



Metal-Incorporated Beta Zeolites: a Versatile class of Catalysts for Continuous Glucose Upgrading

Thesis submitted in accordance with the requirements of
Cardiff University for the degree of doctor in philosophy by

Luca Botti

School of Chemistry

Cardiff University

2020

Supervisor

Dr. Ceri Hammond

Abstract

Glucose upgrading to chemical commodities is an essential step to employ biomass as a novel and renewable source of carbon for chemical production.

Sn-Beta zeolite is known to efficiently catalyse the upgrading of glucose to several commodities such as fructose, α -hydroxy esters and furanic compounds. Nonetheless, Sn-Beta is a catalyst of academic interest only; the lack of knowledge on its stability and selectivity over continuous processes represent an important drawback to its application in the chemical industry. During my PhD studies I focused on tackling this problem investigating and improving the kinetic performance of Sn-Beta zeolite during glucose upgrading to fructose and α -hydroxy esters, five experimental chapters are presented in the manuscript, from chapter 2 to chapter 6. In chapter 2 the causes of Sn-Beta deactivation in methanol were explored, and small traces of water in the feed of reaction were found to increment the stability of the processes carried out by Sn-Beta zeolite. In the third chapter it was shown how the activity and stability of this material are strongly affected by the methodology of preparation, and how the hydrothermal synthesis leads to the most performant material. In chapter 4 the “pre-activation” protocol of Sn-Beta was unveiled, this new treatment enhanced the performances of Sn-Beta for glucose upgrading by tuning the active site and the textural properties of the material. In chapter 5, a new Hf-incorporated Beta zeolite was discovered as a more selective catalyst for glucose isomerisation to fructose, achieving over 50 % yield in fructose with no loss of substrate. In the last experimental chapter of the manuscript the experience gained throughout the whole project allowed to expand the scope of *operando* UV-Vis glucose upgrading, benchmarking the different interactions between the substrate and the catalyst. In this chapter different UV-Vis interactions between catalyst and sugars were attributed to different chemical pathway, generating therefore a powerful methodology to monitor the catalyst deactivation during sugars upgrading.

Throughout this project a better understanding of the performances of Sn-Beta zeolite in continuous conditions was achieved, important developments were brought to the field and new issues were raised suggesting the next challenges to tackle.

Acknowledgment

I would like to thank first of all Dr. Ceri Hammond for the support and the guidance he offered through my PhD project. The scientific discussions we had in these years were always stimulating and allowed me to grow as a researcher. Throughout these discussions I learned not only scientific notions, but I also grew my critical thinking becoming more independent as a professional and as individual. Furthermore, I am grateful for the opportunity of being part of this such stimulating PhD project in collaboration with Haldor Topsøe A/S (Copenhagen, DK) that contributed to sponsor my PhD fellowship. I am sincerely grateful to the whole Haldor Topsøe team with particular mention for Dr. Esben Taarning, Dr. Søren Tolborg and Dr. Juan S. Martinez Espin. They always engaged a stimulating scientific discussion which brought the essential industrial contribution to my academic research. They also host me in their facilities for over two months in my final year of PhD giving me the opportunity to boost my professional growth. On this note I cannot thank them enough for their support during the Covid-19 pandemic.

I would like to thank also the members of Ceri Hammonds' group, they offered an amazing professional and moral support throughout the last three years we spent together in the lab.

Special acknowledgment to Marica and my friends, the good time I had with them in the past years helped me to stay always positive and motivated, and they made me realise that this is probably what life is really about.

Finally and most importantly I would like thank my parents, Gigi and Meri, their high regard for education is what pushed me to start my journey in a tough environment such as scientific research. They thought me that the easiest and short-sighted route in life is never the right one. Their support was essential to face this challenge, and now I am ready for whatever will come.

Table of Contents

Chapter 1: Introduction

1.1 Environmental consequences of CO ₂ anthropologic emissions.....	1
1.2 Biomass as an opportunity for renewable carbon.....	2
1.3 Upgrading of biomass: ethical problem and hurdles in economic sustainability...3	
1.4 Fossil-feedstock and biomass: the need for bio-refinery.....	4
1.5 Biomass for plastic production.....	6
1.6 Composition and typology of biomass.....	7
1.7 Upgrading of biomass.....	9
1.8 Upgrading of glucose.....	11
1.9 Continuous vs discontinuous process.....	15
1.10 Zeolite: properties and activity.....	18
1.11 Activity of metal-incorporated zeolites: Al-, Ti- and Sn-zeotypes.....	21
1.12 Glucose upgrading carried out by Sn-Beta zeolite.....	23
1.13 Zeolite synthesis and the case of Sn-Beta.....	25
1.14 Sn-Beta active site.....	27
1.15 Zeolite deactivation.....	29
1.15 Constant of deactivation from O. Levenspiel.....	30
1.17 Aim of the thesis.....	31
1.18 Reference.....	33

Equation Appendix.....34

Chapter 2: Active site hydration governs the stability of Sn-Beta during continuous sugars conversion

2.1 Introduction.....	43
2.2 Experimental details	
2.2.1 Catalyst synthesis.....	44
2.2.2 Catalyst characterisation.....	44
2.2.3 Kinetic evaluation and analytical methods.....	45
2.3 Results and Discussion	
2.3.1 Water effect on the stability of Sn-Beta.....	46
2.3.2 Understanding the stabilising role of water.....	52
2.3.3 Site selective spectroscopic studies.....	57
2.3.4 Kinetic confirmation of active site hydration effects.....	67
2.3.5 Regeneration studies.....	69
2.4 Conclusion.....	72
2.5 Reference.....	73

Chapter 3: Influence of composition and preparation method on the continuous performance of Sn-Beta for glucose-fructose isomerisation

3.1 Introduction.....	77
3.2 Experimental details	
3.2.1 Catalyst synthesis.....	78
3.2.2 Catalyst characterisation.....	78
3.2.3 Kinetic evaluation and analytical methods.....	79
3.3 Results and Discussion	
3.3.1 Performance of different loading of Sn-Beta during continuous glucose isomerisation.....	80
3.3.2 Glucose upgrading to ML carried out by different loadings of Sn-Beta.....	88
3.3.3 Effect of different preparations methodologies on Sn-Beta performances.....	90
3.3.4 Glucose upgrading to ML carried out by hydrothermal and post-synthetic Sn-Beta.....	92
3.3.5 Structure-activity correlation for different preparations of Sn-Beta...	94
3.4 Conclusion.....	101
3.4 Reference.....	102

Chapter 4: From thermal regeneration to pre-activation of Sn-Beta zeolite.

4.1 Introduction.....	104
4.2 Experimental details	
4.2.1 Catalyst synthesis.....	105
4.2.2 Catalyst characterisation.....	105
4.2.3 Kinetic evaluation and analytical methods.....	106
4.3 Results and discussion: from regeneration to pre-activation	
4.3.1 Preliminary regeneration studies.....	107
4.3.2 Preliminary spectroscopic studies.....	113
4.3.3 Catalyst pre-activation studies.....	116
4.3.4 Spectroscopic studies of pre-activated Sn-Beta zeolite.....	122
4.4 Comparison of different Sn-Beta preparations	
4.4.1 Catalyst synthesis and characterisation.....	127
4.4.2 α -hydroxy-esters production and influence of promoters.....	131
4.5 Conclusions.....	141
4.6 Reference.....	142

Chapter 5: Hf-Beta zeolite: a new selective catalyst for continuous glucose isomerisation

5.1 Introduction.....	145
5.2 Experimental details	
5.2.1 Catalyst synthesis.....	146
5.2.2 Catalyst characterisation.....	146
5.2.3 Kinetic evaluation and analytical methods.....	147
5.3 Results and Discussion	
5.3.1 Kinetic studies.	148
5.3.2 Spectroscopic analysis of Hf-Beta.....	157
5.3.3 Intensification of the process.....	160
5.4 Conclusion.....	163
5.5 Reference.....	164

Chapter 6: Mechanistic studies of continuous glucose upgrading over Lewis acid silicates by *operando* UV-Vis and HSQC NMR

6.1 Introduction.....	167
6.2 Experimental details	
6.2.1 Catalyst synthesis.....	169
6.2.2 Catalyst characterisation.....	170
6.2.3 Kinetic evaluation and analytical methods.....	170
6.3 Results and Discussion	
6.3.1 Identification of optical intermediates by <i>operando</i> UV-Vis spectra..	170
6.3.2 Assignment of selective reaction pathways to <i>operando</i> spectra.....	177
6.3.3 Assignment of non-selective pathways (λ_{442} and λ_{360}) to <i>operando</i> spectra.....	181
6.3.4 Discussion on the nature of the UV-Vis absorptions.....	185
6.3.5 Use of <i>operando</i> UV-Vis to probe mechanistic phenomena.....	188
6.4 Conclusion.....	192
6.5 Reference.....	193

Chapter 7: Conclusions and pertaining challenges

7.2 Next challenges and discussion.....	195
7.2 Next challenges: bullet-points.....	200
7.2 Reference.....	201

Appendix A: Equation appendix.....	202
---	------------

Appendix B: GC Chromatogram.....	203
---	------------

Appendix C: HPLC-ELSD Chromatogram.....	204
--	------------

1.0 Introduction

“We are running the most dangerous experiment in history right now, which is to see how much carbon dioxide the atmosphere can handle before there is an environmental catastrophe”

E. Musk

1.1 Environmental consequences of CO₂ anthropologic emissions

This quote perfectly frames the human behaviour over the last two decades. Scientific data have highlighted an almost perfect correlation between the concentration of CO₂ in the atmosphere and variations in global temperature over the last 800 thousand year (figure 1).¹

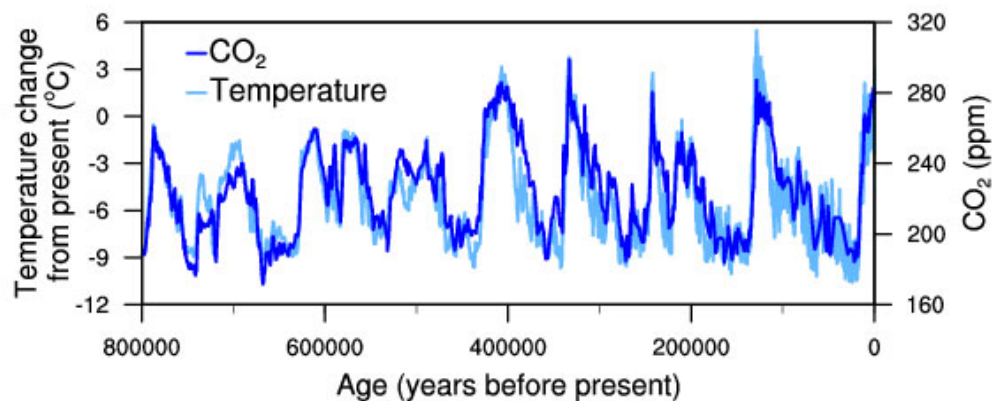


Figure 1. CO₂ concentration in the atmosphere as a function of global temperature variation over the last 800.000 years.¹

However, this has not prevented humanity from dramatically increasing the consumption of carbon-based fossil feedstocks and the subsequent release of CO₂ in the atmosphere, the level of which has increased exponentially since the industrial revolution, reaching a concentration over 400 ppm in the atmosphere.² Although criticisms have been made concerning the link between anthropological activity and CO₂ concentration in the atmosphere, during the last 800.000 years it has never been detected an equally steep increment of greenhouse gasses as it has been monitored in the last 70 years of technological evolution (figure 2).

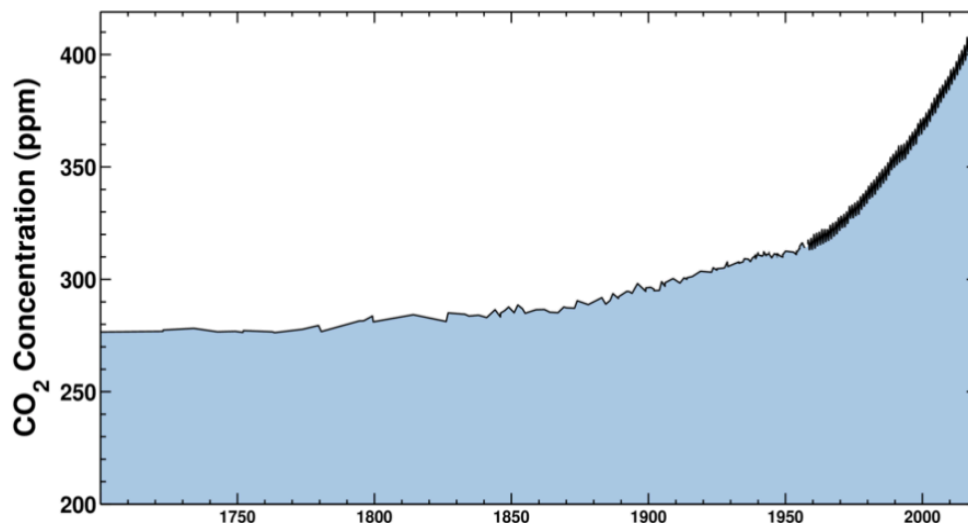


Figure 2. CO₂ concentration in the atmosphere plotted over the last three centuries, showing a dramatic increase of almost 80 % in the last 50 years.¹

This sharp increase was accompanied by an increment in global temperature, which threatens to trigger disasters that might jeopardize life on earth as we know it. Therefore, immediate measures must be taken by the human race to face this challenge, which might be the hardest and most important one humanity will ever face. To prevent further increments in temperature, the quantity of CO₂ released by anthropological activity needs to be sharply reduced. As energy, food and material production are the main areas responsible for CO₂ emission and/or fossil feedstock usage, important and effective investments need to be made in these three sectors to address the problem with the highest priority.³

1.2 Biomass as an opportunity for renewable carbon

As afore mentioned, the accumulation of CO₂ in the atmosphere is mainly due to the large exploitation of fossil-feedstock for the production of energy and plastic material, leading to 5 Gt y⁻¹ of global oil consumption.⁴ Therefore, measures must be taken to promptly decrease the usage of this non-renewable carbon feedstock. One of the most promising form of renewable carbon is biomass. Biomass derives from plant and/or animal waste, and, as such represents an easily available source of carbon atoms, with a reported annual amount of 100 Gt y⁻¹.⁵ The renewability of biomass is due to the fast regeneration of carbon materials from which biomasses are gathered, which helps in closing this carbon cycle.⁶ Considering the vast availability of this substrate, biomass appears as a suitable candidate to fully replace fossil feedstock. Nonetheless the comparison on a weight basis is somewhat misleading, as biomass has a lower energy and carbon density than crude oil; on a weight basis, oil contains approximately twice the amount of carbon atoms and chemically stored energy as biomass.^{6,7} Thus, as the use of biomass in industry increases, it will at some point become a scarce resource, and its utilisation should for this reason be considered wisely. Therefore, it is unrealistic to design processes which consider a zero or negative price for

biomass as feedstock process, because large scale production considerably alter the market and availability of biomass worldwide.⁴ For these reasons it is important to pay attention to the limitations and to the ethical problems which may arise from large-scale processing of biomass.

1.3 Upgrading of biomass: ethical problems and hurdles in economic sustainability

As afore mentioned, the demand for biomass for chemical industry may exponentially increase if several processes for the large scale production of market molecules are developed using this source of carbon as principal feedstock. In turn, this might affect the food market if the production of biomass will be aimed for the chemical market and no longer for food production.^{7,8} The possible competition between the food and chemical market is a factor to be kept in consideration when evaluating a consistent usage of biomass as carbon feedstock. Vast increase in biomass consumption for biofuels and bio-plastic might in fact undermine the stability of the food sector, leading to an increase in prices which can eventually compromise food availability for less wealthy individuals in the society. On this matter is important to distinguish between two typologies of biomass: first generation biomass is directly linked to the production of edible products, whereas second generation biomass is derived from a wide array of feedstocks such as lignocellulosic materials, organic wastes and terrestrial or marine biomass not involved in the food chain.⁶⁻⁸ Hence scientists are studying and developing processes based on second generation biomasses. In this way, it can be ensured that the food market and its related prices can be maintained constant developing alongside chemical processes from biomass.⁸ Although second generation biomass is not directly a food-competitor, the usage of field that could be used for first-generation biomass production still constitutes an indirect source of potential competition which will eventually require regulation from governments.⁹ However, this ethical challenge is not yet an important concern, since the chemical processes employing biomass as carbon source is still an open challenge. One issue related to this slow innovation may arise from the variety of products that can be potentially made from biomasses and the consequent complications in identifying the right market for biomass-based products. In many countries, such as South America, fermentation of biomass to bio-ethanol is a widespread process to produce biofuel which can be added to normal gasoline¹⁰ in order to diminish usage of petrol derived fuel. Although this is a green route that helps decrease the CO₂ emissions related to passenger transports, the exclusive employment of biomass for bio-ethanol production lacks economic sustainability.^{11,12} In fact, economic competitiveness is the second big hurdle in developing a chemical industry based on biomass exploitation, a clear example of which is given when analysing the energy market: heating energy derived from fossil feedstock is sold at a price of 8 \$ GJ.^{1,11} This means that considering a harvest of 10 tonnes dry weight per hectare per year, the average earning is around 640 \$ per hectare of field. This income is too low for an economically sustainable

production of biomass for this purpose only.¹¹ Therefore to develop economically sustainable routes for biomass upgrading the right chemical sector and products must be identified.

1.4 Fossil-feedstock and Biomass: the need for bio-refinery

For the reasons described above, the study of the upgrading of biomasses is looking to integrate the bio-fuel production with the production of higher added-value molecules.¹³

To achieve this goal, scientists have identified two different strategies, as shown in figure 3. The first, known as “drop in approach”, is the conversion of biomass into already existing organic chemical commodities,⁴ which are molecules produced in vast amount (Mt per year).¹⁴ Over the last 50 years of research on fossil feedstock, several processes to synthesise bulk molecules such as xylene, caprolactam, and cumene, were developed; the chemistry of which was largely developed as a mean to upgrade the chemical building blocks present in fossil resources to useful molecules for industry. Herein lies one of the main hurdles in biomass upgrading; in fact, fossil and renewable feedstock are two extremely different feedstocks, with diverse properties and chemical composition. Hence, the synthesis of the same platform molecules produced from fossil feedstock may be challenging when a different source of carbon is employed.¹⁵ The second market strategy for biomass upgrading is the formation a new group of platform molecules that can be easily generated from biomass, and further upgrading of these new platform molecules to produce new bio-based materials.⁴ Obviously, in this case, a major hurdle is the necessity to develop a new set of reactions, materials and market of which little (if nothing) is currently known. Therefore, even though this solution may appear to be the most promising in the long term, a consistent investment should be done to create this portfolio of knowledge for future exploitation of these new classes of molecules and chemical processes.^{4,16} At present, it is impossible to identify the right direction to take, and each specific scenario needs to be singularly evaluated. Nonetheless, the “drop in” approach (if economically sustainable) is the easiest and the more immediate solution to apply, although on the long-term perspective new materials and new platform molecules will probably be developed.

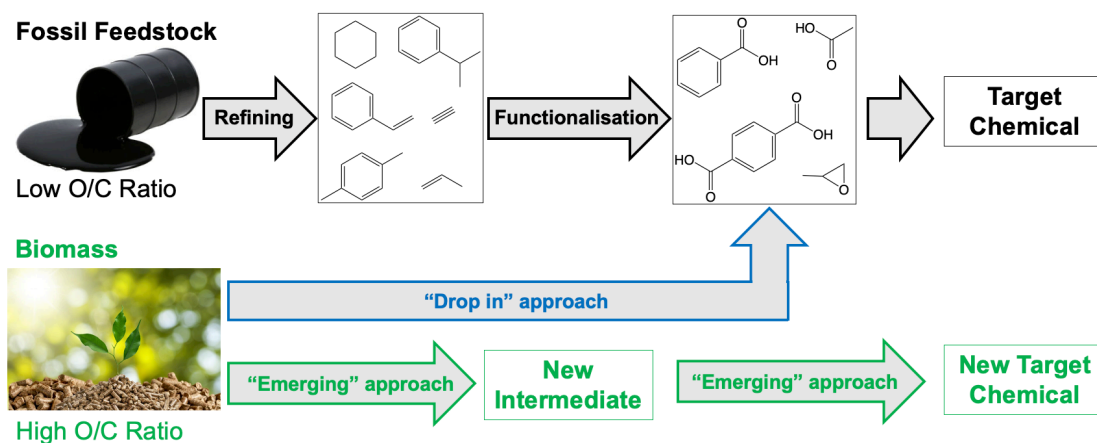


Figure 3. Market strategies for possible upgrading of biomasses to valuable molecules.

One of the main challenges scientists need to cope with whilst working on biomass upgrading is the drastic difference in oxygen content that this feedstock has when compared to the petrochemical one. Fossil feedstock, employed as carbon source in the chemical industry throughout the last century, has a relatively low O/C ratio (oxygen content against carbon content). This property lead to the development of specific processes adapted to this need, which, in most of the case, involve gaseous phase oxidations of the feedstock to achieve functionalised molecules. Conversely, biomass already possess a relatively high O/C ratio, which does not require further oxidation for downstream functionalisation. However, in most cases, the high O/C ratio prevents direct use of biomass as fuel. Moreover, the high boiling point of the molecules involved in such processes, represents a challenge for the development of gas phase systems. Hence, new liquid phase processes for the treatment of biomasses should be investigated, representing a major technological change from the classical petrochemical processes, which are almost exclusively performed in gas phase. This is the direction that researchers are pursuing to expand the usage of this renewable source of carbon.¹⁷

In the previous section some of the main hurdles in biomass upgrading were shown. However, the main obstacle concerning the chemical conversion of biomass is the lack of knowledge regarding this subject. Contemporary chemical industry based on petrochemical carbon source was developed over the last 70 years, in comparison the research on biomass is still at its dawn and the true potential of this renewable feedstock has not yet been entirely expressed.¹⁸ Therefore, it is possible to forecast that in the decades ahead several types of flexible processes will be developed from biomass, which chemical nature is extremely diverse: different typology of biomass are available with a wide array of chemical composition. The diversity and complexity of the biomass matrix is an obstacle to the development of selective processes for biomass upgrading, therefore at present, it is utopian to imagine a single and straightforward process for biomass upgrading. Instead, parallel and flexible processes need to be developed to economically valorise at best biomass for production of molecules, heat and fuels. The integration of several flexible processes for production of different economically valuable products can be summarised in one word: 'biorefinery'.¹⁹

Classic refinery processes already exist to extract the best economic value from petroleum. In fact, although the production of chemicals accounts for only a small fraction of the petrochemical refinery technologies, such routes provide the highest economic gain to the industry. A conceptually similar, but chemically different approach, thus, needs to be developed to ensure the full replacement of fossil feedstock with biomass for our planet.

1.5 Biomass for plastic production

The previously mentioned ethical problems in the exploitation of biomass on large-scale, the hurdles in developing complex and integrated processes able to compete with fossil-derived fuels and the rising of alternative sources of clean energy (solar, wind, nuclear and hydrogen) are limiting the applicability of biomass as a source of biofuels.

Therefore, researchers are focusing their attention on the exploitation of biomass for the synthesis of polymeric materials. Although plastic nowadays represent the 6 % of the final destination of fossil-feedstock its production has increased from 2 Mt in 1950 to 380 Mt in 2015, corresponding to an annual growth of 8 % y^{-1} .²⁰⁻²² If the production keeps increasing at this rate, it is predicted that the carbon footprint related to the plastic industry will reach 15 % of the global carbon budget by 2050. Therefore, countermeasures must be adopted to contain these emissions; in particular the option to exclusively employ bio-based plastic is widely studied amongst the researchers. A switch from petrochemical to renewable carbon feedstocks (i.e. biomass) has the potential to decrease the carbon footprint associated with polymer industry by 75 % of the reference value.²² Moreover plastic production from biomass, does not only represent a greener alternative to the classic fossil-feedstock, but it also may constitute important technological advantages for the production of materials. As previously mentioned in the comparison with petrochemical feedstock (section 1.4), biomass has drastically different chemical composition, in particular their high oxygen content might facilitate functionalisation processes which are paramount for production of reactive and flexible plastic monomers.^{4,23}

The ratio between hydrogen and carbon atoms in the molecule adjusted for heteroatoms (equation 1), is an important metric to identify chemical similarities between industrial feedstock to plan industrial processes.

$$\text{H/C ratio} = \frac{n(H) - 2n(O)}{n(C)}$$

Equation 1. Calculation of the H/C ratio of biomass. This value is used to classify molecules and feedstock to identify chemical similarity to exploit in industrial syntheses.

Fuels usually possess high H/C ratios (1.3-2), whereas commodities for chemical production typically exhibit lower values (0-1) due to the functionalisation that oxygen atoms provide in the molecules.⁴ Sugars, derived from biomass, have a similar H/C ratio to many functionalised high-value chemicals for plastic production and would therefore represent a more ideal feedstock than fossil resources in some cases. For example, by utilizing biomass as feedstock for the production of chemicals instead of biofuels, the necessity for deoxygenation, which is one of the biggest challenges when making fuels from biomass, is partially or completely avoided.⁴ For these reasons, the upgrading of biomass to plastic materials not only represent a possibility to drive away from fossil-feedstock; but it also

represents an opportunity to simplify the processes involved in this chemical sector. Therefore, in this manuscript the development of catalysts capable to transform biomass into monomers for plastic production will be explored, in order to allow the replacement of the classic fossil resources with renewable carbon feedstocks.

1.6 Composition and typology of biomass

In the last section (1.5) was reported the reason why the exploitation of biomass is shifting towards the replacement of fossil-feedstock for the production of chemical commodities to synthese bio-polymers. However, the diverse nature of biomass requires selective and tailored processes for its upgrading, therefore a complete understanding of their chemical composition is required to understand the complexity if their selective upgrading. The word biomass embeds a broad range of materials derived from animals or plants. As such, the structure of biomass is highly diverse depending by the type of biomass that is being taken into account. In general, biomass is composed from different structures, diverse in nature and complexity. Taking as example biomass derived from agricultural waste (which is the most readily available and, hence, most widely studied), it is possible to identify three main structures: hemicellulose, cellulose and lignin.^{24,25} Cellulose is a polysaccharide formed by hundreds or thousands of D-glucose units linked together by β (1 \rightarrow 4) glycosidic bonds (figure 4).^{24,25} Due to its high crystallinity cellulose is a rigid and robust material that gives structural strengths to cell walls. For this reason, cellulose is relatively hard to depolymerise into its basic units by hydrolysis, and several strategies have been explored to solve this challenge.^{25,26}

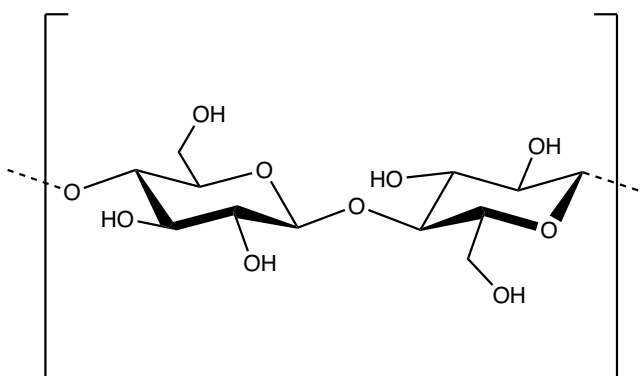


Figure 4. Basic structure of cellulose formed by β 1 \rightarrow 4 glycosidic bonds between D-glucose monomers.

Hemicellulose has a more complex structure than cellulose, and this portion of biomass contains several kinds of sugars besides glucose, including both 6 membered ring sugars such as mannose and galactose, and 5 membered ring monosaccharides, including xylose and arabinose. Due to the diverse nature of the building blocks constituting this portion of

biomass, the overall structure possesses less crystallinity, and is thus more prone to be hydrolysed in acidic or basic conditions.²⁴ Lignin is the last portion of biomass and the most complex matrix to depolymerise and upgrade to valuable chemicals. Several types of lignin exist depending on the source of biomass from where it is gathered and the whole structure of this material is still not fully known. However, it is generally composed by phenolic polymers, which confer high mechanical and chemical resistance to the whole material. This structure in fact is usually found in cell walls of wood and bark (figure 5).^{27,28}

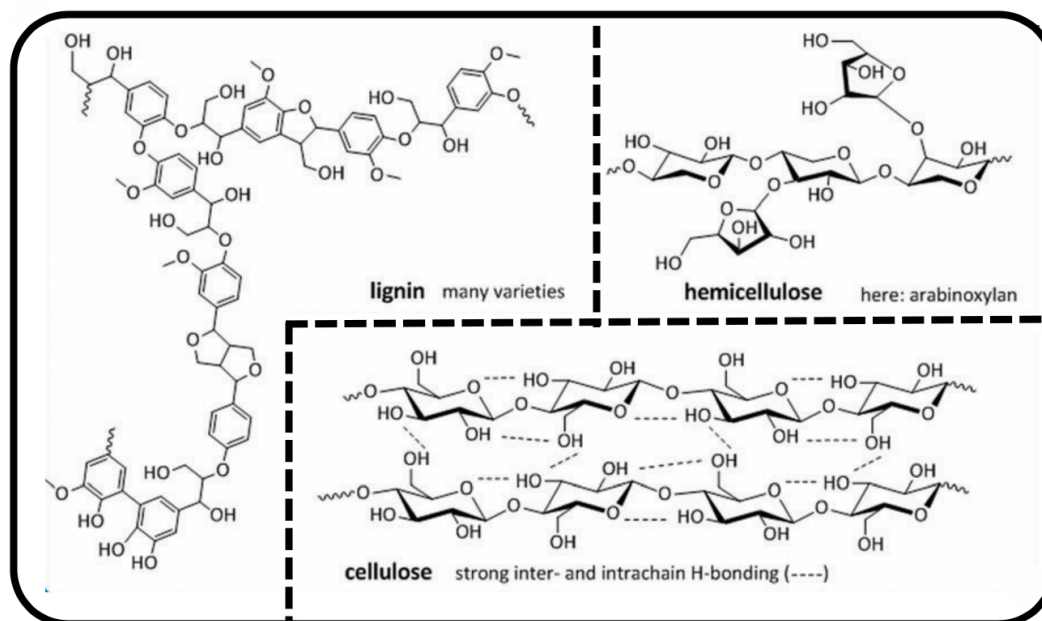


Figure 5. Overview of the three main components of biomass: lignin, cellulose and hemicellulose.²⁸

However, agricultural waste is not the only type of biomass that is attracting attention for its potential as a renewable carbon source. In fact, nowadays many sectors of the food industry produce biological waste that may be used as natural feedstock of carbon. An example of which is chitin, a polymer of N-acetylglucosamine (a derivative of glucose) that is a primary component of the exoskeleton of arthropods such as crustaceans and insects (figure 6). This biopolymer has a structure similar to cellulose since the monomeric units are linked in an analogous manner, via β (1 \rightarrow 4) bonds, and, therefore, similar technologies can be applied to upgrade these two compounds.^{27,28} The annual production of chitin obtained by living organisms in the ocean is around 10^{12} - 10^{14} ton, and this large quantity would supply a sufficient raw material for industry provided that commercial procedures are developed for the upgrading of chitin to platform molecules.²⁹

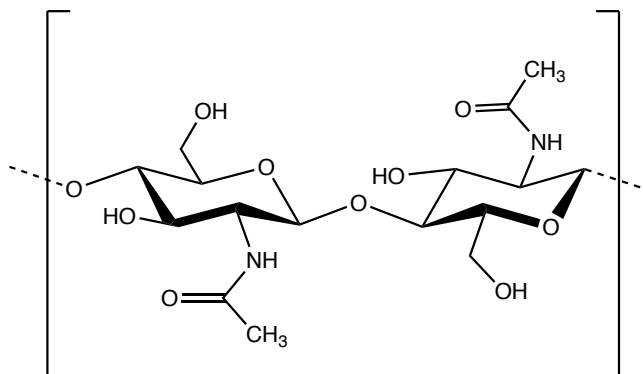


Figure 6. Chitin structural unit formed by N-acetylglucosamine units linked via β (1 \rightarrow 4) bonds.

1.7 Upgrading of biomass

The process of biomass upgrading to chemicals or energy can be performed in different ways.³⁰ In general, it is possible to identify three main approaches to treat biomass feedstock: thermal, bio-enzymatic and catalytic.^{31,32} The thermal treatment of biomass can be further divided into three different methodologies: combustion, gasification and pyrolysis (figure 7).⁸ During combustion, the entire biomass feedstock is burnt to ashes in excess of oxygen. This process produces heat that is further transformed into energy. This resultant energy is therefore derived from renewable carbon sources, whose carbon footprint is lower than the classic fossil feedstocks. However, although this methodology can efficiently lead to energy production, it does not valorise the possible chemicals that might be gathered from these sources of carbon. For this reason, pyrolysis and gasification could be considered a better alternative.^{8,11}

Gasification is usually conducted in the presence of a small amount of air or oxygen, and it goes through three steps: drying, during which the residual water in the material is purged out from the solid mass (heating up to 120 °C); devolatilisation in a temperature range of 120 - 350 °C, during which volatile species are released and char is produced; finally, at temperatures above 350 °C gasification takes place, during which the char reacts with oxygen to form CO, CO₂ and H₂O, which can subsequently lead to H₂ production via water gas shift reaction.³³ Gasification, therefore, produces gasses that might be used in a second instance to generate energy or chemicals. For example, the syngas produced (H₂, CO, CO₂) may be converted to synthetic fuel through Fischer-Tropsch reaction.^{11,33}

Pyrolysis takes place at temperatures up to 350 °C / 400 °C in oxygen-free environment. During this process, a consistent amount of liquid is produced alongside char and syngas. The liquid fraction, mainly composed by carbon and oxygen, is usually further treated to extract platform molecules to deoxygenate to produce biofuels; different compounds are obtained depending from the composition of the biomass used in the process.¹⁹

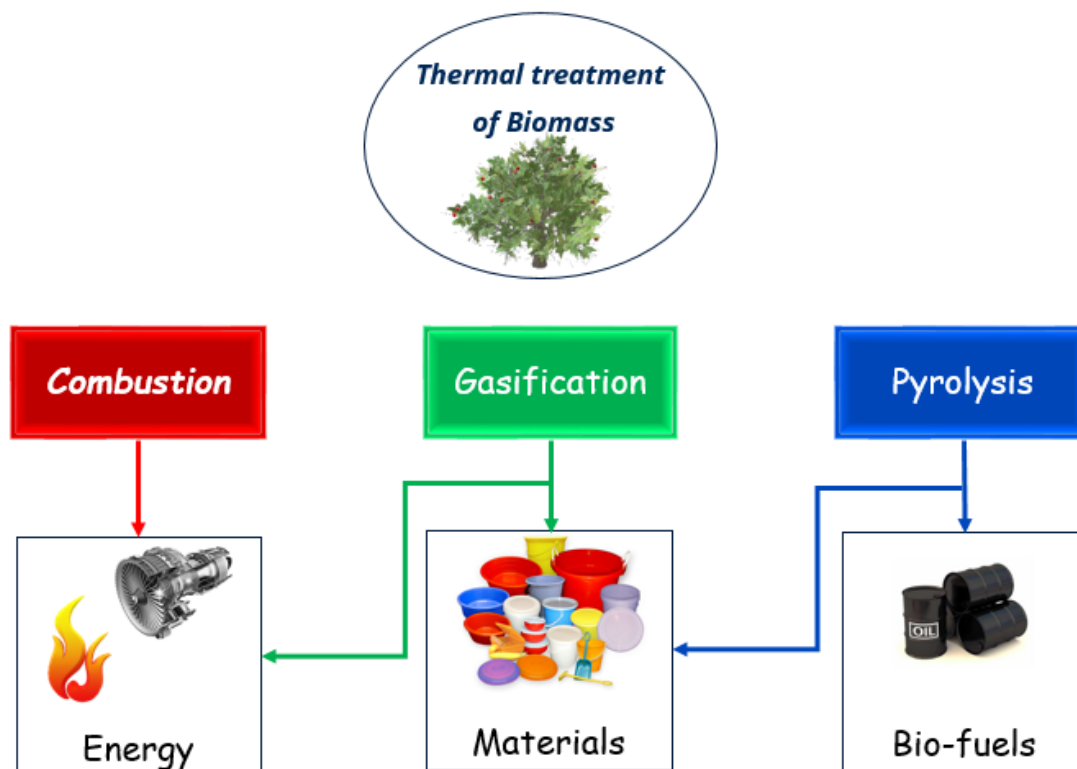


Figure 7. Strategies for direct upgrading of biomass by thermal treatment of biomass with related products.

Thermal conversion of biomass usually involves simple processes which make their application relatively straightforward, however, this set of transformations is not specifically tailored to exploit the functional group present in this feedstock.^{33,34} It rather deoxygenate the biomass yielding to char or liquid with similar composition to the fossil feedstock. This yielding material requires further functionalisation (i.e. oxidation) to obtained chemical commodities for bio-materials production.^{4,8} As previously described in paragraph 1.5, biomasses are already characterised by an H/C ratio similar to several chemical commodities, therefore, researchers are focusing on upgrading this feedstock directly to chemical without an intermediate thermal passage, which only contributes to increase the process costs.

To achieve this goal, other ways to directly upgrade biomass have been developed. The first approach is its biochemical conversion which has shown outstanding results in producing important chemical commodities with high selectivity. During this process biological catalysts such as enzymes and bacteria are employed to convert the carbon feedstock in platform molecules for industry.³⁴ The most important results in this area were obtained for production of succinic acid, ethanol and high fructose corn syrup (HFCS).³⁵ Succinic acid fermentation is promoted by genetically engineered *Escherichia Coli* with high selectivity and productivity.^{35,36} This process has been extremely important to reduce the costs of succinic acid production, previously obtained via n-butane conversion to maleic

anhydride and further conversion to succinic acid.³⁶ Ethanol fermentation from monosaccharides is carried out by microbial agents (yeast) and the product of this process is mainly used as transportation fuel, particularly common in South America.^{32,37} HFCS production, instead, is mainly exploited for food purposes due to the high cost of the product, which production will be thoroughly discussed later in the chapter (Section 1.8). Although these processes are typically characterised by high selectivity due to the use of enzymes, their application is limited to a handful of products for plastic materials. The reason for this low applicability is due the high operating costs that these processes require, in fact, it is known how these biological catalysts are efficient only in narrow conditions of temperature, pH and substrate purity.^{30,31} Such strict conditions require high purifications, buffer solutions and low temperature, which represent important drawbacks, incrementing the price of the final products, which, in many cases, are not economically competitive with commodities synthesised from fossil fuels. For this reason, researchers are focusing on the inorganic catalytic conversion of biomass. Such inorganic catalysts are typically cheaper than biological catalysts, and they usually can withstand harsher operative conditions (in terms of pressure, temperature and pH) when compared to the ones exploited in the biochemical biomass upgrading.^{38,39}

Therefore, the catalytic conversion of biomass aims to achieve more productive and flexible transformations of this feedstock through the robustness of these inorganic catalysts. Moreover it aims to produce platform molecules for bio-based material by tailored chemical processes that selectively modify the functional groups already present in the feedstock. In this way, a plethora of important intermediates can be efficiently produced and implemented at different levels of the chemical industry, replacing building blocks typically derived from fossil feedstock.

1.8 Upgrading of glucose

The catalytic upgrading of biomass, therefore, needs to proceed from the monomeric units of this feedstock, to further upgrade them to the desired molecules. As previously mentioned (Section 1.6) the monomeric units that comprise an important fraction of biomass is glucose. Glucose is the most abundant sugar on the planet, efficiently extracted via hydrolysis from cellulose and hemicellulose.^{40,41} The resulting material is glucose syrup, consisting of approximately 70-90 % glucose in the dry matter. Glucose syrup is a chemical commodity with a worldwide annual production reaching 20 million tonnes for a price of roughly 300 \$ per ton.⁴⁰ Glucose is mainly found as a six-membered ring monosaccharide. Although glucose is considered an aldose since in its open form it possesses an aldehyde terminal group, this compound can also be found in its furanose form (figure 8).⁴¹

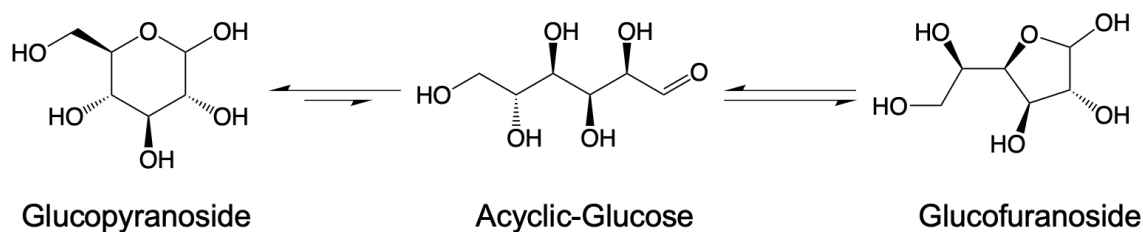
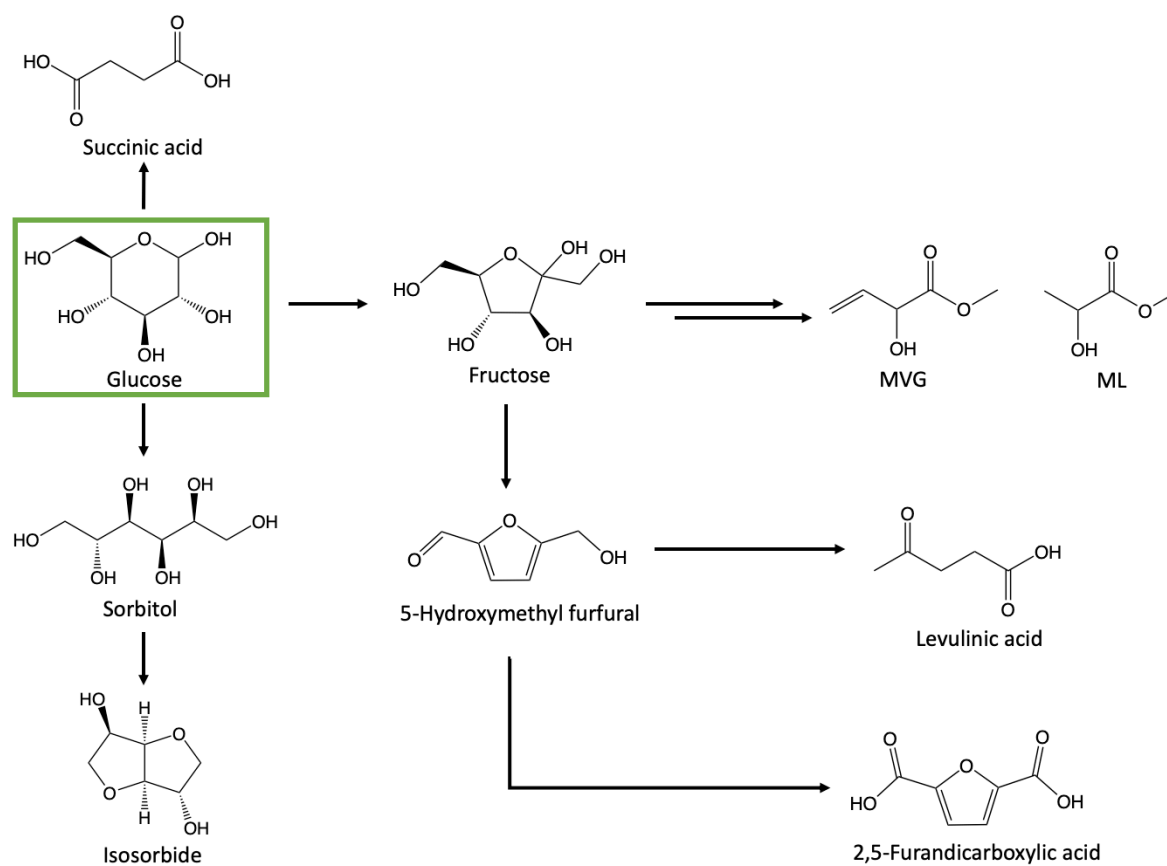


Figure 8. Different forms of glucose that can be found in solution.

Since glucose is the most abundant and cheapest monosaccharide produced from biomass, its upgrading to valuable molecules is paramount for efficient biomass valorisation.^{36,37,42} Therefore, different pathways for production of several kinds of commodities starting from glucose have been studied (scheme 1).



Scheme 1. Some of the platform molecules that can be derived from glucose upgrading.

From this scheme is possible to understand how dehydration and retro-aldol reaction are two important routes for glucose upgrading, as the generated products (including 5-hydroxymethyl furfural, HMF, furfural and methyl lactate) are valuable molecules for the chemical industry.^{43,44} However, for many of these processes the direct functionalisation of glucose is not favoured, above all the dehydration to HMF is not selective when glucose is employed as substrate. This reaction leads to degradation of the substrate rather than formation of the desired product, thus, prior isomerisation of glucose to fructose is essential

for process intensification.^{54,55} Accordingly, the acidic pathway for isomerisation of glucose to fructose will be explored throughout this manuscript. Fructose itself is nowadays produced via glucose isomerisation catalysed by *xylose isomerase*, which is an enzyme able to convert glucose to fructose. This process leads to the production of HFCS, which is used as sweetener in the food industry. The global market for this commodity is around 5.9 billion dollars and it is expected to grow by more than 30 % the next 5 years.⁵⁶

Three types of catalysis have been studied for the glucose isomerisation reactions; enzymatic, homogeneous and heterogeneous catalysis.⁵⁷ Enzymatic catalysis employs glucoamylase and alpha-amylase to convert starch to glucose, and the resulting solution of glucose is then converted to HFCS by immobilised *xylose isomerase* (figure 10).⁵⁵ Following conversion by the enzyme, the sugar solution comprises of 50 % glucose and 42 % fructose (mannose and some polysaccharides are still present in the final mixture).⁵⁸ The yielding product is HFCS, which can be further concentrated by liquid chromatography to reach a fructose concentration of 90 %.⁵⁹



Figure 10. Structure of D-xylose isomerase, the enzyme exploited in the industrial process for glucose isomerisation to fructose for HFCS production.

This process is characterised by high selectivity towards fructose and the formation of by-products is negligible.⁴⁹ However, despite its remarkable performances, HFCS obtained by enzymatic catalysis is not economically competitive with fossil derived molecules for bulk chemical manufacture.⁶⁰ Moreover, enzymes are extremely sensitive to the reaction conditions (temperature, pH and pressure). In particular, temperatures above 80-90 °C should be avoided to ensure enzyme integrity during the process.^{54,61} Unfortunately, the requirement for low temperature negatively impacts the process. In fact, as shown in figure 9, the reaction is governed by a thermodynamic equilibrium, and, being this transformation endothermic, an increment of reaction temperature could theoretically allow to shift the equilibrium towards fructose.⁴⁹⁻⁵¹ Therefore, this limitation strongly impacts the process both

by limiting equilibrium yields and also limiting the productivity of the overall process. Moreover, the cost of the enzymes, generally higher than the ones of classic inorganic catalysts, must be added to the already elevated costs of the process.⁶²

Due to these disadvantages, several technologies have started to be studied as alternative to the enzymatic route, and the necessity to shift away from this costly and fragile catalysts lead to the development of inorganic approaches for glucose isomerisation. In homogeneous catalysis the catalyst and the substrate are in the same phase. This technology allowed to reach interesting performances in presence of acid catalysts for glucose isomerisation, whereas inorganic basic catalysts lead to drastically lower selectivity in the process due to the degradation of the substrate.⁵² Amongst homogeneous catalysts, AlCl_3 and CrCl_3 have been thoroughly studied for this reaction leading to interesting results.^{58,61,63} One of the major benefits of this kind of processes is the ease of the catalyst-substrate interaction. In contrast, in heterogeneous catalysis this interaction might be affected by diffusion problems of the substrate in the catalytic material. However, this route has also several disadvantages that drastically affect the sustainability of the process: homogeneous processes require, in fact, important investments in downstream separation of the products and recycle of the catalyst.⁶⁰

Heterogeneous catalysis employs a solid catalyst in presence of liquid or gaseous stream of the substrate. This process usually generates less liquid waste to dispose of than the classic homogeneous route and the separation of the catalyst from the reaction mixture is not particularly demanding since they already are different phases. Moreover, in continuous systems the catalyst is usually immobilised in a catalytic bed and the separation of the catalyst is not needed at all.⁶⁴ Although this type of process might suffer from mass transfer problems arising from interaction of the liquid substrate with a solid catalyst, the ease of its scalability makes heterogeneous processes suitable for production of high market volume molecules.⁶⁵ Therefore, considering the volume of biomass wastes produced per year (100 billion metric tons of carbon), their low price and the vast market of target commodities, heterogeneous processes seem to be the best choice for glucose upgrading.^{4,13,20}

1.9 Continuous vs discontinuous process

As previously mentioned, the upgrading of biomass cannot be considered a process at zero-cost feedstock (Section 1.2), due to the enormous demand that might be generated from a possible applicability of this feedstock as renewable source of carbon for plastic material. Therefore, optimal productivity is required from these processes to convert at best this valuable substrate.⁴ For chemical production to be economically efficient, selecting the right type of catalysis alone is not enough, but the right operative conditions and reactor configuration are necessary to ensure the competitiveness of the process. Generally, for chemical processes is possible to find two types of systems: continuous and discontinuous, more commonly known as 'batch'. Herein a brief description of these technologies is reported.⁶⁶

In classic batch systems, the catalyst and the substrate are loaded together in a batch reactor. The reaction is subsequently run for a set period of time, after which the reaction is quenched. Subsequent filtration of the crude reaction is essential to isolate the catalyst from the reaction mixture, which is then further treated to obtain the desired products. A simplified scheme of a discontinuous reactor is shown in figure 11.

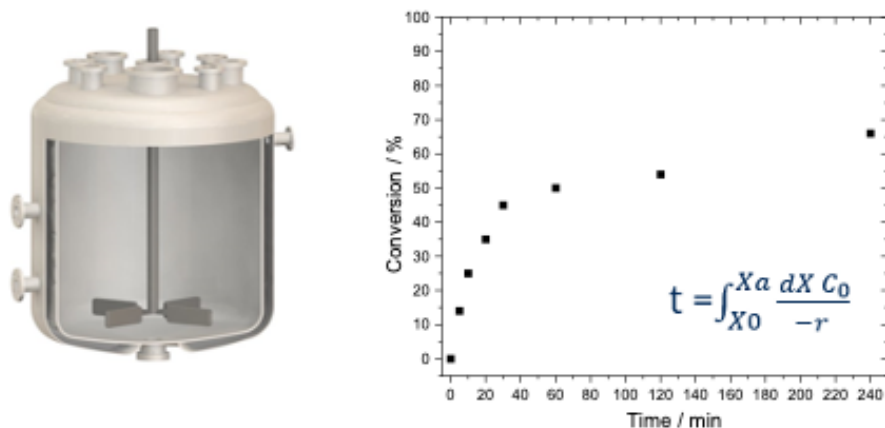


Figure 11. Example of batch reactor with related kinetic plot and relative kinetic equation.

This process is simple and intuitive, its costs of installation are usually relatively low, but several disadvantages are associated to this system. First of all, discontinuous systems do not guarantee optimal productivity due to down period of the process during which the reactor needs to be loaded and unloaded of the contents of the reaction (substrate, solvent and catalyst).⁶⁴⁻⁶⁶ Over time, these periods represent a consistent increment in variable costs due to time and energy required to start, quench and load of the reactor. Furthermore, these discontinuous phases are not only a loss of productivity, but they are also the most dangerous moments from a safety perspective. In fact, discontinuous processes are sensitive to human error, which can lead to the economic loss of an entire batch of product, or in worse cases, to serious safety accidents.⁶⁵ Therefore, batch processes need to be continuously monitored and specific procedure must be followed to decrease the possibility of accidents. Despite these drawbacks, batch processes possess some benefits, in fact, the low costs of process and high flexibility of these systems make discontinuous processes ideal for small scale market productions of chemicals with high added value. This class of chemicals does not need a consistent and continuous production throughout the year and might have a short time window of competitiveness on the market, therefore, the capital investment for continuous upgrading of these process may not be justified. Conversely, for high volume market chemicals with low added values a different kind of process is required. The low added value of this molecules and their high annual demand results in need for less flexible and more productive processes which better controls the variable costs, the safety concerns and, more importantly, needs to ensure the highest economic return for rapidly recovering the fixed costs related to the plant installation.⁶⁷ For these reasons continuous processes are needed for the production of chemicals with high market volumes.

As such, the use of glucose as a building block for to the chemical industry most certainly needs the employment of continuous systems to be competitive with the fossil-derived molecules.⁶⁸

Such continuous reactors are different to the batch ones (figure 12). Firstly, the catalyst is contained or immobilised in an area of the reactor in which the substrate is flown through it and the effluent is already free from the solid catalyst. Furthermore, the resulting kinetic plot for these reactors are different. In fact, they do not have a proper time of reaction as the classic discontinuous reactors (figure 11), but the substrate has a specific contact time (τ) with the catalyst. This value is given by the flow of reactant (F), relative to the volume of the catalytic bed (V), as shown in figure 12. This value defines the performance of the process and allows an operator to tune the conditions (conversion of the substrate and yield of the products) at which the process needs to be run.

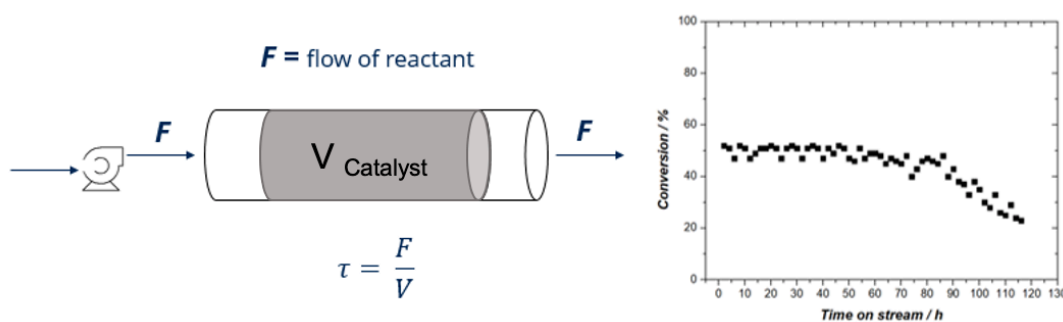


Figure 12. Schematic representation of a continuous reactor (PFR, plug flow reactor) with related kinetic plot.

In figure 12 is reported a general scheme for a continuous reactor, this specific kind of continuous reactor is called tubular reactor and the movement of the fluid inside it is described by the PFR model (Plug Flow Reactor).⁶⁹ This model aims to ensure the best performance of the reactor by designing the motion of the inner fluid with a laminar flow regime. The laminar regime is essential to avoid the back mixing of the liquid phase throughout the catalytic bed, ensuring that the contact time of the molecules flowing through the reactor is constant during the whole process.^{65,67} Figure 12 also shows that the kinetic profile of these systems may be affected by possible contribution from catalyst deactivation, which is identified by a loss of activity. Due to the impact such deactivation events can have on the performances of the catalyst, in this type of system it is not only important to assess the activity and selectivity of the process, but also to perform systematic research on the stability of the catalyst, which becomes an essential factor to ensure the best productivity and economic sustainability of the process.

1.10 Zeolites: properties and activity

After having shown the reactor choice needed for biomass, and specifically glucose upgrading, elucidations on the right catalyst to test for this reaction must be given. Due to the importance of glucose conversion over heterogeneous catalysts, a large amount of research has focused over the last two decades on the development of catalysts capable of performing this chemistry. From these studies appeared that the catalyst exhibiting the best performances in this process is Sn-Beta zeolite.⁷⁰⁻⁷³

To better define Sn-Beta zeolite an explanation of the properties and structure of zeolites is necessary to fully understand the topic. The word “zeolite” describes a vast group of aluminosilicate materials, in which aluminium and silicon atoms are bonded to oxygen atoms in a tetrahedral geometry (figure 13). These tetrahedral units are linked together to form precise crystal structures, which ultimately result in the formation of pores and channels. These channels form a microporous structure (pore size up to 20 Å) which is typical of zeolites, the assignment and the arrangement of these pores are determining the classification of these materials. Due to their high porosity, and the presence of aluminium atoms, zeolites generally tend to absorb large amounts of water. This property gives to this class of materials their name; in fact, zeolite derives from the Greek “ζέω” (zéō), which means “to boil” and “λίθος”(lithos), which means “stone”, due to the fact that the rapid heating of this material produces a considerable amount of steam.⁷⁴

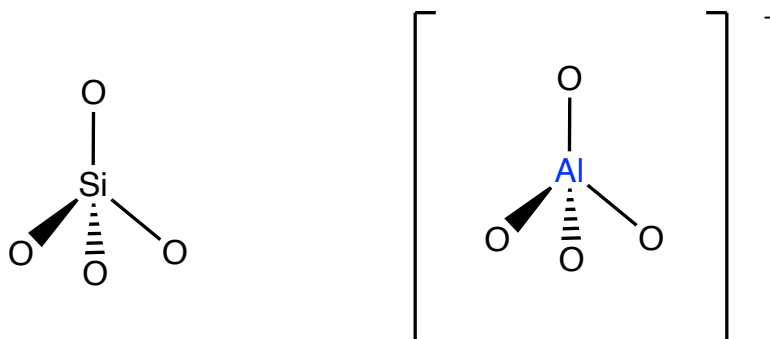


Figure 13. Silicon and aluminium tetrahedral structure of zeolite monomers.

The crystalline structures of zeolites are diverse and numerous. The silicon and the heteroatoms incorporated in the framework occupy a precise and defined position in the repetitive units of the crystals. These positions are called T-sites. Each T-site has a tetrahedral structure, but the angles of the bonds in each T-site are different, as are their degrees of accessibility. This means that the free-energy related to each T-site is slightly different, and heteroatoms with diverse sizes might have energetic preference towards a specific T-site which better accommodates its dimension in the framework.⁷⁵

Aluminosilicates are widely found in nature as minerals (faujasite, amicitite, clinoptilolite), but several more structures have been synthetically obtained alongside the incorporation of new heteroatoms other than aluminium. To date, over 230 different frameworks of zeolite

are known and the international zeolite association (IZA) is responsible for identifying and classifying each framework with a three letter code.⁷⁶ One of the most well-known structures is the MFI (figure 14), which is formed by 10, 6, 5 and 4 membered rings structure and can allow the diffusion of molecules up to 4.7 Å of diameters. For example, the famous ZSM-5 zeolite (Exon Mobil), widely employed for alkane isomerisation, is included in the MFI family.⁷⁷

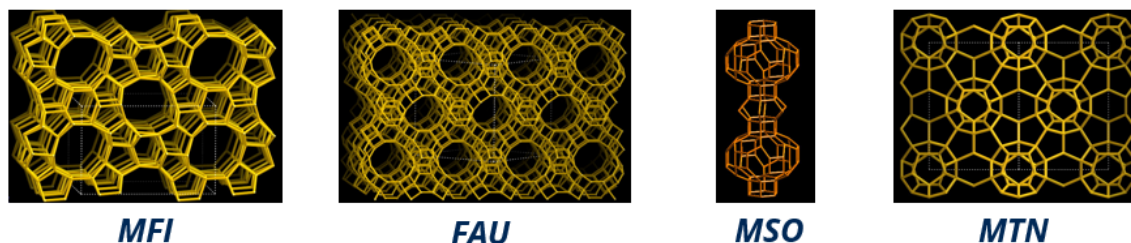


Figure 14. Framework of MFI, FAU, MSO and MTN zeolite, in these images is possible to appreciate the different pore size of the materials.⁸¹

Another family of zeolites which is worthy of note is the one possessing the “FAU” structure (named after the mineral faujasite, figure 14), this group of zeolites is formed by 12, 6 and 4 membered rings and allows diffusion of molecules up to 7.5 Å of diameter.⁷⁸ An important member of this family is zeolite Y, which is employed in the fluid catalytic cracking (FCC) of fossil feedstock due to its large pores.⁷⁹ Besides these relatively large-pore frameworks, also smaller pores zeolite (figure 14) can be found, such as the MSO and the MTN structures, which possess 6 membered rings as largest rings in the structure and allow diffusion of only small molecules (2.5-2.7 Å).⁸⁰

Finally, the structure that will be explored throughout this thesis is the Beta zeolite, which is formed by 12, 6, 5, and 4 membered rings and can allow diffusion of molecule with 6.5 Å of diameter (figure 15).⁸¹ Due to this channel size, open chain glucose molecules fits inside the BEA framework and allow its reaction to form valuable compounds. The Beta zeolite can be found in three different polymorphs: A, B and C. Following synthesis, different ratios of these polymorphs are usually found in the resulting material, and to date only polymorph C has been isolated in 100 % purity (zeolite BEC).^{81,82}

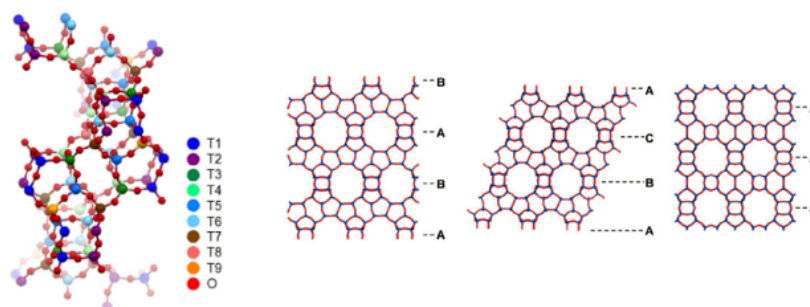


Figure 15. BEA zeolite framework structure with its related 9 T-sites shown and related polymorphs A, B and C.⁸²

These differences in porosity and accessibility of the zeolite structures are responsible for one of the most important properties of zeolites: shape selectivity. Shape selectivity is based upon the fact that only certain size of molecules can access the inner channels of the zeolites, and from these channels only molecules of particular size can diffuse out of them.^{74,77} The size of molecules that can diffuse through the framework is determined by the opening of the zeolite channel throughout its whole structure.

The shape selectivity of zeolites allows reactions which would not be otherwise energetically favoured to be performed, by creating a kinetic channel which the reactants cannot escape from. To best explain this phenomenon, the conversion of toluene by alkylation or disproportion by zeolite ZSM-5 is illustrated in figure 16. This reaction leads to the production of *para*-xylene which is widely exploited as precursor of terephthalic acid, the largely produced monomer for PET production (a light, flexible and resistant plastic material used in packaging of several products such as beverages).^{47,74,77}

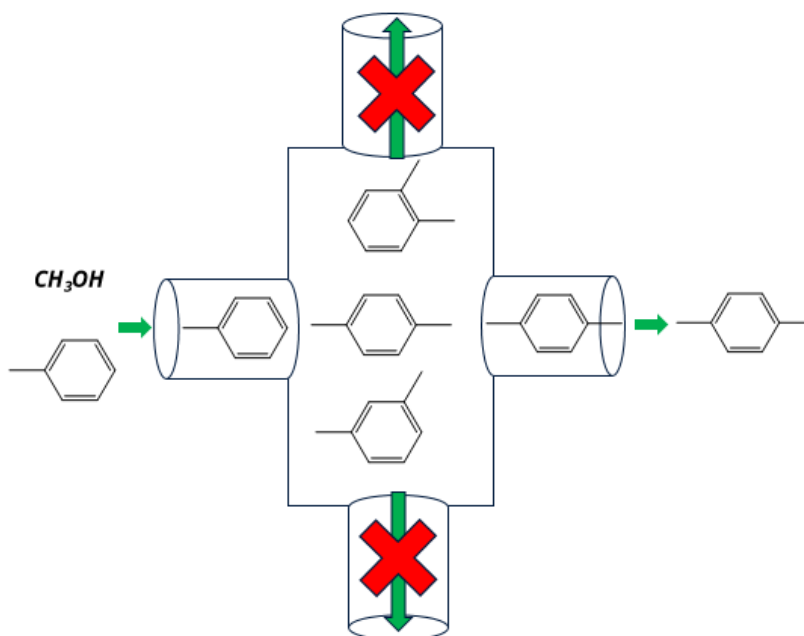


Figure 16. Schematic representation of toluene alkylation to *para*-xylene driven from shape selectivity by ZSM-5 zeolite.

As shown in figure 16, the substrate diffuses along the zeolite channels and reacts inside its structure. Here, although all the isomers can be formed, *meta*- and *ortho*-xylene cannot diffuse out of the zeolite framework. Accordingly, they further react until the *para*-isomer is synthesised. Only when *para*-xylene is formed can the yielding molecule diffuse out of the framework of the zeolite and, therefore, escape from the acid sites of the catalyst. Thanks to this constrain, *para*-xylene is preferred as product against the more energetic favoured *meta*-xylene.⁷⁷ The “shape selectivity” property can then be combined with the choice of different metals to incorporate in the framework of the material to open different reaction pathways and reactivities for this material.⁷⁴

1.11 Activity of metal-incorporated zeolites: Al-, Ti- and Sn-zeotypes.

As previously described, the properties of zeolites do not depend only from their structure and channels conformation, but also from the chemical functionality of the different metals that can be incorporated inside the structure.⁷⁴ Natural zeolites are mainly aluminosilicates, therefore, any atom a part from aluminium, oxygen and silicon present in the zeolitic structure is defined as heteroatom.⁸³ However, with the development of synthetic zeolites several other metals have successfully been incorporated into zeolites structures. Examples include the incorporation of Fe, B, Ga, Sn, Ti, Zr and Hf, amongst others.⁸⁴⁻⁸⁹

The incorporation of different metals generates zeolites with different properties depending on the size, oxidation state and electronegativity of the incorporated atoms. Although several kinds of zeolites with different metals were synthesised in the last decades, hereafter will be introduced examples of the most known and influential zeolites that have impacted the chemistry of important industrial processes.

Aluminium is naturally incorporated in zeolites, this atom forms tetrahedral units with oxygen $[\text{AlO}_4]^-$ which have an overall negative charge of -1, since the aluminium is on its own a trivalent atom with oxidation state +3 (figure 13). These units incorporated in the zeolite structure are surrounded by silicon tetrahedral units, $[\text{SiO}_4]$, which have neutral charge. As such, the entire material possesses a global negative charge. This negative charge is neutralised by external cations (NH_4^+ , H^+ , Na^+ , K^+). In most of the cases the cations are protons, which are responsible for the strong Brønsted acidity of aluminium-containing zeolites.⁹⁰ The external proton is in fact highly reactive and this reactivity is exploited in several processes in which zeolites are widely used nowadays. This tuneable level and strength of Brønsted acidity is the reason behind the widespread utilisation of zeolites in the petrochemical industry. Aluminium zeolites are now largely used in industry, one of their most important application is the Fluid Catalytic Cracking (FCC) of high boiling points, high molecular weight hydrocarbon fractions of crude oils into more valuable products.^{74,91} Aluminium is not the only trivalent atom incorporated in the zeolitic structure, but B-zeolite (boron), In-zeolites (Indium) and Ga-zeolites (gallium) are other examples of synthetic zeolite in which trivalent heteroatom were incorporated.^{83,85}

Titanium incorporated zeolite are also widespread in the chemical industry. The most famous zeolite known in this class of materials is TS-1 (titanium silicalite). TS-1 possesses an MFI structure in which atoms of titanium are isomorphously substituted in the framework. This material has been shown in various studies to possess excellent activity for various oxidation reactions, including the epoxidation of propylene to propylene oxide (figure 17). This compound is known to be an important intermediate molecule for the production of polyols, largely used in the production of polyurethane plastics.⁹² The partial oxidation of propylene catalysed by TS-1, discovered by ENI researchers between the 80's and the 90's, has resulted in several improvements relative to the existing state of the art including decreased water usage, improved selectivity, longer lifetime, diminished waste production

and avoiding chlorine as reaction intermediate, allowing a more economic sustainability of the process.⁹²

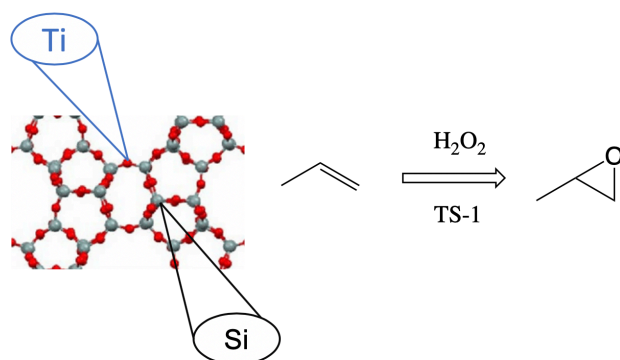


Figure 17. Propylene oxide synthesis catalysed by TS-1 in presence of hydrogen peroxide.

Titanium is in group IV of the periodic table, and within this group also lie Zr (zirconium) and Hf (hafnium). Although no industrial process is carried out from zeolites incorporated with these metals, their application in H-transfer reactions and aldol condensation reactions has shown interesting results.^{93,94}

Sn containing zeolites have gathered the interest of researchers in the last two decades following the discovery that Sn-Beta zeolites are highly active catalysts for the reduction of ketones to alcohols by Meerwein-Ponndorf-Verley reaction (MPV, figure 18)^{95,96} and the oxidation of ketones to esters^{97,98} (Baeyer Villiger Oxidation, BVO shown in figure 18). This catalyst shows high activity for these reactions due to the strong Lewis acidity of the Sn atom originated by the empty orbitals present in the 4d¹⁰ configuration of the Sn^(IV) site.^{99,100} These empty orbitals are able to coordinate the negative electron charge of the oxygen atoms of the carbonyl groups in the substrate molecules, activating the carbon for a nucleophilic attack.^{101,102}

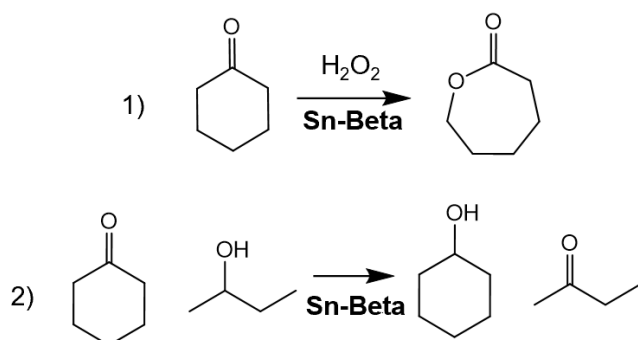


Figure 18. 1) BVO reaction of cyclohexanone to caprolactone catalysed by Sn-Beta. 2) MPV reaction of cyclohexanone to cyclohexanol with 2-butanol as H-donor catalysed by Sn-Beta.

A decade after the discovery of the capability of Sn-Beta to catalyse BVO and H-transfer reactions, this material was shown to be able to carry out glucose isomerisation to fructose,

the hexoses retro-aldol cleavage to dihydroxyacetone and glyceraldehyde and their transformation to methyl lactate.¹⁰³ Since these discoveries, several frameworks have been investigated as hosts in, but to date the best performances have been shown by Beta zeolite, and, therefore, this material will be the main topic of this section.

1.12 Glucose upgrading carried out by Sn-Beta zeolite

As previously mentioned, Sn-Beta zeolite proved to be an efficient catalyst for glucose upgrading. However, alongside the glucose transformation in fructose and lactates, this catalyst can promote a plethora of reactions which potentially lead to valuable products.^{103,104}

In figure 19 is reported a scheme of products and intermediates for glucose upgrading catalysed by Sn-Beta zeolite. The ratio and quantity of these products, and hence the overall selectivity of a particular process, may vary changing the conditions of reaction such as temperature, solvents and contaminants concentration in the reaction environment.^{104,105}

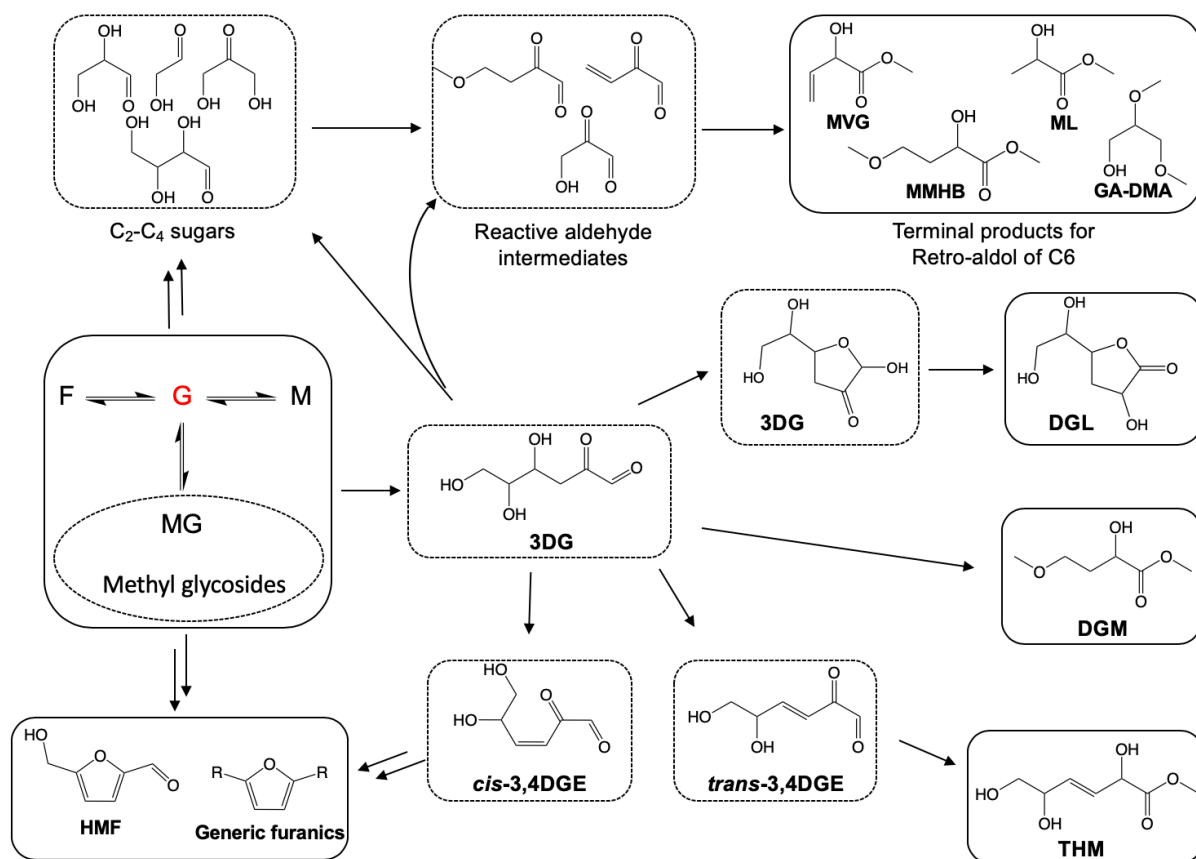


Figure 19. Different pathways in the conversion of glucose catalysed by Sn-Beta zeolite. (G = glucose, M = mannose, F = fructose).¹⁰⁴

The first reaction that Sn-Beta can perform is the isomerisation of glucose (G) to mannose (M) and fructose (F).⁷⁰⁻⁷² The isomerisation reaction of glucose catalysed by Sn-Beta takes place by intramolecular H-shift reaction. During this reaction, the carbonyl and the hydroxyl

group, respectively on the carbon in position 1 and on the carbon in position 2, are simultaneously coordinated to the Lewis acid Sn centre incorporated in the catalyst structure.¹⁰⁶ This coordination polarises the carbonyl atom, and, hence, facilitates the H-shift reaction of the hydride ion in C2 to the carbon in position 1, as shown in figure 20.⁷³

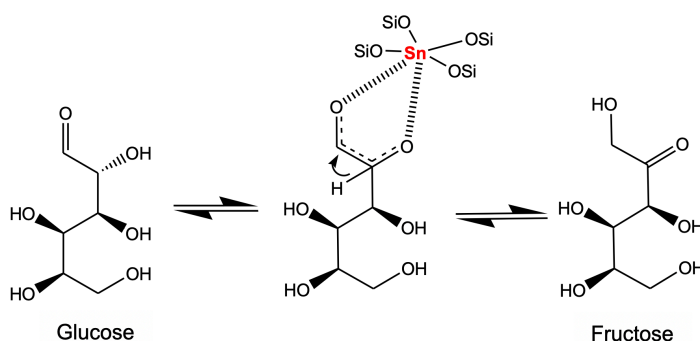


Figure 20. H-Shift reaction mechanism for glucose isomerisation to fructose carried out by Sn Beta zeolite.

In addition to isomerisation, glucose can also be converted to different end products by additional reaction pathways. The first one involves the retro-aldol cleavage of glucose to glycolaldehyde (GA) and erythrose (2+4 retro-aldol). In this pathway, erythrose is further converted to MVG by beta-dehydration of two molecules of water and by addition of methanol with subsequent H-transfer to the final product. Glycolaldehyde (GA) can also be converted to MVG via the aldol condensation of two molecules of glycolaldehyde to erythrose.^{103,104,107} The second pathway is the beta-dehydration of glucose to 3 deoxy-D-erythrosulose (3DG), which can be further converted to 5,6-dihydroxy-2-oxohex-3-enal (3,4-DGE). If this molecule is formed in *cis*-form it will further be converted to furanic compounds by the ring closure of *cis* 3,4-DGE. Alternatively, if the *trans*-form is produced then *trans*-3,4-DGE undergoes addition of methanol and intramolecular H-transfer to yield *trans*-2,5,6-trihydroxy-3-hexenoic methyl ester (THM) which is a terminal product. If methanol addition takes place before the dehydration of 3,4-DGE, 3DG is instead converted to 3-deoxy-gluconic methyl ester (3DGM) as terminal product.¹⁰⁴ Finally, 3DG can also undergo a retro-aldol reaction to glyceraldehyde and pyruvaldehyde (3+3 retro-aldol), which can then be transformed into ML by the same mechanism that governs the transformation of erythrose to MVG. In this manner, when glucose is isomerised to fructose by Sn-Beta, the retro-aldol fragmentation of fructose to glyceraldehyde and dihydroxyacetone occurs, and these products can be further converted to ML. Small quantities of furanic compounds can be formed as co-product of this reaction.¹⁰⁴ Furthermore, it is important to highlight how fructose and glucose may be converted to methyl gluco-pyranoside and methyl fructo-furanoside.^{104,108} These two methylated sugars can be formed in the presence of a Brønsted acid catalyst. The methylated form of glucose is highly stable, and it is therefore considered to be an undesired final product, whereas the methylated form of fructose is in equilibrium

with its free-form and this equilibrium can be exploited for shifting the glucose isomerisation reaction towards the ketose products.¹⁰⁸

Having now acquired an overview of the reactions that Sn-Beta is capable to carry out from glucose as substrate, it is possible to understand how this material presents a good activity for H-transfer reactions, retro-aldol reactions and retro Michael de-hydration. These reactions occur via a reaction intermediate in which the Sn strongly binds a hydroxyl and a carbonyl group of the substrate, confirming the capability of Sn to strongly attract electrons from these functional groups.¹⁰⁹

Due to the diverse activity that Sn-Beta possesses, the average selectivity towards fructose and methyl lactate of this material is not optimal per se due to the several by-products that can be formed. To overcome this challenge, Tolborg *at al.*^{104,105} recently showed how adding small quantities of alkali salts to the reaction mixture can enhance the selectivity of Sn-Beta towards methyl lactate at 160 °C. When the same alkali salts were employed at lower temperature (110 °C), Sn-Beta showed a high tendency to promote the epimerisation to mannose rather than the isomerisation reaction to fructose.¹¹⁰ G. Elliot *at al.*¹¹¹ showed how the alkali salts interact with the Sn sites of the catalyst by exchanging nearby protons. However, several alternative hypothesis on the role of alkali during the catalytic event have been made, and the scientific community is still divided on this matter. Although the impact of alkali salts helped in channelling the selectivity of this material, Sn-Beta is not yet fully selective towards production of industrially interesting α -hydroxy esters (MVG and ML) and the literature referring to these reactions is not taking into account the performance that this material might show in a continuous process.¹¹⁰⁻¹¹³ As previously explained (figure 12), the applicability of a catalyst in this system is essential for developing productive and economically efficient processes. Despite this, the ability of Sn-Beta to perform these reactions make Sn-Beta an ideal catalyst to start optimising the production of different kinds of α -hydroxy esters from glucose, which may open a wide range of industrial applications.

1.13 Zeolite synthesis and the case of Sn-Beta

Zeolite synthesis is not trivial and needs to be taken in consideration when evaluating the sustainability and applicability of a process that exploits zeolites as catalysts. The main hurdle in zeolite synthesis is to achieve the formation of a well-defined crystalline structure in which the reactants can diffuse and interact with the active sites present in the material. Therefore, zeolites synthesis usually involves periods of crystallisation that have different lengths depending on the nature of the desired material.¹¹⁴ This period can vary from few hours to even months, drastically changing the impact of the catalyst synthesis on the economy of a whole process.¹¹⁵ Different methodologies have been developed to synthesise zeolites in the attempt to find cheaper and sustainable synthetic procedures for this class of materials. The two approaches that are employed in zeolite synthesis are: *hydrothermal* and *post-synthetic* syntheses.¹¹⁴

The *hydrothermal* approach occurs via formation of a synthesis gel, which is composed by the silica source such as tetraethyl-ortho silicate (TEOS), the source of the heteroatom(s) to be crystallised within the zeolite, and an organic structure directing agent (OSDA),¹¹⁶ more commonly known as ‘template’. This compound is not always needed and steers the crystallisation of the structure towards the desired zeolite framework. Usually the OSDA for the BEA zeolite structure is tetraethylammonium hydroxide (TEAOH), whereas a chloride precursor is frequently used to insert tin as heteroatom (SnCl_4). This mixture is usually left stirring to reach the homogenisation of the final gel, or to let the ethanol or water evaporate to reach the required gel-composition. The composition of the gel is given in any catalyst recipe and it is the key to obtain the wanted material. This yielding mixture is then left to crystallise until formation of the desired structure (figure 21).¹¹⁷

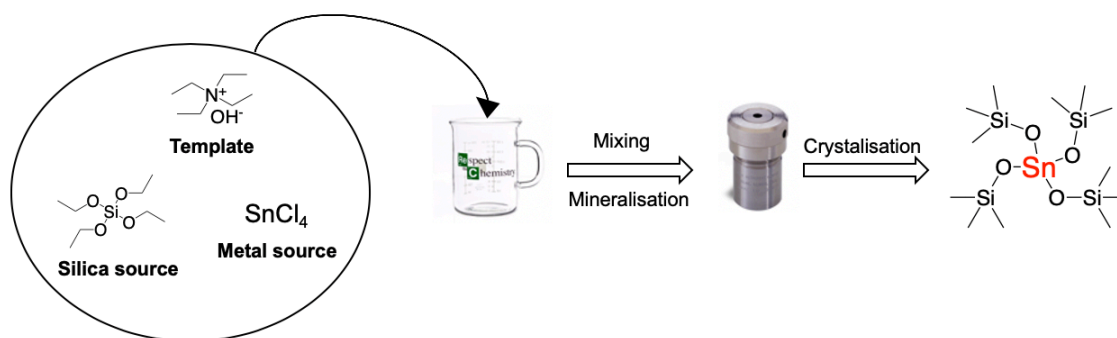


Figure 21. Generic scheme for hydrothermal synthesis of Sn-Beta zeolites.

The other process of synthesis of zeolites, the post-synthetic approach, employs the transformation of an already synthesised zeolite to obtain a different material (figure 22).¹¹⁸ Several kinds of methodologies have been developed in this area, the most common employs the dealumination of an aluminosilicate to create a material available for further metal-incorporation. During dealumination, aluminium atoms are extracted from a previously synthesised aluminosilicate by acid treatment.^{119,120} This treatment leaves defects in the structure (silanol nests) which can be later filled with a different metal through various methods of incorporation (impregnation, solid state incorporation, chemical vapour deposition).¹¹⁵

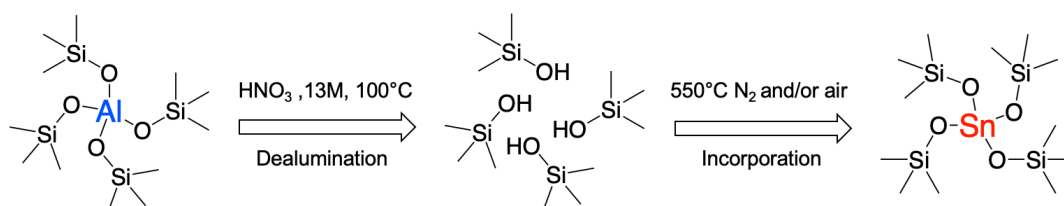


Figure 22. Example of post-synthetic synthesis of zeolites by acid stripping of aluminium to form silanol nests.

Usually this methodology is performed on aluminium zeolites whose hydrothermal synthesis is more feasible also at an industrial scale. However, processes for de-metalation have also been developed for others zeotypes as well. In fact, deboronation, degermanation and degallation processes are also feasible from the respective parent zeolites.^{84,121} Another important process included in the post-synthetic approaches is desilication. Desilication involves a basic treatment of the zeolite to strip out silica units from the frameworks, which results in the creation of larger defect sites and cavities.¹²² By this approach, mesoporosity (pores of dimension between 20 and 500 Å) can also be introduced in these zeolites, which are called “hierarchical zeolites” due to the combination of microporous and mesoporous cavities.¹²³ The alkaline treatment prevents the accumulation of organic material inside the zeolite framework during a common catalytic event, delaying therefore pore blockage, which is one of the main reasons of catalyst deactivation when working with zeolites.^{122,123} Sn-Beta zeolite was first synthesised via the hydrothermal approach mixing the silica source (tetraethyl-ortho silicate), the template and the tin source (SnCl₄).¹²⁴ In the original preparation method hydrofluoric acid (HF) was used as mineralising agent and long crystallisation times were required (70 days).^{100,102,117} Although interesting catalytic performances were exhibited by this material, the environmental impact of HF and unsustainable crystallisation times demanded for the development of a different route of synthesis. Nowadays, different methods of Sn-Beta synthesis have been explored, and this material can now be synthesised by several post synthetic approaches starting from Al-Beta zeolite.^{72,125-128} These processes usually involve dealumination in nitric acid (HNO₃) at elevated temperature (100 °C) and concentration (< 13 M) (figure 22).¹¹⁸ Following dealumination, the resulting dealuminated zeolite possesses silanol nests, which can be subsequently filled with tin using the appropriate precursor and methodology of incorporation. Several incorporation processes have been developed as the wet impregnation of tin chloride (SnCl₄) and the solid state incorporation of tin acetate.^{72,117}

1.14 Sn-Beta active site

The different preparations of Sn-Beta listed above result in the formation of catalysts with very different properties. For example, the hydrothermal preparation of Sn-Beta produces a catalyst that is hydrophobic and defect free, whereas generally the post-synthetic preparations lead to more hydrophilic and defective material.^{129,130} The performance of the catalyst (as will be shown in chapter 3 in detail) is highly dependent on the type of preparation of the catalyst, suggesting differences in the active site(s).^{129,130} However, until now, a difference in type of active sites has not been definitely proved between different Sn-Beta preparations. On one hand it is commonly accepted in the scientific community how Sn-Beta can possess two main types of active sites: “open” tin site and “closed” tin site, Boronat *et al.*¹³¹ first proposed this classification showing how in the “open” active site the Sn-O-Si bond is hydrolysed and, therefore, the “open” active site is composed by a

hydroxyl group bonded to the tin atom adjacent to a silanol group (figure 23). The “closed” tin site instead, is simply isomorphously substituted tin incorporated in the zeolite framework. As reported in the literature, these sites can be found in hydrated or in dehydrated form.^{132,133}

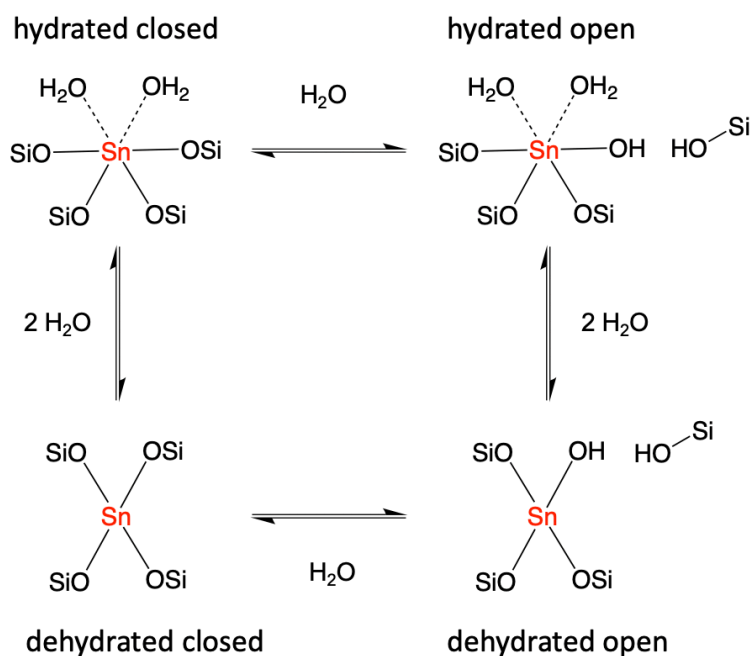


Figure 23. Scheme of different forms of Sn-Beta active site in equilibrium with water molecules.

To further validate the hypothesis of the existence of the “open” tin site several computational works have calculated the stability and activation energy of closed and open site. In particular, Li *at al.*¹³² showed how the open tin site in Sn-Beta, in comparison to its closed analogue, exhibits a lower activation barrier energy for glucose isomerisation to fructose due to the stabilising effect of the adjacent silanol on the oxygen bonded to the C2 of the glucose molecule. (figure 24)

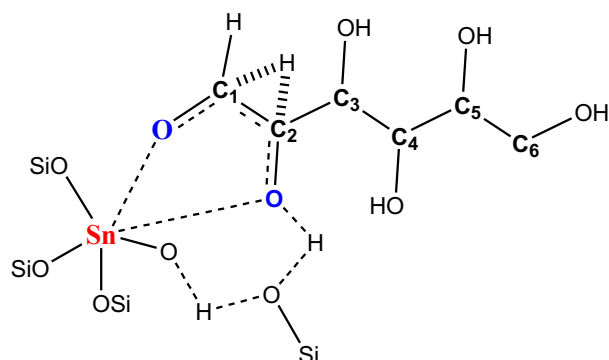


Figure 24. Stabilising effect of adjacent silanol groups on the C2 carbon atom of a glucose molecule in the open active site of Sn-Beta during glucose isomerisation to fructose.

Although the distinction between open and closed sites is commonly accepted, is also important to remember how these materials can strongly interact with the solvent in the

reaction environment or the moisture in the atmosphere, leading to possible modifications of the active sites which are yet to be fully comprehended.^{129,134,135} Therefore, more than a rigid distinction between these forms as immutable and stable over time, it would be more correct to think at them in a dynamic environment where they can actively interact with moisture and chemicals (figure 23), particularly during the reaction process itself. As such, conclusions made from previous theoretical and spectroscopic studies performed under 'ideal' reaction environments do not necessarily represent the real chemistry occurring in these complicated materials and processes.

1.15 Zeolite deactivation

Catalysts are usually evaluated by two important factors, which are activity and selectivity. The activity describes the number of moles of reactant that a material can convert in a precise unit of time and it is expressed in terms of turnover frequency (TOF).^{66,136} Needless to say, the higher the number, the better the performances of the material and therefore the higher its possibilities for use in industrial applications.

However, for an active material to be industrially interesting it must possess a good selectivity as well. The selectivity value expresses how much of the converted substrate yields the desired product. As such, the higher the selectivity, the higher is the quantity of the valuable product obtained per quantity of substrate converted.^{66,137} Although these features are essential to benchmark the performance of a catalyst, activity and selectivity alone do not give the complete picture for its evaluation. Alongside these features, the lifetime of a material must also be considered to have a clearer landscape of its performances.⁶⁶ To determine this value it is important to evaluate the stability of a catalyst. This can be defined as the time in which the catalyst can run with sufficient activity and selectivity.

Deactivation of zeolite (or a general catalyst) is the loss of activity or stability, which necessitates the regeneration or substitution of the catalyst. Deactivation of zeolites can take place by different processes, which can also be found in other types of catalysts, but for the scope of this manuscript only those of relevance to zeolite catalysts will be discussed. The deactivation of a catalyst can be permanent or not permanent. In the first case, the catalyst needs to be disposed of and its regeneration is not possible. Typical examples of permanent deactivation processes include amorphization of the catalyst or leaching of the active phase.¹³⁶⁻¹³⁹ In contrast, if a catalyst is not permanently deactivated, it can easily be regenerated. A classic example is the continuous regeneration of zeolites during FCC, in this process the coked zeolite exhausted is calcined to burn the organic material accumulated inside the pores during the reaction.^{82,136 140} The most common mechanisms of zeolite deactivation include:

- Fouling, which consists of the blockage of the zeolite pores by carbonaceous species leftover from the possible degradation of the substrate and/or various

reaction products. These compounds block the channels of the zeolite framework, inhibiting the diffusion of substrate throughout the material and, thus, decreasing the catalytic performance.^{122,137,139,140}

- Poisoning, by chemisorption of reactive species, which compromises the correct functioning of the catalyst.^{136,139,141}
- Sintering, which is the process leading to the thermodynamically driven growth of crystals. This process leads to a loss of surface area, reduction in density of active sites and, in some cases, collapse of the crystalline structure.^{136,139,142,143}
- Leaching of the active sites in the reaction environment. This is a mechanism of deactivation for the zeotypes whose heteroatoms might be easily leached from the structure in presence of high percentage of water or acid in the stream. This particular kind of deactivation does not only represent a problem for the stability of the catalyst, but the material leached from the structure is also a pollutant for the products of reaction.^{136,139,142,143}

Therefore, when approaching the study of the stability of a catalyst, it is essential to understand the mechanisms by which these catalysts deactivate so that strategies to overcome the deactivation of the material can be developed, therefore, increasing its stability and its lifetime.

1.16 Constant of deactivation from O. Levenspiel: Chemical Reaction Engineering.¹⁴⁴

In the previous paragraph the different causes of deactivation of a catalyst, and in particular of zeolites, were introduced. Although the understanding of the underlying phenomena is essential, more quantitative approaches can be exploited to evaluate different deactivation regimes. On this regard O. Levenspiel elaborated an approach to calculate the deactivation constant of a determined process, which is extensively explained in his well-known manuscript: "Chemical Reaction Engineering".

Levenspiel in his manuscript distinguished two different kinds of deactivation the *dependent deactivation*, which is influenced by the concentration of a chemical in the stream of reaction and *independent deactivation* which depends only by the time for which the catalyst is operating (i.e. sintering of the catalyst). These different kinds of deactivation can be expressed as a function of temperature of reaction, of the concentration and of the present state of the catalyst (equation 1 and 2).

$$\text{Deactivation Rate} = f(\text{Temp.}) \times f(\text{Conc.}) \times f(\text{state of cat.}) \quad \text{eq.(1)}$$

$$\frac{-da}{dt} = k_{d0} \cdot e^{-\frac{E_d}{RT}} \cdot C_i^m \cdot a^d \quad \text{eq. (2)}$$

Where a is considered the relative activity of the catalyst on its initial activity a_0 , d and m show respectively the order of deactivation and the concentration dependency and Ed is the temperature dependency of the deactivation.

This useful definition of the rate of deactivation shows already how assigning a value to the catalyst rate of deactivation is not trivial. The dependency from the concentration and the order of deactivation are needed for a complete evaluation of the phenomena.

The equations 1 and 2 are general equations to broadly describe the process of deactivation. However in paragraph 1.9 is extensively discussed how the use of a continuous set-up is needed to evaluate at best Sn-Beta deactivation in scalable conditions. Therefore the equation adapted to the PFR system (Plug Flow Reactor) can be used to evaluate the deactivation constant of the process studied in the manuscript (equation 3).

$$\ln \ln \left(\frac{C_{A0}}{C_A} \right) = \ln(k' \cdot \tau') - k_d \cdot t \quad \text{eq.(3)}$$

This equation implies an order of deactivation of 1 and no dependency from the concentration of the species. It is important to consider these approximations when applying this model. To simply apply equation 3 to the experiments carried out routinely is possible to reformulate the equation in:

$$\ln \ln \left(\frac{1}{1-X} \right) = -k_d \cdot t + \ln(k' \cdot \tau') \quad \text{eq.(4)}$$

Throughout this expression is possible to plot the function of the conversion (X) in the left hand side of the equation, as a function of the time on stream (t). The slope of the straight line resulting from the plotting of the data will be equal to the constant of deactivation of the catalyst (Figure 25).

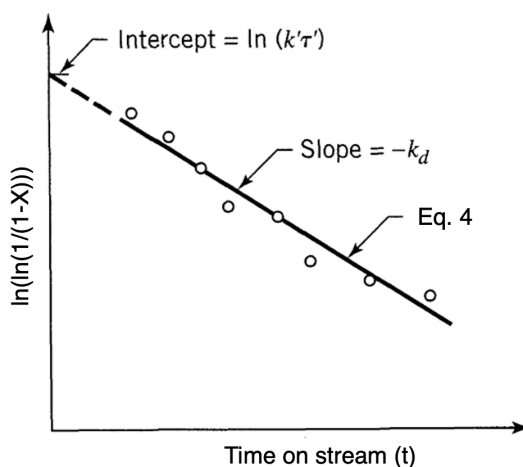


Figure 25. Levenspiel function for catalyst deactivation plotted as a function of the time on stream to identify the deactivation constant K_d .

This correlation will be used throughout the manuscript to evaluate the different deactivation constants related to the each system. For the application of these equations several assumptions need to be done and are herein reported:

- the process deactivation was assumed to be not-dependent from the concentration of chemicals in the system. This is fairly assumed since the primary reason for catalyst deactivation is due to its interaction with the solvent, which concentration can be assumed as constant.
- The order of deactivation was considered as one throughout all the manuscript, since this fitting was effectively carried out for Chapter 2 in which is explored the primary cause of catalyst deactivation.

a more thorough application of the Levenspiel equation is needed to extrapolate the order of the deactivation and the quantitative influence of secondary means of deactivation. Although these information are paramount for the optimisation of a large scale process, the aim of the project is to understand the main cause of catalyst deactivation and further evaluation of secondary deactivation mechanisms are not taken into account at this stage of the research.

Glucose upgrading by Sn-Beta zeolite, has been shown over recent years to yield to a vast number of interesting chemical commodities. Therefore, this catalyst could represent an important development in producing bio-based material from sugars, replacing fossil-feedstock derived polymers. Considering the enormous annual exploitation of plastic materials, the production of the related monomers from biomass must become large-scale processes, where the vast availability of the substrate can ensure continuous production of the desired commodities. These commodities have to be sold at a price comparable with the already existing products obtained by fossil feedstock in order to be competitive on the real market. As such, this type of process needs to be carried out in continuous conditions to ensure economic feasibility of this route of biomass upgrading. Unfortunately, lack of knowledge in this complicated area is strongly affecting the possible industrialisation of Sn-Beta; in fact, at the start of the project (January 2017), no data was available on the performance of Sn-Beta for continuous glucose upgrading.

Therefore, during the course of my PhD project, I intended to explore the performance of Sn-Beta during continuous operation. Data on the stability and selectivity of the material during long operational times are necessary to understand whether Sn-Beta could one day be employed as suitable catalyst for continuous operations. Throughout the project were explored also multiple preparations of Sn-Beta zeolite: hydrothermal and post-synthetic (figure 21 and 22). Thus, the impact of these different protocols of synthesis on the lifetime of the material was evaluated. In this way, I aimed to understand which preparation yields the best performing catalyst during continuous operations. Sn-Beta has also shown a broad reactivity, catalysing the formation of several products from glucose (HMF, α -hydroxy esters and fructose) alongside some unwanted by-products (figure 19). Although this may be scientifically interesting, it is essential to address the selectivity of this material towards the right products to ensure best valorisation of the substrate. Therefore, efforts in the project were pointed towards identifying new conditions and/or catalytic materials, to channel the selectivity of the process towards the desired products.

1.18 Reference

- (1) Hileman, B. Ice Core Record Extended. *Chem. Eng. News Arch.* **2005**, 83 (48), 7.
- (2) IPCC AR5 WG1 (2013), Stocker, T.F.; et al. (eds.), *Climate Change 2013: The Physical Science Basis. Working Group 1 (WG1) Contribution to the Intergovernmental Panel on Climate Change (IPCC) 5th Assessment Report (AR5)*, Cambridge University Press Climate Change 2013 Working Group 1 website
- (3) Nordhaus, W. Erratum: Critical Assumptions in the Stern Review on Climate Change. *Science.* **2007**, 317 (5845), 1682.
- (4) Vennestrøm, P. N. R.; Osmundsen, C. M.; Christensen, C. H.; Taarning, E. Beyond Petrochemicals: The Renewable Chemicals Industry. *Angew. Chemie Int. Ed.* **2011**, 50 (45), 10502–10509.
- (5) Wang, Y. Catalytic Fast Pyrolysis of Lignocellulosic Biomass. **2014**, 43 (22).
- (6) Liu, C.; Wang, H.; Karim, A. M.; Sun, J.; Wang, Y. Catalytic Fast Pyrolysis of Lignocellulosic Biomass. *Chem. Soc. Rev.* **2014**, 43 (22), 7594–7623.
- (7) Matas Güell, B.; Sandquist, J.; Sørum, L. Gasification of Biomass to Second Generation Biofuels: A Review. *J. Energy Resour. Technol.* **2013**, 135 (1), 1007.
- (8) Tuck, C. O. Valorization of Biomass: Deriving More Value from Waste *Science.* **2012**, 338 (6107), 604.
- (9) Liu, C.; Wang, H.; Karim, A. M.; Sun, J.; Wang, Y. Catalytic Fast Pyrolysis of Lignocellulosic Biomass. *Chem. Soc. Rev.* **2014**, 43 (22), 7594–7623.
- (10) Bordonal, R. de O.; Carvalho, J. L. N.; Lal, R.; de Figueiredo, E. B.; de Oliveira, B. G.; La Scala, N. Sustainability of Sugarcane Production in Brazil. A Review. *Agron. Sustain. Dev.* **2018**, 38 (2).
- (11) Soimakallio, S.; Koponen, K. How to Ensure Greenhouse Gas Emission Reductions by Increasing the Use of Biofuels? - Suitability of the European Union Sustainability Criteria. *Biomass and Bioenergy* **2011**, 35 (8), 3504–3513.
- (12) Zhang, Z.; Donaldson, A. A.; Ma, X. Advancements and Future Directions in Enzyme Technology for Biomass Conversion. *Biotechnol. Adv.* **2012**, 30 (4), 913–919.
- (13) Farmer, T. J.; Comerford, J. W.; Pellis, A.; Robert, T. Post-Polymerization Modification of Bio-Based Polymers: Maximizing the High Functionality of Polymers Derived from Biomass. *Polym. Int.* **2018**, 67 (7), 775–789.
- (14) Sølvhøj, A.; Taarning, E.; Madsen, R. Methyl Vinyl Glycolate as a Diverse Platform Molecule. *Green Chem.* **2016**, 18 (20), 5448–5455.
- (15) Huber, G. W.; Iborra, S.; Corma, A. Synthesis of Transportation Fuels from Biomass: Chemistry, Catalysts, and Engineering. *Chem. Rev.* **2006**, 106 (9), 4044–4098.
- (16) Taylor, G. Biofuels and the Biorefinery Concept. *Energy Policy* **2008**, 36 (12), 4406–4409.
- (17) Chheda, J. N.; Huber, G. W.; Dumesic, J. A. Liquid-Phase Catalytic Processing of Biomass-Derived Oxygenated Hydrocarbons to Fuels and Chemicals. *Angew. Chemie - Int. Ed.* **2007**, 46 (38), 7164–7183.
- (18) Kohli, K.; Prajapati, R.; Sharma, B. K. Bio-Based Chemicals from Renewable Biomass for Integrated Biorefineries. *Energies* **2019**, 12 (2)
- (19) Clark, J. H.; Luque, R.; Matharu, A. S. Green Chemistry, Biofuels, and Biorefinery. *Annu. Rev. Chem. Biomol. Eng.* **2012**, 3 (1), 183–207.

- (20) Geyer, R.; Jambeck, J. R.; Law, K. L. Production, Use, and Fate of AllPlastics Ever Made. *Sci. Adv.* **2017**, *3* (7), 25–29.
- (21) Sheldon, R. A. Green and Sustainable Manufacture of Chemicals from Biomass: State of the Art. *Green Chem.* **2014**, *16* (3), 950–963.
- (22) Zheng, J.; Suh, S. Strategies to Reduce the Global Carbon Footprint of Plastics. *Nat. Clim. Chang.* **2019**, *9* (5), 374–378.
- (23) Hillmyer, M. The promise of plastic from plant. *Science.* **2016**, *351* (6278), 1154–1155.
- (24) Collard, F. X.; Blin, J. A Review on Pyrolysis of Biomass Constituents: Mechanisms and Composition of the Products Obtained from the Conversion of Cellulose, Hemicelluloses and Lignin. *Renew. Sustain. Energy Rev.* **2014**, *38*, 594–608.
- (25) Delidovich, I.; Leonhard, K.; Palkovits, R. Cellulose and Hemicellulose Valorisation: An Integrated Challenge of Catalysis and Reaction Engineering. *Energy Environ. Sci.* **2014**, *7* (9), 2803.
- (26) Collard, F. X.; Blin, J. A Review on Pyrolysis of Biomass Constituents: Mechanisms and Composition of the Products Obtained from the Conversion of Cellulose, Hemicelluloses and Lignin. *Renew. Sustain. Energy Rev.* **2014**, *38*, 594–608
- (27) Ponnusamy, V. K.; Nguyen, D. D.; Dharmaraja, J.; Shobana, S.; Banu, J. R.; Saratale, R. G.; Chang, S. W.; Kumar, G. A Review on Lignin Structure, Pretreatments, Fermentation Reactions and Biorefinery Potential. *Bioresour. Technol.* **2019**, *271* (August), 462–472.
- (28) Ennaert, T.; Van Aelst, J.; Dijkmans, J.; De Clercq, R.; Schutyser, W.; Dusselier, M.; Verboeckend, D.; Sels, B. F. Potential and Challenges of Zeolite Chemistry in the Catalytic Conversion of Biomass. *Chem. Soc. Rev.* **2016**, *45* (3), 584–611.
- (29) Yadav, M.; Goswami, P.; Paritosh, K.; Kumar, M.; Pareek, N.; Vivekanand, V. Seafood Waste: A Source for Preparation of Commercially Employable Chitin/Chitosan Materials. *Bioresour. Bioprocess.* **2019**, *6* (1).
- (30) Sanders, J.; Scott, E.; Weusthuis, R.; Mooibroek, H. Bio-Refinery as the Bio-Inspired Process to Bulk Chemicals. *Macromol. Biosci.* **2007**, *7* (2), 105–117.
- (31) Osmundsen, C. M.; Egeblad, K.; Taarning, E. *Trends and Challenges in Catalytic Biomass Conversion*; Elsevier B.V., 2013.
- (32) Alvira, P.; Tomás-Pejó, E.; Ballesteros, M.; Negro, M. J. Pretreatment Technologies for an Efficient Bioethanol Production Process Based on Enzymatic Hydrolysis: A Review. *Bioresour. Technol.* **2010**, *101* (13), 4851–4861.
- (33) Bridgwater, A. V. Review of Fast Pyrolysis of Biomass and Product Upgrading. *Biomass and Bioenergy* **2012**, *38*, 68–94
- (34) Alonso, D. M.; Bond, J. Q.; Dumesic, J. A. Catalytic Conversion of Biomass to Biofuels. *Green Chem.* **2010**, *12* (9), 1493–1513.
- (35) Lin, X.; Wu, Z.; Zhang, C.; Liu, S.; Nie, S. Enzymatic Pulp of Lignocellulosic Biomass. *Ind. Crops Prod.* **2018**, *120* (April), 16–24.
- (36) Song, H.; Lee, S. Y. Production of Succinic Acid by Bacterial Fermentation. *Enzyme Microb. Technol.* **2006**, *39* (3), 352–361.
- (37) Baruah, R.; Dixit, M.; Basarkar, P.; Parikh, D.; Bhargav, A. Advances in Ethanol Autothermal Reforming. *Renew. Sustain. Energy Rev.* **2015**, *51* (August), 1345–1353.
- (38) Cherubini, F. The Biorefinery Concept: Using Biomass Instead of Oil for Producing Energy and Chemicals. *Energy Convers. Manag.* **2010**, *51* (7), 1412–1421.

- (39) Wang, J.; Zhang, M.; Chen, M.; Min, F.; Zhang, S.; Ren, Z.; Yan, Y. Catalytic Effects of Six Inorganic Compounds on Pyrolysis of Three Kinds of Biomass. *Thermochim. Acta* **2006**, *444* (1), 110–114.
- (40) Christoph, R.; Schmidt, B.; Steinberner, U.; Dilla, W.; Karinen, R. Furfural and Derivatives. *Ullmann's Encycl. Ind. Chem.* **1998**, *16*, 67–82.
- (41) Hudson, C. S.; Dale, J. K. Studies on the Forms of D-Glucose and Their Mutarotation. *J. Am. Chem. Soc.* **1917**, *39* (2), 320–328.
- (42) Herbst, A.; Janiak, C. MOF Catalysts in Biomass Upgrading towards Value-Added Fine Chemicals. *CrystEngComm* **2017**, *19* (29), 4092–4117.
- (43) Liu, Z.; Li, W.; Pan, C.; Chen, P.; Lou, H.; Zheng, X. Conversion of Biomass-Derived Carbohydrates to Methyl Lactate Using Solid Base Catalysts. *Catal. Commun.* **2011**, *15* (1), 82–87.
- (44) Kuster, B. F. M. 5-Hydroxymethylfurfural (HMF). A Review Focussing on Its Manufacture. *Starch - Stärke* **1990**, *42* (8), 314–321.
- (45) Assary, R. S.; Kim, T.; Low, J. J.; Greeley, J.; Curtiss, L. A. Glucose and Fructose to Platform Chemicals: Understanding the Thermodynamic Landscapes of Acid-Catalysed Reactions Using High-Level Ab Initio Methods. *Phys. Chem. Chem. Phys.* **2012**, *14* (48), 16603–16611.
- (46) Yang, G.; Pidko, E. A.; Hensen, E. J. M. Mechanism of Bronsted Acid-Catalyzed Conversion of Carbohydrates. *J. Catal.* **2012**, *295*, 122–132.
- (47) Eerhart, A. J. J. E.; Faaij, A. P. C.; Patel, M. K. Replacing Fossil Based PET with Biobased PEF; Process Analysis, Energy and GHG Balance. *Energy Environ. Sci.* **2012**, *5* (4), 6407–6422.
- (48) Groeger, H. ChemInform Abstract: Enzymatic Routes to Enantiomerically Pure Aromatic α -Hydroxy Carboxylic Acids: A Further Example for the Diversity of Biocatalysis. *ChemInform* **2010**, *32* (49), no-no.
- (49) Li, H.; Yang, S.; Saravanamurugan, S.; Riisager, A. Glucose Isomerization by Enzymes and Chemo-Catalysts: Status and Current Advances. *ACS Catal.* **2017**, *7* (4), 3010–3029.
- (50) Dehkordi, A. M.; Tehrany, M. S.; Safari, I. Kinetics of Glucose Isomerization to Fructose by Immobilized Glucose Isomerase (Sweetzyme IT). *Ind. Eng. Chem. Res.* **2009**, *48* (7), 3271–3278.
- (51) Son, P. A.; Nishimura, S.; Ebitani, K. Preparation of Zirconium Carbonate as Water-Tolerant Solid Base Catalyst for Glucose Isomerization and One-Pot Synthesis of Levulinic Acid with Solid Acid Catalyst. *React. Kinet. Mech. Catal.* **2014**, *111* (1), 183–197.
- (52) Takasaki, Y. Kinetic and Equilibrium Studies on D-Glucose-d-Fructose Isomerization Catalyzed by Glucose Isomerase from *Streptomyces* Sp. *Agric. Biol. Chem.* **1967**, *31* (3), 309–313.
- (53) ¹ Tewari, Y. B.; Steckler, D. K.; Goldberg, R. N. Thermodynamics of Isomerization Reactions Involving Sugar Phosphates. *J. Biol. Chem.* **1988**, *263* (8), 3664–3669.
- (54) Souza, R. O. L.; Fabiano, D. P.; Feche, C.; Rataboul, F.; Cardoso, D.; Essayem, N. Glucose-Fructose Isomerisation Promoted by Basic Hybrid Catalysts. *Catal. Today* **2012**, *195* (1), 114–119.
- (55) Choudhary, V.; Pinar, A. B.; Lobo, R. F.; Vlachos, D. G.; Sandler, S. I. Comparison of Homogeneous and Heterogeneous Catalysts for Glucose-to-Fructose Isomerization in Aqueous Media. *ChemSusChem* **2013**, *6* (12), 2369–2376.
- (56) Camacho-Rubio, F.; Jurado-Alameda, E.; González-Tello, P.; Luzón-González, G. Kinetic Study of Fructose-glucose Isomerization in a Recirculation Reactor. *Can. J. Chem. Eng.* **1995**, *73* (6), 935–940.
- (57) Delidovich, I.; Palkovits, R. Catalytic Isomerization of Biomass-Derived Aldoses: A Review. *ChemSusChem* **2016**, *9* (6), 547–561.

- (58) Zhang, N.; Meng, X. G.; Wu, Y. Y.; Song, H. J.; Huang, H.; Wang, F.; Lv, J. Highly Selective Isomerization of Glucose into Fructose Catalyzed by a Mimic Glucose Isomerase. *ChemCatChem* **2019**, *11* (9), 2355–2361.
- (59) Parker, K.; Salas, M.; Nwosu, V. C. High Fructose Corn Syrup : Production , Uses and Public Health Concerns. **2010**, *5*, 71–78.
- (60) Ciriminna, R.; Pagliaro, M. Biodegradable and Compostable Plastics: A Critical Perspective on the Dawn of Their Global Adoption. *ChemistryOpen* **2020**, *9* (1), 8–13.
- (61) Tosi, I.; Elliot, S. G.; Jessen, B. M.; Riisager, A.; Taarning, E.; Meier, S. Uncharted Pathways for CrCl₃ Catalyzed Glucose Conversion in Aqueous Solution. *Top. Catal.* **2019**, *62* (7–11), 669–677.
- (62) Marianou, A. A.; Michailof, C. M.; Pineda, A.; Iliopoulou, E. F.; Triantafyllidis, K. S.; Lappas, A. A. Glucose to Fructose Isomerization in Aqueous Media over Homogeneous and Heterogeneous Catalysts. *ChemCatChem* **2016**, *8* (6), 1100–1110.
- (63) Corma, A.; Garci, H. Lewis Acids : From Conventional Homogeneous to Green Homogeneous and Heterogeneous Catalysis. **2003**.
- (64) Coperet, C.; Chabanas, M.; Saint-Arroman, R. P.; Basset, J.-M. Homogeneous and Heterogeneous Catalysis: Bridging the Gap Through Surface Organometallic Chemistry. *ChemInform*. **2003**.
- (65) Macario, A.; Giordano, G.; Onida, B.; Cocina, D.; Tagarelli, A.; Giuffrè, A. M. Biodiesel Production Process by Homogeneous/Heterogeneous Catalytic System Using an Acid-Base Catalyst. *Appl. Catal. A Gen.* **2010**, *378* (2), 160–168.
- (66) Costandy, J. G.; Edgar, T. F.; Baldea, M. Switching from Batch to Continuous Reactors Is a Trajectory Optimization Problem. *Ind. Eng. Chem. Res.* **2019**, *58* (30), 13718–13736.
- (67) Hartman, R. L.; McMullen, J. P.; Jensen, K. F. Deciding Whether to Go with the Flow: Evaluating the Merits of Flow Reactors for Synthesis. *Angew. Chemie - Int. Ed.* **2011**, *50* (33), 7502–7519.
- (68) Hammond, C. Intensification Studies of Heterogeneous Catalysts: Probing and Overcoming Catalyst Deactivation during Liquid Phase Operation. *Green Chem.* **2017**, *19* (12), 2711–2728.
- (69) Oshima, Y.; Bijanto, B.; Koda, S. PFR and CSTR Analyses of Supercritical Water Oxidation of Methanol. *J. Chem. Eng. Japan* **2000**, *33* (3), 507–513.
- (70) Moliner-Marín, M.; Roman-Leshkov, Y.; Davis, M. E.; Nikolla, E. Isomerisation of glucose to fructose by means of Lewis acid-zeolite catalysts. **2011**, *2* (19), 1–23. EP3067362A1
- (71) Moliner, M.; Román-Leshkov, Y.; Davis, M. E. Tin-Containing Zeolites Are Highly Active Catalysts for the Isomerization of Glucose in Water. *Proc. Natl. Acad. Sci. U. S. A.* **2010**, *107* (14), 6164–6168.
- (72) Dijkmans, J.; Gabriels, D.; Dusselier, M.; de Clippel, F.; Vanelderen, P.; Houthoofd, K.; Malfliet, A.; Pontikes, Y.; Sels, B. F. Productive Sugar Isomerization with Highly Active Sn in Dealuminated Beta Zeolites. *Green Chem.* **2013**, *15*, 2777–2785.
- (73) Román-Leshkov, Y.; Moliner, M.; Labinger, J. A.; Davis, M. E. Mechanism of Glucose Isomerization Using a Solid Lewis Acid Catalyst in Water. *Angew. Chemie - Int. Ed.* **2010**, *49* (47), 8954–8957.
- (74) Auerback, S.M.; Carrado, K. A. & Dutta, P. K. Handbook of Zeolite science and technology. (CRO,**2003**)

- (75) Pérez-Pariente, J.; Sanz, J.; Fornés, V.; Corma, A. 298i and 27A1 MAS NMR Study of Zeolite / 3 with Different Si / Al Ratios 29Si Spectra. *J. Catal.* **1990**, *124*, 217–223.
- (76) The International Zeolite Association available at <http://www.iza-online.org>
- (77) Liu, J.; Yang, Y.; Wei, S.; Shen, W.; Rakovitis, N.; Li, J. Intensified p -Xylene Production Process through Toluene and Methanol Alkylation. *Ind. Eng. Chem. Res.* **2018**, *57* (38), 12829–12841.
- (78) Scherzer, J. Catalysis Reviews: Science and Engineering FCC Catalysts : Scientific and Technical Aspects. *Catal. Rev. - Sci. Eng.* **1989**, *31* (3), 215–354
- (79) Liu, B.; Chen, F.; Zheng, L.; Ge, J.; Xi, H.; Qian, Y. Synthesis and Structural Properties of Hierarchically Structured Aluminosilicates with Zeolite γ (FAU) Frameworks. *RSC Adv.* **2013**, *3* (35), 15075–15084.
- (80) Anurova, N. A.; Blatov, V. A.; Ilyushin, G. D.; Proserpio, D. M. Natural Tilings for Zeolite-Type Frameworks. *J. Phys. Chem. C* **2010**, *114* (22), 10160–10170.
- (81) The International Zeolite Association available at <http://www.iza-online.org> /IZA-SC/framework.php?STC=BEA
- (82) Cantín, Á.; Corma, A.; Díaz-Cabañas, M. J.; Jordá, J. L.; Moliner, M.; Rey, F. Synthesis and Characterization of the All-Silica Pure Polymorph C and an Enriched Polymorph B Intergrowth of Zeolite Beta. *Angew. Chemie - Int. Ed.* **2006**, *45* (47), 8013–8015.
- (83) Vogt, E. T. C.; Weckhuysen, B. M. Fluid Catalytic Cracking: Recent Developments on the Grand Old Lady of Zeolite Catalysis. *Chem. Soc. Rev.* **2015**, *44* (20), 7342–7370
- (84) Fricke, R.; Kosslick, H.; Lischke, G.; Richter, M. Incorporation of Gallium into Zeolites: Syntheses, Properties and Catalytic Application. *Chem. Rev.* **2000**, *100* (6), 2303–2405.
- (85) Hammond, C.; Forde, M. M.; Ab Rahim, M. H.; Thetford, A.; He, Q.; Jenkins, R. L.; Dimitratos, N.; Lopez-Sanchez, J. A.; Dummer, N. F.; Murphy, D. M.; et al. Direct Catalytic Conversion of Methane to Methanol in an Aqueous Medium by Using Copper-Promoted Fe-ZSM-5. *Angew. Chemie - Int. Ed.* **2012**, *51* (21), 5129–5133
- (86) Guo, Q.; Fan, F.; Pidko, E. A.; Van Der Graaff, W. N. P.; Feng, Z.; Li, C.; Hensen, E. J. M. Highly Active and Recyclable Sn-MWW Zeolite Catalyst for Sugar Conversion to Methyl Lactate and Lactic Acid. *ChemSusChem* **2013**, *6* (8), 1352–1356.
- (87) Kots, P. A.; Zabilska, A. V.; Ivanova, I. I. Selective Self-Condensation of Butanal over Zr-BEA Zeolites. *ChemCatChem* **2020**, *12* (1), 248–258.
- (88) Tang, B.; Li, S.; Song, W. C.; Yang, E. C.; Zhao, X. J.; Guan, N.; Li, L. Hierarchical FAU-Type Hafnosilicate Zeolite as a Robust Lewis Acid Catalyst for Catalytic Transfer Hydrogenation. *ACS Sustain. Chem. Eng.* **2019**, *7* (19), 16329–16343.
- (89) Cavani, F.; Teles, J. H. Sustainability in Catalytic Oxidation: An Alternative Approach or a Structural Evolution? *ChemSusChem* **2009**, *2* (6), 508–534.
- (90) Derouane, E. G.; Védrine, J. C.; Ramos Pinto, R.; Borges, P. M.; Costa, L.; Lemos, M. A. N. D. A.; Lemos, F.; Ramôa Ribeiro, F. The Acidity of Zeolites: Concepts, Measurements and Relation to Catalysis: A Review on Experimental and Theoretical Methods for the Study of Zeolite Acidity. *Catal. Rev. - Sci. Eng.* **2013**, *55* (4), 454–515
- (91) Vogt, E. T. C.; Weckhuysen, B. M. Fluid Catalytic Cracking: Recent Developments on the Grand Old Lady of Zeolite Catalysis. *Chem. Soc. Rev.* **2015**, *44* (20), 7342–7370.

- (92) Guo, Q.; Sun, K.; Feng, Z.; Li, G.; Guo, M.; Fan, F.; Li, C. A Thorough Investigation of the Active Titanium Species in TS-1 Zeolite by in Situ UV Resonance Raman Spectroscopy. *Chem. - A Eur. J.* **2012**, *18* (43), 13854–13860.
- (93) Lewis, J. D.; Van De Vyver, S.; Crisci, A. J.; Gunther, W. R.; Michaelis, V. K.; Griffin, R. G.; Román-Leshkov, Y. A Continuous Flow Strategy for the Coupled Transfer Hydrogenation and Etherification of 5-(Hydroxymethyl)Furfural Using Lewis Acid Zeolites. *ChemSusChem* **2014**, *7* (8), 2255–2265.
- (94) Koehle, M.; Lobo, R. F. Lewis acidic zeolite Beta catalyst for the Meerwein–Ponndorf–Verley reduction of furfural. *Cat. Sci. & Tech.* **2016**, 3018–3026.
- (95) Canos, A. C.; Valencia, V.; Us, I. L.; Domine, M. E.; Es, V. United States Patent. **2001**, 1 (12).
- (96) Corma, A.; Domine, M. E.; Nemeth, L.; Valencia, S. Al-Free Sn-Beta Zeolite as a Catalyst for the Selective Reduction of Carbonyl Compounds (Meerwein-Ponndorf-Verley Reaction). *J. Am. Chem. Soc.* **2002**, *124* (13), 3194–3195.
- (97) Corma, A.; Nemeth, L. T.; Renz, M.; Moscoso, G. J. Oxidation of ketones to esters using a tin substituted zeolite beta **2002**, *1* (12), 1–6. US6344583B1
- (98) Corma, A.; Nemeth, L. T.; Renz, M.; Valencia, S. Sn-Zeolite Beta as a Heterogeneous Chemoselective Catalyst for Baeyer-Villiger Oxidations. *Nature* **2001**, *412* (6845), 423–425.
- (99) Paniagua, M.; Morales, G.; Melero, J. A.; Iglesias, J.; López-Aguado, C.; Vidal, N.; Mariscal, R.; López-Granados, M.; Martínez-Salazar, I. Understanding the Role of Al/Zr Ratio in Zr-Al-Beta Zeolite: Towards the One-Pot Production of GVL from Glucose. *Catal. Today* **2020**, No. December 2019, 1–11.
- (100) Boronat, M.; Corma, A.; Renz, M. Mechanism of the Meerwein-Ponndorf-Verley-Oppenauer (MPVO) Redox Equilibrium on Sn- and Zr-Beta Zeolite Catalysts. *J. Phys. Chem. B* **2006**, *110* (42), 21168–21174.
- (101) Román-Leshkov, Y.; Davis, M. E. Activation of Carbonyl-Containing Molecules with Solid Lewis Acids in Aqueous Media. *ACS Catal.* **2011**, *1* (11), 1566–1580.
- (102) Shetty, S.; Pal, S.; Kanhere, D. G.; Goursot, A. Structural, Electronic, and Bonding Properties of Zeolite Sn-Beta: A Periodic Density Functional Theory Study. *Chem. - A Eur. J.* **2005**, *12* (2), 518–523.
- (103) Holm, M. S.; Saravanamurugan, S.; Taarning, E. Conversion of Sugars to Lactic Acid Derivatives Using Heterogeneous Zeotype Catalysts. *Science* **2010**, *328* (5978), 602–605.
- (104) Tolborg, S.; Meier, S.; Sádaba, I.; Elliot, S. G.; Kristensen, S. K.; Saravanamurugan, S.; Riisager, A.; Fristrup, P.; Skrydstrup, T.; Taarning, E. Tin-Containing Silicates: Identification of a Glycolytic Pathway via 3-Deoxyglucosone. *Green Chem.* **2016**, *18* (11), 3360–3369.
- (105) Tolborg, S.; Sádaba, I.; Osmundsen, C. M.; Fristrup, P.; Holm, M. S.; Taarning, E. Tin-Containing Silicates: Alkali Salts Improve Methyl Lactate Yield from Sugars. **2015**, No. MI, 613–617.
- (106) Yang, G.; Pidko, E. A.; Hensen, E. J. M. The Mechanism of Glucose Isomerization to Fructose over Sn-BEA Zeolite: A Periodic Density Functional Theory Study. *ChemSusChem* **2013**, *6* (9), 1688–1696.
- (107) Dusselier, M.; De Clercq, R.; Cornelis, R.; Sels, B. F. Tin Triflate-Catalyzed Conversion of Cellulose to Valuable (α -Hydroxy-) Esters. *Catal. Today* **2017**, *279*, 339–344.

- (108) Shunmugavel, S.; Tosi, I.; Rasmussen, K.; Jensen, R.; Taarning, E.; Meier, S.; Riisager, A. Facile and Benign Conversion of Sucrose to Fructose Using Zeolites with Balanced Brønsted and Lewis Acidity. *Catal. Sci. Technol.* **2017**, *7*, 2782–2788.
- (109) Dusselier, M.; VanWouwe, P.; deClippel, F.; Dijkmans, J.; Gammon, D. W.; Sels, B. F. Mechanistic Insight into the Conversion of Tetrose Sugars to Novel α -Hydroxy Acid Platform Molecules. *ChemCatChem* **2013**, *5* (2), 569–575
- (110) Bermejo-Deval, R.; Orazov, M.; Gounder, R.; Hwang, S. J.; Davis, M. E. Active Sites in Sn-Beta for Glucose Isomerization to Fructose and Epimerization to Mannose. *ACS Catal.* **2014**, *4* (7), 2288–2297.
- (111) Elliot, S. G.; Tosi, I.; Meier, S.; Martinez-Espin, J. S.; Tolborg, S.; Taarning, E. Stoichiometric Active Site Modification Observed by Alkali Ion Titrations of Sn-Beta. *Catal. Sci. Technol.* **2019**, *9* (16), 4339–4346.
- (112) Tang, B.; Li, S.; Song, W. C.; Yang, E. C.; Zhao, X. J.; Guan, N.; Li, L. Fabrication of Hierarchical Sn-Beta Zeolite as Efficient Catalyst for Conversion of Cellulosic Sugar to Methyl Lactate. *ACS Sustain. Chem. Eng.* **2020**, *8* (9), 3796–3808.
- (113) Zhang, J.; Wang, L.; Wang, G.; Chen, F.; Zhu, J.; Wang, C.; Bian, C.; Pan, S.; Xiao, F. S. Hierarchical Sn-Beta Zeolite Catalyst for the Conversion of Sugars to Alkyl Lactates. *ACS Sustain. Chem. Eng.* **2017**, *5* (4), 3123–3131.
- (114) Cundy, C. S.; Cox, P. A. The Hydrothermal Synthesis of Zeolites: Precursors, Intermediates and Reaction Mechanism. *Microporous Mesoporous Mater.* **2005**, *82* (1–2), 1–78.
- (115) Hammond, C.; Padovan, D.; Tarantino, G. Porous Metallosilicates for Heterogeneous, Liquid-Phase Catalysis: Perspectives and Pertaining Challenges. *R. Soc. Open Sci.* **2018**, *5* (2).
- (116) Schmidt, J. E.; Fu, D.; Deem, M. W.; Weckhuysen, B. M. Template–Framework Interactions in Tetraethylammonium-Directed Zeolite Synthesis. *Angew. Chemie - Int. Ed.* **2016**, *55* (52), 16044–16048.
- (117) Tolborg, S.; Katerinopoulou, A.; Falcone, D. D.; Sadaba, I.; Osmundsen, C. M.; Davis, R. J.; Taarning, E.; Fristrup, P.; Holm, M. S. Incorporation of Tin Affects Crystallization, Morphology, and Crystal Composition of Sn-Beta. *J. Mater. Chem. A* **2014**, *2* (47), 20252–20262.
- (118) Hammond, C.; Conrad, S.; Hermans, I. Simple and Scalable Preparation of Highly Active Lewis Acidic Sn-?? *Angew. Chemie - Int. Ed.* **2012**, *51* (47), 11736–11739.
- (119) Van Bokhoven, J. A.; Koningsberger, D. C.; Kunkeler, P.; Van Bekkum, H.; Kentgens, A. P. M. Stepwise Dealumination of Zeolite Beta at Specific T-Sites Observed with ^{27}Al MAS and ^{27}Al MQ MAS NMR. *J. Am. Chem. Soc.* **2000**, *122* (51), 12842–12847.
- (120) Müller, M.; Harvey, G.; Prins, R. Comparison of the Dealumination of Zeolites Beta, Mor-denite, ZSM-5 and Ferrierite by Thermal Treatment, Leaching with Oxalic Acid and Treatment with SiCl_4 by ^1H , ^{29}Si and ^{27}Al MAS NMR. *Microporous Mesoporous Mater.* **2000**, *34* (2), 135–147.
- (121) Shamzhy, M. V.; Eliašová, P.; Vitvarová, D.; Opanasenko, M. V.; Firth, D. S.; Morris, R. E. Post-Synthesis Stabilization of Germanosilicate Zeolites ITH, IWW, and UTL by Substitution of Ge for Al. *Chem. - A Eur. J.* **2016**, *22* (48), 17377–17386.
- (122) Al-Nayili, A.; Yakabi, K.; Hammond, C. Hierarchically Porous BEA Stannosilicates as Unique Catalysts for Bulky Ketone Conversion and Continuous Operation. *J. Mater. Chem. A* **2015**, *00*, 1–10.
- (123) Holm, M. S.; Taarning, E.; Egeblad, K.; Christensen, C. H. Catalysis with Hierarchical Zeolites. *Catal. Today* **2011**, *168* (1), 3–16.

- (124) Bare, S. R.; Kelly, S. D.; Sinkler, W.; Low, J. J.; Modica, F. S.; Valencia, S.; Corma, A.; Nemeth, L. T. Uniform Catalytic Site in Sn- β -Zeolite Determined Using X-Ray Absorption Fine Structure. *J. Am. Chem. Soc.* **2005**, *127* (37), 12924–12932.
- (125) Li, P.; Liu, G.; Wu, H.; Liu, Y.; Jiang, J. G.; Wu, P. Postsynthesis and Selective Oxidation Properties of Nanosized Sn-Beta Zeolite. *J. Phys. Chem. C* **2011**, *115* (9), 3663–3670.
- (126) Wolf, P.; Hammond, C.; Conrad, S.; Hermans, I. Post-Synthetic Preparation of Sn-, Ti- and Zr-Beta: A Facile Route to Water Tolerant, Highly Active Lewis Acidic Zeolites. *Dalton Trans.* **2014**, 43 (11), 4514–4519.
- (127) Liu, M.; Jia, S.; Li, C.; Zhang, A.; Song, C.; Guo, X. Facile Preparation of Sn- β Zeolites by Post-Synthesis (Isomorphous Substitution) Method for Isomerization of Glucose to Fructose. *Cuihua Xuebao/Chinese J. Catal.* **2014**, *35* (5), 723–732.
- (128) Dijkmans, J.; Dusselier, M.; Gabriëls, D.; Houthoofd, K.; Magusin, P. C. M. M.; Huang, S.; Pontikes, Y.; Trekels, M.; Vantomme, A.; Giebelers, L.; et al. Cooperative Catalysis for Multistep Biomass Conversion with Sn/Al Beta Zeolite. *ACS Catal.* **2015**, *5* (2), 928–940.
- (129) Pérez-Ramírez, J.; Christensen, C. H.; Egeblad, K.; Christensen, C. H.; Groen, J. C. Hierarchical Zeolites: Enhanced Utilisation of Microporous Crystals in Catalysis by Advances in Materials Design. *Chem. Soc. Rev.* **2008**, *37* (11), 2530–2542.
- (130) Botti, L.; Navar, R.; Tolborg, S.; Martinez-Espin, J. S.; Padovan, D.; Taarning, E.; Hammond, C. Influence of Composition and Preparation Method on the Continuous Performance of Sn-Beta for Glucose-Fructose Isomerisation. *Top. Catal.* **2019**, *62* (17–20), 1178–1191.
- (131) Boronat, M.; Concepción, P.; Corma, A.; Renz, M.; Valencia, S. Determination of the Catalytically Active Oxidation Lewis Acid Sites in Sn-Beta Zeolites, and Their Optimisation by the Combination of Theoretical and Experimental Studies. **2005**, *234*, 111–118.
- (132) Li, G.; Pidko, E. A.; Hensen, E. J. M. Synergy between Lewis Acid Sites and Hydroxyl Groups for the Isomerization of Glucose to Fructose over Sn-Containing Zeolites: A Theoretical Perspective. *Catal. Sci. Technol.* **2014**, *4* (8), 2241–2250.
- (133) Wolf, P.; Valla, M.; Rossini, A. J.; Comas-Vives, A.; Núñez-Zarur, F.; Malaman, B.; Lesage, A.; Emsley, L.; Copéret, C.; Hermans, I. NMR Signatures of the Active Sites in Sn-BEA Zeolite. *Angew. Chemie - Int. Ed.* **2014**, *53* (38), 10179–10183.
- (134) Padovan, D.; Botti, L.; Hammond, C. Active Site Hydration Governs the Stability of Sn-Beta during Continuous Glucose Conversion. *ACS Catal.* **2018**, *8* (8), 7131–7140.
- (135) Yakimov, A. V.; Kolyagin, Y. G.; Tolborg, S.; Vennestrøm, P. N. R.; Ivanova, I. I. ^{119}Sn MAS NMR Study of the Interaction of Probe Molecules with Sn-BEA: The Origin of Penta- and Hexacoordinated Tin Formation. *J. Phys. Chem. C* **2016**, *120* (49), 28083–28092.
- (136) Sádaba, I.; López Granados, M.; Riisager, A.; Taarning, E. Deactivation of Solid Catalysts in Liquid Media: The Case of Leaching of Active Sites in Biomass Conversion Reactions. *Green Chem.* **2015**, *17* (8), 4133–4145.
- (137) Yakabi, K.; Milne, K.; Buchard, A.; Hammond, C. Selectivity and Lifetime Effects in Zeolite-Catalysed Baeyer–Villiger Oxidation Investigated in Batch and Continuous Flow. *ChemCatChem* **2016**, *8* (22), 3490–3498.
- (138) Boskovic, G.; Baerns, M. Catalyst Deactivation. *Springer Ser. Chem. Phys.* **2004**, *75*, 477–503.

- (139) Lari, G. M.; Dapsens, P. Y.; Scholz, D.; Mitchell, S.; Mondelli, C.; Pérez-Ramírez, J. Deactivation Mechanisms of Tin-Zeolites in Biomass Conversions. *Green Chem.* **2016**, *18* (5), 1249–1260.
- (140) Hinrichs, M. United States Patent (19). **1982**, No. 19.
- (141) Bartholomew, C. H. Mechanisms of Catalyst Deactivation. *Appl. Catal. A Gen.* **2001**, *212* (1–2), 17–60.
- (142) Dai, C.; Zhang, S.; Zhang, A.; Song, C.; Shi, C.; Guo, X. Hollow Zeolite Encapsulated Ni-Pt Bimetals for Sintering and Coking Resistant Dry Reforming of Methane. *J. Mater. Chem. A* **2015**, *3* (32), 16461–16468.
- (143) Padovan, D.; Botti, L.; Hammond, C. Active Site Hydration Governs the Stability of Sn-Beta during Continuous Glucose Conversion. *ACS Catal.* **2018**, *8* (8), 7131–7140.
- (144) Levenspiel, O. *Chemical Reaction Engineering*; 1999; Vol. 38.

Chapter 2

Active site hydration governs the stability of Sn-Beta during continuous sugars conversion

The content of this chapter was published in the following manuscripts:

React. Chem. Eng. **2018**, 3 (2), 155–163.

ACS Catal. **2018**, 8 (8), 7131–7140.

2.1 Introduction

In the main introduction of the manuscript (Chapter 1, Section 1.1), it was described how the implementation of renewable feedstock for chemical production is essential to break away from the excessive use of common fossil feedstock, the consumption of which contributes to increased emissions of CO₂ in the atmosphere and therefore aggravates already alarming anthropogenic climate change.¹⁻³ Sugar derived from biomass is one of the most promising sources of renewable carbon, and its efficient conversion is paramount to develop new competitive green process to replace the actual chemical production for fossil feedstock.^{4,5} In Chapter 1 (Section 1.8) it was thoroughly shown how the enzymatic catalytic approach have been successfully applied at this scope. However, the high operational costs of these catalysts affect the economic competitiveness of biomass upgrading; therefore, efforts were addressed in developing inorganic heterogeneous catalysts which could more efficiently promote sugars upgrading. As described in Chapter 1 (Section 1.12) Sn-Beta zeolite is known in the literature to be one of the best catalysts for the processing of sugars. Although several studies focused on the development of this catalyst for sugars upgrading,^{6,7} little was known on the stability of this material in 2017 when this project commenced. At time a limited number of studies were showing continuous testing to assess the life-time of the material and these rare works in the literature were involving model-reactions.⁸⁻¹¹ Although the useful insight that these systems gave, a more industrially interesting system was needed to assess the stability of Sn-Beta for realistic applications. The lack of essential knowledge regarding the stability of the catalyst and its ability to operate continuously represented an important drawback for the future application of this catalyst in this kind of market. As explained in Chapter 1 (Section 1.9), the large volume of biomass and the vast annual production of chemical commodities require continuous substrate conversion for maintaining an economic competitiveness with fossil feedstock.^{12,13} For these reasons in this chapter of the thesis, the performances of Sn-Beta for sugar upgrading in continuous conditions will be studied. Specifically, the isomerisation of glucose to fructose at low temperature (110 °C), and the conversion of fructose to methyl lactate

(ML) at high temperature (160 °C) will be investigated.¹⁴ These reactions are both industrially relevant since glucose and ML are both important intermediates for bio-plastic and bio-fuels production.¹⁵⁻¹⁷ In this work new process conditions are explored to improve Sn-Beta stability during continuous sugar upgrading. In particular the effect of traces of water on the stability of Sn-Beta is monitored. Successively, a thorough mechanistic study employing MAS-NMR analysis coupled with *operando* analysis is carried out to ascertain the cause of the catalyst deactivation during these processes.¹⁸

2.2. Experimental details:

2.2.1 Catalyst synthesis

For glucose isomerisation (GI) experiments, a commercial zeolite Al-Beta (Zeolyst, NH₄⁺-form, Si/Al = 19) was dealuminated by treatment in HNO₃ solution (13 M HNO₃, 100 °C, 20 mL g⁻¹ zeolite, 20 h). Solid-state stannation of dealuminated zeolite *BEA was performed the procedure reported in reference 19 by grinding the appropriate amount of tin (II) acetate (Sigma Aldrich, > 99.9 %) with the necessary amount of dealuminated zeolite for 10 minutes in a pestle and mortar. Following this procedure, the sample was heated in a combustion furnace (Carbolite MTF 12/38/400) to 550 °C (10 °C min⁻¹ ramp rate) first in a flow of N₂ (3 h) and subsequently air (3 h) for a total of 6 h. Gas flow rates of 60 mL min⁻¹ were employed at all times. For methyl lactate production experiments, Sn-Beta was prepared using a commercial zeolite (Zeolyst, NH₄⁺-form, Si/Al = 19), this material was calcined at 550 °C for 6 h and treated in a solution of HNO₃ (65 %, 80 °C, 10 mL g⁻¹ zeolite). After thoroughly washing of the dealuminated sample, the solid was recovered by vacuum filtration and tin was introduced using tin(II) chloride (Sigma-Aldrich, 98 %) dissolved in water by incipient wetness impregnation to yield a Si/Sn ratio of 125 in the material. The catalyst was finalized by drying the sample at 110 °C for 12 h followed by calcination (550 °C, 6 h, 2 °C min⁻¹).

2.2.2 Catalyst characterisation

X-Ray Diffraction analyses were carried out by a PANalytical X'PertPRO X-ray. A CuK α radiation source (40 kV and 30 mA) was utilised. Diffraction patterns were recorded between 6–55° 2 θ (step size 0.0167°, time/step = 150 s, total time = 1 h).

Specific surface area was determined from nitrogen adsorption using the BET equation, and microporous volume was determined from nitrogen adsorption isotherms using the *t*-plot method. Porosimetry measurements were performed on a Quantachrome Quadrasorb, and samples were degassed prior to use (115 °C, 6 h, nitrogen flow). Adsorption isotherms were obtained at 77 K.

TGA analysis was performed on a Perkin Elmer system. Samples were held isothermally at 30 °C for 30 minutes, before being heated to 550 °C (10 °C min⁻¹ ramp rate) in air. TPD-MS measurement were carried out on a home-made system formed by a Bruker Tensor II equipped with a Harrick praying mantis DRIFT cell connected with the MS. The catalyst was placed inside the drift cell and its surface was constantly monitored by the IR spectrometer. The cell was heated from 30 to 550 °C (ramp rate 10 °C min) and a constant flow of air was kept throughout

the experiment. The outlet of the DRIFT cell was connected to a Hiden QGA mass spectrometer for the online analysis of the gas phase.

Operando UV–Vis measurements were performed with a homemade tubular reactor equipped with a fiber optic UV–Vis probe. UV–Vis measurements were performed with a light source (Ocean Optics DH-2000), spectrometer (Maya 2000 Pro, Ocean Optics), and a 600- μm UV–Vis fiber. The light was directed onto an optically transparent reactor column, located within a heated aluminium block. *Ex situ* UV–Vis analyses were performed in a similar manner, with the exception that the fibre was focused directly on the powder samples.

MAS NMR analysis was performed at Durham University through the National Solid-State NMR service. All the samples were nonenriched and were measured on a Bruker Avance III HD spectrometer at operating frequencies of 400, 100, 149, and 79 MHz for ^1H , ^{13}C , ^{119}Sn , and ^{29}Si , respectively. Typically, between 50 and 100 mg of solid sample was packed in a 4 mm rotor and spun at $\pm 12\,000$ Hz. For ^{119}Sn MAS NMR, samples were measured by the CPMG method as described in references.^{20,21} Spectra were acquired in both direct excitation and cross-polarization modes. Recycle delay times of 1 and 2 s were applied for ^{119}Sn CP CPMG MAS NMR and ^{119}Sn DE CPMG MAS NMR, respectively.

DRIFT spectroscopy analyses were performed in a Harrick praying mantis cell. The spectra were recorded on a Bruker Tensor Spectrometer over a range of $4000\text{--}650\text{ cm}^{-1}$ at a resolution of 2 cm^{-1} . Alcohol adsorption studies with DRIFT spectroscopy were performed on the pre-treated zeolite powder (heated to $110\text{ }^\circ\text{C}$ for 30 min in nitrogen at 40 mL min^{-1} prior to adsorption). The alcohol was dosed by passing the gas stream through a saturator module. Samples were maintained at $110\text{ }^\circ\text{C}$ during the experiment to simulate reaction conditions. Spectra were recorded after 20 min of absorption.

2.2.3 Kinetic evaluation and analytical methods

Continuous GI reactions were performed in a plug flow, stainless steel, tubular reactors. The reactor was connected to an HPLC pump in order to regulate the reactant flow and allow operation at elevated pressures. The catalyst was mixed with a diluent material (SiC, particle size of $63\text{--}75\text{ }\mu\text{m}$), and the catalytic bed placed in between two plugs of quartz wool. The diluted sample was densely packed into a $1/4$ " stainless steel tube (4.1 mm internal diameter), and a frit of $0.5\text{ }\mu\text{m}$ was placed at the reactor exit. The reactor was subsequently immersed in a thermostatted oil bath at the desired reaction temperature. Pressure in the system was controlled by means of a backpressure regulator, typically set at 10 bar, in order to allow operations above the boiling temperature of the solvent. Aliquots of the reaction solutions were taken periodically from a sampling valve placed after the reactor and analysed by an Agilent 1260 Infinity HPLC equipped with a Hi-Plex Ca column and ELS detector and quantified against an external standard (sorbitol) added to the sample prior the injection. Where applicable, periodic regeneration was performed by heating the whole reactor in a combustion furnace (Carbolite MTF 12/38/400) to $550\text{ }^\circ\text{C}$ ($10\text{ }^\circ\text{C min}^{-1}$) in air (3 h). In the second part of the chapter, in which

the focus was on the *operando* and on the *ex situ* characterisation of the catalyst, SiC was no longer used to dilute the catalytic bed. Instead, Sn-Beta zeolite was introduced in the reactor after pelletisation to particle sizes between 63 and 77 μm .

Methyl lactate production was performed using 250 mg of Sn-Beta catalyst in a 1/4" stainless steel tube fractioned to a size of 300–600 μm and placed between two quartz plugs. A solution of 12.5 g L⁻¹ fructose, 2.5 mg L⁻¹ K₂CO₃ in varying H₂O : MeOH (0 : 100 and 1 : 99) mixtures was led over the bed using a Knauer pump. 250 mg of catalyst (Sn-Beta, Si/Sn = 125) and a flow rate of 0.15 mL min⁻¹ were employed. Reactions were performed at 160 °C. Sampling was done at regular intervals using a Valco autosampler (VICI®). *Ex situ* thermal regeneration of the catalyst was performed by removing the catalyst from the reactor and treating the sample at 550 °C for 6 h in a muffle furnace (Nabertherm). Unconverted sugars were quantified on an Agilent 1200 HPLC with an Aminex HPX-87H (BioRad) column equipped using a diluted sulphuric acid eluent (0.004 M H₂SO₄, 0.6 mL min, 65 °C) was used to quantify unconverted sugars using the response factor of fructose. Methyl lactate (ML) was quantified on an Agilent 7890A GC-FID with a SolGel-WAX column (Phenomenex) equipped. The glucose employed as substrate was provided by Sigma Aldrich (>99.5 %, monohydrate), methanol anhydrous as solvent was provided by Sigma Aldrich (99.8 %), deionised water was added to the reaction feed. Standard of fructose, mannose, methyl lactate were provided by Sigma Aldrich (> 99.9 %).

2.3 Results and Discussion

2.3.1 Water effect on the stability of Sn-Beta

Sn-Beta zeolite is known to be an excellent catalyst for glucose upgrading to fructose (via isomerisation) and methyl lactate (via retro-aldol fragmentation). For both of these reactions, Sn-Beta is known to exhibit a good level of activity when the reaction is performed either in alcoholic solvent, such as methanol or ethanol, and water.²²⁻²⁴

Given that the choice of reaction media can dramatically influence the catalyst stability, the impact of the solvent with respect to catalyst stability was first evaluated. As such, preliminary stability studies were focused on continuous glucose isomerisation (GI), using a 10 % wt. Sn-Beta zeolite (henceforth 10Sn-Beta) material prepared by Solid State incorporation (SSI) as catalyst, as this has been shown to be one of the highest performing catalysts in the literature per gram of material for this reaction (equation 1, in the equation appendix).¹⁹

Preliminary studies were undertaken by performing the isomerisation reaction in various solvents under otherwise similar conditions (1 % wt. glucose, 110 °C figure 1). For these preliminary studies, the contact time (equation 2, in the equation appendix) was adjusted so that all reactions were performed at similar levels of substrate conversion (equation 3, in the equation appendix), to ensure catalyst stability was probed at a similar stage of the reaction coordinate. The initial level of conversion in each case was approximately 40 %, below the equilibrium level,²⁵ allowing the rate of deactivation to be accurately assessed. To better evaluate catalyst stability at slightly

different levels of conversion, stability is evaluated as relative performance (equation 4, in the equation appendix) against time on stream.

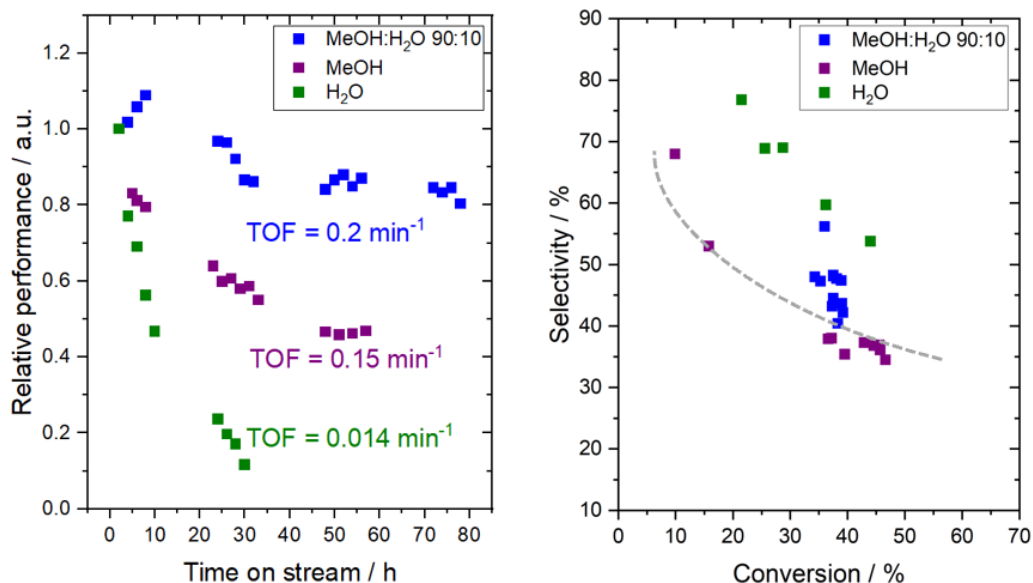


Figure 1. (Left) Influence of the solvent on the stability and (Right) Selectivity of fructose plotted against the conversion of glucose of 10Sn-Beta for low temperature glucose–fructose isomerisation. The initial level of conversion in all cases was between 33–40 %. Experimental details: 1 % wt. glucose, 110 °C , 10 bar. MeOH: 0.2 mL min⁻¹ over 30 mg of catalyst. MeOH:H₂O 90:10: 0.25 mL min⁻¹ over 30 mg of catalyst. H₂O: 0.1 mL min⁻¹ over 65 mg of catalyst.

In good agreement with the results reported in the literature, extensive deactivation of Sn-Beta is observed when GI is performed in an aqueous medium, with 90 % loss of activity observed within 30 h on stream (figure 1 Left).⁸ Whilst deactivation in methanol is less severe, it is still prevalent with approximately 50 % loss of activity observed over 50 h on stream. In contrast, a dramatic improvement in stability is observed when a mixture of water and methanol is employed as solvent (figure 1 Left). Indeed, the addition of just 10 % wt. water to methanol (henceforth denoted MeOH:H₂O 90:10) results in dramatic improvements in catalyst stability, with less than 10 % deactivation being observed even after 80 h on stream. In figure 1 Right is shown the selectivity (equation 8 in the equation appendix) of fructose at the same rate of conversion for each reaction carried out by 10Sn-Beta with different solvents. Interestingly water shows the best selectivity of the series, which is unfortunate due to the scarce activity (0.014 min⁻¹) and low stability of the system. Similar level of selectivity were achieved in the process in MeOH and in MeOH:H₂O 90:10, these results lays on the same selectivity-conversion curve. Therefore, henceforth the selectivity of the catalyst will not be showed for favouring the clearness of the data. In addition, two different kind of deactivation observed when using the catalyst in pure methanol or in pure water, in the first the catalyst does not show permanent deactivation and the material can be regenerated by thermal treatment (550 °C, 3 h, air), whereas when the catalyst is exposed to water the material does not recover the lost activity if thermally treated (figure 2).

Notably the catalyst regenerated by thermal treatment after methanol reaction shows an improvement in performance, the explanation of this behaviour is beyond the scope of this chapter and it will be thoroughly treated in Chapter 4.

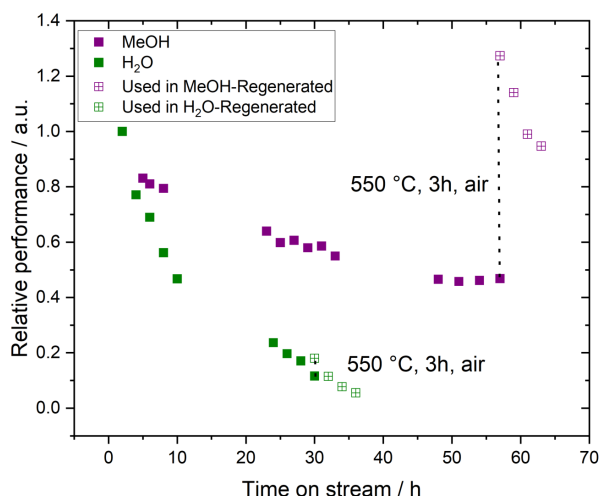


Figure 2. Regeneration by thermal treatment at 550 °C in air for 3 h for 10Sn-Beta used in MeOH (purple) and water (green) at 110 °C. Experimental details: 1 % wt. glucose, 110 °C, 10 bar. MeOH: 0.2 mL min⁻¹ over 30 mg of catalyst. MeOH:H₂O 90:10: 0.25 mL min⁻¹ over 30 mg of catalyst. Regeneration was performed by thermal treatment in air at 550 °C for 3 h.

Secondary analysis in analysis (figure 3) of the time on stream data reveals that the rate of deactivation (k_d)²⁶ experienced by 10Sn-Beta decreases by an order of magnitude as the solvent is changed from pure methanol to MeOH:H₂O 90:10 (0.02 X% h⁻¹ to 0.002 X% h⁻¹), despite water itself being a very unfavourable solvent (0.07 X% h⁻¹). The rate of deactivation is calculated by linearly fitting the Levenspiel function of conversion as function of time on stream as shown in equation 5 in the equation appendix.

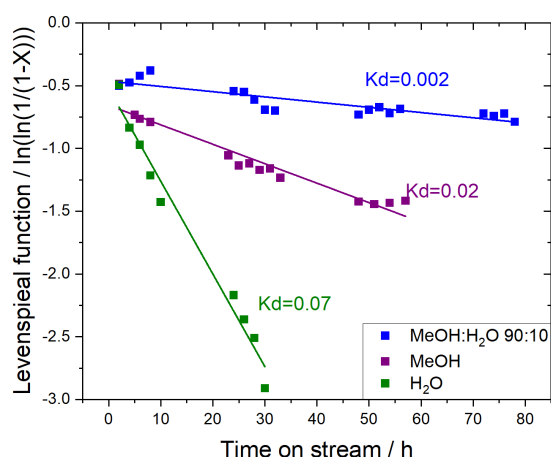


Figure 3. Levenspiel function plotted as a function of time on stream for 10Sn-Beta used in GI in MeOH:H₂O 90:10 (blue), MeOH (purple) and water (green) at 110 °C. Experimental details: 1 % wt. glucose, 110 °C, 10 bar. MeOH: 0.2 mL min⁻¹ over 30 mg of catalyst. MeOH:H₂O 90:10: 0.25 mL min⁻¹ over 30 mg of catalyst. H₂O: 0.1 mL min⁻¹ over 65 mg of catalyst.

Based on the dramatic improvement to stability observed in the presence of water, a variety of other solvent compositions, ranging from 0 % water (i.e. pure methanol) to 100 % water were explored (figure 4). In each case, the stability (k_d) and the activity in terms of turn over frequency (TOF_0 , equation 6 in the equation appendix) of the catalyst was determined during continuous operation. This analysis demonstrated that there was a clear optimal window for high levels of stability to be obtained, with the lowest k_d values being observed between 1 % and 10 % wt. water.

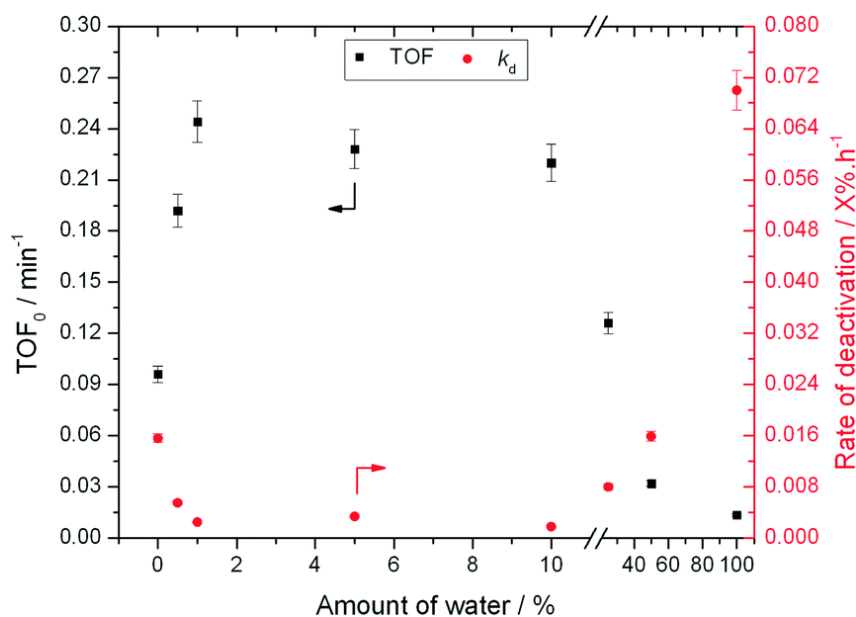


Figure 4. Influence of solvent composition in terms of activity (TOF_0) and rate of deactivation (k_d) during low temperature glucose–fructose isomerisation. Experimental details: 1 % wt. glucose, 110 °C , 10 bar. MeOH: 0.2 mL min^{-1} over 30 mg of catalyst. MeOH:H₂O (90:10): 0.25 mL min^{-1} over 30 mg of catalyst. H₂O: 0.1 mL min^{-1} over 65 mg of catalyst. MeOH:H₂O (99.5:0.5): 0.25 mL min^{-1} over 30 mg of catalyst. MeOH:H₂O (99:1): 0.25 mL min^{-1} over 30 mg of catalyst. MeOH:H₂O (95:5): 0.25 mL min^{-1} over 30 mg of catalyst. MeOH:H₂O (75:25): 0.25 mL min^{-1} over 30 mg of catalyst. MeOH:H₂O (75:25): 0.11 mL min^{-1} over 70 mg of catalyst.

The addition of water also improves intrinsic reactivity. To ensure that the stability studies were performed at a similar stage of the reaction coordinate (figure 1), the contact time, and hence the number of substrate turnovers (equation 7 in the equation appendix) had to be adjusted. Consequently, despite exhibiting similar levels of absolute substrate conversion, TOF_0 is higher when the reaction is performed in MeOH:H₂O 90:10 (0.20 min^{-1}) than when it is performed in H₂O (0.014 min^{-1}) or MeOH (0.15 min^{-1}) alone.

To better understand the impact of water on the intrinsic reactivity of 10Sn-Beta *i.e.* TOF_0 , a series of experiments were repeated, this time under identical reaction conditions and contact times. As can be seen (figure 5), as the fraction of water is increased from 0 % to 1 %, TOF_0 more than doubles from 0.1 min^{-1} in pure methanol to 0.25 min^{-1} in MeOH:H₂O 99:1. Whilst activity is

maintained at this high level up to at least MeOH:H₂O 90:10, further increasing the water fraction beyond 10 % results in decreasing values of TOF₀, with poorest levels of performance being obtained in H₂O only.

Notably, the beneficial effect of water in terms of improving stability can also be extended to lower loading of Sn-Beta (table1). This shows how the effect of water is applicable also to lower loading of Sn-Beta.

Table 1 Rate of Deactivation (k_d) of 2Sn-Beta and 10Sn-Beta during continuous glucose isomerisation in MeOH or MeOH:H₂O 90:10.

Catalyst	K_d MeOH	K_d MeOH:H ₂ O 90:10
10Sn-Beta	0.02	0.002
2Sn-Beta	0.028	0.005

To understand whether the beneficial effect of water was present also for the upgrading of sugars to methyl lactate, fructose processing was performed at higher temperature (160 °C). This reaction is potentially interesting since methyl lactate is an expensive and interesting compound that finds application as monomer in plastic materials.²⁷ For this system 1.5 % wt. Sn-Beta zeolite (henceforth 1.5Sn-Beta) was exploited. A lower loading sample was chosen to match the final set of GI data (table 1), and aid future spectroscopic studies.

To carry out these experiments a solution of fructose in methanol was used as feed for the high temperature reaction (160 °C), due to the higher solubility of fructose in methanol at room temperature compared to sucrose and glucose. Alkali (K₂CO₃) was also added to the feed at a level of 2.5 mg L⁻¹ (36 μM), to increase the selectivity towards methyl lactate, as demonstrated in previous reports.²⁸ In good agreement to the GI system, a gradual decrease in the conversion of fructose during continuous operation was observed in pure methanol, with conversion decreasing from 87 % to 65 % after the first 94 h on stream (figure 5). Deactivation in this case was non-permanent, since full activity of the material could be restored by thermal treatment of the catalyst after 90 h on stream. This *ex situ* treatment was performed by removing the catalyst from the reactor and heating it in air at 550 °C for 6 h.

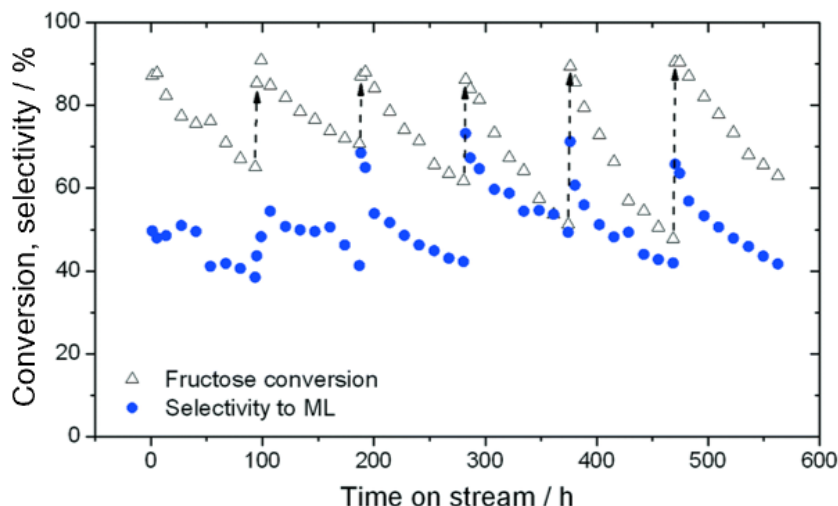


Figure 5. Time on stream data showing the selectivity towards methyl lactate (blue circles) and conversion of fructose (hollow triangles) using 1.5Sn-Beta at 160 °C in methanol. Regeneration by thermal treatment was performed every 96 h (dashed arrows). Experimental details: 1.5 % wt. fructose in methanol (2.5 mg L⁻¹, K₂CO₃), 160 °C, 20 bar. 0.15 mL min⁻¹ over 250 mg of catalyst.

These data were kindly provided by Dr. S.Tolborg, Manager of research in Haldor Topsøe (DK), in the role of sponsor and collaborator of the project

As found for GI, the addition of water to methanol in small amounts (<10 % wt.) resulted in a dramatic increase in catalyst stability. Figure 6 presents three consecutive cycles of the same 1.5Sn-Beta material under the same conditions as figure 5, but with 1 % wt. of water added to the reaction feed. Two different modes of deactivation can again be observed. Firstly, an initial transient regime during the initial 60 h of operation, during which conversion decreases and selectivity towards methyl lactate increases slightly. Secondly, an apparent steady state regime over the following 400 h, where conversion only decreases slightly, and ML selectivity (equation 8, in the equation appendix) is maintained at approximately 60 %. By comparing the rate of deactivation (k_d) in this reaction (0.008–0.017 X% h⁻¹) to that observed in the absence of water (0.23–0.59 X% h⁻¹), it is obvious that there is a drastic increase in 1.5Sn-Beta stability following the addition of small amounts of water to the feed, in excellent agreement to the low temperature GI studies. Due to the increase in stability, regeneration was only performed twice (456 h and 912 h), for indicative purposes. This resulted in a total of 1366 h TOS, corresponding to a substrate turnover of >25 600, with only minor losses in activity.

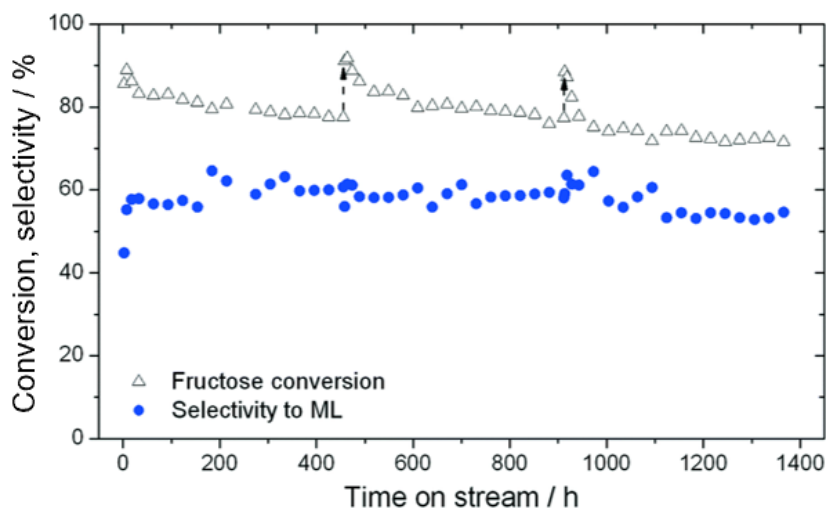


Figure 6. Time on stream data showing the selectivity towards methyl lactate (blue circles) and conversion of fructose (hollow triangles) using 1.5Sn-Beta at 160 °C in the presence of 1 % wt. water in methanol. The catalyst was regenerated periodically by thermal treatment (dashed arrows). Experimental details: 1.5 % wt. fructose in methanol (2.5 mg L⁻¹, K₂CO₃), 160 °C , 20 bar. 0.15 mL min⁻¹ over 250 mg of catalyst.

These data were kindly provided by Dr. S.Tolborg, Manager of research in Haldor Topsøe (DK), in the role of sponsor and collaborator of the project

2.3.2 Understanding the stabilising role of water

The possibility of expanding the stabilising effect of water to conversion of monosaccharide at high temperature makes this discovery extremely interesting from an industrial prospective. Therefore, the understanding of this phenomenon is compelling to further understand the effect of these continuous liquid processes on heterogeneous catalysts.

To elucidate the molecular level origin of the water effect, structure–activity–lifetime relationships were generated, primarily for samples of 10Sn-Beta following operation in MeOH or MeOH:H₂O for 50–60 h. Over this time period, the catalyst exhibited approximately 55 and 5 % loss of activity in MeOH and H₂O:MeOH, respectively (figure 1). Considering the ease in performing structure–activity correlations on pure materials, characterization studies of the undiluted (*i.e.* SiC-free), "ex reactor" samples were performed with XRD, TGA, TPO-MS, and ¹³C MAS NMR.

The results of XRD analyses (figure 7) clearly show how the reaction in pure methanol and in MeOH:H₂O 90:10 do not shows drastic differences in the restructuring of the catalyst crystal structure. However, when the reaction is carried out in pure water, two broad reflections arise at 26.7° and 51.8°, both of which are related to the crystal structure of SnO₂.¹⁹

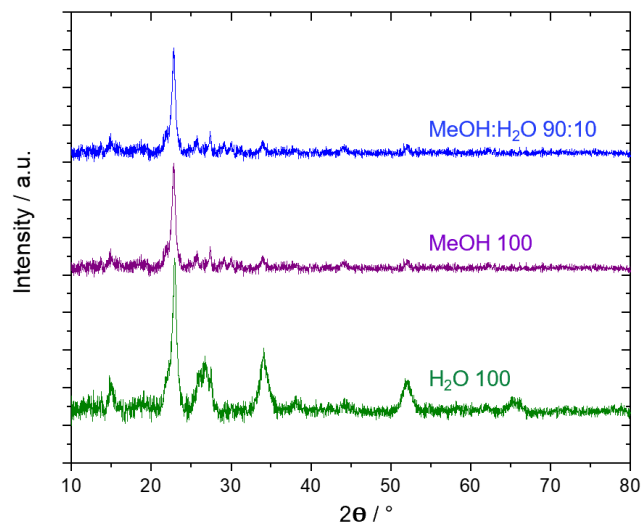


Figure 7. Powder X-ray diffraction analysis on used 10Sn-Beta zeolite after continuous glucose isomerisation in pure water (green line), in pure methanol (purple line) and in 10 : 90 H₂O : MeOH (blue line)

This evidence implies that in pure water the Sn incorporated in the zeolite is removed from the framework, resulting in the formation of tin oxide. Obviously, this restructuring is not reversible via thermal treatment and the catalyst is thus not regeneratable after reaction. Although this technique effectively showed how the use of pure water was not beneficial for the performance of 10Sn-Beta, it did not provide an explanation of the difference in stability in pure methanol and in MeOH:H₂O 90:10. TGA analysis (figure 8) for the fresh 10Sn-Beta zeolite shows a major loss of weight at 110 °C that can be associated with physisorbed water in the pores of the zeolite. The TGA analyses related to the catalysts exploited in GI in pure methanol and in H₂O:MeOH instead show further loss of weight at higher temperatures (280 °C and 400 °C).

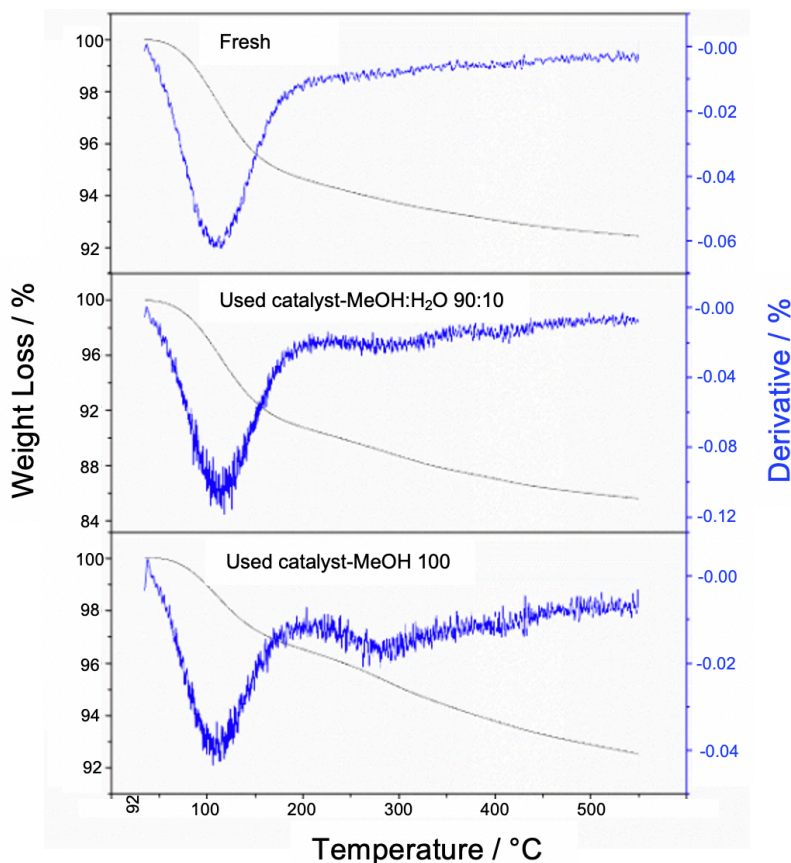


Figure 8. Thermo-gravimetric analysis of the 10Sn-Beta as (top) fresh i.e. unused catalyst, (middle) 10Sn-Beta used in MeOH:H₂O 90:10 and (bottom) 10Sn-Beta following reaction in pure MeOH. The relative mass loss (black line) and its derivative (blue line) are reported against the temperature.

In particular the fresh 10Sn-Beta experience a 5 % mass loss at 110 °C, this temperature is strongly related to moisture present in the hydrophobic structure of the zeolite which is released. The same loss of mass is present in the catalyst used in pure MeOH and in MeOH:H₂O 90:10, however in the latter the loss of mass at this temperature reached almost 10 % whereas in the catalyst used in pure methanol only 3 % mass loss was recorded at 110 °C. This is in agreement with the fact that the catalyst used in MeOH:H₂O 90:10 might adsorb more water, but it is interesting how the catalyst used in pure methanol and dried at room temperature is retaining less water than the fresh material. Moreover the catalyst used in MeOH showed a further loss of mass at 280 °C of roughly 3 % of the starting mass, this signal was not detected for the fresh sample and was on the edge of the detection limit in 10Sn-Beta used in MeOH:H₂O 90:10. This small mass loss can be attributed to some carbonaceous species retained in the reactor after reaction. However, the poor intensity of these signals and the lack of references samples result in a need for further TPO-MS analysis of the spent catalysts. During these experiments, reference material could also be analysed, which were produced by treating the catalysts in the chosen solvent at the temperature of reaction (figure 9).

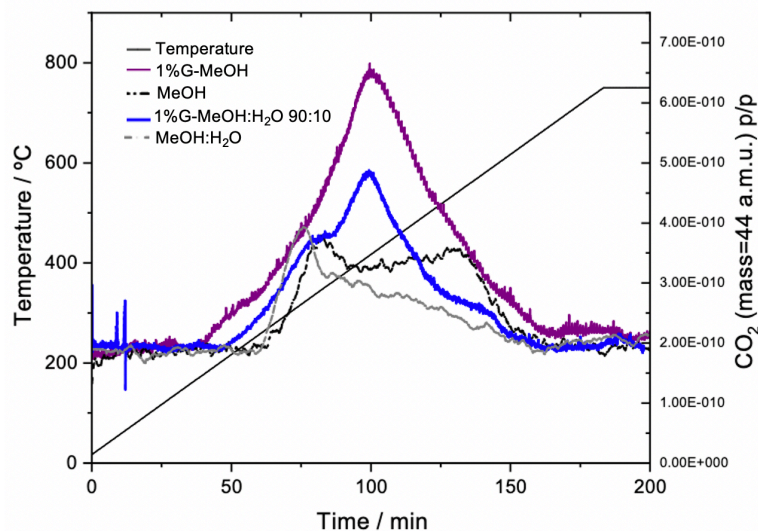


Figure 9. Comparison of the intensity of the $m/e = 44$ signal in the effluent from the TPO-MS analysis of 10Sn-Beta following glucose isomerisation (GI) in MeOH (purple), GI in MeOH:H₂O 90:10 (blue), and following solvothermal treatment in MeOH only (black dotted) and MeOH:H₂O 90:10 only (grey dotted). Air was used as carrier gas at 10 mL min⁻¹. Relative pressure of the gases (right Y axis) and cell temperature (left Y axis) are displayed

These analyses clearly show how different species of carbon are retained in the catalyst depending on the solvent used. In fact, three distinct CO₂ signals can be identified due to the combustion of different carbonaceous species (250 °C, 400 °C and 500 °C). Thanks to the reference materials, it is possible to address the two species at 250 °C and 500 °C to be generated by the interaction of the catalyst with the solvent. As such, by process of elimination the signal at 400 °C can be assigned to the reaction of the sugar substrate with Sn-Beta. Therefore in terms of the CO₂ released this analysis indicate that a large fraction of these residues arise from the solvent alone (figure 9). This agrees well with ¹³C MAS NMR analyses, which indicate that only one detectable resonance ($\delta = 49.8$ ppm) is observed in all used samples, characteristic of retained methanol (figure 10). Accounting for the fact that each retained sugar molecule provides six times more CO₂ during TPO than a molecule of solvent, and that only one resonance is observed by MAS NMR, it is evident that the major species retained in the catalyst after reaction arise from the solvent.

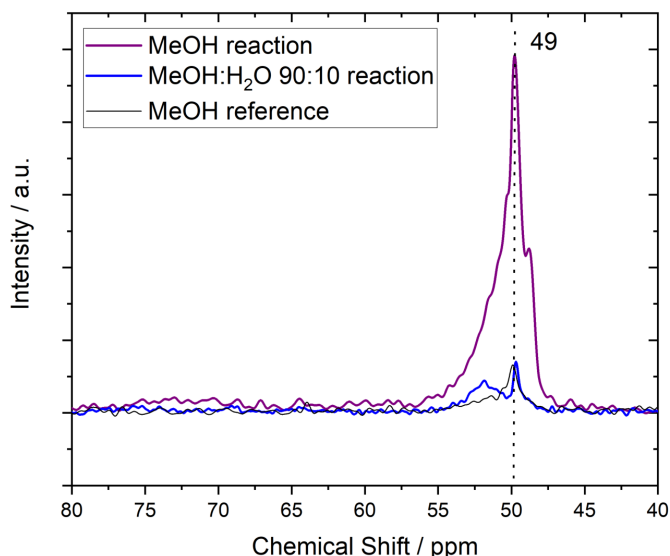


Figure 10. ^{13}C MAS NMR analysis of 10Sn-Beta following GI in MeOH and $\text{H}_2\text{O}:\text{MeOH}$.

This first set of experiment addressed at detecting the carbon retained in 10Sn-Beta after reaction, clearly showed how small amounts of organic are trapped in the catalyst after reaction, potentially causing problem of diffusion through the crystal framework of the zeolite.

Given that pore fouling is an established form of Sn-Beta deactivation (Chapter 1, 1.18),²⁹⁻³² it is possible that the decrease in the quantity of carbonaceous residues upon the addition of water to the feed may minimise the contribution of fouling to deactivation. Consequently, porosimetry analysis of the partially deactivated samples following glucose isomerisation was also performed (table 2). Interestingly, both used samples (MeOH and MeOH: H_2O 90:10) demonstrated a loss of porosity following continuous operation. However, a direct correlation between remaining porosity of the sample and the extent of activity loss is not evident, as both samples lose approximately 15–25 % pore volume during this operational period. Although it cannot be ruled out that deactivation arises from the retention of a specific type of residue, and/or blockage of a particular type of active site, these measurements already suggest that minimized pore fouling is not the dominant role of water.

Table 2. Porosity data for 10Sn-Beta catalysts prior to, and following, continuous operation for GI.

Catalyst	SSA ($\text{m}^2 \text{g}^{-1}$)	V_{micro} ($\text{cm}^3 \text{g}^{-1}$)	Activity lost (%)
10Sn-Beta pelletized (63-75 μm)	351	0.226	/
10Sn-Beta used in GI (MeOH)	279	0.178	55
10Sn-Beta used in GI (MeOH: H_2O)	294	0.192	5

Porosity data determined by N_2 isotherms. Specific surface area (SSA) calculated from BET method, and micropore volume (V_{micro}) derived from the t-plot method.

2.3.3 Site selective spectroscopic studies

In addition to pore fouling, the loss and/or reorganization of active sites is also a primary cause of zeolite deactivation. To gain further insight regarding the impact of water, site selective spectroscopic studies were thus performed. Given its sensitivity to the active sites of the catalyst, in addition to other chromophoric species that could be formed during the reaction, UV–Vis spectroscopy represents a powerful method of gaining insight into the impact of water.^{6,33} However, to maximize the scientific rigor of the analysis, UV–Vis analysis was performed *in operando*, following development of a continuous reactor capable of permitting UV–Vis spectra to be collected throughout continuous operation of the catalyst (so-called *operando* spectroscopy).^{34,35} Notably, measuring the absorption spectra *in operando* permits the rate of evolution of each band to be correlated against real kinetic performance. Importantly, the kinetic data obtained from this reactor was identical to that obtained for the same system in a conventional reactor (figure 11).

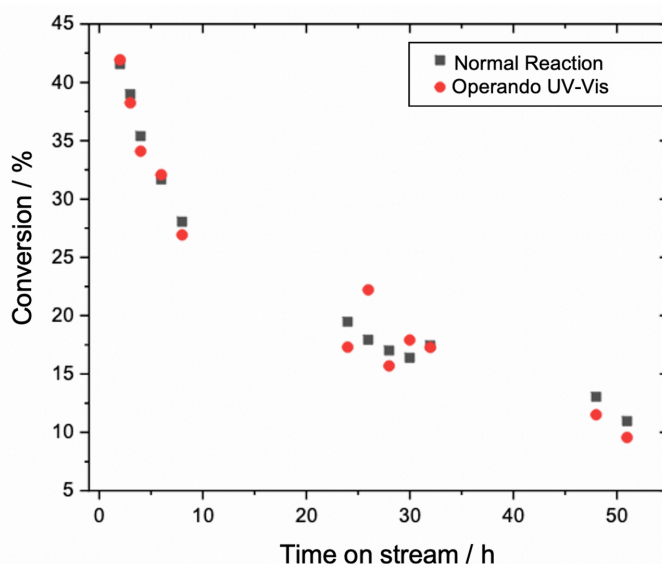


Figure 11. Catalytic performance of 10Sn-Beta for GI in MeOH, as obtained from the in situ UV-Vis reactor (red circles) compared to the catalytic performance obtained during the reaction without measurement in situ (black squares). Experimental details: 1 % wt. Glucose in MeOH or MeOH:H₂O 90:10, 110°C, 10 bar, 100 mg of 10Sn-Beta, 0.65 mL min⁻¹ of flow.

To aid comparison of the evolution of the optical spectra of the experiments as a function of time on stream, spectra are shown in “difference” mode, background subtracted to the spectra of the fresh catalyst recorded at the beginning of each reaction. Accordingly, positive signals represent absorption features gained during the reaction, while negative signals represent those features lost during reaction.

Preliminary control experiments in figure 12, performed by treating 10Sn-Beta and dealuminated Beta with various reactants under otherwise operational conditions for 1 h on stream, revealed the following:

- 1) all chromophoric changes were related to Sn (i.e., in the absence of Sn, no absorption changes were observed)
- 2) interaction between Sn and pure methanol results in the formation of two positive absorption features (260 and 315 nm), and a negative absorption signal at 223 nm
- 3) interaction between Sn and glucose results in absorptions at 341 and 440 nm (figure 12).

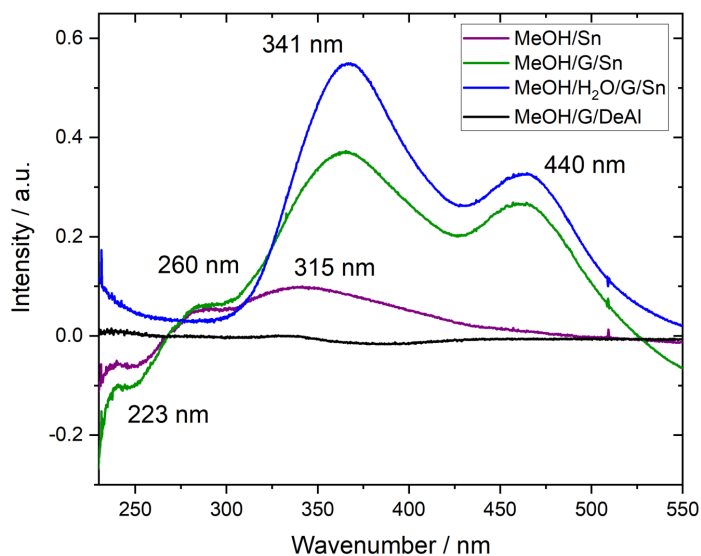


Figure 12. Control samples performed for assignment of UV–Vis spectra, achieved by dosing 10Sn-Beta and dealuminated Beta with pure methanol (MeOH), methanol/glucose (MeOH/G), and methanol/water/glucose (MeOH/H₂O/G) solutions.

Figure 13 presents the difference spectra of 10Sn-Beta during GI in MeOH and MeOH:H₂O, by collection of the absorption spectra “*in operando*”. The contact time in each reaction was adjusted so that both systems presented an initial conversion of 40 %, to ensure both reactions were monitored over similar stages of the reaction coordinate. As expected from control experiments, the 300–450 nm region rapidly increases in absorbance during the very early stages of both reactions, due to the interactions between Sn–methanol (223, 260, 315 nm) and Sn–glucose (341, 440 nm). Interestingly, intensity in this region is slightly higher when water is present, possibly indicating preferential transport of glucose to Sn in the co-presence of water. In MeOH, intensity above 350 nm diminishes after approximately 10 h on stream, whereas in MeOH:H₂O 90:10, the intensity remains largely consistent until longer times on stream. The lower energy Sn–glucose feature (440 nm) is also present at the very early stages of both catalytic reactions. However, its intensity diminishes rapidly in both systems, particularly so in pure methanol.

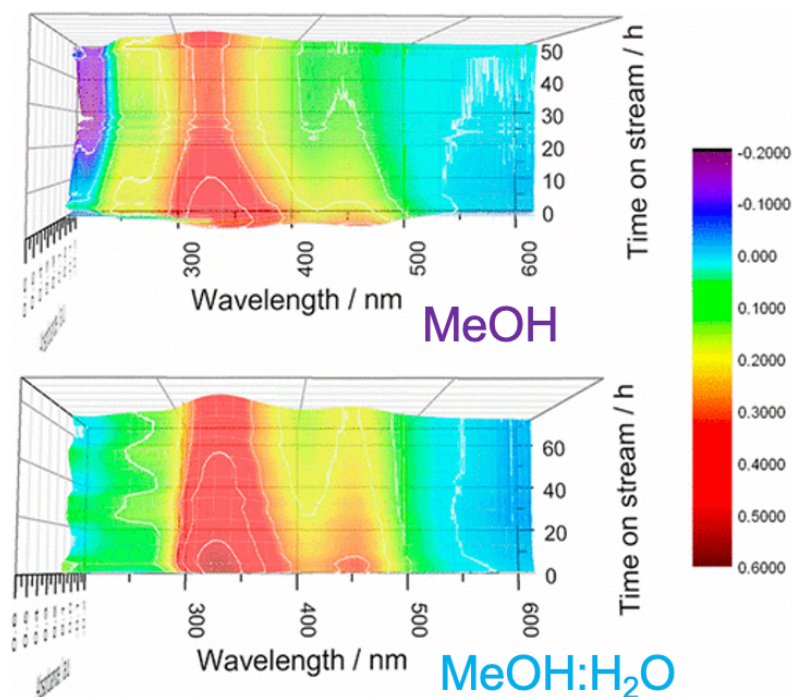


Figure 13. Difference UV–Vis spectra of 10Sn-Beta during GI in (top) MeOH, and (bottom) H₂O:MeOH. Spectra were recorded “in *operando*”. Experimental details: 1 % wt. Glucose in MeOH or MeOH:H₂O 90:10, 110 °C, 10 bar, 100 mg of 10Sn-Beta, 0.65 mL min⁻¹ of flow.

An obvious difference in the high energy region of both systems is also evident. Indeed, while intensity in the high energy region (210–300 nm) remains relatively constant in MeOH:H₂O 90:10, a decrease in intensity at 223 nm and an increase in intensity at 260 nm is observed when the reaction is performed in MeOH. Interestingly, the degree of change in this region also correlates to time on stream in both systems, remaining relatively consistent in MeOH:H₂O 90:10, but gradually increasing in magnitude throughout the operational period in MeOH as the catalyst suffers deactivation.

To better compare the impact of these changes, particularly with respect to kinetic performance, the difference spectra of each reaction, collected at 25 h on stream, are presented in figure 14 Left, alongside the relative performance of the catalyst in both systems at that same point in time (figure 14 Right). When correlated to the performance of the catalyst over both operational periods (figure 13), in addition to the relative performance of the catalyst in both solvents at one fixed point in time (figure 14), it is clear that only two of the changes correlate to loss of activity. These include the change of intensity in the high energy region (decrease at 223 nm, increase at 260 nm, shown to be due to methanol in the solvent) and the decrease in intensity between 350 and 400 nm. Crucially, the absence of water is essential for these spectral changes to occur, and each change occurs at similar time periods of the reaction in MeOH.

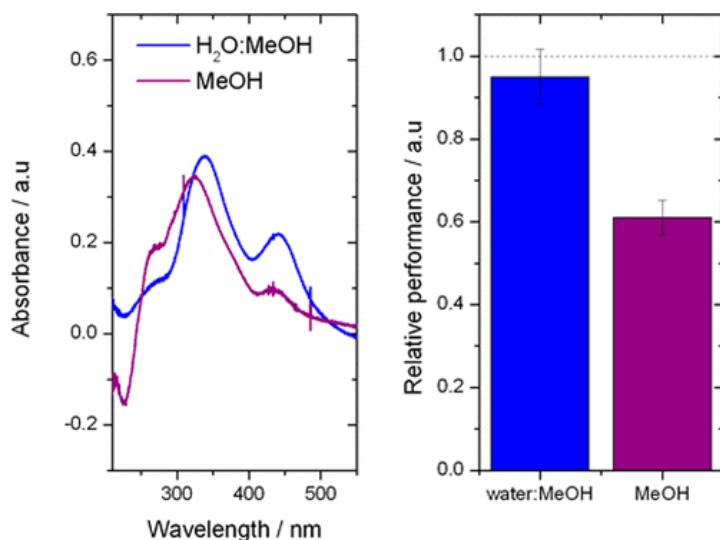


Figure 14. (Left) Difference UV-Vis spectra of 10Sn-Beta during GI in MeOH and MeOH: H₂O at 25 h on stream, and (Right) relative performance of 10Sn- β for GI in MeOH and MeOH: H₂O at 25 h. Experimental details: 1 % wt. Glucose in MeOH or MeOH:H₂O 90:10, 110 °C, 10 bar, 100 mg of 10Sn-Beta, 0.65 mL min⁻¹ of flow.

As control studies indicate that the changes in the high energy region arise from interaction of the catalyst with pure methanol (figure 12), the ability of the solvent alone to diminish the activity of 10Sn-Beta was investigated. To do so, GI was performed after solvothermally treating 10Sn-Beta in pure methanol for 24 h prior to operation (i.e., glucose was introduced into the feed after treating the catalyst in methanol for 24 h at 110 °C and 10 bar of backpressure). As can be seen in figure 15, the starting conversion obtained after treating the catalyst in methanol for 24 h (18 %) matches the conversion value observed after continuous operation of the catalyst during a standard reaction over the same period of time, even though no glucose has passed over the catalyst during the first 24 h. This strongly indicates that changes occurring to 10Sn-Beta due to the solvent, and not factors related to the presence of substrate, are the primary reasons for catalyst deactivation.

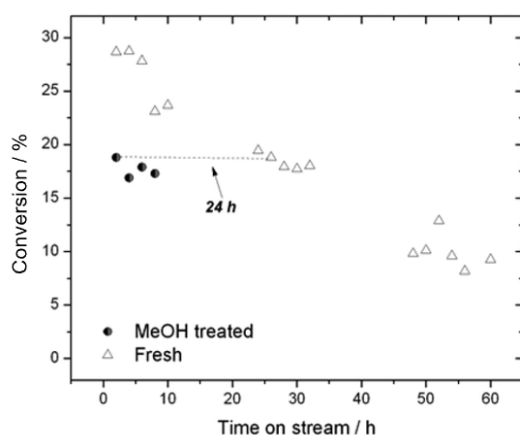


Figure 15. Catalytic performance of 10Sn-Beta for GI in MeOH as a fresh catalyst (open triangles) and after a 24-h pretreatment period in methanol (black circles). Experimental details: 1 % wt. Glucose in methanol, 110 °C, 10 bar, 100 mg of 10Sn-Beta, 0.65 mL min⁻¹ of flow. Pre-treatment carried out in the same condition without glucose.

The high energy region of the UV–Vis spectra is related to the ligand-to-metal charge transfer (LMCT) bands of the Sn^{4+} sites of the catalyst.^{33,36} Hence, changes in this spectral region relate to changes to the coordination sphere of Sn^{4+} , possibly through ligand exchange, and/or changes in its speciation, such as its agglomeration into oxidic particles. Thus, to better understand the changes that occur to the Sn sites of the zeolite during operation, ^{119}Sn MAS NMR experiments were performed on the fresh and used catalytic materials.^{37,38} In line with recent developments, spectra were recorded by Carr–Purcell–Meiboom–Gill (CPMG) echo-train acquisition methods, as exemplified by the Ivanova group.^{21,21} Due to the signal enhancements made possibly by CPMG methods, spectra could be recorded on materials containing naturally abundant quantities of Sn. All “ex reactor” samples were measured without prior heat treatment, in order to preserve integrity of the samples following operation and were thus compared to fresh samples also in their hydrated forms. Figure 16 Left presents the direct excitation CPMG (DE-CPMG) ^{119}Sn MAS NMR spectrum of 10Sn-Beta prior to reaction (a), and following 50 h of reaction in MeOH (b) and MeOH:H₂O 90:10 (c). Given differences in t_1 relaxation times, precise quantification of the percentage of each species is not possible. However, systematic comparison prior to, and following reaction, still allows a (semi)-quantitative insight of the changes in speciation that occur, provided identical acquisition methods are employed.

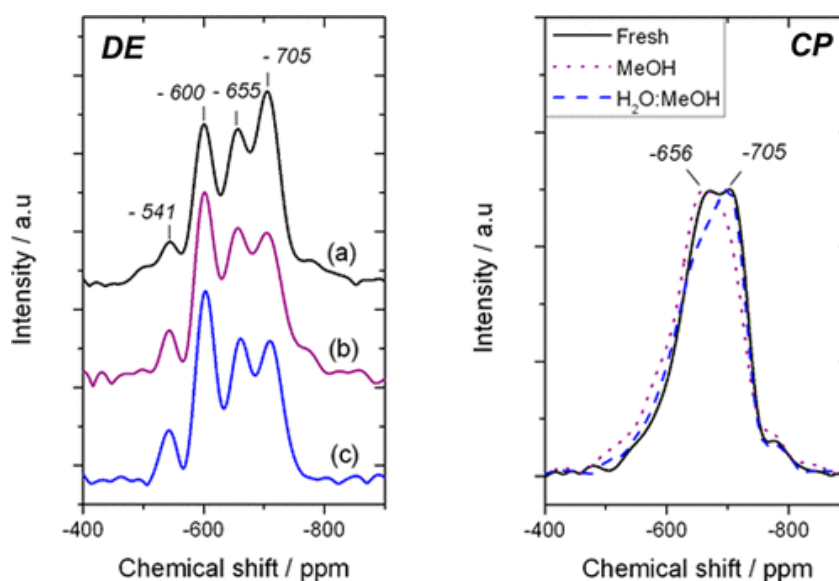


Figure 16. (Left) ^{119}Sn DE-CPMG MAS NMR spectra of 10Sn-Beta prior to (a) and following reaction in MeOH (b) and MeOH:H₂O 90:10 (c). (Right) ^{119}Sn CP-CPMG MAS NMR spectra of 10Sn-Beta prior to and following reaction in MeOH and MeOH:H₂O 90:10.

In figure 16 four dominant resonances are observed in the fresh catalyst, at chemical shifts of -705, -655, -600, and -541 ppm. The presence of multiple signals indicates the presence of multiple Sn species, as a consequence of the high Sn loading of the sample (10 % wt. Sn). In fact, the signals at -541 and -600 ppm are indicative of pentacoordinated

Sn and extra-framework (inactive) SnOx species, respectively,^{18,39,40} which have previously demonstrated to be spectators during catalytic operation.¹⁷ As further evidence of this, is it possible to refer to table 1, which demonstrate the same kinetic phenomena in the presence of water is observed irrespective of the loading of Sn employed. In addition to these signals, two major resonances at -655 and -705 ppm are also observed. Resonances at these chemical shifts are typically assigned to the framework Sn sites of the catalyst in their hydrated form (i.e., octahedral, framework Sn sites).³⁹⁻⁴¹ However, as the precise chemical shift of these species depends on multiple factors, including T-site occupation, degree of Sn, the number and type of proximal defects, and the exact method of analysis, both resonances are simplistically treated as one type of site, that being octahedrally coordinated framework Sn⁴⁺ sites in a hydrated state. Notably, analysis of 1Sn-Beta zeolite, possessing only 1 % wt. Sn but exhibiting a 2-fold higher turnover frequency (i.e., activity per gram of Sn) indicates that the species responsible for the signal at -705 ppm is likely the most important site, as the relative intensity of this signal dominates at lower loadings when the highest levels of TOF are obtained (figure 17).

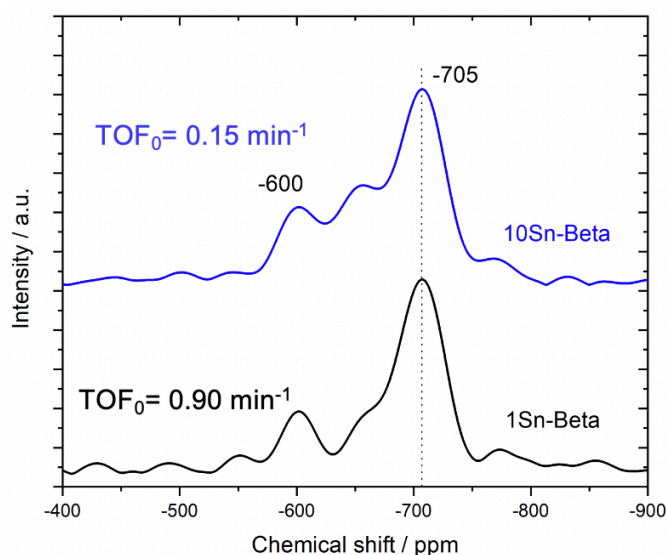


Figure 17. ¹¹⁹Sn DE-CPMG MAS NMR spectra of 1Sn-Beta (black) and 10Sn-Beta (blue).

Following continuous operation in MeOH (b) and MeOH:H₂O 90:10 (c), only minor changes to the Sn sites are observed by DE-CPMG (Left). Most notable among these is the relative growth in intensity for the -600 ppm signal, and a small increase in the relative ratio of the -655 to the -705 ppm signal. These indicate the formation of some additional, inactive, SnOx sites, in addition to minor modification to the T sites of the catalyst, respectively.⁴² Although it is not possible to quantify the extent of this restructuring within each particular sample (*vide supra*), it is evident that these changes are almost identical in both systems, despite the dramatic differences in relative activity after 50–60 h on stream. Hence, these changes are unlikely to correlate to decreased performance, which is much more dramatic when the reaction was performed in pure MeOH. This also indicates that the formation of

extra-framework SnOx is not the only reason behind the increase in absorption at 260 nm during continuous operation in MeOH (figure 14), as this absorption signal does not form during continuous operation in MeOH:H₂O 90:10 despite a similar amount of SnOx forming during this reaction. Taken together, DE-CPMG indicates that the same types of Sn species are mainly present in the catalytic material after reaction regardless of the choice of solvent. This rules out dramatic changes to the Sn site speciation as being the primary reason for deactivation.

In contrast, clear differences in both *ex reactor* samples could be identified when cross-polarization (¹H–¹¹⁹Sn, CP-CPMG) methods were employed (figure 16 Right). In the fresh sample, both signals between –655 and –700 ppm are clearly amenable to cross-polarization, indicating both Sn species have protons in their vicinity. However, a clear decrease in the signal at –705 ppm is observed following reaction in pure methanol. This indicates that the proton(s) in the vicinity of this particular Sn species are lost during reaction. Notably, this effect only occurs when water is absent, as the –705 ppm signal remains present following reaction in MeOH:H₂O 90:10, where very little deactivation is observed. Considering that the relative ratio between the –655 and –705 ppm signals does not change dramatically following both reactions, as evidenced by DE-CPMG, complementary CP-CPMG studies indicate that it is the environment that surrounds the Sn sites that changes in the absence of water. As the –705 ppm signal is dominant at lower loadings (figure 17), when the highest levels of intrinsic activity are observed, changes to the environment of this species are likely to lead to consequences for kinetic performance. According to previous studies, the formation of Sn–OH species following interaction of Sn-Beta with water is also accompanied by the formation of Si–OH groups, particularly at the reaction temperatures employed in this study.⁴³ In good agreement to this, it is notable that both the fresh catalyst and the sample following reaction in H₂O:MeOH exhibit Q3 resonances (–103 ppm) in the ²⁹Si MAS NMR spectra, indicating the presence of Si–OH groups (figure 18).⁴⁴ However, a much lower signal at this chemical shift was observed in the used sample obtained after reaction in MeOH. The absence of this signal indicates that the absence of water also permits the loss of Si–OH to occur, that can be possibly accompanied by a loss in Sn–OH. Given that the loss of these protons is only observed following substantial deactivation of the catalyst in pure methanol, it is clear that keeping hydration in the active site environment by maintaining the presence of some water is essential for stability to be maintained. Considering water is known to more readily adsorb to Sn-Beta compared to other substrates, such as NH₃, alcohols, and acetonitrile,⁴⁵⁻⁴⁷ this may account for the positive effect of water even when present at low levels (1 % wt.).

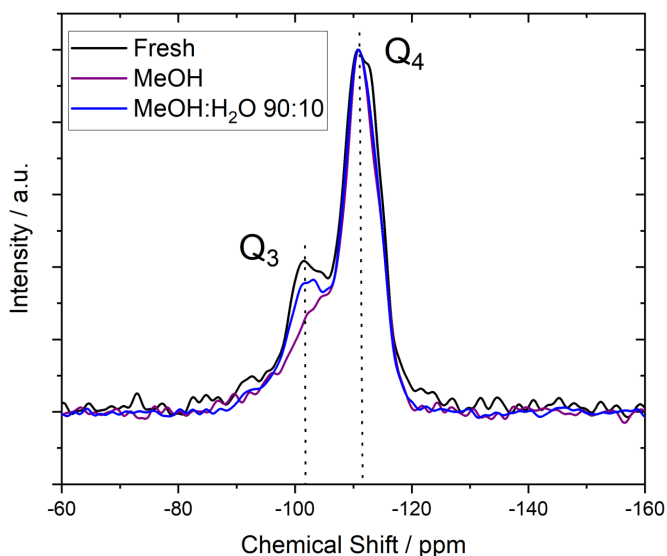


Figure 18. ^{29}Si MAS NMR of 10Sn-Beta zeolite, prior to reaction, and following GI in MeOH and MeOH:H₂O 90:10.

The loss of Si–OH and/or Sn–OH protons could be attributed to ligand exchange at the active site (i.e., the displacement of coordinated water for methanol and/or alkoxylation of a putative Sn–OH bond with methanol) or alternatively to (re)condensation of the structure, with the (re)formation of Sn–O–Si bonds. Although no concrete methodologies for identifying Sn–OH exist, and hence direct differentiation of these pathways is not feasible, spectroscopic studies with DRIFTS reveal the formation of metal-alkoxylates to be at least partially responsible for the loss of signal. In figure 19 Left is shown the “*in situ*” DRIFT methanol absorption over 2Sn-Beta zeolite. A lower loaded catalyst was chosen instead of 10Sn-Beta zeolite since the significant amount of tin oxide present in this material can contribute to the spectra, and hence compromises the clarity of the characterisation. In this experiment methanol was flushed over the catalyst which was heated at 110 °C to simulate at the best the conditions of reaction. figure 19 Left presents the spectrum of the fresh zeolite in black, whereas in the purple lines are shown the spectra of the zeolite flushed with methanol for 10 and 20 minutes.

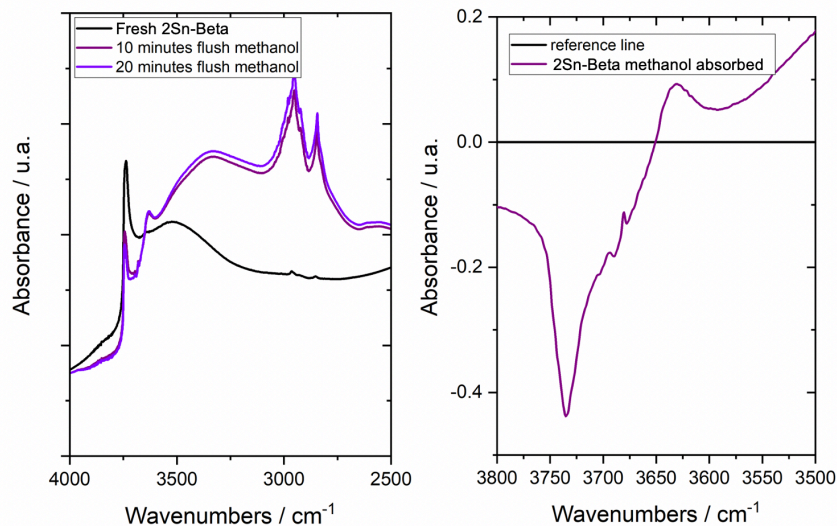


Figure 19. (Left) “*in situ*” methanol dosing DRIFT of 2Sn-Beta zeolite. (Right) differential spectrum magnified in the high energy region of the graph.

This experiment clearly shows that once 2Sn-Beta enters in contact with methanol, the signal related to the Si-OH bond at 3735 cm^{-1} decreases in intensity, meanwhile at 3630 cm^{-1} a new peak arises due to the interaction between methanol and the catalyst. On the right of figure 19 is shown the differential graph between the catalyst flushed with methanol and the fresh 2Sn-Beta zeolite. This figure clearly shows the loss in intensity of the peak at 3735 cm^{-1} , as a negative signal, and the appearing of the signal at 3630 cm^{-1} , as a positive feature. The same experiment was then performed flushing different alcohols on 2Sn-Beta and on its dealuminated precursor. The results in figure 20 Left show how the wavenumber of the new feature arising at 3630 cm^{-1} shifts to lower energy when the alcohol used in the dosing increases in molecular weight. Moreover, a shift of 6 cm^{-1} is always present between the spectrum gathered from 2Sn-Beta and the dealuminated Beta zeolite. This implies that this new feature is present also when Sn is not incorporated in the material, but when Sn is added it somehow bring a contribution to this signal. On the right of figure 20 is plotted the wavenumber of the new vibrational signal against the molecular weight of the alcohol from which it is generated. It is possible to notice that is present a linear proportion between the reduced mass of the alcohols and the frequency of the new signals; implying so that the alcohols is directly involved in the formation of this new feature.

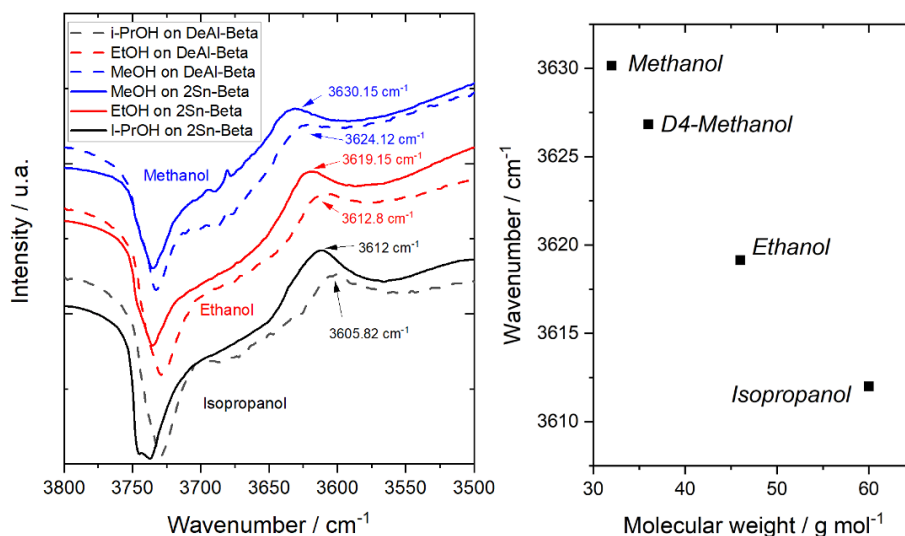


Figure 20. (Left) Differential DRIFTS spectra of 2Sn-Beta and dealuminated Beta following the adsorption of various probe molecules at 110 °C. (Right) Influence of molecular weight of the R-OH probe on the final vibrational wavenumber of the new vibration.

Therefore, from these analyses it is clear that after treating 2Sn-Beta in alcohols at 110 °C a bond involving Sn and the alcohols is present. Whereas this observation does not rule out a contribution from framework condensation (Sn-O-Si formation) during the reaction, it clearly indicates that the formation of Sn-alkoxy species is at least partly responsible for the loss of Sn-OH and Si-OH species. The formation of such alkoxy species were previously hypothesized by the group of Roman-Leshkov, during their study focused on the transfer hydrogenation and etherification of carbonyl compounds.^{8,48} Notably, flushing the DRIFTS cell with water following formation of the Sn-alkoxy species results in its removal from the DRIFTS spectrum, even when a large amount of physisorbed methanol was still present in the sample as evidenced by the C-H stretches present at 3000-2800 cm^{-1} (figure 21). These observations indicate both the reversibility of alkoxy formation and the preferential binding of water over methanol.

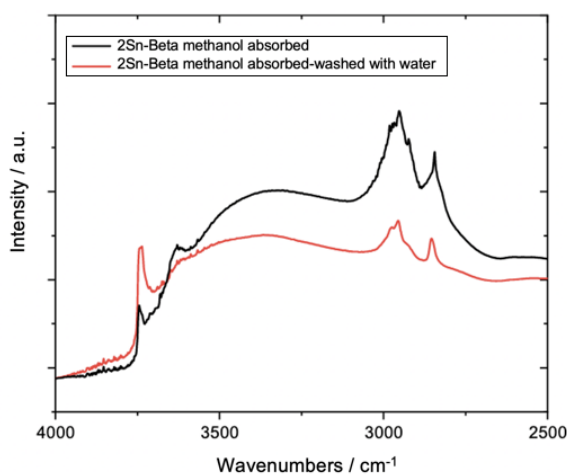


Figure 21. DRIFTS spectra of 2Sn-Beta after dosing with methanol at 110 °C (black line) and following dosing of the methanol saturated sample with water (red line).

2.3.4 Kinetic Confirmation of Active Site Hydration Effects

Operando UV–Vis, ^{119}Sn CPMG MAS NMR, ^{29}Si MAS NMR, and DRIFTS studies indicate that deactivation of the catalyst in the absence of water is accompanied by the loss of Sn–OH and Si–OH species, at least partly due to ligand exchange at the active site. The loss of these sites could lead to deactivation through two distinct means. First, maintaining hydration at the active site and its vicinity may simply favour the transportation of sugars to and from the active site (transport hypothesis). An alternative role of hydration may be the stabilization of a more intrinsically active Sn site (kinetic hypothesis). For example, several studies have reported that the open form of Sn-Beta, where one or more Sn–OH and Si–OH bonds are present due to partial hydrolysis of the framework, is the most active form of the catalyst.⁴⁹ In fact, theoretical studies have hypothesized that the temperature dependence of Sn-Beta increases by approximately 30 kJ mol^{-1} when the site is fully closed, due to the loss of proximal Si–OH species that can contribute to H-bonding of the substrate.⁵⁰

To conclusively differentiate between the kinetic and transport hypotheses, an additional series of kinetic experiments focused on determining the temperature dependence of the catalyst at various stages of deactivation was performed. If the system becomes limited by the uptake of glucose, the reaction should exhibit very low temperature dependence indicative of transport limitations after interaction with methanol. In contrast, the formation of a less catalytically active Sn site should result in an increment in the temperature dependence of the system, relative to the fresh catalyst. Finally, no change in the temperature dependence of the system would simply indicate that the same active sites are present, but that their concentration is lower, due to the formation of inactive (spectator) Sn species. Figure 22 Left, presents the effective temperature dependence of the fresh catalyst and that of the catalyst following solvothermal treatment in methanol for 24 h. As can be seen, following pretreatment of the sample in pure methanol for 24 h, which induces approximately 35 % deactivation (figure 15), the apparent temperature dependence of the reaction increases substantially, from 39 to 67 kJ mol^{-1} (figure 22 Left). The increase calculated from experiment (28 kJ mol^{-1}) is in excellent agreement to the increase predicted from theory to occur following the loss of cooperating Sn–OH and Si–OH sites, further indicating the loss of hydrated active sites.³¹

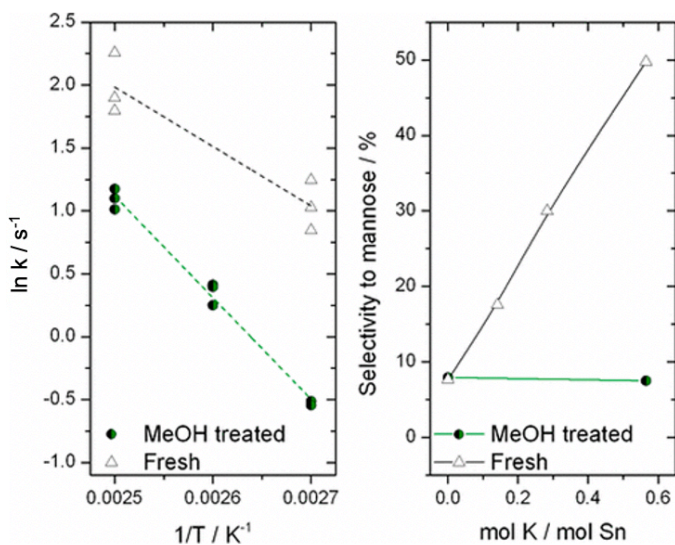


Figure 22 (Left) Apparent temperature dependence of fresh 10Sn-Beta and 10Sn-Beta pretreated in pure methanol for 24 h prior to operation. A contact time of 0.19 min was employed throughout both experiments, and temperatures of 100, 110, and 120 °C were used. (Right) Influence of K_2CO_3 on the selectivity to mannose (epimerization product) during GI at 110 °C in pure methanol. 10Sn-Beta and 10 Sn-Beta pretreated in pure methanol for 24 h prior to operation were used as catalysts. Reaction conditions: 1 % wt. glucose 110 °C, 900 rpm, glucose/Sn molar ratio of 50.

To further verify the hypothesis that it is the loss of Si–OH and Sn–OH that results in diminished performance, the influence of alkali exchange was examined (figure 22 Right). Indeed, several experimental studies have demonstrated that ion-exchange of Sn-Beta zeolite with alkali salts can dramatically impact its selectivity performance. For GI, ion exchange has been shown to result in switch in reaction selectivity, with epimerization to mannose dominating in the presence of alkali metals, as opposed to the classical isomerization to fructose in the absence of such additives.^{51,52} Likewise, ion exchange at these positions during methyl lactate production results in an increased selectivity to retroaldol product formation.^{7,28} As can be seen in figure 22 Right, whereas the presence of K_2CO_3 results in a dramatic increase in mannose selectivity for the fresh catalyst, the methanol-treated sample is not modified by the presence of alkali (table 3). This strongly indicates the absence of ion-exchangeable Si–OH and Sn–OH species following partial deactivation of the catalyst, in excellent agreement to the spectroscopic and kinetic evidence.

Table 3 Influence of alkali on the selectivity of selectivity of fresh and methanol treated 10 Sn-Beta during glucose fructose isomerisation

Catalyst	mol K/mol Sn	X _(GLU) / %	Y _(FRU) / %	Y _(MAN) /%
Fresh 10Sn-Beta	0	20.2	14.8	1.4
	0.141	18.5	10.8	2.9
	0.283	18.0	8.4	5.4
	0.565	21.5	4.5	10.7
MeOH treated 10Sn-Beta	0	23.9	15.8	1.9
	0.565	25.3	15.5	1.9

2.3.5 Regeneration studies

From the spectroscopic and kinetic experiments presented above, it is clear that deactivation of the catalyst relates to the loss of Sn–OH and Si–OH species in the absence of water. Considering that dissociative adsorption of water, and the concurrent formation of Sn–OH and Si–OH species, is reportedly rapid when Sn-Beta is exposed to water,⁴³ it was hypothesized that activity should be restored in deactivated samples through simple solvothermal treatment of the sample (low temperature regeneration). According to this hypothesis, the loss of Si–OH and Sn–OH should be reversible by reintroducing water into the feed, without the need for classical high-temperature thermal treatment being performed. To probe this, a variety of washing protocols on partially deactivated samples of 10Sn-Beta were performed, following an initial cycle of GI in methanol for 60 h. As can be seen in figure 23, solvothermally treating a partially deactivated sample of 10Sn-Beta allows initial catalytic activity to be fully restored. Interestingly, the regeneration is sensitive to the solvent of choice, in addition to the time of treatment (12 h vs 20 h). Indeed, whereas a solution of MeOH:H₂O is able to fully restore catalytic activity within 20 h, employing methanol alone results in no recovery being achieved. This is in agreement to the conclusion that it is methanol that is the primary cause of deactivation. Interestingly, when water alone is employed as wash solution, no regeneration is observed, even when the time of treatment is adjusted so that the same total quantity of water is flowed over the partially deactivated catalyst (2 h versus 20 h). This clearly emphasizes the need to optimize the concentration of water in order to balance active site recovery against leaching of active site to SnO_x, which is known to occur in bulk water at these temperatures (figure 7).

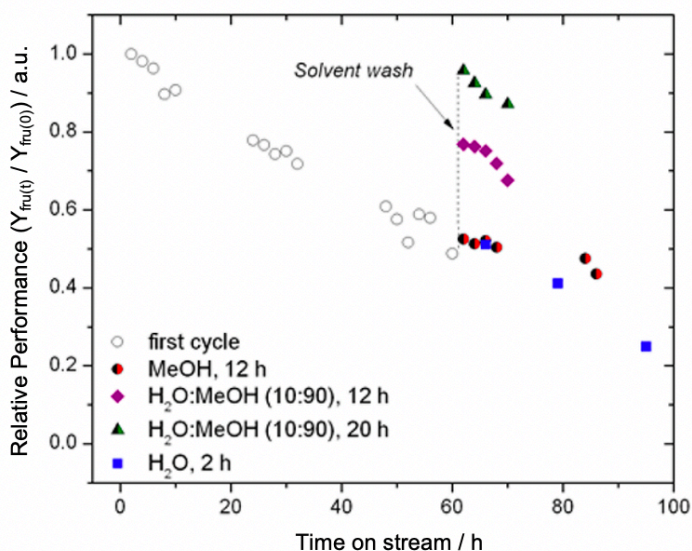


Figure 23. Low temperature, solvothermal regeneration of Sn-Beta, following an initial cycle of GI in pure methanol. Second cycles were also performed in pure methanol. Experimental details: 1 % wt. Glucose in methanol, 110 °C, 10 bar, 100 mg of 10Sn-Beta, 0.65 mL min⁻¹ of flow. Solvothermal regeneration was carried out in the same conditions feeding the reactor with a MeOH:H₂O 90:10.

To gain a better understanding of the regeneration process, and hence to gain additional indirect insight regarding the mechanism(s) of deactivation, spectroscopic studies of the catalyst following regeneration were performed (table 4). Porosimetry revealed that washing the sample in MeOH:H₂O 90:10 restored a large fraction of pore volume, indicating removal of the carbonaceous residue. This is in good agreement with the observation that the presence of water in the feed results in decreased retention of residue (figure 9, Table 2). Notably, although regeneration of the catalyst does not occur by treating the sample in MeOH alone, a large fraction of the lost pore volume is still recovered by this treatment. The fact that carbonaceous residue is removed without regeneration being observed further indicates that the accumulation of such residue, and pore fouling in general, is not the primary cause of deactivation and that the removal of such residue is not the primary role of water.

Table 4 Porosimetry Data for Various Sn-Beta Catalysts Prior to and Following Solvothermal Regeneration

Catalyst	V _{micro} (cm ³ g ⁻¹)	Activity (%)
Fresh 10Sn-Beta pellet	0.226	100
10Sn-Beta, used in MeOH 50h	0.178	48
Used 10Sn-Beta, after washing in MeOH:H ₂ O 90:10	0.218	90
Used 10Sn-Beta, after washing in MeOH	0.198	54

Porosity data determined by N₂ isotherms and micropore volume (V_{micro}) derived from the t-plot method. Activity is calculated by calculating the percentage of conversion lost keeping as benchmark fresh 10Sn-Beta pellet.

To verify whether solvothermal regeneration of the catalyst results in restoration of the hydrated state of the catalyst, additional ¹¹⁹Sn CP-CPMG MAS NMR and UV-Vis measurements on the regenerated sample were performed (figure 24). As can be seen, regeneration of the sample by flushing in MeOH:H₂O 90:10 results in regeneration of both the signal at -705 ppm in the ¹¹⁹Sn CP-CPMG MAS NMR spectrum, in addition to reversal of the high energy changes in the UV-Vis spectra, both of which correlate to decreased kinetic performance. The ability to regenerate the catalyst without resorting to classical high-temperature (>550 °C) thermal treatment also represents a major breakthrough, as solvothermal treatment of the catalyst means the reactor does not need to be drained prior to regeneration, reduces overall energy input, and negates the requirement for high-temperature heating provision.

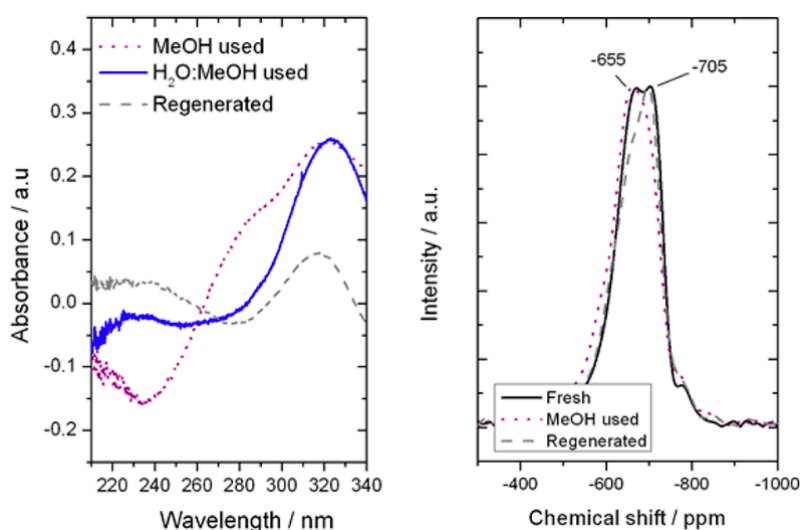


Figure 24. (Left) UV-Vis of 10Sn-Beta deactivated in MeOH (purple dotted line), 10Sn-Beta deactivated in MeOH:H₂O 90:10 (blue solid line), and following regeneration of 10Sn-Beta in H₂O:MeOH (gray dashed line). (Right) ¹¹⁹Sn CP-CPMG MAS NMR spectra of fresh 10Sn-Beta prior to (black) and following reaction in pure methanol (purple), and following regeneration in MeOH:H₂O (grey).

2.4 Conclusion

Based on this, continuous operation for up to 1500 h was achieved for the conversion of fructose to methyl lactate and the activity of Sn-Beta was improved by a factor of 10. Alongside the improvement in stability the adding of water increases the solubility of sugar in the reaction media leading to a potential improvement of the productivity of the process. Furthermore, the mechanistic study of Sn-Beta deactivation in pure methanol clarified the cause of the deactivation of this material in pure methanol. By *operando* UV-Vis, MAS NMR, TGA, porosimetry and TPO-MS, it is revealed that deactivation is accompanied by condensation and/or alkoxylation of the active sites, resulting in loss of Si-OH and Sn-OH sites. Activity can be maintained either by addition of water to the feed (between 1-10 % wt.), or can be restored following reaction by re-hydrating the active sites. In particular, this information allowed to design a new protocol for the regeneration of Sn-Beta zeolite after reaction in methanol. This protocol proceeds through the solvothermal washing of the catalyst in MeOH:H₂O for 20 h at 110 °C. These conditions are less energetic demanding than the classic regeneration protocols, which typically exploit high temperature (>500 °C) treatment in air. Moreover, this regeneration method can be carried out *in situ* without extracting the catalyst from the reactor saving operational time on a hypothetical plant.

These whole findings boosted the performance of the processes carried out from Sn-Beta in continuous showing how there is a big potential unexplored in this area of research.

Although the results are promising, more work is required to understand how to improve not only the stability but also the selectivity of the process through a more advanced catalyst design that may be able to optimise the active sites present to achieve a more efficient process for biomass conversion. On this topic the analysis of different preparations of Sn-Beta will need to be tested in these conditions to ascertain which kind of catalyst preparations reported in Chapter 1 (1.13) is yielding to the best material for continuous processing.

2.5 Reference

- (1) Delidovich, I.; Leonhard, K.; Palkovits, R. Cellulose and Hemicellulose Valorisation: An Integrated Challenge of Catalysis and Reaction Engineering. *Energy Environ. Sci.* 2014, 7 (9), 2803.
- (2) Zhang, X.; Wilson, K.; Lee, A. F. Heterogeneously Catalyzed Hydrothermal Processing of C5-C6 Sugars. *Chem. Rev.* 2016, 116 (19), 12328–12368
- (3) Ennaert, T.; Van Aelst, J.; Dijkmans, J.; De Clercq, R.; Schutyser, W.; Dusselier, M.; Verboekend, D.; Sels, B. F. Potential and Challenges of Zeolite Chemistry in the Catalytic Conversion of Biomass. *Chem. Soc. Rev.* 2016, 45 (3), 584–611.
- (4) Vennestrøm, P. N. R.; Osmundsen, C. M.; Christensen, C. H.; Taarning, E. Beyond Petrochemicals: The Renewable Chemicals Industry. *Angew. Chemie - Int. Ed.* 2011, 50 (45), 10502–10509.
- (5) Luo, H. Y.; Lewis, J. D.; Román-Leshkov, Y. Lewis Acid Zeolites for Biomass Conversion: Perspectives and Challenges on Reactivity, Synthesis, and Stability. *Annu. Rev. Chem. Biomol. Eng.* 2016, 7 (1), 663–692.
- (6) Moliner, M.; Roman-Leshkov, Y.; Davis, M. E. Tin-Containing Zeolites Are Highly Active Catalysts for the Isomerization of Glucose in Water. *Proc. Natl. Acad. Sci.* 2010, 107 (14), 6164–6168.
- (7) Tolborg, S.; Meier, S.; Sádaba, I.; Elliot, S. G.; Kristensen, S. K.; Saravanamurugan, S.; Riisager, A.; Fristrup, P.; Skrydstrup, T.; Taarning, E. Tin-Containing Silicates: Identification of a Glycolytic Pathway via 3-Deoxyglucosone. *Green Chem.* 2016, 18 (11), 3360–3369.
- (8) Lari, G. M.; Dapsens, P. Y.; Scholz, D.; Mitchell, S.; Mondelli, C.; Pérez-Ramírez, J. Deactivation Mechanisms of Tin-Zeolites in Biomass Conversions. *Green Chem.* 2016, 18 (5), 1249–1260.
- (9) Lewis, J. D.; Van De Vyver, S.; Crisci, A. J.; Gunther, W. R.; Michaelis, V. K.; Griffin, R. G.; Román-Leshkov, Y. A Continuous Flow Strategy for the Coupled Transfer Hydrogenation and Etherification of 5-(Hydroxymethyl)Furfural Using Lewis Acid Zeolites. *ChemSusChem* 2014, 7 (8), 2255–2265.
- (10) Hammond, C. Intensification Studies of Heterogeneous Catalysts: Probing and Overcoming Catalyst Deactivation during Liquid Phase Operation. *Green Chem.* 2017, 19 (12), 2711–2728.
- (11) Padovan, D.; Parsons, C.; Simplicio Grasina, M.; Hammond, C. Intensification and Deactivation of Sn-Beta Investigated in the Continuous Regime. *Green Chem.* 2016, 18 (18), 5041–5049.
- (12) Yakabi, K.; Milne, K.; Buchard, A.; Hammond, C. Selectivity and Lifetime Effects in Zeolite-Catalysed Baeyer-Villiger Oxidation Investigated in Batch and Continuous Flow. *ChemCatChem* 2016, 8 (22), 3490–3498.
- (13) Hartman, R. L.; McMullen, J. P.; Jensen, K. F. Deciding Whether to Go with the Flow: Evaluating the Merits of Flow Reactors for Synthesis. *Angew. Chemie - Int. Ed.* 2011, 50 (33), 7502–7519.
- (14) Holm, M. S.; Saravanamurugan, S.; Taarning, E. Conversion of Sugars to Lactic Acid Derivatives Using Heterogeneous Zeolite Catalysts. *Science.* 2010, 328 (5978), 602–605.
- (15) Vink, E. T. H.; Rábago, K. R.; Glassner, D. A.; Gruber, P. R. Applications of Life Cycle Assessment to NatureWorks™ Polylactide (PLA) Production. *Polym. Degrad. Stab.* 2003, 80 (3), 403–419.
- (16) Dai, Y.; King, C. J. Selectivity between Lactic Acid and Glucose during Recovery of Lactic Acid with Basic Extractants and Polymeric Sorbents. *Ind. Eng. Chem. Res.* 1996, 35 (4), 1215–1224.

- (17) Lima, D. M.; Fernandes, P.; Nascimento, D. S.; Cássia, R. De; Ribeiro, L. F.; Assis, S. A. De. Fructose Syrup : A Biotechnology Asset. 2011, 9862 (4), 424–434.
- (18) Padovan, D.; Botti, L.; Hammond, C. Active Site Hydration Governs the Stability of Sn-Beta during Continuous Glucose Conversion. *ACS Catal.* 2018, 8, 7131–7140.
- (19) Hammond, C.; Padovan, D.; Al-Nayili, A.; Wells, P. P.; Gibson, E. K.; Dimitratos, N. Identification of Active and Spectator Sn Sites in Sn- β Following Solid-State Stannation, and Consequences for Lewis Acid Catalysis. *ChemCatChem* 2015, 7 (20), 3322–3331.
- (20) Yakimov, A. V.; Kolyagin, Y. G.; Tolborg, S.; Vennestrøm, P. N. R.; Ivanova, I. I. ^{119}Sn MAS NMR Study of the Interaction of Probe Molecules with Sn-BEA: The Origin of Penta- and Hexacoordinated Tin Formation. *J. Phys. Chem. C* 2016, 120 (49), 28083–28092.
- (21) Kolyagin, Y. G.; Yakimov, A. V.; Tolborg, S.; Vennestrøm, P. N. R.; Ivanova, I. I. Application Of ^{119}Sn CPMG MAS NMR for Fast Characterization of Sn Sites in Zeolites with Natural ^{119}Sn Isotope Abundance. *J. Phys. Chem. Lett.* 2016, 7 (7), 1249–1253.
- (22) Moliner, M.; Román-Leshkov, Y.; Davis, M. E. Tin-Containing Zeolites Are Highly Active Catalysts for the Isomerization of Glucose in Water. *Proc. Natl. Acad. Sci. U. S. A.* 2010, 107 (14), 6164–6168.
- (23) Padovan, D.; Parsons, C.; Simplicio Grasina, M.; Hammond, C. Intensification and Deactivation of Sn-Beta Investigated in the Continuous Regime. *Green Chem.* 2016, 18 (18), 5041–5049.
- (24) Osmundsen, C. M.; Spangsberg Holm, M.; Dahl, S.; Taarning, E. Tin-Containing Silicates: Structure-Activity Relations. *Proc. R. Soc. A Math. Phys. Eng. Sci.* 2012, 468 (2143), 2000–2016.
- (25) Takasaki, Y. Kinetic and Equilibrium Studies on D-Glucose-d-Fructose Isomerization Catalyzed by Glucose Isomerase from *Streptomyces* Sp. *Agric. Biol. Chem.* 1967, 31 (3), 309–313.
- (26) Levenspiel, O. *Chemical Reaction Engineering*; 1999; Vol. 38.
- (27) Dusselier, M.; De Clercq, R.; Cornelis, R.; Sels, B. F. Tin Triflate-Catalyzed Conversion of Cellulose to Valuable (α -Hydroxy-) Esters. *Catal. Today* 2017, 279, 339–344.
- (28) Tolborg, S.; Sádaba, I.; Osmundsen, C. M.; Fristrup, P.; Holm, M. S.; Taarning, E. Tin-Containing Silicates: Alkali Salts Improve Methyl Lactate Yield from Sugars. *ChemSusChem* 2015, 8 (4), 613–617.
- (29) Al-Nayili, A.; Yakabi, K.; Hammond, C. Hierarchically Porous BEA Stannosilicates as Unique Catalysts for Bulky Ketone Conversion and Continuous Operation. *J. Mater. Chem. A* 2015, 00, 1–10.
- (30) Sádaba, I.; López Granados, M.; Riisager, A.; Taarning, E. Deactivation of Solid Catalysts in Liquid Media: The Case of Leaching of Active Sites in Biomass Conversion Reactions. *Green Chem.* 2015, 17 (8), 4133–4145.
- (31) Alaba, P. A.; Sani, Y. M.; Mohammed, I. Y.; Wan Daud, W. M. A. Insight into Catalyst Deactivation Mechanism and Suppression Techniques in Thermocatalytic Deoxygenation of Bio-Oil over Zeolites. *Rev. Chem. Eng.* 2016, 32 (1), 71–91.
- (32) Lange, J. P. Renewable Feedstocks: The Problem of Catalyst Deactivation and Its Mitigation. *Angew. Chemie - Int. Ed.* 2015, 54 (45), 13187–13197.
- (33) Lange, J. P. Renewable Feedstocks: The Problem of Catalyst Deactivation and Its Mitigation. *Angew. Chemie - Int. Ed.* 2015, 54 (45), 13187–13197.
- (34) Bañares, M. A. Operando Methodology: Combination of in Situ Spectroscopy and Simultaneous Activity Measurements under Catalytic Reaction Conditions. *Catal. Today* 2005, 100 (1–2), 71–77.

- (35) Chakrabarti, A.; Ford, M. E.; Gregory, D.; Hu, R.; Keturakis, C. J.; Lwin, S.; Tang, Y.; Yang, Z.; Zhu, M.; Banares, M. A.; et al. A Decade of Operando Spectroscopy Studies. *Catal. Today* 2017, 283, 27–53.
- (36) Ferrini, P.; Dijkmans, J.; De Clercq, R.; Van de Vyver, S.; Dusselier, M.; Jacobs, P. A.; Sels, B. F. Lewis Acid Catalysis on Single Site Sn Centers Incorporated into Silica Hosts. *Coord. Chem. Rev.* 2017, 343, 220–255.
- (37) Gunther, W. R.; Michaelis, V. K.; Caporini, M. A.; Griffin, R. G.; Román-Leshkov, Y. Dynamic Nuclear Polarization NMR Enables the Analysis of Sn-Beta Zeolite Prepared with Natural Abundance ^{119}Sn Precursors. *J. Am. Chem. Soc.* 2014, 136 (17), 6219–6222.
- (38) Hwang, S. J.; Gounder, R.; Bhawe, Y.; Orazov, M.; Bermejo-Deval, R.; Davis, M. E. Solid State NMR Characterization of Sn-Beta Zeolites That Catalyze Glucose Isomerization and Epimerization. *Top. Catal.* 2015, 58 (7–9), 435–440.
- (39) Wolf, P.; Valla, M.; Rossini, A. J.; Comas-Vives, A.; Núñez-Zarur, F.; Malaman, B.; Lesage, A.; Emsley, L.; Copéret, C.; Hermans, I. NMR Signatures of the Active Sites in Sn-Beta Zeolite. *Angew. Chemie - Int. Ed.* 2014, 53 (38), 10179–10183.
- (40) Wolf, P.; Liao, W. C.; Ong, T. C.; Valla, M.; Harris, J. W.; Gounder, R.; van der Graaff, W. N. P.; Pidko, E. A.; Hensen, E. J. M.; Ferrini, P.; et al. Identifying Sn Site Heterogeneities Prevalent Among Sn-Beta Zeolites. *Helv. Chim. Acta* 2016, 99 (12), 916–927.
- (41) Wolf, P.; Valla, M.; Núñez-Zarur, F.; Comas-Vives, A.; Rossini, A. J.; Firth, C.; Kallas, H.; Lesage, A.; Emsley, L.; Copéret, C.; et al. Correlating Synthetic Methods, Morphology, Atomic-Level Structure, and Catalytic Activity of Sn- β Catalysts. *ACS Catal.* 2016, 6 (7), 4047–4063.
- (42) Kolyagin, Y. G.; Yakimov, A. V.; Tolborg, S.; Vennestrøm, P. N. R.; Ivanova, I. I. Direct Observation of Tin in Different T-Sites of Sn-BEA by One- and Two-Dimensional ^{119}Sn MAS NMR Spectroscopy. *J. Phys. Chem. Lett.* 2018, 9 (13), 3738–3743.
- (43) Courtney, T. D.; Chang, C. C.; Gorte, R. J.; Lobo, R. F.; Fan, W.; Nikolakis, V. Effect of Water Treatment on Sn-BEA Zeolite: Origin of 960 cm^{-1} FTIR Peak. *Microporous Mesoporous Mater.* 2015, 210, 69–76.
- (44) Dijkmans, J.; Dusselier, M.; Janssens, W.; Trekels, M.; Vantomme, A.; Breynaert, E.; Kirschhock, C.; Sels, B. F. An Inner-/Outer-Sphere Stabilized Sn Active Site in β -Zeolite: Spectroscopic Evidence and Kinetic Consequences. *ACS Catal.* 2016, 6 (1), 31–46.
- (45) Kulkarni, B. S.; Krishnamurty, S.; Pal, S. Probing Lewis Acidity and Reactivity of Sn- and Ti-Beta Zeolite Using Industrially Important Moieties: A Periodic Density Functional Study. *J. Mol. Catal. A Chem.* 2010, 329 (1–2), 36–43.
- (46) Yang, G.; Pidko, E. A.; Hensen, E. J. M. Structure, Stability, and Lewis Acidity of Mono and Double Ti, Zr, and Sn Framework Substitutions in BEA Zeolites: A Periodic Density Functional Theory Study. *J. Phys. Chem. C* 2013, 117 (8), 3976–3986.
- (47) Van der Graaff, W. N. P.; Tempelman, C. H. L.; Li, G.; Mezari, B.; Kosinov, N.; Pidko, E. A.; Hensen, E. J. M. Competitive Adsorption of Substrate and Solvent in Sn-Beta Zeolite During Sugar Isomerization. *ChemSusChem* 2016, 9 (22), 3145–3149.
- (48) Moliner, M. State of the Art of Lewis Acid-Containing Zeolites: Lessons from Fine Chemistry to New Biomass Transformation Processes. *Dalt. Trans.* 2014, 43 (11), 4197–4208.

- (49) Boronat, M.; Concepción, P.; Corma, A.; Renz, M.; Valencia, S. Determination of the Catalytically Active Oxidation Lewis Acid Sites in Sn-Beta Zeolites , and Their Optimisation by the Combination of Theoretical and Experimental Studies. 2005, 234, 111–118.
- (50) Li, G.; Pidko, E. A.; Hensen, E. J. M. Synergy between Lewis Acid Sites and Hydroxyl Groups for the Isomerization of Glucose to Fructose over Sn-Containing Zeolites: A Theoretical Perspective. *Catal. Sci. Technol.* 2014, 4 (8), 2241–2250.
- (51) Bermejo-Deval, R.; Orazov, M.; Gounder, R.; Hwang, S. J.; Davis, M. E. Active Sites in Sn-Beta for Glucose Isomerization to Fructose and Epimerization to Mannose. *ACS Catal.* 2014, 4 (7), 2288–2297.
- (52) Li, S.; Josephson, T.; Vlachos, D. G.; Caratzoulas, S. The Origin of Selectivity in the Conversion of Glucose to Fructose and Mannose in Sn-BEA and Na-Exchanged Sn-BEA Zeolites. *J. Catal.* 2017, 355, 11–16.

Chapter 3

Influence of composition and preparation method on the continuous performance of Sn-Beta for glucose-fructose isomerisation

The content of this chapter was published in the following manuscripts:

Top. Catal. **2019**, 62 (17–20), 1178–1191.

3.1 Introduction

In the previous chapter (Chapter 2), it was shown how Sn-Beta zeolite has the potential to catalyse glucose upgrading in continuous flow, particularly as the stability of Sn-Beta could be successfully improved by adding small amounts (1-10 % wt.) of water in the feed of reaction. The stabilising effect of water was exploited successfully for two systems: the isomerisation of glucose to fructose (GI) and the upgrading of fructose to methyl-lactate (ML). Despite this important finding it was pointed out how the stability of Sn-Beta stability over continuous process is seriously compromised by its interaction with the reaction solvent (methanol), which leads to condensation and alkoxylation of the active sites.

As thoroughly showed in Chapter 1 (Section 1.13) several methodologies are known to produce Sn-Beta zeolite and high flexibility in terms of loading is achieved when synthesizing the material by post-synthetic preparation reaching up to 10 % wt. loaded Sn-Beta zeolites.¹⁻⁴ Hammond *et al.*¹ showed how increasing the loading of Sn-Beta through solid state incorporation synthesis (SSI) the TOF (equation 6 in the equation appendix) decreased drastically due to the formation of SnOx as non-active phase in the catalyst. Moreover Wolf *et al.*⁵ showed that throughout post-synthetic preparations not only SnOx are formed alongside the incorporation of Sn, but different speciation of Sn are detected, meaning that multiple active sites might be formed, which activity can be diverse as a function of its properties (hydration, T-sites, geometry...).⁵⁻⁷ Furthermore it is reported in the literature how hydrothermal and post-synthetic preparations of Sn-Beta zeolite are yielding different catalysts, with different level of stability⁸ and activity.⁹ In particular Gounder *et al.*¹⁰ showed how water has drastically different impact on the activation of different preparations of Sn-Beta. Although these studies have given essential insight on properties of different Sn-Beta preparations, the use of model reactions or not scalable conditions makes the impact of this works less relevant for industrial purposes. Therefore exploring the synthesis of different Sn-Beta zeolites through different preparations and compositions represents a potential way to produce a material intrinsically less sensitive to deactivation for the continuous transformation of glucose to relevant chemical commodities.⁸ Therefore in this chapter the influence of the loading of Sn in Sn-Beta zeolites synthesized by solid state

incorporation was studied, and this post synthetic route of synthesis was compared with the hydrothermal synthesis of Sn-Beta in order to understand how these two extremely different routes of synthesis might impact on the properties of the material.

These catalysts were tested for the continuous isomerisation of glucose to fructose at 110 °C and for the continuous glucose upgrading to methyl lactate (henceforth ML) carried out at 160 °C in pure methanol. Pure methanol was chosen as solvent to accelerate the rate of deactivation (accelerated ageing), so as to achieve fundamental insights into the stability of the catalysts in a more time efficient manner.¹¹ The results from these experiments were used to understand which of these preparations yield to the best catalyst from an activity and stability prospective. Structure-activity correlations were explored for these materials to rationalise the different kinetic behaviour shown by these catalysts.

3.2. Experimental details

3.2.1 Catalyst synthesis

Post synthetic Sn-Beta samples were prepared by SSI. Commercial Al-Beta (Zeolyst, NH_4^+ -form, $\text{Si}_2\text{O}/\text{Al}_2\text{O}_3 = 38$) was dealuminated by treatment in HNO_3 solution (13 M HNO_3 , 100 °C, 20 mL g^{-1} zeolite, 20h). SSI of dealuminated zeolite Beta was performed by grinding the appropriate amount of tin (II) acetate with the necessary amount of dealuminated zeolite for 10 min in a pestle and mortar. Following this procedure, the samples were heated in a combustion furnace (Carbolite MTF12/38/400) to 550 °C (10 °C min^{-1} ramp rate) first in a flow of N_2 (3 h) and subsequently air (3 h) for a total of 6 h. Gas flow rates of 60 mL min^{-1} were employed at all times.⁴

The hydrothermal synthesis of Sn-Beta was performed following a procedure described in literature in reference 12: 30.6 g of tetraethyl orthosilicate (TEOS) was added to 33.1 g of tetraethylammonium hydroxide (TEAOH) under careful stirring, forming a two-phase system. After 60–90 min, one phase was obtained and the desired amount of the tin source, typically $\text{SnCl}_4 \cdot 5\text{H}_2\text{O}$ dissolved in 2.0 mL of H_2O , was added dropwise. The solution was then left for 48 h under stirring until a viscous gel was formed. The gel was finalised by the addition of 3.1 g HF in 1.6 g of demineralized H_2O yielding a solid gel with the molar composition; 1.0Si: 0.005Sn: 0.02 Cl^{-1} : 0.55 TEA^+ : 0.55 F^{-1} : 7.5 H_2O . The obtained gel was transferred in a Teflon lined stainless steel autoclave and kept for 7 days at 140 °C to crystallise. The obtained crystals were filtered and washed with deionised water. Calcination at 550 °C (2 °C min^{-1}) for 6 h under static air was carried out in order to remove the organic template.

3.2.2 Catalyst characterisation

X-Ray Diffraction analyses were carried out by a PANalytical X'PertPRO X-ray. A $\text{CuK}\alpha$ radiation source (40 kV and 30 mA) was utilised. Diffraction patterns were recorded between 6–55° 2θ (step size 0.0167°, time/step = 150 s, total time = 1 h).

Specific surface area was determined from nitrogen adsorption using the BET equation, and microporous volume was determined from nitrogen adsorption isotherms using the t -plot

method. Porosimetry measurements were performed on a Quantachrome Quadrasorb, and samples were degassed prior to use (115 °C, 6 h, nitrogen flow). Adsorption isotherms were obtained at 77 K. The same instrument was employed for vapor absorption analysis. Samples were degassed as suggested above and the adsorption isotherms were obtained with vapours of methanol and water at 20 °C.

TPD-MS measurement were carried out on a home-made system formed by a Bruker Tensor II equipped with a Harrick praying mantis DRIFT cell connected with the MS. The catalyst was placed inside the drift cell and its surface was constantly monitored by the IR spectrometer. The cell was heated from 30 to 550 °C (ramp rate 10 °C min⁻¹) and a constant flow of air was kept throughout the experiment. The outlet of the DRIFT cell was connected to a Hiden QGA mass spectrometer for the online analysis of the gas phase.

Operando UV–Vis measurements were performed with a homemade tubular reactor equipped with a fibre optic UV–Vis probe. UV–Vis measurements were performed with a light source (Ocean Optics DH-2000), spectrometer (Maya 2000 Pro, Ocean Optics), and a 600-µm UV–Vis fiber. The light was directed onto an optically transparent reactor column, located within a heated aluminium block.

MAS NMR analysis was performed at Durham University through the National Solid-State NMR service. All the samples were nonenriched and were measured on a Bruker Avance III HD spectrometer at operating frequencies of 400, 100, 149, and 79 MHz for ¹H, ¹³C, ¹¹⁹Sn, and ²⁹Si, respectively. Typically, between 50 and 100 mg of solid sample was packed in a 4-mm rotor and spun at ±12 000 Hz. For ¹¹⁹Sn MAS NMR, samples were measured by the CPMG method as described in references.^{13,14} Spectra were acquired in both direct excitation and cross-polarization modes. Recycle delay times of 1 s, 2 s and 135 s were applied for ¹¹⁹Sn CP CPMG MAS NMR and ¹¹⁹Sn DE CPMG MAS NMR, respectively.

Scanning Electron Images were captured using a Hitachi Tabletop microscope TM3030. Images were acquired at 5 kV and 15 kV at different magnifications as specified in the text.

3.2.3 Kinetic evaluation and analytical methods

Continuous GI reactions were performed in a plug flow, stainless steel, tubular reactor. The reactor was connected to an HPLC pump in order to regulate the reactant flow and allow operation at elevated pressures. The catalyst was pelletised to precise particle size (particle size of 63–75 µm), and the catalytic bed placed in between two plugs of quartz wool. The diluted sample was densely packed into a 1/4" stainless steel tube (4.1 mm internal diameter), and a frit of 0.5 µm was placed at the reactor exit. The reactor was subsequently immersed in a thermostatted oil bath at the desired reaction temperature. Pressure in the system was controlled by means of a backpressure regulator, typically set at 10 bar, in order to allow operations above the boiling temperature of the solvent. Aliquots of the reaction solutions were taken periodically from a sampling valve placed after the reactor and analysed by an Agilent 1260 Infinity HPLC equipped with a Hi-Plex Ca column and ELS detector and quantified against an external

standard (sorbitol) added to the sample prior the injection. The flow of reaction feed was adjusted over the mass of catalyst in order to have an initial conversion of glucose around 40 %. Glucose upgrading to ML was carried out in an identical system but setting the temperature of reaction at 160 °C and the backpressure regulator at 20 bars. ML generated during glucose upgrading was analysed by GC (Agilent 7820, 25 m CP-Wax 52 CB column), and quantified against a biphenyl external standard.

The glucose employed as substrate was provided by Sigma Aldrich (>99.5 %, monohydrate), methanol anhydrous as solvent was provided by Sigma Aldrich (99.8 %). Standards of fructose, mannose, methyl lactate were provided by Sigma Aldrich (> 99.9 %).

3.3 Results and Discussion

3.3.1 Performance of different loading of Sn-Beta during continuous glucose isomerisation

In order to investigate how the Sn loading affects the activity and stability of Sn-Beta for glucose isomerisation, Sn-Beta catalysts with four different metal loadings (1, 2, 5 and 10 % wt.) were synthesised by SSI, following the procedure described previously.¹ The catalyst are henceforth denoted XSn-Beta, where X represents the Sn loading in % wt. XRD analysis (figure 1) confirms that the crystallinity of the material does not substantially change even when elevated loadings of Sn are employed.

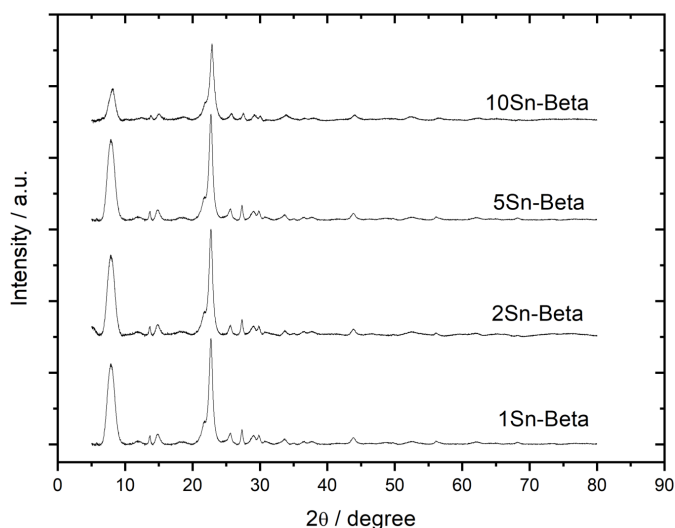


Figure 1. X-Ray Diffraction analysis for 1,2, 5 and 10Sn-Beta catalysts fresh prior reaction.

However, porosimetry measurements on the sample series reveal a small but steady decrease in specific surface area and micropore volume as the loading of Sn increases (table 1).

Table 1 Porosimetry data for 1,2,5 and 10Sn-Beta.

Catalyst	Specific surface area (m ² g ⁻¹)*	Micropore Volume (cm ³ g ⁻¹)*
1Sn-Beta	581	0.245
2Sn-Beta	528	0.225
5Sn-Beta	488	0.210
10Sn-Beta	422	0.179

*Specific surface area was obtained by using BET equation and micropore volume was obtained from t-plot method

¹¹⁹Sn MAS NMR is the technique that has shown to be the most effective for characterising Sn sites in zeolites, as it is able to distinguish between framework and extra-framework Sn species.^{15,16} During recent years, much effort has been made in order to improve the typically low signal-to-noise ratio, with the recent application of a CPMG sequence by Ivanova and co-workers greatly improving this parameter.^{12,13} Thus, ¹¹⁹Sn CPMG MAS NMR was employed to study how the Sn distribution changes as the loading of the metal increases beyond 2 % wt. Sn (figure 2). The acquisition time for each measurement was adjusted according to the amount of Sn present, so that comparable total signal was achieved in each case.

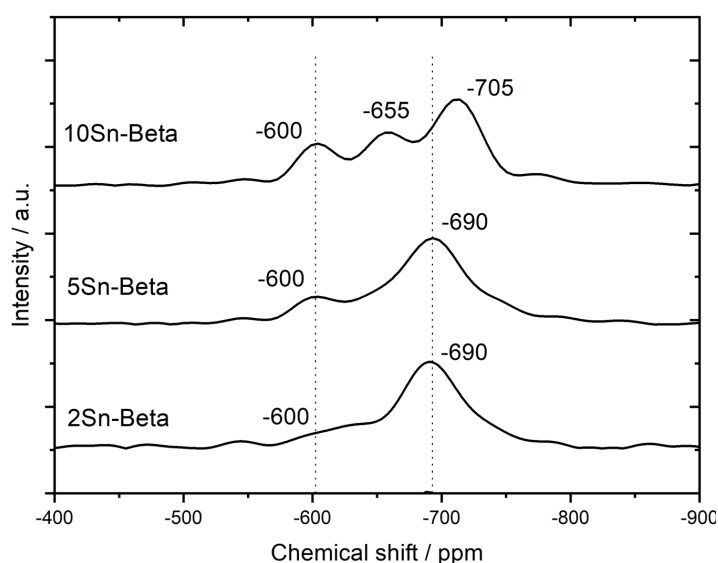


Figure 2. ¹¹⁹Sn CPMG MAS NMR acquired in direct excitation for 2, 5 and 10Sn-Beta catalysts. Experimental details: D¹=2 s

As can be seen, a similar distribution of Sn is observed for 2 and 5Sn-Beta, with two major resonances centred at -600 and -700 ppm observed, the final of which is by far the most dominant. These resonances are indicative of extra-framework Sn (both oligomeric and oxidic, henceforth denoted SnOx) and hexa-coordinated framework Sn i.e. hydrated Sn isomorphously substituted into the lattice, respectively. In contrast, a clear difference in the

Sn site distribution of 10Sn-Beta is observed. The signal of SnOx is still present, but its intensity is higher, indicating that a larger fraction of SnOx is present at the highest loading. Furthermore, the resonance at -690 ppm is no longer observed, with two signals, located at -710 and -655 ppm, instead present. Although both signals are present in the region of chemical shift associated with hydrated framework Sn, the differences in chemical shift indicate that the active sites present at the highest loading are somewhat different to those at the lowest loadings. Wolf *et al.*⁵ previously observed Sn site heterogeneity for a large number of Sn-Beta samples prepared by different synthetic methodologies, and attributed this to changes in the T-site distribution of Sn.^{5,6} Together, these observations indicate that increasing the Sn loading increases the heterogeneity of Sn within the zeolite, and also influences the precise nature of the isomorphously substituted Sn atoms.

This observation of increasing heterogeneity is in line with a previous study, in which it was observed that the progressive incorporation of Sn into the BEA framework above levels of 5 % wt. leads to the formation of extra-framework species.¹ In addition to lowering the intrinsic activity of the material during batch operation (*i.e.* Turnover frequency, TOF) such species can also partially block access to the micropores of the material, likely accounting for the slight decrease in porosity exhibited by 10Sn-Beta (table 1). However, nothing is known yet about how this increasing heterogeneity of active sites influences continuous operation of the catalyst, in terms of activity and stability. Accordingly, the four catalysts were tested in continuous flow for the glucose isomerisation reaction, with pure MeOH used as solvent. Being aware that mixtures of MeOH/water greatly increase the stability of the process by several orders of magnitude (Chapter 2),¹⁷ the intentional choice of using MeOH as solvent in this work was done in order to have faster rates of deactivation *i.e.* to allow a systematic study to be performed in a relatively short period of time. Furthermore, utilising pure MeOH allows identification of which materials are intrinsically more stable to deactivation through the mechanisms identified for Sn-Beta deactivation in Chapter 2.

Figure 3 presents the relative performance (equation 4 in the equation appendix) of various Sn-Beta catalysts, containing between 1 and 10 % wt. Sn, for glucose isomerisation in MeOH at 110 C as a function of time on stream. The contact time (equation 2 in the equation appendix) of each reaction was adjusted in order that every reaction started from a similar level of conversion (equation 3 in the equation appendix) (ranging between 35 % and 40 %), allowing accurate comparison of the stability of the catalysts at similar points of the reaction coordinate.^{11,18} As a preliminary analysis, it can be seen that all the catalysts lose at least 50 % of their initial activity within 48 h on stream. However, 10- and 5Sn-Beta demonstrate a lower level of stability, losing *ca.* 90 % and 60 % of their initial activity, respectively after only 30 h of operation. In contrast, 1- and 2Sn-Beta appear to have very similar stability during the reaction, showing a loss of approximately 40 % of initial activity over the same 30 h period.

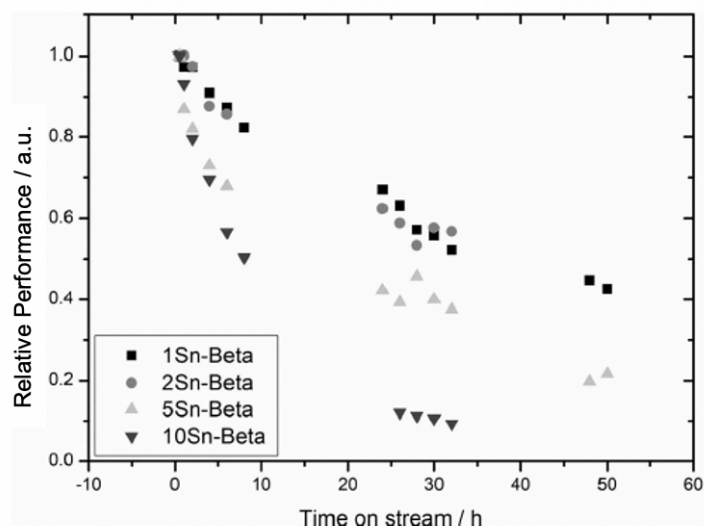


Figure 3. Relative performance of various Sn-Beta catalysts with different metal loadings for glucose isomerisation as a function of time on stream. Experimental details: 1 % wt. glucose in methanol, 110 °C, 10 bar, 100 mg of catalyst. Flow was adjusted to obtain 35-40 % as starting conversion: 1 mL min⁻¹ for 10Sn-Beta, 1 mL min⁻¹ for 5Sn-Beta, 0.7 mL min⁻¹ for 2Sn-Beta, 0.6 mL min⁻¹ for 1Sn-Beta.

When talking about stability, however, it is often more appropriate to compare the performance of different catalysts against substrate turnover number (indicative of the quantity of substrate that has passed over the catalytic bed, equation 7 in the equation appendix). In fact, it is often more important to evaluate the catalyst stability as a function of the number of reactant molecules that have been processed rather than the time on stream, particularly if disparate levels of activity are observed between catalytic materials.¹¹ Therefore, the relative performances of the catalysts were also compared as function of substrate turnovers in figure 4. This analysis shows how much greater the differences of stability are. In fact, after only 1000 substrate turnover, 10Sn-Beta has lost approximately 90 % of its activity, whilst 5Sn-Beta has lost only 50 % of its initial activity. On the other hand, 1 and 2Sn-Beta have lost just 10 % of their initial activity at the same number of substrate turnovers, showing remarkably improved stability.

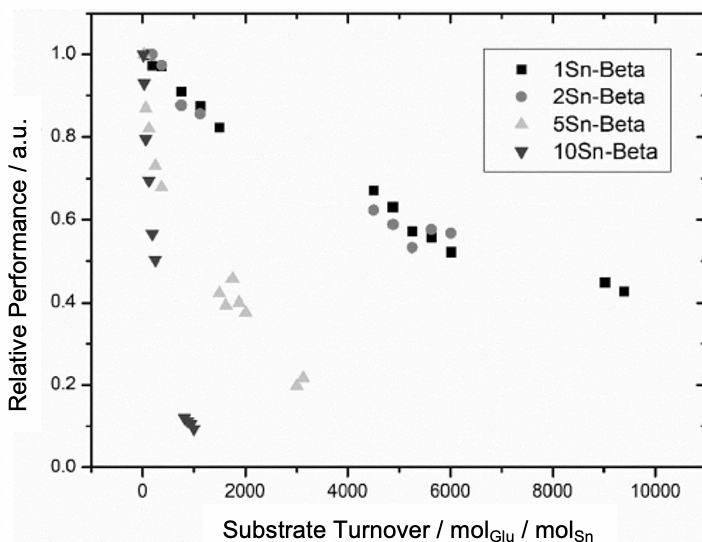


Figure 4. Relative performance as function of substrate turnover for glucose isomerisation reaction performed with Sn-Beta at different metal loadings. Experimental details: 1 % wt. glucose in methanol, 110 °C, 10 bar, 100 mg of catalyst. Flow was adjusted to obtain 35-40 % as starting conversion: 1 mL min⁻¹ for 10Sn-Beta, 1 mL min⁻¹ for 5Sn-Beta, 0.7 mL min⁻¹ for 2Sn-Beta, 0.6 mL min⁻¹ for 1Sn-Beta.

We further note that in all of these reactions, the fructose selectivity (equation 8 in the equation appendix) of the system overlaps at all levels of conversion, implying that the Sn loading of the catalyst does not drastically alter the selectivity of the reaction (figure 5).

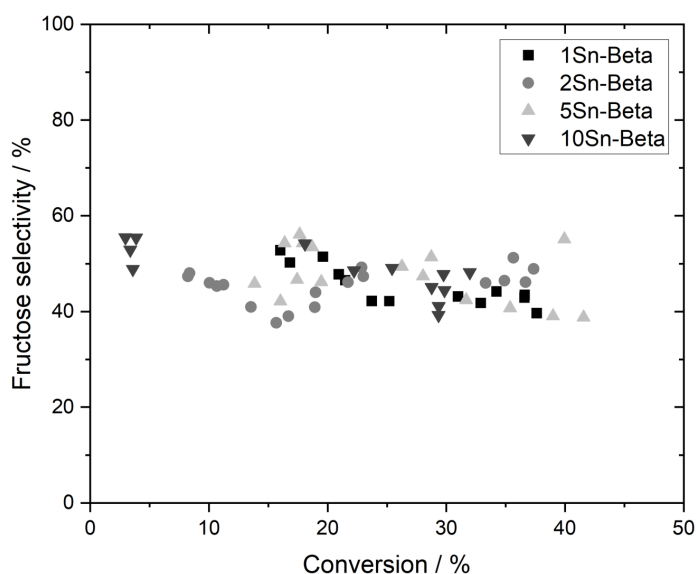


Figure 5. Selectivity in fructose plotted against glucose conversion for glucose isomerisation reaction performed with Sn-Beta at different metal loadings. Experimental details: 1 % wt. glucose in methanol, 110 °C, 10 bar, 100 mg of catalyst. Flow was adjusted to obtain 35-40 % as starting conversion: 1 mL min⁻¹ for 10Sn-Beta, 1 mL min⁻¹ for 5Sn-Beta, 0.7 mL min⁻¹ for 2Sn-Beta, 0.6 mL min⁻¹ for 1Sn-Beta.

To compare the performance of the series of catalyst in a more quantitative way, the deactivation rate (k_d) of each catalyst was calculated using the approach described by

Levenspiel (equation 5).¹⁹ Additionally, the intrinsic activity of each catalyst was also calculated according to its initial TOF. As can be seen in table 2, the calculated deactivation rate showed that samples containing lower amounts of metal were substantially more stable, with deactivation rates of 0.020 and 0.022 h⁻¹ observed for 1Sn-Beta and 2Sn-Beta, respectively. Slightly faster deactivation was observed for 5Sn-Beta (0.033 h⁻¹), and an even larger value of k_d observed for 10Sn-Beta (0.08 h⁻¹). Analysis of the TOF of each sample also showed that at higher loadings of Sn, the intrinsic activity decreased substantially, in line with what was previously identified during batch operation.¹ However, it should be stressed that the calculation of TOF in continuous flow can be affected by the deactivation, i.e. some contribution of deactivation may already have occurred by the time the first sample was taken. Thus, it can be expected that the precise values of TOF are underestimated, and that the extent of this is different for each sample depending on the deactivation rate of the catalyst.

Table 2. Deactivation constant and TOF value for different loadings of Sn-Beta (1,2,5 and 10Sn-Beta zeolite) Experimental details: 1 % wt. glucose in methanol, 110 °C , 10 bar, 100 mg of catalyst. Flow was adjusted to obtain 35-40 % as starting conversion: 1 mL min⁻¹ for 10Sn-Beta, 1 mL min⁻¹ for 5Sn-Beta, 0.7 mL min⁻¹ for 2Sn-Beta, 0.6 mL min⁻¹ for 1Sn-Beta.

Catalyst	Deactivation constant (Kd)	Turnover frequency (TOF)
1Sn-Beta	0.020	70
2Sn-Beta	0.022	55
5Sn-Beta	0.033	27
10Sn-Beta	0.080	10

It was previously reported that the formation of extra-framework SnOx species was the cause of the decrease in the initial TOF of Sn-Beta catalysts at elevated loadings, and that this process became relevant for loadings higher than 5 % wt.¹ However, in previous studies, was investigated the performance of samples with > 2 % wt. Sn.¹ Although the decreased TOF of 10Sn-Beta in this study is in line with previous literature, it is notable that the TOF also decreases slightly between 1- and 2Sn-Beta. As the ¹¹⁹Sn CPMG MAS NMR spectra show that extra-framework SnOx formation is not a major factor at loadings lower than 5 % wt. (figure 1), some other factors must govern the higher intrinsic activity of Sn-Beta at the very lowest loadings. At this stage, it can be hypothesised that below 2 % wt. of metal, Sn may generally occupy more favourable positions in the framework *i.e.* different T-sites, and that this site is more active resulting in slightly higher TOF values for this material. In a similar manner, the large decrease in TOF of 10Sn-Beta, relative to 5Sn-Beta, may also be related to the different distribution of active sites in this sample, in addition to the higher quantities of extra-framework SnOx observed in this material (figure 2).

This data provides evidence that the metal loading of Sn-Beta affects not just its intrinsic activity, but also its stability. In particular, when the relative performance of the catalyst is

compared as a function of substrate turnover, it appears clear that higher loading catalysts are more prone to deactivate, in addition to being lower in intrinsic activity. This demonstrates that optimal performance, in terms of activity and stability, is attained at the lowest loadings (figure 6). As it was shown in Chapter 2 (2.3.4) that the loss of crystallinity and pore fouling are not important factors with respect to deactivation of Sn-Beta for glucose isomerisation in MeOH, different possible causes of deactivation must explain the lower stability observed at higher loadings of Sn.

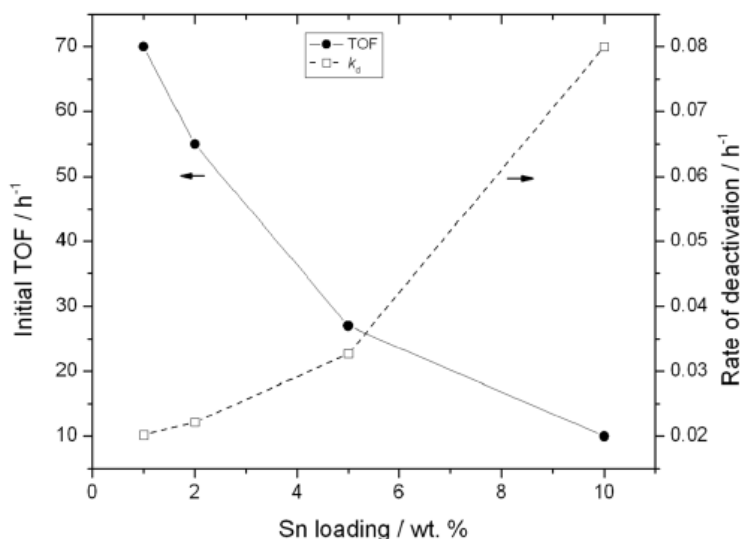


Figure 6. Impact of Sn loading of Sn-Beta on the initial activity of the catalyst (TOF, left Y axis) and its rate of deactivation (k_d , right Y axis) during glucose isomerisation. Experimental details: 1 % wt. glucose in methanol, 110 °C, 10 bar, 100 mg of catalyst. Flow was adjusted to obtain 35-40 % as starting conversion: 1 mL min⁻¹ for 10Sn-Beta, 1 mL min⁻¹ for 5Sn-Beta, 0.7 mL min⁻¹ for 2Sn-Beta, 0.6 mL min⁻¹ for 1Sn-Beta.

One of the main differences between 10Sn-Beta and the samples of lower loading is the increased quantity of extra-framework SnOx present, as evidenced by the increased signal at -600 ppm in the ¹¹⁹Sn CPMG MAS NMR spectrum (figure 2). Although previous studies¹ have suggested that such extra-framework SnOx species are spectators during catalysis (i.e. they do not contribute to catalytic performance of the material for glucose isomerisation) no knowledge about their potential impact on the lifetime of the catalyst has been described in the literature. In fact, the co-presence of extra-framework SnOx could still contribute to deactivation of the catalyst, even if such species are inactive for glucose isomerisation, either by participating in a negative side reaction, or by altering the overall physical properties of the material such as lowering its porosity, or facilitating its interaction with methanol. Thus, to investigate the possible impact of extra-framework SnOx species on the lifetime of the material, a continuous flow reaction employing a physical mixture of 2Sn-Beta and SnO₂ (at a Sn loading corresponding to 2 % wt. thus a total of 4 % wt.) was run under identical reaction conditions to an experiment performed with 2Sn-Beta alone (figure 7). As can be seen, the performance of both systems is equal throughout the reaction period.

Although it should be stressed that such a physical mixture containing bulk SnO₂ may not be fully representative of the SnO_x-type clusters found as a secondary species in the SSI-prepared materials, this strongly indicates that the co-presence of SnO_x itself in 10Sn-Beta does not directly influence the stability of the catalyst.

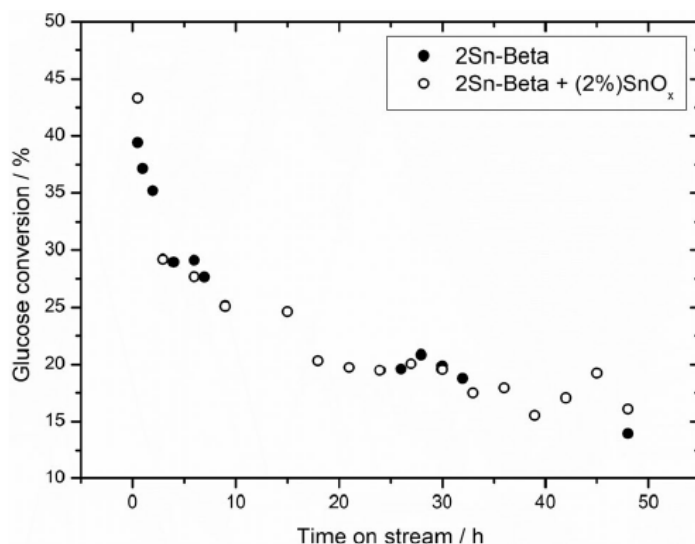


Figure 7. Conversion as function of time on stream of 2Sn-Beta alone, and a physical mixture of 2Sn-Beta and 2SnO_x. Experimental details: 1 % wt. glucose in methanol, 110 °C, 10 bar, 100 mg of catalyst. Flow was adjusted to obtain 35-40 % as starting conversion: 0.7 mL min⁻¹ for 2Sn-Beta.

The different rate of deactivation amongst the different loading of Sn-Beta therefore is not related to the extra framework tin species. This implies that the origin of this difference is related to the in-framework tin species, which differ at increasing Sn loadings. In Chapter 2 (2.3.3) was already shown how the active sites of the catalyst deactivates due to interaction with methanol, and it could be that different Sn specie might have different tendency to interact with the methanol leading so to a different rate of deactivation. From this set of data, the lower loading of Sn-Beta seems to be the most suitable and active material for glucose isomerisation. However, from an industrial perspective the productivity of the catalyst (equation 1 in the equation index) is an equal important property to consider. This feature defines the quantity of product yielded per volume or mass of catalyst, giving therefore an important guideline to start sizing the process. In figure 8 the productivity for different loadings of Sn-Beta was plotted, interestingly this picture shows how the highest productivity is achieved increasing the loading. In fact, 5 and 10Sn-Beta shows almost a double productivity than 1Sn-Beta zeolite. This complicates the choice for the best loading of Sn in Sn-Beta to perform glucose isomerisation, in fact a compromise between stability and productivity needs to be made in this contest.

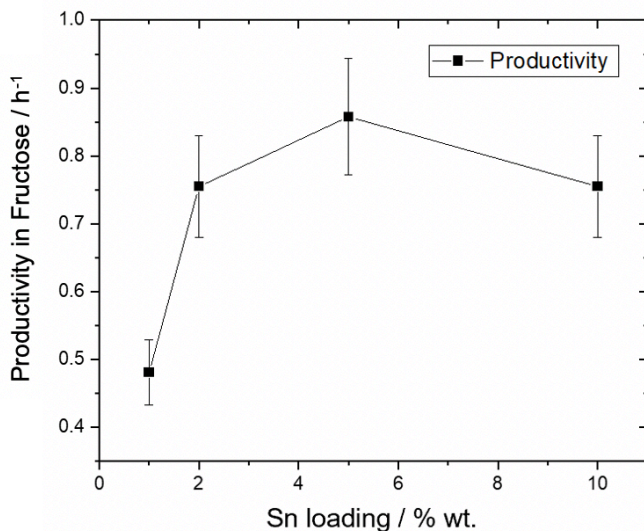


Figure 8. Productivity of different loadings of Sn-Beta zeolites for glucose isomerisation carried out in continuous flow. Experimental details: 1 % wt. glucose in methanol, 110 °C, 10 bar, 100 mg of catalyst. Flow was adjusted to obtain 35-40 % as starting conversion: 1 mL min⁻¹ for 10Sn-Beta, 1 mL min⁻¹ for 5Sn-Beta, 0.7 mL min⁻¹ for 2Sn-Beta, 0.6 mL min⁻¹ for 1Sn-Beta.

3.3.2 Glucose upgrading to ML carried out by different loadings of Sn-Beta

As mentioned previously in the introduction of the chapter Sn-Beta is known to be an effective catalyst also for the upgrading of glucose to ML.²⁰ This reaction requires higher temperature for catalysing the cleavage of the C₆ sugar. The glucose cleavage consists in a retro-aldol reaction yielding to C₃ molecules (dihydroxyacetone and glyceraldehyde) catalysed by the Sn-Lewis acid sites present in the material.²¹ Therefore, the performance of Sn-Beta for glucose upgrading to ML was studied for different loadings in continuous conditions to understand the effect of the metal loading on the catalytic performance. In figure 9 are shown the kinetic for glucose upgrading to ML carried out by 1 and 10Sn-Beta zeolite. In this case all the reactions were performed with the same conditions flowing 1 mL min⁻¹ of feed (1 % glucose in methanol) over 100mg of catalyst at 160 °C.

The complex pathway of this reaction (Chapter 1, Section 1.12) in comparison to GI, requires a different approach in carrying out the experiments and displaying the related data. The kinetic experiments were performed obtaining a full conversion of glucose to further convert the intermediates of reaction which leads to ML, to aid in the comparison amongst these systems all the processes were carried out at the exact same conditions and the results were plotted as conversion of glucose and yields in ML (equation 9, in the equation appendix).

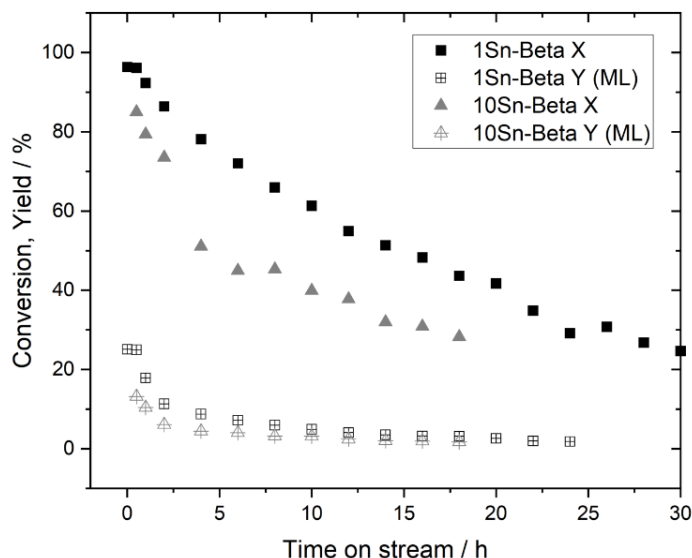


Figure 9. Glucose upgrading to ML carried out by 1 and 10Sn-Beta zeolite in continuous conditions at 160 °C in pure methanol (1 % glucose). Conversion (X) of glucose and yield at the time t (Y) of the product (ML) are plotted against time on stream. Experimental details: 1 % wt. glucose in methanol, 160 °C, 10 bar, 100 mg of catalyst, 1mL min⁻¹ of flow.

Interestingly both materials have comparable initial performance keeping the conditions of reaction constant. The starting conversion for 1Sn-Beta is slightly higher than the one for 10Sn-Beta zeolite (97 % vs 85 %); and the yield in ML is higher with the lower loaded material (28 % vs 13 %). These data already suggest that the performance of Sn-Beta for glucose upgrading to ML respond to the loading of Sn differently than when the catalyst is employed for glucose isomerisation carried out at 110°C.

In figure 10 are shown the performance of Sn-Beta loadings in terms of turnover frequency and productivity during glucose upgrading to ML. Interestingly the TOF for 1Sn-Beta is twelvefold higher than the one for 10Sn-Beta. This difference is higher than that found during glucose isomerisation, where 1Sn-Beta was 7 time more active per atom of tin than 10Sn-Beta. This suggests how all the tin incorporated into the catalyst above 1 % wt. of loading is substantially less active for the reaction.

Comparing these materials by the starting productivity the higher loaded material is showing a third of the productivity of 1 Sn-Beta (figure 10). The results from this prospective are radically different from the ones shown for glucose isomerisation, in particular 10Sn-Beta showed higher productivity towards fructose than the low loaded catalyst, whereas for ML production at 160 °C the 1Sn-Beta showed the best results.

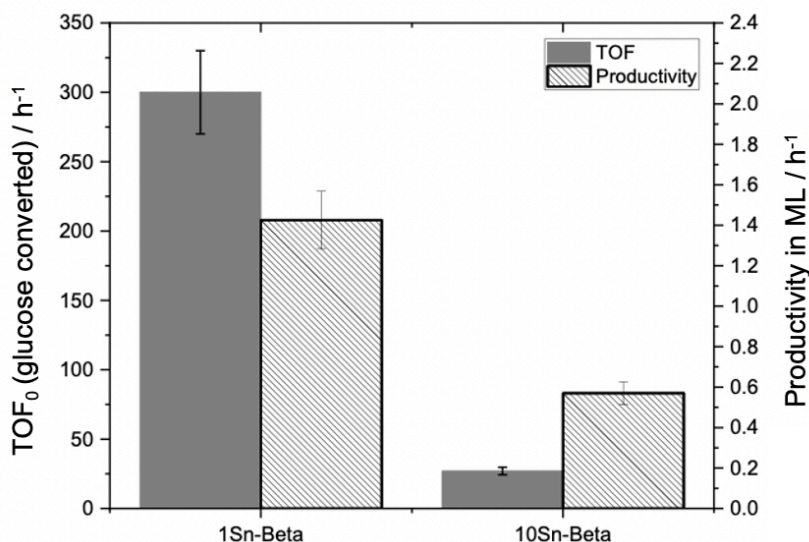


Figure 10. Turnover frequency (TOF) and productivity for 1 and 10Sn-Beta zeolite during continuous glucose upgrading at 160 °C in pure methanol. Experimental details: 1 % wt. glucose in methanol, 160 °C, 10 bar, 100 mg of catalyst, 1 mL min⁻¹ of flow.

The dramatic difference in these two systems point towards the fact that the level of Sn incorporation in the BEA structure strongly affect the behaviour of this material, in particular the Sn speciation which is produced inserting progressively more metal in the zeolite framework is highly diverse when a level above 5 % wt. of Sn is reached (figure 2). This diversification of sites at higher loading of metal might be the cause of the different reactivity of 1Sn-Beta and 10Sn-Beta when these materials are employed in these systems.

3.3.3 Effect of different preparations methodologies on Sn-Beta performances

It is generally recognised that Sn-Beta materials prepared by classical hydrothermal synthesis possess different intrinsic characteristics to those prepared by emerging post-synthetic methods such as SSI. For example, hydrothermally synthesised materials are reportedly more hydrophobic than post-synthetically prepared ones.²²⁻²⁴ In several reports, the intrinsic activity of the hydrothermal synthesised catalyst also differs to that of its post-synthetic counterpart. These differences are generally attributed to a more efficient incorporation of the Sn into the structure when hydrothermal synthesis is employed, and the more hydrophobic nature of the fluoride-synthesised material.^{13,14,16} However, no clear information about differences of stability between the two classes of Sn-Beta catalysts is known, as extended time on stream testing of otherwise analogous materials has not performed for glucose isomerisation. In order to study these important parameters, a 1Sn-Beta sample synthesised by classical fluoride synthesis (named 1Sn-Beta_{HDT}) was tested in the continuous flow system at similar operational conditions to 1Sn-Beta, henceforth re-named as 1Sn-Beta_{PS}. Due to its superior activity, the contact time of the reaction with 1Sn-Beta_{HDT} was adjusted that both catalysts start from an initial conversion of 32–40 %. Figure 11 shows the relative performance of 1Sn-Beta_{HDT} and 1Sn-Beta_{PS} as a function of time of stream.

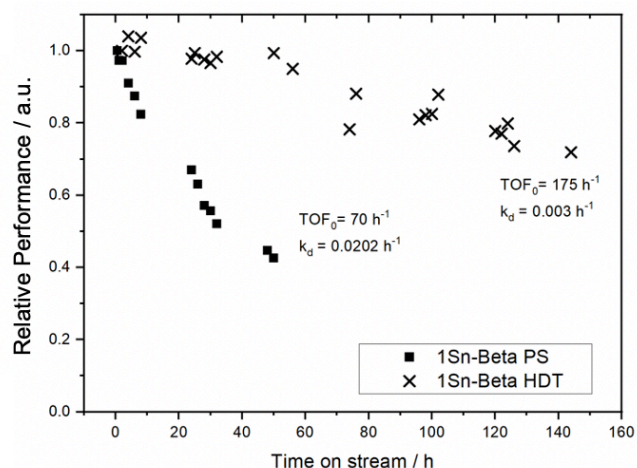


Figure 11. Relative performance of 1Sn-Beta_{PS} and 1Sn-Beta_{HDT} for glucose isomerisation as a function of time on stream. Experimental details: 1 % wt. glucose in methanol, 110 °C , 10 bar, 100 mg of catalyst. Flow was adjusted to obtain 35-40 % as starting conversion: 1.4 mL min⁻¹ for 1Sn-Beta_{HDT}, 0.6 mL min⁻¹ for 1Sn-Beta_{PS}

It can be immediately seen from the initial TOF values of both samples that 1Sn-Beta_{HDT} is approximately 2.5 times higher in activity than the post-synthetic material. However, an even greater difference arises when the stability of both the materials is examined. In fact, the k_d values calculated for 1Sn-Beta_{HDT} and 1Sn-Beta_{PS} are 0.003 and 0.020 h⁻¹, respectively. Hence, an almost sevenfold increase in stability is observed due to the differences in the method of material preparation. A more meaningful comparison of the two systems can again be made by comparing the stability of the catalyst as a function of substrate turnover (figure 12). In this case the difference is even more remarkable.

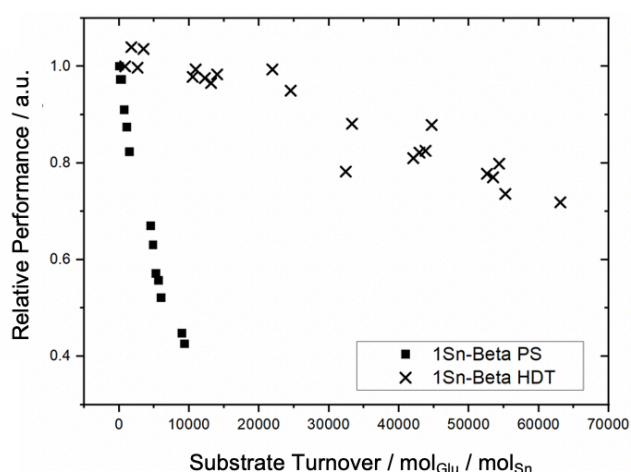


Figure 12. Relative performances of 1Sn-Beta_{PS} and 1Sn-Beta_{HDT} for glucose isomerisation as a function of substrate turnovers. Experimental details: 1 % wt. glucose in methanol, 110 °C , 10 bar, 100 mg of catalyst. Flow was adjusted to obtain 35-40 % as starting conversion: 1.4 mL min⁻¹ for 1Sn-Beta_{HDT}, 0.6 mL min⁻¹ for 1Sn-Beta_{PS}.

After 10,000 substrate turnovers, the post-synthetic material has lost 60% of its initial activity, while the hydrothermal material has retained almost its entire initial activity. It can be noticed that on average, the fructose selectivity for the hydrothermal material is slightly lower when compared at the same level of conversion to that of the post-synthetic material (figure 13). In fact, at glucose conversion levels of 30–40 %, the values of fructose selectivity lay around 35 % for the hydrothermal catalyst, and 45 % in the case of the post-synthetic material. Given its much higher levels of activity and resistance to deactivation, it is suggested that hydrothermal synthesis is a more suitable method of Sn-Beta preparation in the context of continuous operation.

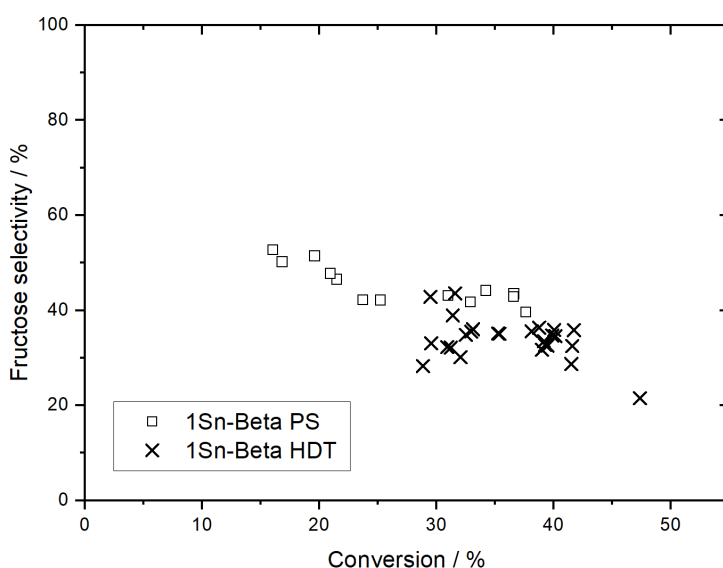


Figure 13. Fructose selectivity as a function of glucose conversion for 1Sn-Beta_{PS} and 1Sn-Beta_{HDT}. Experimental details: 1 % wt. glucose in methanol, 110 °C , 10 bar, 100 mg of catalyst. Flow was adjusted to obtain 35-40 % as starting conversion: 1.4 mL min⁻¹ for 1Sn-Beta_{HDT}, 0.6 mL min⁻¹ for 1Sn-Beta_{PS}

3.3.4 Glucose upgrading to ML carried out by hydrothermal and post-synthetic Sn-Beta

Considering the surprisingly good activity of 1Sn-Beta_{HDT} for glucose isomerisation to fructose, this material was tested as well for glucose upgrading to ML at 160 °C. In figure 14 are shown the kinetic data related to glucose upgrading to ML carried out by 1Sn-Beta_{HDT} and its post synthetic analogue synthesized by solid state incorporation 1Sn-Beta_{PS}. In this experiment the conditions for both the materials were kept constant: 1 mL min⁻¹ of feed (1 % glucose in methanol) was kept over 100mg of catalyst at 160 °C. 1Sn-Beta_{HDT} shows a higher selectivity in ML than 1Sn-Beta_{PS} reaching a yield of 47 % against the 23 %. Furthermore, it is possible to notice how in the first 20 h of the reactions only 20 % activity is lost by Sn-Beta_{HDT} whereas 1Sn-Beta_{PS} loses 70 % of the starting activity.

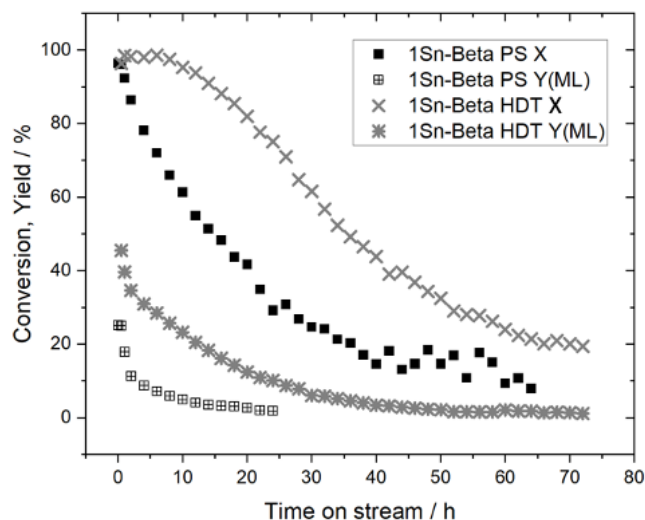


Figure 14. Glucose upgrading to ML carried out by 1Sn-Beta_{PS} and 1Sn-Beta_{HDT} zeolite in continuous conditions at 160 °C in pure methanol (1 % glucose). Conversion (X) of glucose and yield at the time t (Y) of the product (ML) are plotted against time on stream. Experimental details: 1 % wt. glucose in methanol, 160 °C , 10 bar, 100 mg of catalyst, 1mL min⁻¹of flow.

These results are generally in agreement with the ones gathered by glucose isomerisation to fructose (figure 11), where 1Sn-Beta_{HDT} showed to be more than twice more active than 1Sn-Beta_{PS}. In figure 15 is reported the activity (TOF, calculated on glucose conversion) for these two materials alongside the productivity (in terms of ML production). These data shows how these material efficiently convert glucose at the beginning of the reaction, almost 100 % conversion is achieved for both the catalyst, thus TOF is similar for both the material. 1Sn-Beta_{HDT} however show much higher productivity in ML (2.1 Kg_{ML} Kg⁻¹_{cat.} h⁻¹) than 1Sn-Beta_{PS} which only achieved 1.4 Kg_{ML} Kg⁻¹_{cat.} h⁻¹.

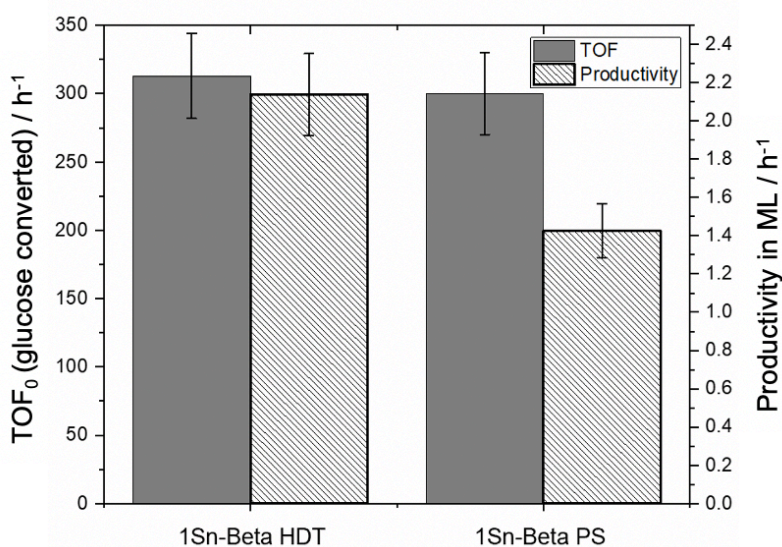


Figure 15. turnover frequency (TOF) and productivity in ML for Sn-Beta_{HDT} and Sn-Beta_{PS} during continuous glucose upgrading at 160 °C in pure methanol. Experimental details: 1 % wt. glucose in methanol, 160 °C , 10 bar, 100 mg of catalyst, 1mL min⁻¹of flow.

The different productivity results are due to the diverse tendency of these material to produce ML in these conditions, in fact the hydrothermal catalyst shows an overall yield in ML of 47 % against 27 % yield achieved by 1Sn-Beta_{PS} (figure 16). Considering that the catalyst were operating at exactly same conditions this clearly shows how 1Sn-Beta_{HDT} seems to be able to convert more selectively glucose in to ML. The missing carbon balance in the process carried out from 1Sn-Beta_{HDT} is 40 % whereas the process catalysed from 1Sn-Beta_{PS} accounts for a loss of 65 % of carbon balance. It was already introduced in Chapter 1 (Section 1.12) how several by-products can be formed by Sn-Beta zeolite, therefore 1Sn-Beta_{PS} might have a higher tendency to form these by-products than 1Sn-Beta_{HDT}. The understanding of the different pathways that can be promoted by different preparations of Sn-Beta is beyond the scope of this chapter and this problem will addressed in Chapter 6.

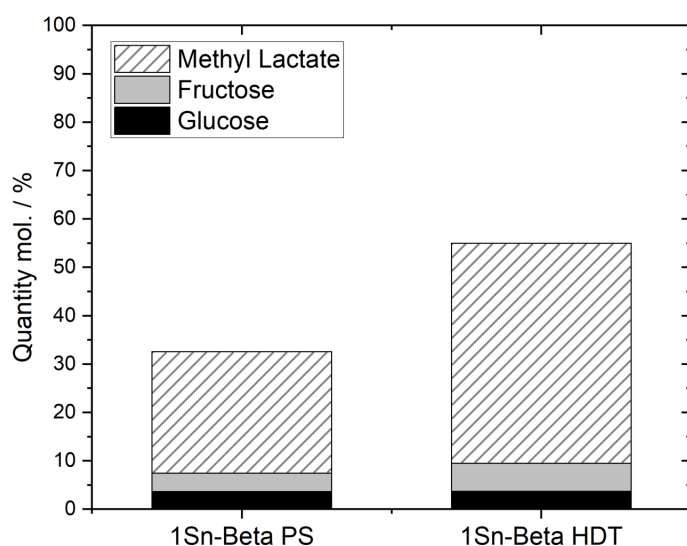


Figure 16. Carbon balance for 1Sn-Beta_{HDT} and 1Sn-Beta_{PS} at the same rate of conversion during glucose upgrading to ML carried out at 160 °C. Experimental details: 1 % wt. glucose in methanol, 160 °C , 10 bar, 100 mg of catalyst, 1mL min⁻¹ of flow.

3.3.5 Structure-activity correlation for different preparations of Sn-Beta

Clearly, a remarkable effect on activity and stability is observed when Sn-Beta samples of similar loading (1 % wt.) are prepared by two different methods. In fact, the hydrothermally synthesised material exhibits a higher activity and stability for both glucose isomerisation to fructose and for glucose upgrading to ML. Such remarkable difference suggests that a profound difference, either in the textural and physical properties of the samples, and/or in the nature of its active sites, exists.

The textural properties of the material, such as crystallinity and pore volume, were first characterised, in order to understand if there were evident differences between the two materials. XRD analysis of the two materials show a difference in intensity between the

diffraction patterns of the two materials, with 1Sn-Beta_{HDT} showing higher levels of intensity than its post-synthetic counterpart (figure 17).

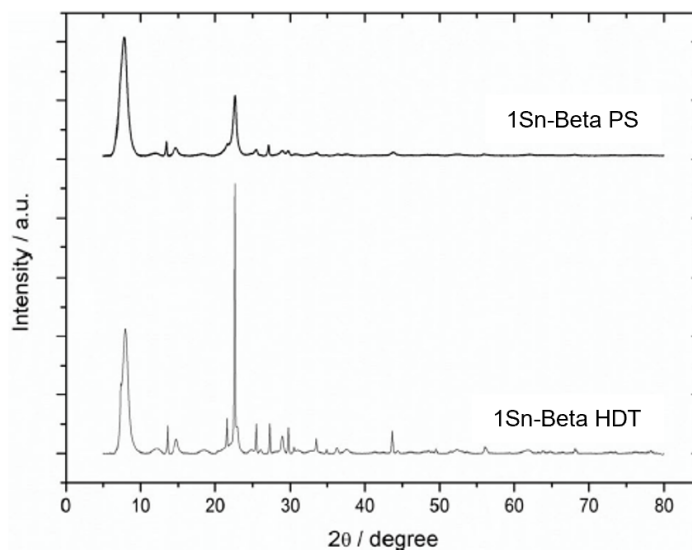


Figure 17. XRD patterns of 1Sn-Beta_{HDT} and 1Sn-Beta_{PS}.

However, complementary analysis of the morphology of the catalysts revealed the increase in intensity for 1Sn-Beta_{HDT} likely arises from its larger crystallite sizes (figure 18). Specifically, 1Sn-Beta_{HDT} exhibits particle sizes of 10–15 μm, whereas particle sizes between 0.5 and 2 μm are found for 1Sn-Beta_{PS}. Moreover, in Chapter 2, it was ruled out that loss of crystallinity was the cause of deactivation of post-synthetic materials. As such, these differences likely do not account for the lower stability 1Sn-Beta_{PS}.

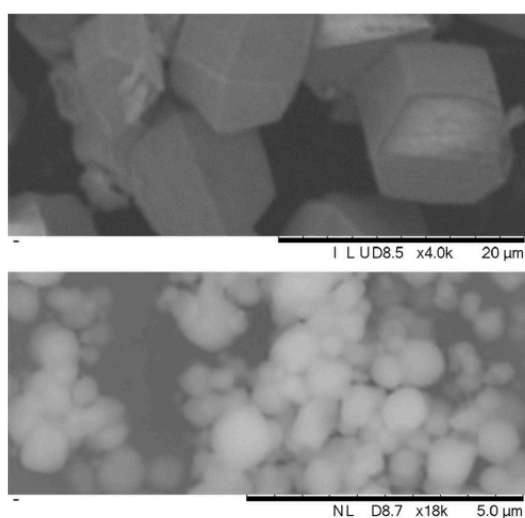


Figure 18. SEM micrographs of 1Sn-Beta_{HDT} (top) and 1Sn-Beta_{PS} (bottom); magnification for each micrograph is specified beneath each box.

Porosimetry analysis on the two materials was also performed in order to see how the specific surface area and pore volume changes according to the different synthetic

methodology (table 3). As can be seen, the two samples demonstrate different levels of microporosity and surface areas, with 1Sn-Beta_{HDT} exhibiting approximately 30 % lower surface area and micropore volume than 1Sn-Beta_{PS}. In light of the lower surface area and porosity exhibited by 1Sn-Beta_{HDT}, and the higher intrinsic activity and stability displayed by this material, it can be hypothesised that the factors governing the catalytic properties and the stability of the material are not strongly related to the textural properties. This is in further agreement with the results gained in Chapter 2, where was demonstrated that pore fouling i.e. blocking of the micropores with carbonaceous residue, is not a major contributing factor to deactivation in this system. In summary, it is clear that whilst XRD data and porosimetry data show there are some intrinsic textural differences present between the two materials, satisfactory and conclusive structure-activity-stability relationships cannot be achieved with these two techniques alone. Hence, studies of the active sites of both samples are required.

Table 3. Porosimetry data for 1Sn-Beta_{HDT} and 1Sn-Beta_{PS}.

Catalyst	Surface Area (m ² g ⁻¹)	Porosimetry (cm ³ g ⁻¹)
1Sn-Beta PS	581	0.245
1Sn-Beta HDT	391	0.168

As described in Chapter 2, the primary mechanism of deactivation during glucose conversion with Sn-Beta arises from the strong interaction between the catalyst and the MeOH solvent. Indeed, *operando* UV–Vis analysis on catalysts performing glucose isomerisation in pure MeOH revealed that a strong negative absorption occurs at around 220 nm upon interaction of Sn with MeOH, and that the appearance of this absorption correlated to deactivation of the catalyst. Thus, to further investigate the improved stability of 1Sn-Beta_{HDT} relative to 1Sn-Beta_{PS}, the two samples were re-examined for glucose isomerisation, this time with *operando* UV–Vis being performed. The resulting spectra of the first 20 h on stream under the UV probe are shown in figure 19. As can be seen, over the course of 20 h on stream, 1Sn-Beta_{PS} experiences a steady decrease in absorbance at 220 nm. Over this period of time, the catalyst also loses approximately 30 % of its catalytic performance. In contrast, the hydrothermal material experiences very little negative absorbance in this region over the same reaction period, clearly demonstrating that interaction between Sn and MeOH is greatly reduced for this sample. Importantly, this sample also exhibits no loss in activity over this reaction period. Alongside this, the band at 340 nm, attributed to interaction between Sn and glucose, is much stronger in 1Sn-Beta_{HDT}, whereas for 1Sn-Beta_{PS} it decreases in intensity with time.

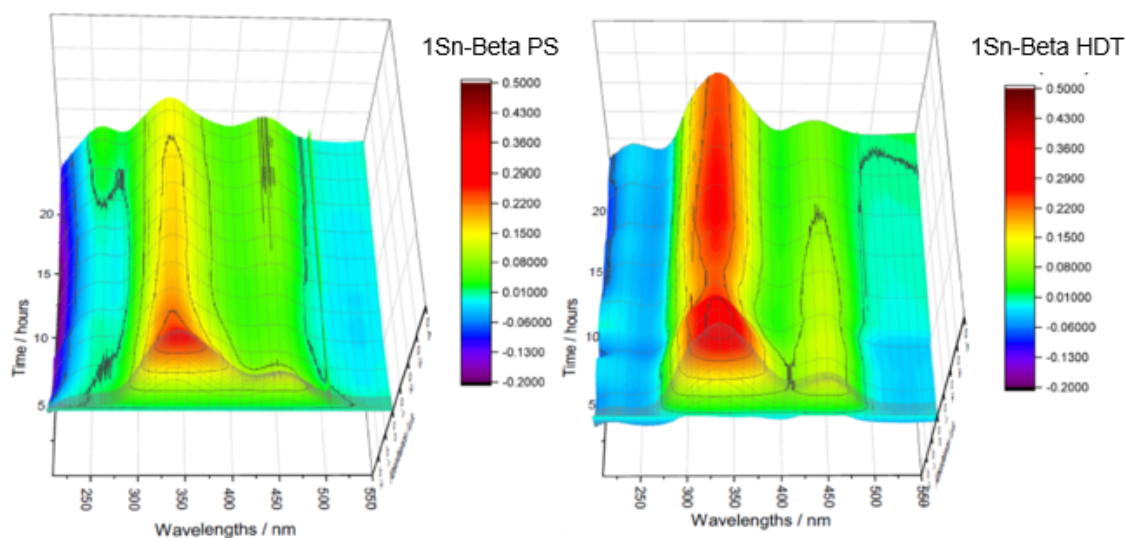


Figure 19. *Operando* UV–Vis following the isomerisation of glucose in pure MeOH for (Left) 1Sn-Beta_{PS} and (Right) 1Sn-Beta_{HDT}.

From the *operando* UV–Vis measurements, it is clear that the hydrothermally synthesised material better inhibits the Sn sites of the catalyst from interacting strongly with MeOH, somehow mimicking what small quantities of water molecules do in the post-synthetic sample, whilst at the same time helping the interaction of Sn with glucose. To further study the interaction between catalyst and MeOH, TPD-MS was performed, following treatment of both samples in pure MeOH at 110 °C for 1 h (figure 20). From this it can be seen that the quantity of MeOH evolved from the two samples is comparable, as the area of the MeOH signal is of similar magnitude for both TPD-MS profiles. However, the temperature at which the MeOH evolved is quite different for the two materials. In particular, in 1Sn-Beta_{HDT} retained MeOH is evolved at approximately 150 °C, while MeOH is desorbed at 220 °C in 1Sn-Beta_{PS}. The similar quantity of MeOH retained in the materials after treatment indicates that MeOH is likely bonded to Sn, since the percentage of metal in the two catalysts is similar. However, the strength of the MeOH-Sn interaction clearly differs. This indicates that the two synthetic routes result in different Sn species, or Sn species present in a different environment. The tendency of 1Sn-Beta_{PS} to interact more strongly with MeOH is in good agreement to the UV–Vis analysis, and the lower stability of the catalyst under reaction conditions.

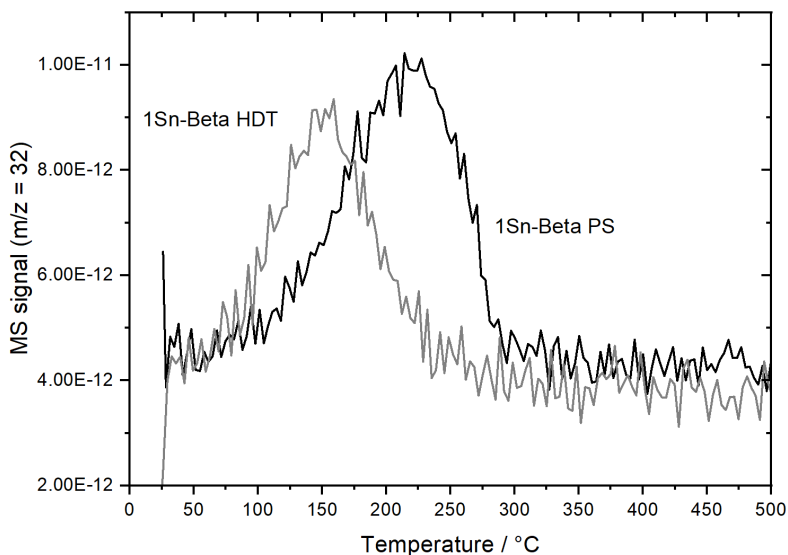


Figure 20. TPD-MS of 1Sn-Beta_{HDT} and 1Sn-Beta_{PS} obtained following dosing of the samples in pure MeOH at 110 °C for 1 h, and subsequent drying at room temperature.

To gain further insight of catalyst-solvent interactions, vapour adsorption isotherms with MeOH and water were performed for 1Sn-Beta_{HDT} and 1Sn-Beta_{PS}. As can be seen (figure 21 Left), both catalysts adsorb different quantities of MeOH by different mechanisms. Specifically, whereas MeOH adsorption over 1Sn-Beta_{PS} is typical of a Type I isotherm, representative of micropore condensation driven by adsorbate-adsorbent interactions, MeOH adsorption over 1Sn-Beta_{HDT} is more typical of a Type V isotherm, representative of micropore condensation driven by adsorbate-adsorbate interactions.²⁵ As such, it is likely that MeOH tends to adsorb to 1Sn-Beta_{PS} directly on the acid sites (Sn, or Si-OH groups close to Sn), but MeOH adsorption by 1Sn-Beta_{HDT} is achieved by MeOH molecules interacting with other MeOH molecules. This observation indicates lower interaction of MeOH with the Sn sites of 1Sn-Beta_{HDT}, in excellent agreement to the lower desorption temperature observed for MeOH for this material compared to 1Sn-Beta_{PS}. In addition to reflecting different adsorption behaviour, it is notable that different quantities of MeOH are also adsorbed by both samples in the low pressure regime, with 1Sn-Beta_{PS} adsorbing approximately twice the amount of MeOH than 1Sn-Beta_{HDT} at $P/P_0 = 0.1$. This observation clearly indicates that 1Sn-Beta_{HDT} is substantially more resistant to MeOH adsorption, even at the same metal loading as 1Sn-Beta_{PS}. More dramatic again is the difference in the amount of water adsorbed by 1Sn-Beta_{HDT} than 1Sn-Beta_{PS} (figure 21, Right). In fact, 1Sn-Beta_{PS} shows a much higher water uptake than the hydrothermal catalyst at comparable pressures, in perfect agreement with previous reports where the more hydrophobic nature of the hydrothermal material has been identified.^{16,26} Taken together, these results clearly demonstrate that the hydrothermally prepared material represents a more protected environment for the Sn sites of the catalyst from both water and MeOH. Even though differences in solvent uptake between the two materials are clearly observed by TPD-MS and vapour absorption measurements, it cannot yet be deduced if this is due to an overall

difference in the zeolite structure itself i.e. different porosity, different number of connectivity defects, presence of silanol groups, amongst others, or whether it relates to a specific type of Sn species uniquely present in 1Sn-Beta_{HDT}.

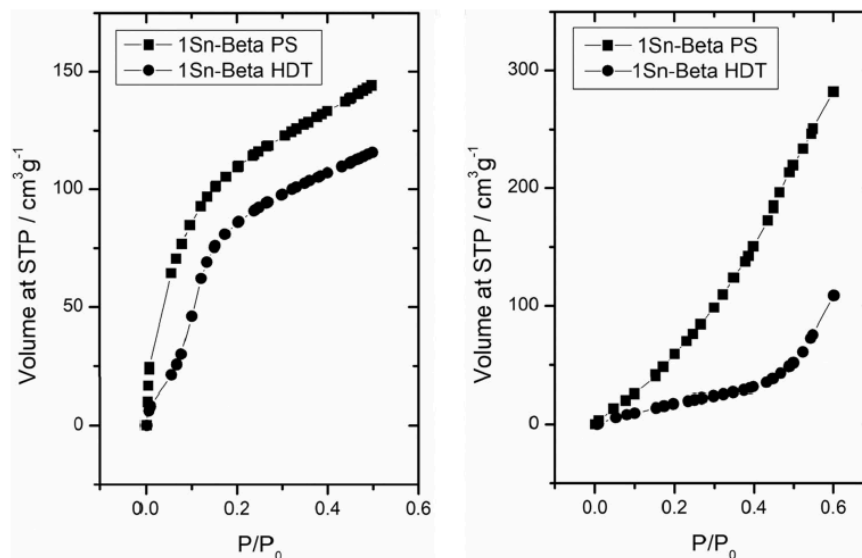


Figure 21. Vapour isotherms of MeOH (Left) and water (Right) for 1Sn-Beta_{HDT} and 1Sn-Beta_{PS} at 20 °C.

Thus, to see if the two diverse synthetic routes generate actual differences in the Sn speciation, ¹¹⁹Sn CPMG MAS NMR was performed. In this experiment a long recycle delay (135s) was kept for both the materials in order to allow a full relaxation of all the tin species in the material, the number of scans was set equal (512 scans) for both the catalysts. From the two spectra shown in figure 22, it can be seen immediately that the major resonances in 1Sn-Beta_{HDT} than 1Sn-Beta_{PS} are slightly shifted, resonating at - 690 and - 710 ppm, respectively. These signals lie in the spectral region representative of hexa-coordinated framework Sn sites, known to result in catalytic activity.^{26,27} In 1Sn-Beta_{PS} a minor signal is also present at - 600 ppm, which indicates the presence of some extra-framework SnO_x species in this sample. As the level of extra-framework SnO_x is low, and with the chosen recycle delay times it is an overestimate of its real contribution to the population, it will not account for the 2.5-fold decrease in TOF exhibited by this sample relative to the hydrothermal, although it will evidently contribute somewhat. However, the precise chemical shift of the isomorphously substituted Sn species present in both samples differs substantially, by approximately 20 ppm. Despite the fact that exact nature of the active sites of the two materials is unknown, such differences in chemical shift clearly relate to differences in the environment and nature of the active sites of both catalysts. In addition to reflecting changes in intrinsic activity, such changes could also result in different degrees of stability. In fact, changes in chemical shift could arise not only from a different form of the active site e.g. open or closed, but also from a different location in the zeolite structure (T site).^{23,24,27} Thus, it can be hypothesised that sites located in different crystallographic

positions of the framework might possess different stability, being more or less intrinsically stable and/or being more or less exposed to the deactivation processes identified. The genesis of this difference likely arises from the different methods of incorporation i.e. direct insertion of Sn into its most favourable T-site during hydrothermal synthesis, versus post-synthetic incorporation of Sn into the most favourable T-site for incorporation of Al.

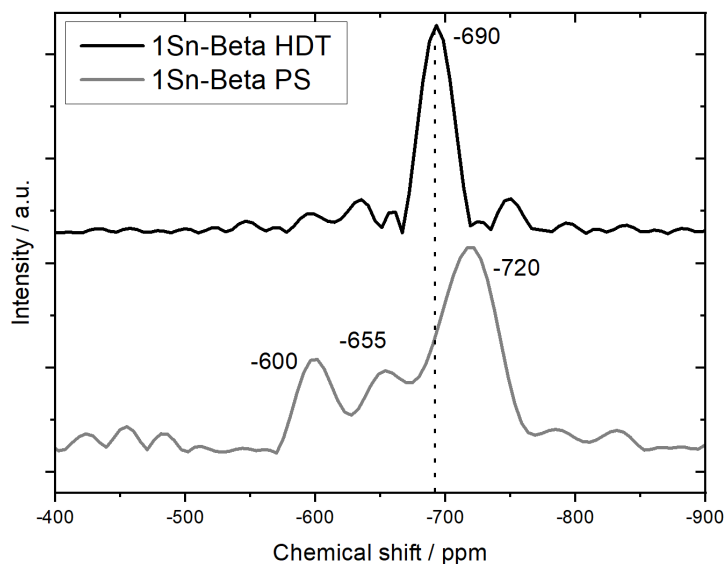


Figure 22. ^{119}Sn DE CPMG MAS NMR spectra of 1Sn-Beta_{PS} (grey line) and 1Sn-Beta_{HDT} (solid line). D1=135 s

3.4 Conclusion:

This study showed how during Sn-Beta zeolite preparation, the increment of the loading of tin and the changing of the synthesis methodology are a key factor to module the catalytic performances of the resultant material. 10Sn-Beta showed the best productivity in fructose when glucose upgrading was performed at 110 °C, whereas 1Sn-Beta showed the best performance for ML production at 160 °C. This different behaviour might be due to the formation of different kinds of active sites as a function of Sn insertion in the material. In fact, increasing the metal loading several speciation of in framework Sn can be detected by ^{119}Sn MAS NMR, these speciation shows drastic difference in activity, selectivity and stability during glucose upgrading in continuous flow.

Moreover, it was shown how post synthetic and hydrothermal preparation of Sn-Beta generate catalysts with different tin speciation and different textural properties. These different properties of the material lead to dramatic difference in the interaction of the catalysts with the solvent (methanol) resulting in drastically different level of stability. The hydrothermal synthesis of Sn-Beta zeolite generated a catalyst more stable and at the same time more active towards glucose upgrading in methanol than the post-synthetic analogue. Nonetheless this method of synthesis presents important hurdles for a hypothetical industrial scale up. In fact, the mineralisation of the synthesis gel with fluoride anion and the long time on synthesis make the preparation of this material not suitable from an economical point of view. Therefore, an important issue still unsolved in the field is the production of a catalyst with properties similar to the one of the hydrothermal Sn-Beta but without recurring to the use of fluorides in the synthesis. An eventual success in this area might lead to a strong advance in Sn-Beta exploitation for continuous biomass upgrading.

Finally this study was essential to benchmark how the catalyst performances respond to different methodologies of preparations and which properties lead to the best performing material for continuous glucose upgrading. Although this study represents an essential first step towards the scale-up of these process, the yields in final products were relatively low (maximum yield of 47 % in ML was achieved), therefore a follow-up study is necessary to understand how the influence of promoters (such as alkali and water)^{9,17,21} impacts on different catalyst preparations. These contaminants in the reaction environment are known to be important promoters for the stability and selectivity of the process, thus their effect on different catalyst preparations will be better examined in Chapter 4.

3.5 Reference

- (1) Hammond, C.; Padovan, D.; Al-Nayili, A.; Wells, P. P.; Gibson, E. K.; Dimitratos, N. Identification of Active and Spectator Sn Sites in Sn- β Following Solid-State Stannation, and Consequences for Lewis Acid Catalysis. *ChemCatChem* **2015**, *7* (20), 3322–3331.
- (2) Dijkmans, J.; Gabriëls, D.; Dusselier, M.; de Clippel, F.; Vanelderen, P.; Houthoofd, K.; Malfliet, A.; Pontikes, Y.; Sels, B. F. Productive Sugar Isomerization with Highly Active Sn in Dealuminated β Zeolites. *Green Chem.* **2013**, *15* (10), 2777.
- (3) Li, P.; Liu, G.; Wu, H.; Liu, Y.; Jiang, J. G.; Wu, P. Postsynthesis and Selective Oxidation Properties of Nanosized Sn-Beta Zeolite. *J. Phys. Chem. C* **2011**, *115* (9), 3663–3670
- (4) Hammond, C.; Conrad, S.; Hermans, I. Simple and Scalable Preparation of Highly Active Lewis Acidic Sn-b *Angew. Chemie - Int. Ed.* **2012**, *51* (47), 11736–11739.
- (5) Wolf, P.; Valla, M.; Rossini, A. J.; Comas-Vives, A.; Núñez-Zarur, F.; Malaman, B.; Lesage, A.; Emsley, L.; Copéret, C.; Hermans, I. NMR Signatures of the Active Sites in Sn-b Zeolite. *Angew. Chemie - Int. Ed.* **2014**, *53* (38), 10179–10183.
- (6) Wolf, P.; Liao, W. C.; Ong, T. C.; Valla, M.; Harris, J. W.; Gounder, R.; van der Graaff, W. N. P.; Pidko, E. A.; Hensen, E. J. M.; Ferrini, P.; et al. Identifying Sn Site Heterogeneities Prevalent Among Sn-Beta Zeolites. *Helv. Chim. Acta* **2016**, *99* (12), 916–927.
- (7) Conrad, S.; Wolf, P.; Müller, P.; Orsted, H.; Hermans, I. Influence of Hydrophilicity on the Sn β -Catalyzed Baeyer–Villiger Oxidation of Cyclohexanone with Aqueous Hydrogen Peroxide. *ChemCatChem* **2017**, *9* (1), 175–182.
- (8) Lari, G. M.; Dapsens, P. Y.; Scholz, D.; Mitchell, S.; Mondelli, C.; Pérez-Ramírez, J. Deactivation Mechanisms of Tin-Zeolites in Biomass Conversions. *Green Chem.* **2016**, *18* (5), 1249–1260.
- (9) Tolborg, S.; Meier, S.; Sádaba, I.; Elliot, S. G.; Kristensen, S. K.; Saravanamurugan, S.; Riisager, A.; Fristrup, P.; Skrydstrup, T.; Taarning, E. Tin-Containing Silicates: Identification of a Glycolytic Pathway via 3-Deoxyglucosone. *Green Chem.* **2016**, *18* (11), 3360–3369.
- (10) Cordon, M. J.; Hall, J. N.; Harris, J. W.; Bates, J. S.; Hwang, S.-J.; Gounder, R. Deactivation of Sn-Beta Zeolites Caused by Structural Transformation of Hydrophobic to Hydrophilic Micropores during Aqueous-Phase Glucose Isomerization. *Catal. Sci. Technol.* **2019**, *9* (7), 1654–1668.
- (11) Hammond, C. Intensification Studies of Heterogeneous Catalysts: Probing and Overcoming Catalyst Deactivation during Liquid Phase Operation. *Green Chem.* **2017**, *19* (12), 2711–2728.
- (12) Tolborg, S.; Katerinopoulou, A.; Falcone, D. D.; Sadaba, I.; Osmundsen, C. M.; Davis, R. J.; Taarning, E.; Fristrup, P.; Holm, M. S. Incorporation of Tin Affects Crystallization, Morphology, and Crystal Composition of Sn-Beta. *J. Mater. Chem. A* **2014**, *2* (47), 20252–20262.
- (13) Yakimov, A. V.; Kolyagin, Y. G.; Tolborg, S.; Vennestrøm, P. N. R.; Ivanova, I. I. ¹¹⁹Sn MAS NMR Study of the Interaction of Probe Molecules with Sn-BEA: The Origin of Penta- and Hexacoordinated Tin Formation. *J. Phys. Chem. C* **2016**, *120* (49), 28083–28092.
- (14) Kolyagin, Y. G.; Yakimov, A. V.; Tolborg, S.; Vennestrøm, P. N. R.; Ivanova, I. I. Application Of ¹¹⁹Sn CPMG MAS NMR for Fast Characterization of Sn Sites in Zeolites with Natural ¹¹⁹Sn Isotope Abundance. *J. Phys. Chem. Lett.* **2016**, *7* (7), 1249–1253.
- (15) Gunther, W. R.; Michaelis, V. K.; Caporini, M. A.; Griffin, R. G.; Román-Leshkov, Y. Dynamic Nuclear Polarization NMR Enables the Analysis of Sn-Beta Zeolite Prepared with Natural Abundance ¹¹⁹Sn Precursors. *J. Am. Chem. Soc.* **2014**, *136* (17), 6219–6222.

- (16) Hwang, S. J.; Gounder, R.; Bhawe, Y.; Orazov, M.; Bermejo-Deval, R.; Davis, M. E. Solid State NMR Characterization of Sn-Beta Zeolites That Catalyze Glucose Isomerization and Epimerization. *Top. Catal.* **2015**, *58* (7–9), 435–440.
- (17) Padovan, D.; Botti, L.; Hammond, C. Active Site Hydration Governs the Stability of Sn-Beta during Continuous Glucose Conversion. *ACS Catal.* **2018**, *8* (8), 7131–7140.
- (18) Scott, S. L. A Matter of Life(Time) and Death. *ACS Catal.* **2018**, *8* (9), 8597–8599.
- (19) Levenspiel, O. *Chemical Reaction Engineering*; 1999; Vol. 38.
- (20) Holm, M. S.; Saravanamurugan, S.; Taarning, E. Conversion of Sugars to Lactic Acid Derivatives Using Heterogeneous Zeotype Catalysts. *Science*. **2010**, *328* (5978), 602–605.
- (21) Tolborg, S.; Spudaba, I.; Osmundsen, C. M.; Fristrup, P.; Holm, M. S.; Taarning, E. Tin-Containing Silicates : Alkali Salts Improve Methyl Lactate Yield from Sugars. **2015**, No. MI, 613–617.
- (22) Gounder, R.; Davis, M. E. Monosaccharide and Disaccharide Isomerization over Lewis Acid Sites in Hydrophobic and Hydrophilic Molecular Sieves. *J. Catal.* **2013**, *308*, 176–188.
- (23) Vega-Vila, J. C.; Harris, J. W.; Gounder, R. Controlled Insertion of Tin Atoms into Zeolite Framework Vacancies and Consequences for Glucose Isomerization Catalysis. *J. Catal.* **2016**, *344*, 108–120.
- (24) Conrad, S.; Wolf, P.; Müller, P.; Orsted, H.; Hermans, I. Influence of Hydrophilicity on the Sn β -Catalyzed Baeyer–Villiger Oxidation of Cyclohexanone with Aqueous Hydrogen Peroxide. *ChemCatChem* **2017**, *9* (1), 175–182.
- (25) Gounder, R.; Davies, M. E. Beyond shape selective catalysis with zeolites: hydrophobic void spaces in zeolites enable catalysis in liquid water. *AIChE J.* **2013**, *59* (9), 3349–3358.
- (26) Yakimov, A. V.; Kolyagin, Y. G.; Tolborg, S.; Vennestrøm, P. N. R.; Ivanova, I. I. ¹¹⁹Sn MAS NMR Study of the Interaction of Probe Molecules with Sn-BEA: The Origin of Penta- and Hexacoordinated Tin Formation. *J. Phys. Chem. C* **2016**, *120* (49), 28083–28092.
- (27) Gounder, R.; Davis, M. E. Monosaccharide and Disaccharide Isomerization over Lewis Acid Sites in Hydrophobic and Hydrophilic Molecular Sieves. *J. Catal.* **2013**, *308*, 176–188.

Chapter 4

From thermal regeneration to pre-activation of Sn-Beta zeolite.

The content of this chapter was published in the following manuscript:

ACS Catal. **2020**, 10,11545-11555

4.1 Introduction:

Chapter 2 of the thesis demonstrated that the stability of Sn-Beta for the valorisation of hexoses could be enhanced dramatically by adding small quantities of water to the conventional sugar/methanol feed.¹ In doing so, the continuous conversion of various hexoses was catalysed for up to 57 days, without experiencing significant levels of deactivation. Through a variety of spectroscopic and kinetic methods, the improvement of the stability of Sn-Beta was attributed to the prevention of the Sn-methanol interactions by the adding of traces of water.² During the same study, an alternative method to achieve catalyst regeneration was also identified (“washing regeneration”), whereby activity could be restored to the catalyst without resorting to classical high temperature thermal treatment, simply by flushing the reactor column with a methanol/water solution at the reaction temperature (110 °C).²

Motivated by this discovery, this chapter presents a study of the deactivation and reactivation of Sn-Beta catalysts during the continuous valorisation of hexoses. Through a variety of kinetic and spectroscopic (¹¹⁹Sn CPMG MAS NMR, FTIR, porosimetry, vapour sorption) methods,³ the changes that occur to these materials is monitored during various regeneration processes, and it is demonstrated how some of these changes correlate favourably to improved activity and stability. By understanding the parameters that govern improved performance following regeneration, it is demonstrated how increased activity and stability can also be accessed prior to reaction by developing “pre-activation protocols”, where the catalyst is solvothermally treated prior to reaction for short periods.

The discovery of this new protocol to enhance Sn-Beta activity is shown to effectively yield a new class of Sn-Beta catalyst, with different speciation, characteristics and performances from the Sn-Beta synthesized by conventional Solid State Incorporation (SSI).⁴ In Chapter 3 the comparison of different preparations of Sn-Beta catalysts showed how the hydrothermal preparation yields to the most active and stable catalyst for glucose isomerisation (GI) and glucose cleavage to methyl lactate (ML).⁵ Nonetheless this preparation of Sn-Beta presents important hurdles during its preparations, such as lengthy crystallisation times and the use of hydrofluoric acid (HF) as mineralising agent.⁶⁻⁸ Therefore

the need to find a valid alternative to this catalyst is paramount for future Sn-Beta applications on an industrial level.

For these reasons, the second part of this chapter recalls the properties of hydrothermal Sn-Beta (Sn-Beta_{HDT}) and compares these to the properties of pre-activated Sn-Beta (Sn-Beta_{PA}). These catalysts are tested in glucose upgrading to α -hydroxy esters at 160 °C in the presence of different promoters such as water and alkali salts.^{2,9,10} This reaction was chosen since the formed products are high added value intermediates which can be used in the production of bio-plastic and surfactants.¹¹⁻¹³ The response of each prepared catalyst to each perturbation is monitored to understand which features of these catalysts are essential for the synthesis of highly active Sn-Beta.

4.2 Experimental details:

4.2.1 Catalyst synthesis

A commercial Al-Beta zeolite (Zeolyst, NH₄⁺-form, Si/Al = 19) was dealuminated by treatment in HNO₃ solution (13 M HNO₃, 100 °C, 20 mL g⁻¹ zeolite, 20 h). SSI was achieved by grinding the appropriate amount of tin(II) acetate with the necessary amount of dealuminated zeolite for 10 minutes in a pestle and mortar. Following this procedure, the sample was heated in a combustion furnace (Carbolite MTF12/38/400) to 550 °C (10 °C min⁻¹ ramp rate) first in a flow of N₂ (3 h) and subsequently air (3 h) for a total of 6 h. Gas flow rates of 60 mL min⁻¹ were employed at all times.

The hydrothermal synthesis of Sn-Beta was performed following a procedure described in literature in reference 14: 30.6 g of tetraethyl orthosilicate (TEOS) was added to 33.1 g of tetraethylammonium hydroxide (TEAOH) under careful stirring, forming a two-phase system. After 60–90 min, one phase was obtained and the desired amount of the tin source, typically SnCl₄·5H₂O dissolved in 2.0 mL of H₂O, was added dropwise. The solution was then left for 48 h under stirring until a viscous gel was formed. The gel was finalised by the addition of 3.1 g HF in 1.6 g of demineralized H₂O yielding a solid gel with the molar composition; 1.0Si: 0.005Sn: 0.02Cl⁻: 0.55TEA⁺: 0.55F⁻: 7.5H₂O. The obtained gel was transferred in a Teflon lined stainless steel autoclave and kept for 7 days at 140 °C to crystallise. The obtained crystals were filtered and washed with deionised water. Calcination at 550 °C (2 °C min⁻¹) for 6 h under static air was carried out in order to remove the organic template.

4.2.2 Catalyst Characterisation

X-Ray Diffraction spectra were acquired using a PANalytical X'PertPRO X-ray diffractometer. A CuK α radiation source (40 kV and 30 mA) was utilised. Diffraction patterns were recorded between 6–55° 2 θ (step size 0.0167°, time/step = 150 s, total time = 1 h).

Specific surface area was determined from nitrogen adsorption using the BET equation, and microporous volume was determined from nitrogen adsorption isotherms using the t-plot method. Porosimetry measurements were performed on a Quantachrome Autosorb-iQ-

MP/XR, and samples were degassed prior to use (115 °C, 6h, nitrogen flow). Vapor adsorption experiments were performed on the same instrument maintaining the sample at 20° and adsorbing water from 0 to 0.7 P/P₀.

Magic Angle Spinning (MAS) solid state NMR analysis was performed at Durham University through the National solid-state NMR service, and at Cardiff University with Cardiff Catalysis Institute (CCI) facilities. All the samples were non-enriched and were measured on a Bruker Avance III HD spectrometer at operating frequencies of 400, 100, 149 and 79 MHz for ¹H, ¹³C, ¹¹⁹Sn and ²⁹Si, respectively. Typically, between 50-100 mg of solid sample was packed in a 4 mm rotor and spun at ± 12,000 Hz. For ¹¹⁹Sn MAS NMR, samples were measured by the Carr-Purcell-Meiboom-Gill (CPMG) method as described in references 15 and 16. Spectra were acquired both in Direct Excitation (DE) and Cross Polarisation (CP, ¹H-¹¹⁹Sn) modes. Recycle delay times (t₁) are shown in table 1.

Table 1. Parameters for ¹¹⁹Sn CPMG MAS NMR analysis on Sn-Beta.

Entry	Analytical centre	Analysis	t ₁ (s)	Scan Number
1	Durham National Solid-state NMR centre	Direct Excitation	2	24000
2	Durham National Solid-state NMR centre	Cross Polarisation	1	14000
3	Cardiff University	Direct Excitation	135	512

DRIFT spectroscopy analyses were performed in a Harrick praying mantis cell, with the spectra recorded on a Bruker Tensor Spectrometer over a range of 4000-650 cm⁻¹ at a resolution of 2 cm⁻¹. Experiments were performed increasing the temperature at 5 °C min⁻¹ up to 300 °C to dehydrate the sample under a flow on N₂ (40 mL min⁻¹)

4.2.3 Kinetic evaluation and analytical methods

Continuous glucose upgrading reactions were performed in a plug flow, stainless steel, tubular reactor. The catalyst was pelletised (size fraction 63 and 77 μm) and densely packed into a ¼" stainless steel tube (4.1 mm internal diameter). Two plugs of quartz wool and a frit of 0.5 μm held the catalyst in location. Temperature control was achieved by a thermostatted oil bath at the desired reaction temperature, and pressurization was achieved by means of a backpressure regulator. Aliquots of the reaction solutions were taken periodically from a sampling valve placed after the reactor and analysed by an Agilent 1260 Infinity HPLC equipped with a Hi-Plex Ca column and ELS detector and quantified against an external standard (sorbitol) added to the sample prior the injection.

Solvothermal regeneration of the catalytic bed was performed by changing the reactor feed to a mixture of methanol:water (90:10 % wt.), which was flowed through the bed for 20 h. The treatment was carried out at the same flow rate and the same temperature at which the reaction was performed (110 °C). Subsequently, the reactor feed was switch back to the reactant solution and a second cycle was performed. Thermal regeneration was performed by disconnecting the stainless-steel reactor tube from the reactor, and heating the entire reactor assembly at 550 °C in a Carbolite 12/38/400 MTF tube furnace.

GI batch studies were performed in a pressurised Ace tubular glass reactor thermally controlled by a hot oil bath on an IKA hot plate. 4 g of reactant solution (1 % wt. glucose in methanol) and catalysts were placed inside the reactor. Samples were periodically collected and analysed by HPLC as described above.

Continuous Bayer Villiger Oxidations (BVO) reactions were performed in a home-made plug flow, stainless steel, tubular reactor with the same system used for continuous GI. Aliquots of the BVO reaction solutions were taken periodically from a sampling valve placed after the reactor, and were analysed chromatographically by a GC (Agilent 7820, 25 m CP-Wax 52 CB column) and quantified against a biphenyl internal standard.

Continuous Transfer Hydrogenation (TH) reactions were performed in a plug flow, stainless steel, tubular reactor with the same system used for continuous GI. Aliquots of the TH reaction solutions were taken periodically from a sampling valve placed after the reactor. All reactants and products during TH were analysed by GC (Agilent 7820, 25 m CP-Wax 52 CB column), and quantified against a biphenyl internal standard.

The glucose employed as substrate was provided by Sigma Aldrich (>99.5 %, monohydrate), methanol anhydrous as solvent was provided by Sigma Aldrich (99.8 %), deionised water was added to the reaction feed. Standard of fructose, mannose, methyl lactate were provided by Sigma Aldrich (> 99.9 %). Methyl Vinyl Glycolate as standard was provided by Tokyo Chemicals Industry (>99.9 %). Cyclohexanone for BVO and TH reaction was provided by Sigma Aldrich (>99.9 %). 2-Butanol and Dioxane used as solvent for BVO and TH were provided by Sigma Aldrich (>99.5 %).

4.3 Results and discussion: from regeneration to pre-activation

4.3.1 Preliminary regeneration studies

Washing regeneration – whereby (partially) deactivated samples of Sn-Beta are regenerated by flushing the reactor column with a methanol:water mixture (90 % wt. MeOH and 10 % wt. H₂O, henceforth methanol:water 90:10) at reaction temperature – offers several potential advantages over thermal regeneration at 550 °C. The most notable of these include the use of milder temperatures and hence minimised energy consumption, avoiding the need to drain the reactor as is required prior to thermal regeneration, and removing the need for the reactor to have provision for high temperature heating and gas flow. However, to be a viable method of catalyst regeneration, washing regeneration must be able to restore catalyst activity over multiple regeneration cycles. Thus, to evaluate the true potential of the washing regeneration process, a series of deactivation-reactivation cycles were investigated for the low temperature (110 °C) isomerisation of glucose to fructose (GI), which is a critical reaction in the context of Sn-Beta catalysis and biomass conversion (Chapter 1, Section 1.8). For these initial experiments, a sample of Sn-Beta prepared by Solid State Incorporation (SSI) and containing 10 % wt. Sn was employed as the primary catalyst. The catalyst is henceforth-denoted 10Sn-Beta.

Figure 1 presents three operational cycles of 10Sn-Beta during two separate GI experiments, which differed only by the choice of regeneration method used between cycles. Cycle 1 of both experiments was identical, whereby GI was performed with a freshly synthesised sample of 10Sn-Beta for a total of 50 h at benchmarked operational conditions (110 °C, 1 wt. % glucose in methanol). Following this initial identical period of operation, the catalyst employed in each experiment was regenerated two times, resulting in three operational cycles being performed for a total of 150 h in each experiment. However, a different method of regeneration was followed in each experiment. In the first experiment, the catalyst was washed in a mixture of methanol:water 90:10 for 20 h at 110 °C between cycles, in line with the discovery presented in Chapter 2. In the second experiment, regeneration of the catalyst between cycles was achieved by classical thermal treatment in air at 550 °C for 3 h. All operational cycles were performed at 110 °C, using pure methanol as solvent (1 wt. % glucose in methanol), as the faster rates of deactivation observed in the absence of water allowed to probe deactivation and reactivation more rapidly (*accelerated ageing*).¹⁷ Experiments were compared by the glucose conversion (equation 3 in the equation appendix) as a function of total time on stream (figure 1 Left), and the fructose selectivity (equation 8 in the equation appendix) of the process as a function of glucose conversion (figure 1 Right).

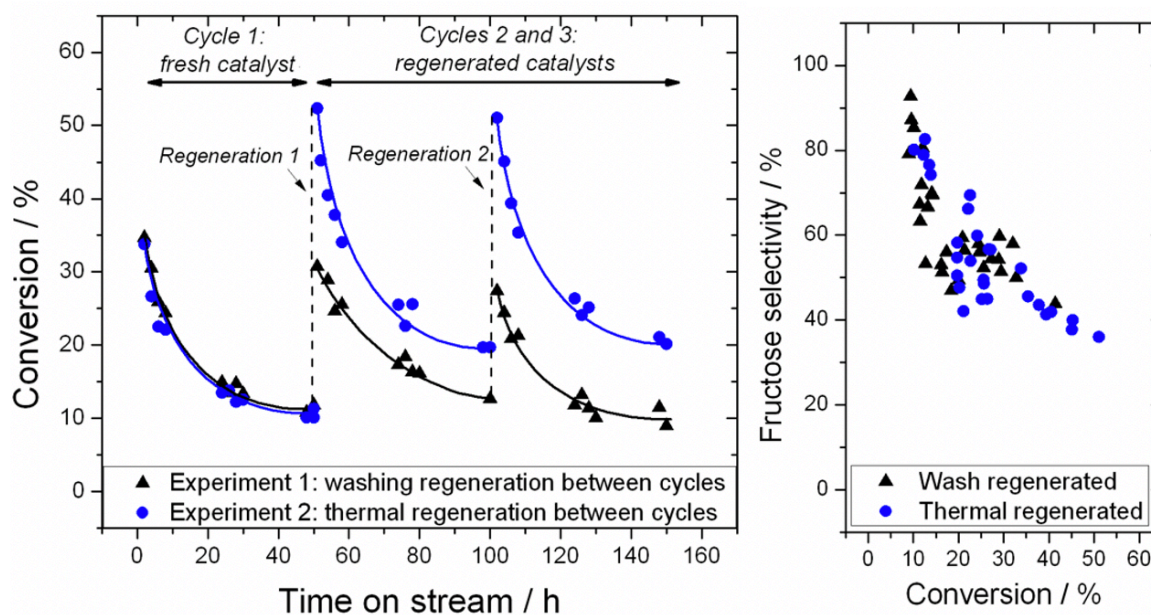


Figure 1. Continuous performance of 10Sn-Beta for glucose isomerisation at 110 °C in MeOH with (Left) conversion of glucose versus time on stream, and (Right) fructose selectivity as a function of glucose conversion. Experimental details: 1 % wt. glucose in methanol, 110 °C , 10 bar, 100 mg of catalyst, flow of reactant: 0.75 mL min⁻¹. Washing regeneration was performed flowing methanol:water 90:10 over the catalytic bed at 0.75 mL min⁻¹. Thermal regeneration was performed by calcining the used catalyst in air at 550 °C for 3h.

As can be seen (figure 1), deactivation of 10Sn-Beta in cycle 1 of both experiments occurred relatively rapidly, and conversion decreased from 35 % to 10 % over 50 h on stream. Over this time frame, the yield (equation 9 in the equation appendix) of fructose also decreased, although more gradually in line with the conversion *versus* fructose selectivity relationship established for the reaction (figure 1). The yield of fructose is not showed on figure 1 Left to facilitate the understanding of the figure, but on figure 1 Right is possible to see how the selectivity at the same rate of conversion is similar for both the cycles of experiments. Following the initial cycle of both experiments, two further operational cycles were carried out for each experiment, but with different regeneration protocols used between each cycle. In the first experiment, regeneration between cycles was achieved by washing regeneration. As can be seen (figure 1, experiment 1) activity was largely restored between cycles upon washing, and the catalyst exhibited similar performance in cycles 2 and 3. However, it is clear that activity was never fully restored following each regeneration procedure, with maximum conversion decreasing from 35 % in cycle 1, to 30 % and 27 % in cycles 2 and 3, respectively. It was demonstrated in Chapter 2 (Section 2.3.5) that washing regeneration of the catalyst removes both carbonaceous residue from the material, and also rehydrates the active site environment. However, since full activity of the catalyst was not restored by washing between cycles, this could indicate that washing does not totally decarbonise or rehydrate the sample, allowing these effects to gradually affect long-term performance. Alternatively, it could indicate that an additional, as-yet unidentified, long-term process also contributes to deactivation.

In contrast, a dramatic improvement to the activity of the catalyst was observed following thermal regeneration. Consequently, in cycles 2 and 3, the maximal activity of the catalyst was in excess of 50 % conversion, and activity did not decrease below 20 % throughout the additional operational periods. These observations show that the relative performance (equation 4 in the equation appendix) of the catalyst increased by 50 % following thermal regeneration. However, it should be noted that as the thermally regenerated catalyst exhibited conversion values close to the equilibrium level of the reaction (57-58 % at 110 °C),^{18,19} the true extent of activity increase following thermal regeneration could be greater than 50 %. Despite being more active, the conversion *versus* selectivity profile for both reactions (figure 1 Right) demonstrates that the selectivity performance of the catalysts was unaffected by the choice of regeneration method at all overlapping levels of conversion.

Although the preparation of 10Sn-Beta by SSI already involves high temperature thermal treatment prior to operation (550 °C, 3 h N₂ followed by 3 h in air),⁴ performing an additional thermal treatment of the catalyst at the conditions of thermal regeneration (550 °C, 3 h, air) prior to undertaking the first catalytic cycle of the experiment did not result in improved performance (figure 2). Clearly, prior interaction with the solvent and/or reactants is required for the effects detailed above to be obtained.

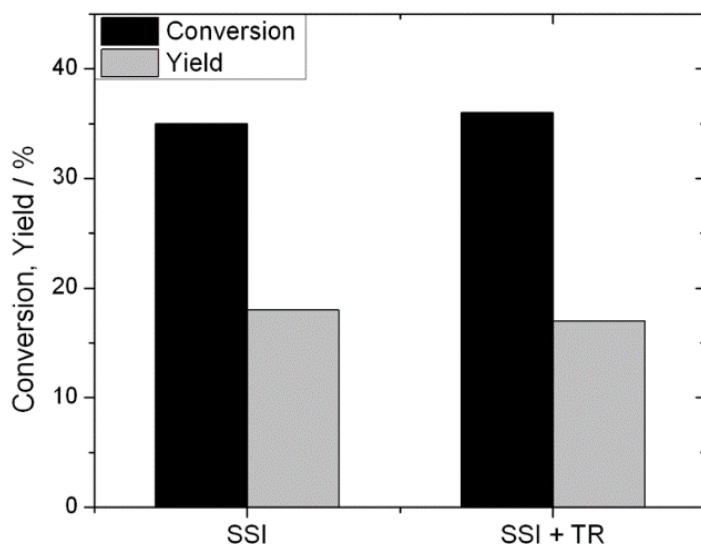


Figure 2. Catalytic activity of 10Sn-Beta for glucose isomerisation at 110 °C after conventional solid state incorporation (the heat treatment procedure of which involves heating to 550 °C for 3 h in N₂, followed by 3 h in air) (SSI), or solid state incorporation followed by an additional thermal treatment at the conditions of thermal regeneration (550 °C, 3 h, air) (SSI+TR). Experimental details: 1 % wt. glucose in methanol, 110 °C , 10 bar, 100 mg of catalyst, flow of reactant: 0.75 mL min⁻¹.

To further probe the effects of regeneration, a series of mixed regeneration protocols was explored following initial operation of the fresh catalyst (figure 3). As can be seen, following thermal regeneration of the sample, the catalyst could no longer be fully regenerated by washing, with conversion and yield values not recovering much above the levels observed at the end of cycle 2. Given that washing clearly regenerated the fresh catalyst, this indicates that after thermal regeneration the catalyst possess different properties making it no longer amenable to regeneration by washing. However, its activity could still be restored by an additional thermal regeneration (cycle 4), confirming the increase in activity observed after cycle 1 to be permanent.

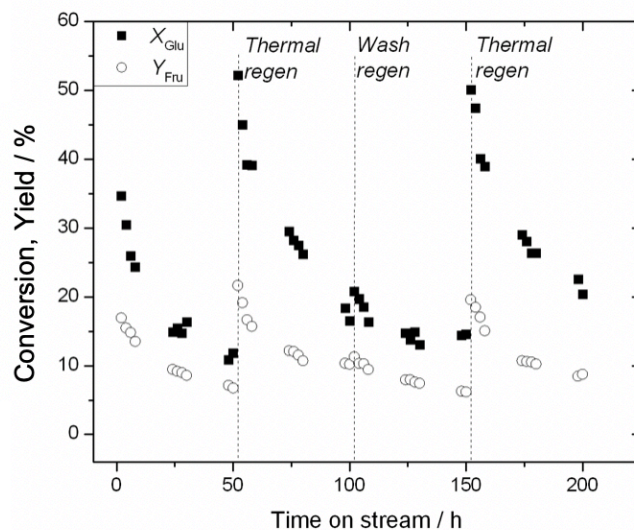


Figure 3. Continuous operation of 10Sn-Beta for glucose isomerisation prior to, and following, various regeneration protocols. Experimental conditions on Table 3. Experimental details: 1 % wt. glucose in methanol, 110 °C , 10 bar, 100 mg of catalyst, flow of reactant: 0.75mL min⁻¹. Washing regeneration was performed flowing methanol:water 90:10 over the catalytic bed at 0.75 mL min⁻¹. Thermal regeneration was performed by calcining the used catalyst in air at 550 °C for 3h.

Similar deactivation-reactivation cycles performed on samples of Sn-Beta containing lower quantities of Sn (2Sn-Beta) revealed that the positive effect of thermal regeneration was observed irrespective of the Sn loading during GI (figure 4).

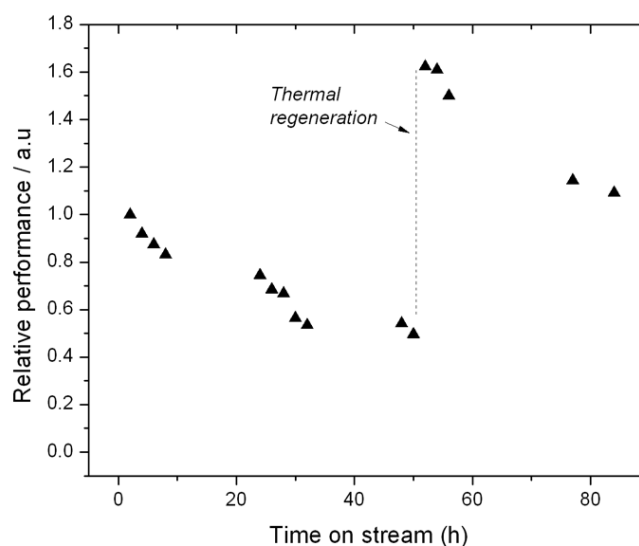


Figure 4. Relative performance of 2Sn-Beta for glucose isomerisation at 110 °C in MeOH prior to and following thermal regeneration. Reaction conditions: 1 wt. % glucose in methanol, 0.8 mL min⁻¹, 100 mg 2Sn-Beta, 110 °C. Thermal regeneration was performed by calcining the used catalyst in air at 550 °C for 3h.

Moreover, regeneration cycles performed on Sn-Beta during other catalytic processes, including the Baeyer-Villiger oxidation (BVO) of ketones with H₂O₂, and the catalytic transfer

hydrogenation (CTH) of furfural, revealed the positive effect of thermal regeneration was also present in other systems, albeit to a much lower degree (ca. 15 % increase in relative performance, figure 5).

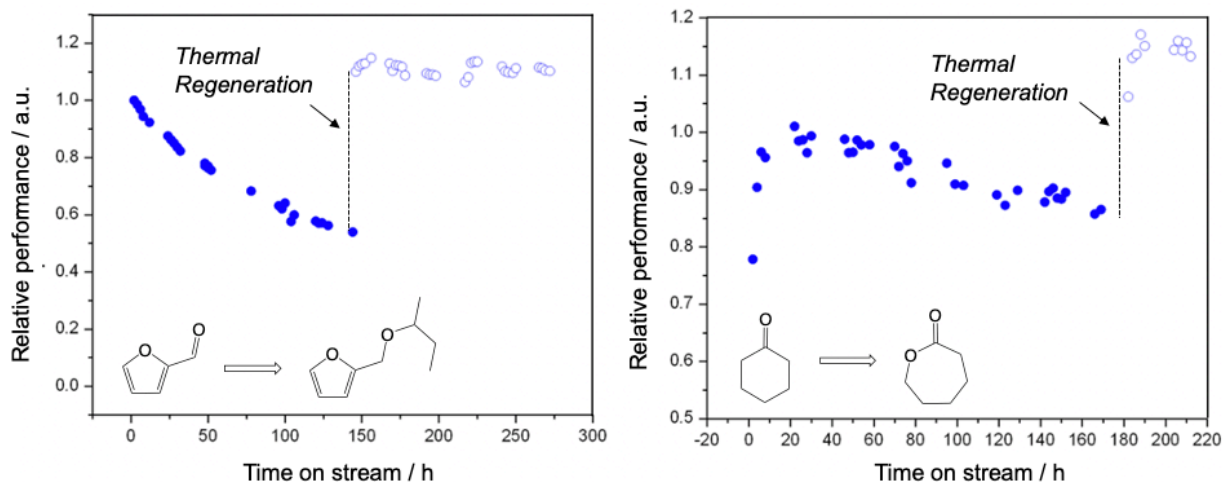


Figure 5. (Left) Relative performance of 2Sn-Beta for the catalytic transfer hydrogenation of furfural as fresh catalyst (cycle 1) and following thermal regeneration. Reaction conditions: 0.2M furfural in 2-butanol, flow rate 0.07 mL min⁻¹, 100 °C, 200 mg 2Sn-Beta. Thermal regeneration was performed by calcining the used catalyst in air at 550 °C for 3h. (Right) Relative performance of 2Sn-Beta for the Baeyer-Villiger oxidation of cyclohexanone prior as fresh catalyst (cycle 1) and following thermal regeneration. Reaction conditions: 0.33M cyclohexanone in 1,4-dioxane, 0.08 mL min⁻¹, 100 °C, 400 mg of 2Sn-Beta. Thermal regeneration was performed by calcining the used catalyst in air at 550 °C for 3h.

As described in figure 1, the excessively high levels of conversion exhibited by the thermally regenerated catalyst under the conditions optimised for the fresh sample may result in its activity being underestimated by operating close to the thermodynamic equilibrium of the reaction.^{18,19} Thus, to gain a better understanding of the kinetic performance of Sn-Beta following thermal regeneration, the activity of the catalyst was evaluated as a function of contact time (equation 2 in the equation appendix), by monitoring the quantity of glucose converted at various weight hourly space velocities (WHSVs, equation 10 in the equation appendix). As can be seen, although the fresh and thermally regenerated catalysts exhibited comparable levels of selectivity as a function of conversion (figure 1 Right), the kinetic performance of the thermally regenerated sample was much improved, exhibiting a first order rate constant over twice that of the fresh sample (9.7 and 4.4 s⁻¹ respectively, figure 6 Left). Thus, it is clear that large improvement in the activity of Sn-Beta is observed following thermal regeneration of the catalyst after the first period of operation.

The improved activity of the catalyst following thermal regeneration could be due to the formation of additional amounts of the original active site, or the generation of a new active site of increased intrinsic reactivity. Accordingly, an Arrhenius expression of both samples, obtained over a temperature range of 90-110 °C, was undertaken (figure 6 Right). This demonstrated that changes to both the activation energy and the pre-exponential factor

were observed following thermal regeneration. Surprisingly given its higher levels of activity, the activation energy of the catalyst increased following thermal regeneration (109 versus 75 kJ mol⁻¹). However, this increase in barrier was accompanied by a substantial increase in the pre-exponential factor (2.9×10¹² versus 2.1×10⁷). Such changes in kinetic values suggest that thermal regeneration is accompanied by the formation of a new type of active site and/or active site environment, characterised by different levels of reactivity and accessibility, compared to that found in the fresh material.²⁰

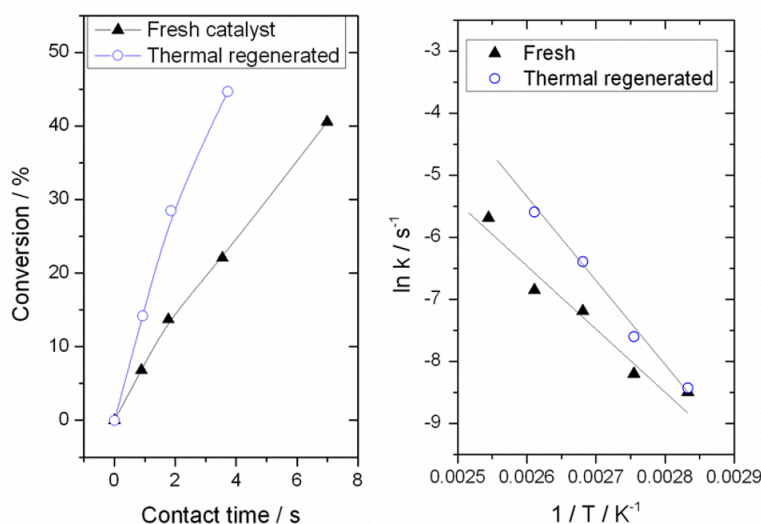


Figure 6. (Left) Kinetic activity of fresh 10 Sn-Beta, and thermally regenerated 10Sn Beta, as a function of contact time at 110 °C. (Right) Arrhenius expression for fresh 10Sn-Beta, and thermally regenerated 10Sn-Beta between 90-110 °C. Reaction conditions: 1% wt. glucose in methanol, 15 bar, 10-20 bar, 1-8 s of contact time, 90-120 °C.

4.3.2 Preliminary spectroscopic studies

To investigate the changes that occur to the catalyst during operation-regeneration cycles, a variety of spectroscopic measurements were performed on the fresh catalytic material, and to the materials obtained following washing and thermal regeneration. Techniques sensitive to the textural and compositional properties of the sample (XRD, porosimetry, ICP-MS) indicated that all three samples (fresh, washing regenerated, thermal regenerated) possess the same level of crystallinity (figure 7), and comparable levels of porosity (table 1)

This indicates that structural modifications to the sample following thermal regeneration, such as topological conversion or the generation of a hierarchial matrix,²¹ are not responsible for the improved levels of performance observed. Notably, the total pore volume of the washing regenerated sample is somewhat lower than the fresh and thermally regenerated samples, likely due to incomplete removal of the carbonaceous residue formed during reaction by washing. Although it was demonstrated in Chapter 2 (2.3.2) that the accumulation of this residue is not a major cause of deactivation of Sn-Beta during this

reaction, the slight accumulation of this residue could account for the gradual loss in maximal activity of Sn-Beta during the three operational cycles discussed in figure 1.

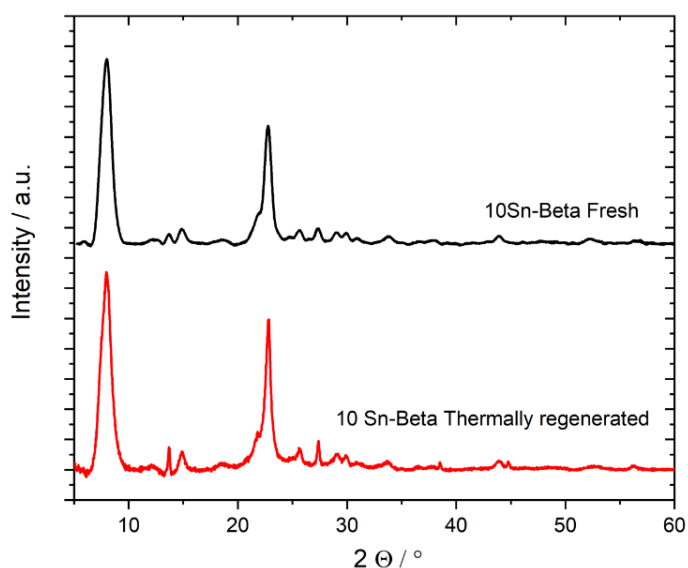


Figure 7. XRD analysis for thermally regenerated (red) and fresh 10Sn-Beta zeolite (black).

Table 1. Textural properties of 10Sn-Beta prior to glucose isomerisation at 110 °C in MeOH, and following, various regeneration protocols.

Entry	Catalyst	BET Area (m ² g ⁻¹) ^a	Total pore volume (cm ³ g ⁻¹) ^b
1	10Sn-Beta (Pelletised, 63-75 um, 7 Tons)	351	0.23
2	10Sn-Beta after cycle 1	279	0.18
3	10Sn-Beta regenerated by washing	334	0.21
4	10Sn-Beta regenerated by heating	356	0.23

a Surface area determined from nitrogen adsorption using BET equation. **b** Micropore volume determined by t-plot method

The changes to the Arrhenius expression of the catalyst following thermal regeneration (figure 6 Right) suggest that changes to the active sites and/or active site environment of the catalyst occur. Therefore, methods sensitive to the active sites of the catalyst were explored. Accordingly, ¹¹⁹Sn MAS NMR was exploited as a more sensitive and selective methodology. Spectra were recorded by Carr-Purcell-Meiboom-Gill (CPMG) echo-train acquisition methods, under the conditions optimised by the Ivanova group ($t_1 = 2$ s).^{15,16} To maintain the integrity of all samples, each samples was measured without additional pre-treatment. Figure 8 presents the ¹¹⁹Sn MAS NMR spectra of 10Sn-Beta prior to operation (a), following reaction in pure methanol (b), following washing regeneration (c) and following thermal regeneration (d) in both Direct Excitation (Left) and Cross Polarisation (Right) modes. In line with recent studies, the fresh catalyst demonstrated four clear resonances at

chemical shifts of -705, -658, -600 and -541 ppm. The resonances at -541 and -600 can be attributed to pentacoordinated framework Sn species and extra-framework oxides of Sn, respectively, whereas the resonances at -660 and -705 are attributable to octahedral framework Sn species. In line with previous Sn-Beta spectra in Chapter 2 (Section 2.3.3), only minor changes to the DE-CPMG spectrum are observed after reaction in pure methanol and after washing regeneration of the catalyst, with the same four resonances observed *albeit* with slight differences in relative intensities. However, following thermal regeneration of the sample, an obvious change to the octahedral framework Sn species occurs. Indeed, the relative intensity of the -658 ppm species decreases substantially, and the dominant resonance arising from octahedrally coordinated framework tin (-705 ppm) shifts to higher values (to -696 ppm). As the precise chemical shift of octahedral framework Sn species depends on their T-site occupation, their degree of hydration, and the number and type of framework defects within the proximity of Sn, an increase of 10 ppm in the chemical shift of this sample indicates a change in the speciation of the active sites of the catalyst.^{21,22} However, despite the clear signal at -696 ppm in the DE-CPMG spectrum of thermally regenerated 10Sn-Beta, no resonance at this chemical shift is observed by ¹H-¹¹⁹Sn cross polarisation in the CP-CPMG spectrum. This indicates the absence of protons in the environment of this signal, despite the samples being measured several weeks after preparation, indicating that this species does not directly interact with protons. This could be due to the absence of Sn-OH species, and/or could indicate that the site is not amenable to hydration (Sn--OH₂). Notably, an inability to hydrate this site agrees to the inability of the thermally regenerated sample to be further regenerated by washing treatment. These observations, alongside the changes observed to the Arrhenius expression of the catalyst, support the hypothesis that thermal regeneration results in the formation of a new type of active site and/or active site environment, characterised by different levels of accessibility and reactivity, to those found in the fresh catalyst, as opposed to the formation of additional quantities of the original active site.

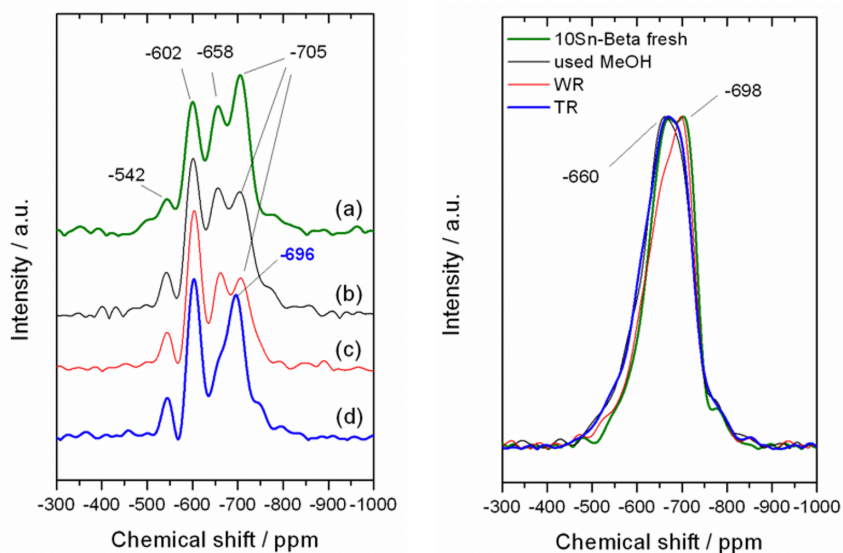


Figure 8. (Left) ^{119}Sn DE-CPMG MAS NMR spectra of 10Sn-Beta prior to operation (a), following reaction in pure methanol (b), following wash regeneration (c) and following thermal regeneration (d). (Right) ^{119}Sn CP-CPMG MAS NMR spectra of 10Sn-Beta prior to operation (green), following reaction in pure methanol (black), following wash regeneration (red) and following thermal regeneration (blue).

4.3.3. Catalyst pre-activation studies

The kinetic findings presented in Section 4.3.1 and Section 4.3.2 demonstrate that beneficial changes to the activity of Sn-Beta occur following operation and thermal regeneration of the catalyst. However, as this effect is only observed when thermal regeneration is performed after the first operational cycle of the catalyst, some prior interaction with the solvent and/or reactants and products is evidently required for improved performance to be achieved.

With the aim of improving macroscopic performance of the catalyst without resorting to an extended initial operational cycle, a series of catalyst “pre-activation” protocols were evaluated, in an attempt to access the more active state of the catalyst at the very start of the reaction. As described in the previous section, an additional thermal treatment of the fresh catalyst at the conditions of thermal regeneration prior to operation resulted in no improvement in activity (figure 2). As such, thermal treatment of the catalyst following various liquid-based “pre-activation” procedures in the continuous reactor was investigated. The performance of the catalyst following each pre-activation procedure was examined for GI at the same conditions as described above, and compared to that of the fresh catalyst. The turnover frequency (TOF_0 , equation 6 in the equation appendix) of each experiment was determined after 0.5 h on stream, and used for comparative purposes.

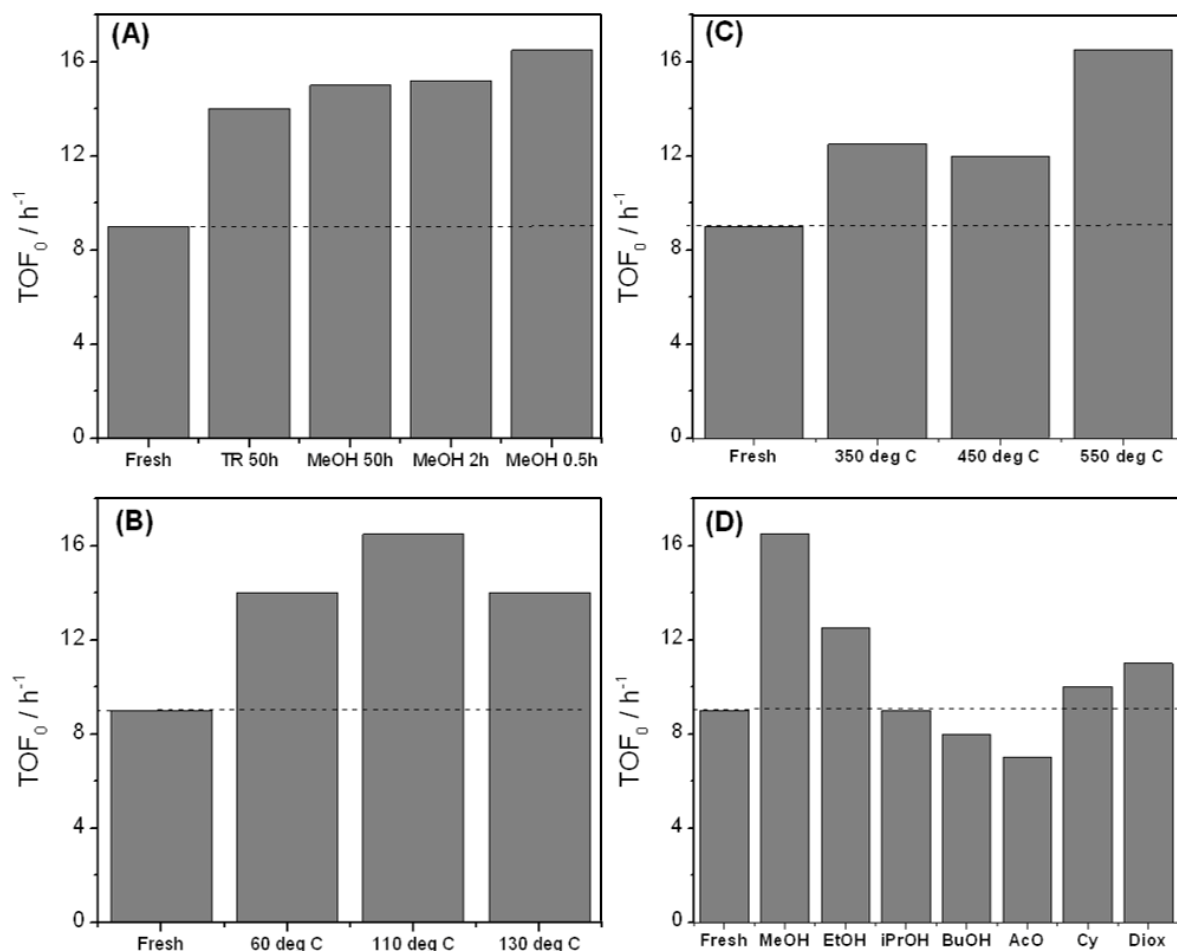


Figure 9. Kinetic activity of 10Sn-Beta-prior to (Fresh) and following various pre-activation protocols gained at 0.5 h of time on stream. (A) Effect of solution composition and pre-activation time on performance of Sn-Beta (TR 50h: 50 h treatment with 1% glucose in methanol). (B) Effect of the pre-activation temperature during pre-activation of the catalyst in pure methanol for 0.5 h. (C) Effect of calcination temperature following pre-activation in pure methanol for 0.5 h at 110 °C. (D) Effect of the choice of solvent during pre-activation at 110 °C for 0.5 h. MeOH, EtOH, iPrOH, BuOH, AcO, Cy and Diox represent methanol, ethanol, *iso*-propanol, butanol, acetone, cyclohexane and 1,4-dioxane, respectively. Thermal treatment performed at 550 °C (or different where specified) for 3h in air. Reaction conditions: 1.5 mL min⁻¹ flow of 1 wt. % glucose in pure methanol over 100 mg of Sn-Beta at 110 °C. Washing in the solvent was performed at 110 °C, 1.5 mL min⁻¹ of flow per 100 mg of catalyst at 10 bar of pressure.

As can be seen (figure 9A), a similar improvement in TOF to that achieved by thermal regeneration after 50 h of operation (TR 50 h) could be obtained by thermal treatment of 10Sn-Beta following treatment in a solution of pure methanol at 110 °C for 50 h. This confirms that the presence of reactants and/or products of the reaction in the feed are not essential for improved activity to be achieved. More importantly, optimising the length of MeOH treatment reveals that improved activity can be obtained following only 0.5 h of pre-activation in pure methanol at reaction temperature (110 °C), and by pre-activating the sample in pure methanol at lower temperatures (figure 9C). However, although the length

and temperature of the solvent step do not dramatically influence final activity of the catalyst, the choice of the calcination temperature does impact ultimate performance, with optimal activity being obtained after heat treating the sample at 550 °C (figure 9B). At the optimised pre-activation conditions (pre-activation in MeOH for 0.5 h at 110 °C, heat treatment at 550 °C), a number of alternative solvents were explored (figure 9D). At these conditions, substantial improvement in performance was only observed for small alcohols, such as methanol and ethanol. Larger alcohols, ketones and hydrocarbons did not lead to improvements in activity over the time period examined (0.5 h), although some improvement was observed for 1,4-dioxane, which may arise from the presence of ethylene glycol impurities observed in solution. Notably, the only solvents that result in substantial improvements in TOF are those that have been shown to be able to coordinate to Sn in a hexacoordinated manner *i.e.* those that are small enough for two solvent molecules to bind simultaneously to the Sn sites of the catalyst.¹⁵ However, some improvement in activity for these other solvents must be feasible, given the 10-15 % improvement in TOF exhibited by 10Sn-Beta during catalytic transfer hydrogenation and Baeyer-Villiger oxidation (figure 4, 5). Likely, for larger solvents, much longer treatment times would be required. Interestingly, a control experiment performed by pre-activating 10Sn-Beta in a batch reactor at 110 °C for 0.5 h was unsuccessful at improving the performance of the catalyst, even when pressurising the reactor with N₂ and ensuring the total quantity of methanol interacting with the catalyst was identical to that achieved in the continuous setup. This indicates that some other factor unique to the plug flow setup is essential for pre-activation to be achieved.

Having identified a suitable pre-activation protocol for 10Sn-Beta, the applicability of this methodology was evaluated for other Sn-Beta catalysts, particularly those with lower loadings of Sn. This is an important step both to understand the practical versatility of pre-activation, and to gain additional mechanistic insight of the process. Accordingly, various samples of Sn-Beta containing between 0.5-10 % wt. Sn were explored as catalysts for GI prior to, and following, pre-activation according to the optimised procedure described above (treatment in methanol at 110 °C for 0.5 h, followed by thermal treatment at calcination 550 °C). To aid comparison, the activity of each Sn-Beta catalyst described in this section was evaluated on a productivity (equation 1 in the equation appendix) basis *i.e.* activity per gram of catalyst material (equation 8, in the equation appendix), as this is more appropriate for comparing the performance of catalysts containing different loadings of Sn and hence quantities of active and inactive sites.

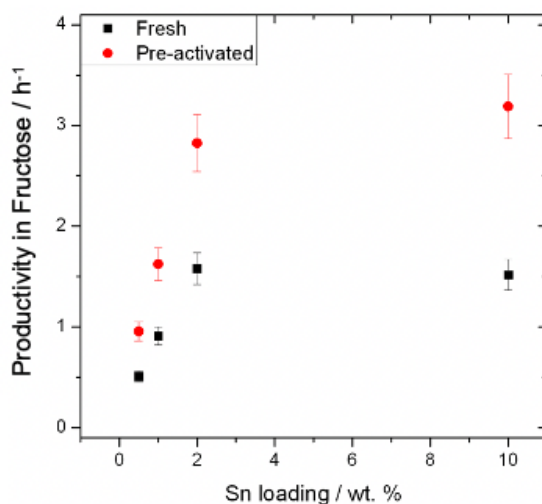


Figure 10. Productivity values exhibited by various Sn-Beta catalysts of different Sn loadings, prior to (black) and following (red) pre-activation in MeOH. Pre-activation performed by wetting in MeOH at 110 °C and 10 bar with a flow of 1.5 mL min⁻¹ and following thermal treatment performed at 550 °C for 3 h in air. Experimental condition reported in table 2.

Table 2. Experimental conditions for different loadings of Sn-Beta zeolite employed in continuous glucose isomerisation to fructose in methanol (1wt. % glucose in methanol). Pre-activation performed by wetting in MeOH at 110 °C and 10 bar with a flow of 1.5 mL min⁻¹ and following thermal treatment performed at 550 °C for 3h in air.

Description	Temperature (°C)	Mass (mg)	Flow (mL min ⁻¹)	X (%)	Y (%)
0.5Sn-Beta	110	0.1	0.3	42	16
1Sn-Beta	110	0.1	0.6	36	13
2Sn-Beta	110	0.1	0.8	37	14
10Sn-Beta	110	0.1	0.1	41	16
0.5Sn-Beta Pre-activated	110	0.1	0.5	46	18
1Sn-Beta Pre-activated	110	0.1	1	35	12
2Sn-Beta Pre-activated	110	0.1	1.2	42	17
10Sn-Beta Pre-activated	110	0.1	1.5	45	18

As can be seen in figure 10, increasing the Sn content of the fresh catalyst from 0.5-2 % wt. resulted in an increase in the productivity of the catalyst. This is due to the formation of additional active sites upon addition of extra Sn to the catalyst.²⁴ However, the increase in productivity was not directly proportional to the increased loading in this range, with the productivity of the catalyst increasing by a factor of three (0.5 to 1.5 h⁻¹) upon increasing the metal loading by a factor of four (0.5 to 2 % wt.). This suggests that some less active Sn sites and/or spectator species were formed even at these lower loadings. Although increasing the loading of Sn beyond 2 % wt. increases the overall productivity of the catalyst further, the increase in productivity levels off substantially at the highest loadings. Based on previous research²⁴ and the ¹¹⁹Sn MAS NMR spectrum presented above (figure 8), this can be attributed to the formation of extra-framework SnO_x species, which results in a large

fraction of the additional Sn content not contributing to activity, and hence not improving the productivity of the catalyst. Notably, an almost identical trend in productivity as a function of Sn loading was observed for the pre-activated series, with productivity increasing steeply between loadings of 0.5 and 2 % wt. Sn, and increasing much more gradually between 2 and 10 % wt. Sn. Yet, it is clear that the absolute productivity value of each catalyst is approximately two-fold higher following pre-activation. In addition to demonstrating the general applicability of the pre-activation protocol, these findings demonstrate that the relative increase in activity upon pre-activation is largely independent of loading (figure 11 Left).

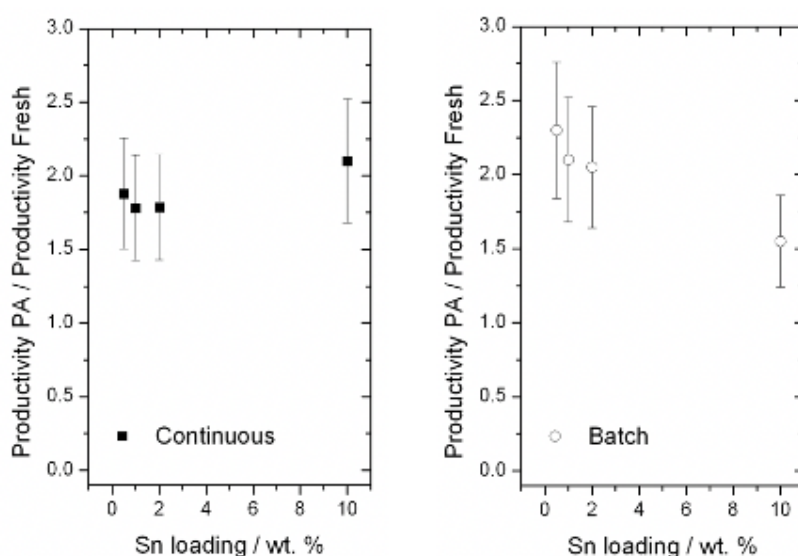


Figure 11. (Left) Relative increase in productivity of various Sn-Beta catalysts with different Sn loadings, following pre-activation, as measured in continuous mode. (Right) Relative increase in productivity of various Sn-Beta catalysts with different Sn loadings, following pre-activation, as measured in batch mode. Pre-activation performed by wetting in MeOH at 110 °C and 10 bar with a flow of 1.5 mL min⁻¹ and following thermal treatment performed at 550 °C for 3 h in air. Experimental condition reported in table 3.

Table 2. Experimental conditions for different loadings of Sn-Beta employed in batch glucose isomerisation to fructose in methanol (1 % wt. glucose in methanol). Pre-activation performed by wetting in MeOH at 110 °C and 10 bar with a flow of 1.5 mL min⁻¹ and thermal treatment performed at 550 °C for 3 h in air.

Description	Temperature (°C)	Mass (mg)	X (%)	Y(%)
0.5Sn-Beta	110	0.1030	10	5.3
1Sn-Beta	110	0.09	6.5	3.6
2Sn-Beta	110	0.07	7.2	5.3
10Sn-Beta	110	0.027	12	8.2
0.5Sn-Beta Pre-activated	110	0.1030	19	9
1Sn-Beta Pre-activated	110	0.09	11	6.8
2Sn-Beta Pre-activated	110	0.07	14	8.2
10Sn-Beta Pre-activated	110	0.027	15	6.9

However, care must be taken when comparing the activity of catalysts in continuous reactors, since deactivation events that occur in the very first stages of operation can influence the precise value(s) of productivity calculated, particularly if the rate of deactivation is high and especially if it differs between samples.²⁵ Accordingly, to rule out that increased activity observed in the continuous reactor was not solely due to increased stability of the catalyst following pre-activation, the activity of the fresh and pre-activated Sn-Beta samples were also evaluated in batch mode. In this case, productivity values were determined at short reaction times (2 minutes), to decouple the influence of deactivation. These experiments demonstrated that all pre-activated samples were approximately twice as productive as their fresh counterparts even in the batch reactor, confirming that pre-activation clearly improves the intrinsic activity of the catalyst, and that the extent of pre-activation does not depend on the loading of Sn in the catalyst (figure 11 Right). However, it should be noted that at very high loadings, the extent of pre-activation observed in batch mode appears to be slightly lower than that observed in the continuous reactor at elevated loadings. This suggests that at least some of the improved activity in the continuous reactor arises from improved stability of the catalyst following pre-activation. This was confirmed by evaluating some of the catalyst materials (1Sn-Beta, 10Sn-Beta) for stability according to the Levenspiel (equation 5 in the equation appendix) approach prior to and following pre-activation (Figure 12).²⁶

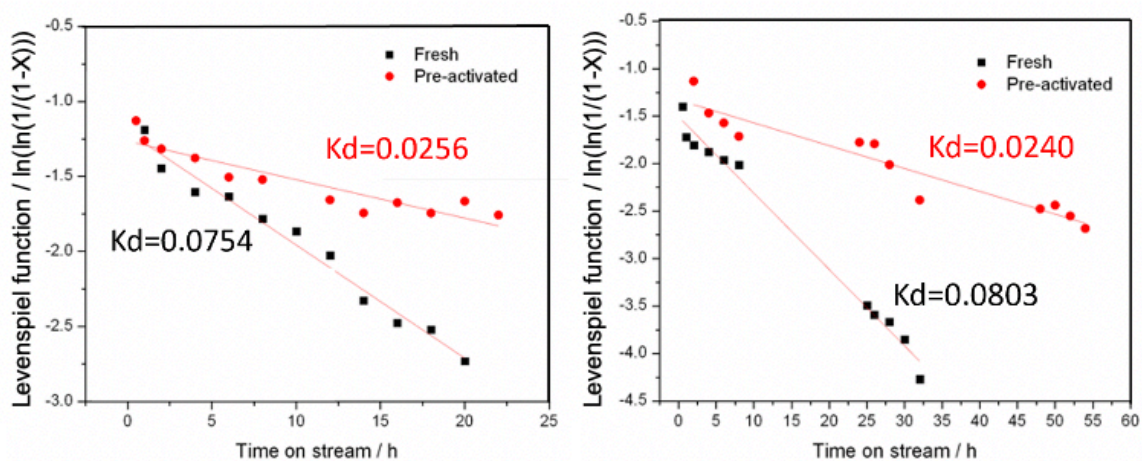


Figure 12. Levenspiel plots for 1Sn-Beta (left) and 10Sn-Beta (right), prior to (black squares) and following (red circles) pre-activation in methanol at 110 °C for 0.5 h. Experimental details: 1 % wt. glucose in methanol, 110 °C, 10 bar, 100 mg of catalyst. Flow was adjusted to obtain 35-40 % as starting conversion: 1 mL min⁻¹ for 10Sn-Beta (1.5 mL min⁻¹ after pre-activation), 0.6 mL min⁻¹ for 1Sn-Beta (1.0 mL min⁻¹ after pre-activation). Pre-activation performed by wetting in MeOH at 110 °C and 10 bar with a flow of 1.5 mL min⁻¹ and following thermal treatment performed at 550 °C for 3 h in air.

From this, it was found that the rate of deactivation decreased by a factor of approximately 3 following pre-activation. Thus, it is clear that pre-activation is applicable to all the Sn-Beta

catalysts studied in this work, and that pre-activation increases the performance of each catalyst through both a large intrinsic activity effect, and also through a less substantial (but still present) increase in stability.

4.3.4 Spectroscopic studies of pre-activated Sn-Beta zeolite

In addition, to determining the general applicability of pre-activation, these experiments provide useful insight into the mechanistic processes occurring during pre-activation. Indeed, it could be reasoned that if pre-activation related to the conversion of inactive Sn sites into additional active Sn sites, the relative increase in pre-activation should be greatest for those samples containing the highest fraction of inactive Sn sites *i.e.* high loaded catalysts. Yet, it is clear that the extent of pre-activation is largely independent of loading (figure 11). Accordingly, it can be hypothesised that pre-activation either relates to the modification of the initial active sites of each catalyst *i.e.* the Sn species that give rise to activity in the fresh samples, and/or to processes that are not directly to Sn itself, such as lattice effects or changes to other chemical properties of the catalyst.

Although preliminary spectroscopic studies of the thermally regenerated samples indicate that clear changes to the active sites of the catalysts occur during pre-activation, lattice effects could also explain the improved activity of Sn-Beta following pre-activation, and could justify the lack of correlation observed between the extent of pre-activation and initial Sn loading (figure 11). Although XRD (figure 7) and porosimetry (table 2) revealed no major structural modifications occurred during thermal regeneration, changes to the properties of the lattice following pre-activation could be observed through DRIFTS and vapour sorption methods. DRIFTS spectra of fresh and pre-activated 1Sn-Beta and 10Sn-Beta were first collected at room temperature (figure 13). At both loadings, consistent changes to the vibrational spectra could be observed following pre-activation. These include; an increased contribution of isolated silanol groups ($\equiv\text{Si-OH}$, 3740 cm^{-1}),¹⁵⁻¹⁷ a decrease in the magnitude of H-bonding interactions ($3200\text{-}3600\text{ cm}^{-1}$); and, a decrease in intensity characteristic of internal defect sites (960 cm^{-1}).^{27,28} Together, these observations indicate that pre-activation results in the formation of a more hydrophobic catalyst possessing fewer defect sites.²⁹ To verify this, DRIFTS spectra of 10Sn-Beta were re-measured after raising the sample cell temperature to $225\text{ }^{\circ}\text{C}$. Although this temperature is typically insufficient to dehydrate Sn-Beta²⁷ (as evidenced by the substantial intensity still observed between $3200\text{-}3600\text{ cm}^{-1}$ in the fresh catalyst at the same temperature), pre-activated 10Sn-Beta is almost fully dehydrated at this temperature.

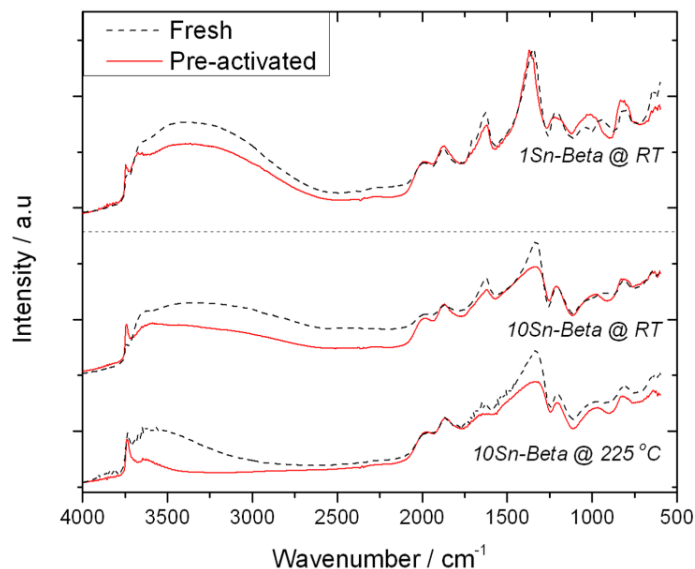


Figure 13. DRIFT spectra of 1- and 10Sn-Beta catalysts, in both fresh and pre-activated states, at various temperatures from room temperature (RT) to 225 °C. Pre-activation performed by wetting in MeOH at 110 °C and 10 bar with a flow of 1.5 mL min⁻¹ and following thermal treatment performed at 550 °C for 3 h in air.

To further verify the impact of pre-activation on the hydrophobic properties of Sn-Beta, vapour adsorption studies of 1Sn-Beta and 10Sn-Beta were performed prior to and following pre-activation, using water as sorbate (figure 14). In good agreement to the DRIFTS measurements, consistent changes to the sorption data are observed following pre-activation. Indeed, whereas both fresh catalysts exhibit more Type I character, which is representative of micropore condensation driven by adsorbate-adsorbent interactions, both pre-activated catalysts exhibit more Type V character. This is notable since Type V isotherms suggest micropore condensation is driven by adsorbate-adsorbate interactions.³⁰ This change in behaviour indicates that sorption is no longer driven by specific catalyst-sorbate interactions, implying that the catalysts become less amenable to directly interact with water following pre-activation. This is further supported by the quantity of water adsorbed by each catalyst. Indeed, at indicative P/P_0 values of 0.2, the volume of water adsorbed by the catalyst following pre-activation decreases by 27 % and 32 % for 10Sn-Beta and 1Sn-Beta, respectively. This supports the observations made from DRIFTS analysis, and confirms that an increase in catalyst hydrophobicity occurs following pre-activation of the catalyst in MeOH. Nevertheless, it should be stressed the quantity of water adsorbed even by the most hydrophobic pre-activated catalyst (1Sn-Beta, 21 cm³ g⁻¹ at $P/P_0 = 0.2$) is still higher than what observed for Sn-Beta materials synthesised by classical (fluoride media) hydrothermal methods (ca. 10 cm³ g⁻¹ at $P/P_0 = 0.2$) in Chapter 3.

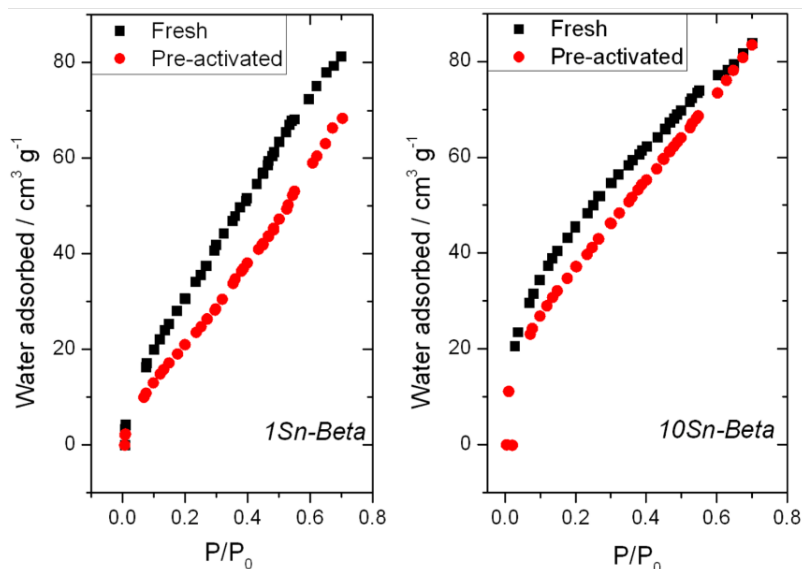


Figure 14. Water sorption isotherms of (Left) 1Sn-Beta and (Right) 10Sn-Beta, in both fresh and pre-activated states. Experimental details: Isotherm gathered at 20 °C from 0 to 0.7 P/P_0 . Pre-activation performed by wetting in MeOH at 110 °C and 10 bar with a flow of 1.5 mL min⁻¹ and following thermal treatment performed at 550 °C for 3 h in air.

To confirm whether the lower affinity for water arises solely from changes to the Sn sites of the catalyst, or occurs also to the lattice alone, similar studies were performed on dealuminated zeolite Beta *i.e.* the Sn-free material, prior to and following its pre-activation in MeOH at the optimised conditions (figure 15). At P/P_0 values of 0.2, the quantity of water adsorbed by the sample decreased from 26.3 cm³ g⁻¹ to 19.0 cm³ g⁻¹, indicating approximately 30 % increase in hydrophobicity.

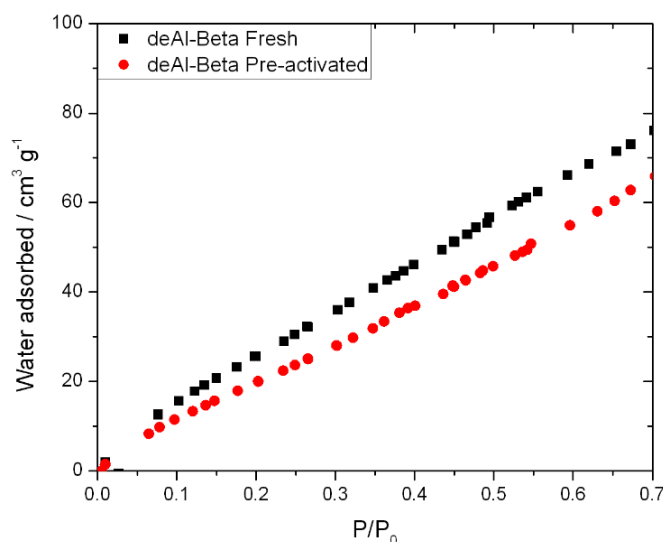


Figure 15. Vapour isotherm of dealuminated Beta prior to (black) and following (red) pre-activation. Experimental details: Isotherm gathered at 20 °C from 0 to 0.7 P/P_0 . Pre-activation performed by wetting in MeOH at 110 °C and 10 bar with a flow of 1.5 mL min⁻¹ and following thermal treatment performed at 550 °C for 3 h in air.

These results show that a similar (28 %) increase in hydrophobicity can be achieved for dealuminated Beta upon pre-activation, even though the catalyst does not contain any Sn.

As such, the lattice effects observed following pre-activation do not appear to require direct interaction between Sn and MeOH to be achieved but are a consequence of solvothermal treatment of the lattice itself in MeOH. Although incorporating Sn into this 'pre-activated' dealuminated Beta did result in the formation of an active catalyst, the activity of this material was only approximately 30 % higher than that of standard 'fresh' catalyst (figure 16). As such, it is clear that although increased hydrophobicity of the lattice itself is beneficial in regard to activity of the catalyst, it does not fully account for the improved performance of the catalyst following pre-activation. Hence, changes to the active sites must also occur during the interaction of Sn and methanol, in line with the original ^{119}Sn CPMG MAS NMR spectrum of thermally regenerated 10Sn-Beta (figure 8).

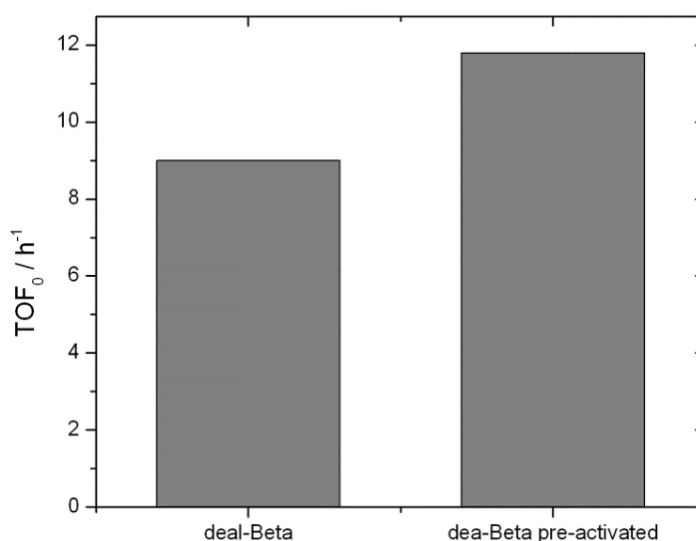


Figure 16. Catalytic performance of 10Sn-Beta depending on whether the dealuminated precursor material was untreated (deal-Beta) or pre-activated (deal-Beta pre-activated) prior to incorporation of Sn. Experimental details: 1 % wt. glucose in methanol, 110 °C , 10 bar, 100 mg of catalyst, flow of reactant: 0.75mL min⁻¹. Pre-activation performed by wetting in MeOH at 110 °C and 10 bar with a flow of 1.5 mL min⁻¹ and following thermal treatment performed at 550 °C for 3h in air.

To better understand the changes that occur to the active sites of the catalyst beyond those established for thermally regenerated 10Sn-Beta (figure 4), additional ^{119}Sn CPMG MAS NMR studies were performed. However, since the extent of pre-activation is comparable for all Sn-Beta samples (figure 11), these final experiments were focused on samples containing lower Sn loadings, where the changes in Sn species could be more evident by minimising the spectral crowding that occurs at high loading. In particular, samples of 1Sn-Beta were studied prior to and following pre-activation, as these provide an appropriate compromise between maximal productivity, active site uniformity, and hence signal to noise ratio. To further maximise insight, these final measurements were performed in a more quantitative manner, employing a recycle delay time shown to be long enough to fully relax all the Sn sites ($t_1 = 135$ s).⁵ Moreover, no normalisation of intensity was performed, with

each sample run for 512 scans in order to provide an accurate comparison of intensities and chemical shift.

As can be seen (figure 17), the spectrum of the fresh catalyst exhibits three major resonances, at chemical shift values of -600, -650 and -720. The first resonance arises from the presence of extra-framework SnO_x species, which have been shown to be spectators to Lewis acid catalysis.²⁴ In contrast, the additional resonances at -650 and -720 ppm are indicative of hexa-coordinated framework Sn species, which are known to contribute to catalytic performance. As the precise chemical shift of these species depends on the environment, geometry and chemical reactivity of each Sn site, the presence of two resonances in this region is indicative of the presence of more than one active site in the fresh material.^{15,31,32} However, it was previously demonstrated the -720 ppm signal to be most abundant in the samples of the highest TOF (Chapter 2, 2.3.3) and hence it is presumed that this resonance is the one that provides the catalyst with the largest fraction of its activity. Following pre-activation, the distribution of active site clearly changes. Although there are no changes to the intensity of extra-framework SnO_x species – in good agreement to the lack of correlation between the presence of spectator sites and extent of pre-activation (figure 11) - changes in the spectral region of hexa-coordinated framework Sn are observed. Notable amongst these are an-almost entire loss of intensity at -650ppm; a shift in the dominant resonance at -720 ppm to -690 ppm, and the generation of new resonances at -740 and -780 ppm. Thus, in addition to increasing the hydrophobicity of the lattice, it is clear that pre-activation of Sn-Beta leads to substantial changes to the relative population of Sn species in the catalyst. From the NMR spectrum alone, it cannot be concluded whether the changes in Sn environment are due to the increased hydrophobicity of the catalyst, or are in addition to increased hydrophobicity. Yet, as the incorporation of Sn into a pre-activated (and more hydrophobic) sample of dealuminated-Beta did not result in the same two-fold increase in performance (figure 16), it can be hypothesised that at least some of the changes to the Sn species occur in addition to the increased hydrophobicity of the catalyst.

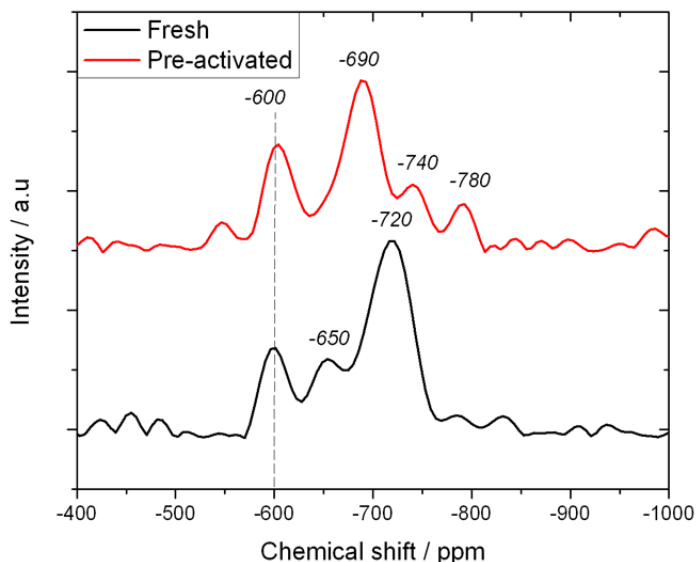


Figure 17. ^{119}Sn CPMG MAS NMR spectrum of 1Sn-Beta materials prior to (black) and following (red) pre-activation. Pre-activation performed by wetting in MeOH at 110 °C and 10 bar with a flow of 1.5 mL min⁻¹ and following thermal treatment performed at 550 °C for 3 h in air.

Based on previous spectroscopic studies, it has been hypothesised that differences in the chemical shift values of Sn in zeolite materials can arise from differences in T-site occupancy, and/or coordinative changes due to presence/absence of defect sites.^{31,32} Although these NMR spectra do not allow discrimination between which of these potential processes also occurs upon pre-activation, it is clear that the active site environment in the catalyst is markedly different following pre-activation, in line with the changes observed to the Arrhenius expression (figure 3). The change in active site environment, alongside the increased levels of hydrophobicity observed following pre-activation, clearly result in the genesis of new catalytic materials characterised by increased levels of activity and stability for GI. The formation of a more hydrophobic active site environment characterised by elevated levels of activity and stability draws clear parallels to the active site environment found in Sn-Beta materials synthesised by classical hydrothermal synthesis (Chapter 3).

4.4 Comparison of different Sn-Beta preparations

4.4.1 Catalyst synthesis and characterisation

In Chapter 3 of the thesis, the hydrothermal preparation of Sn-Beta zeolite was introduced. 1 % wt. Sn loaded Sn-Beta hydrothermal (1Sn-Beta_{HDT}) showed superior performance when compared to the post synthetic prepared Sn-Beta (1 % wt. Sn, Solid State Incorporated, SSI, 1Sn-Beta_{SSI}). Kinetic reactions for glucose isomerisation (GI) and glucose upgrading to ML showed how 1Sn-Beta_{HDT} was better performing in these reactions (Chapter 3, Section 3.3.4). These differences in reactivity between the 1Sn-Beta_{HDT} and 1Sn-Beta_{SSI} were accompanied by remarkable differences in active site speciation, hydrophobicity and particles sizes. Therefore in this part of the manuscript the pre-activated 1 % wt. Sn-Beta

zeolite (1Sn-Beta_{PA}) is tested against 1Sn-Beta_{HDT} and 1Sn-Beta_{SSI} for the glucose upgrading to α -hydroxy-esters at 160 °C in presence of different reaction promoters.^{11,12,33} The protocol of pre-activation in this section is kept consistent in what was reported on the first part of the chapter: methanol is flown at 1.5 mL min⁻¹ over 100 mg of 1Sn-Beta_{SSI} at 110 °C, 10 bar in a PFR reactor. The catalyst was subsequently calcined at 550 °C, air, 3 h yielding to 1Sn-Beta_{PA}.

Textural analysis of 1Sn-Beta_{SSI}, pre-activated 1Sn-Beta_{PA} and 1Sn-Beta_{HDT} by XRD and porosimetry showed that each catalyst possessed a crystalline, microporous structure, characteristic of the BEA framework, in line with previous reports (table 3, figure 18).^{24,25,34}

Table 3. Textural properties of 1Sn-Beta HDT, PA and SSI

Catalyst	BET Area (m ² g ⁻¹) ^a	Total pore volume (cm ³ g ⁻¹) ^b
1Sn-Beta HDT	398	0.21
1Sn-Beta SSI	581	0.24
1Sn-Beta PA	564	0.23

a Surface area determined from nitrogen adsorption using BET equation. **b** Micropore volume determined by t-plot method

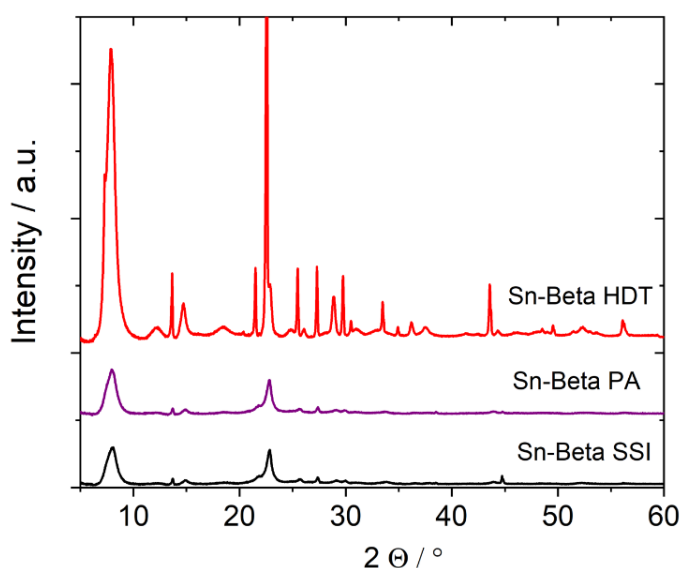


Figure 18. X-Ray Diffraction analysis for 1Sn-Beta_{SSI} (purple,) 1Sn-Beta_{HDT} (red) and 1Sn-Beta_{PA} (black).

In order to compare and analyse the active site distributions of the three catalyst materials, ¹¹⁹Sn MAS NMR spectroscopy analysis was performed.^{15,16} The technique was performed on hydrated materials to emulate the state of the catalyst upon placement into the reactor.

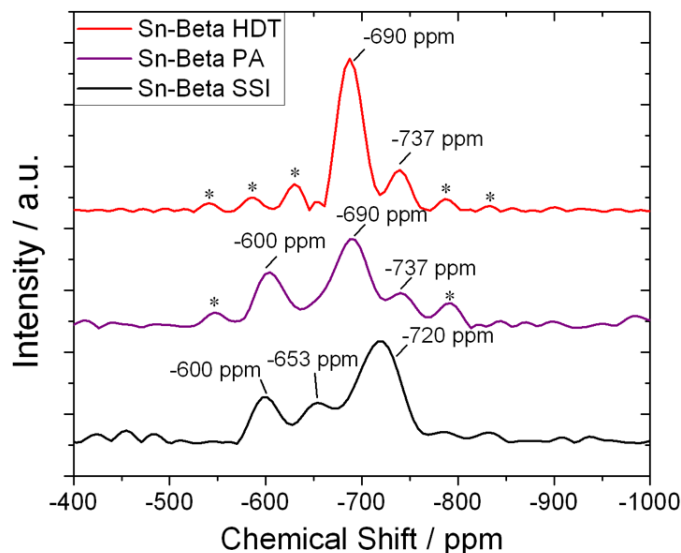


Figure 19. ^{119}Sn CPMG MAS NMR spectrum of Sn-Beta samples prepared by hydrothermal synthesis (1Sn-Beta_{HDT}, top line) and post-synthetic methods (1Sn-Beta_{PA}, middle line and 1Sn-Beta_{SSI}, bottom line).

Figure 19 presents the ^{119}Sn CPMG MAS NMR spectra of 1Sn-Beta_{HDT} (top line), 1Sn-Beta_{PA} (middle line) and 1Sn-Beta_{SSI} (bottom line). In line with the data showed in Chapter 3, 1Sn-Beta_{HDT} did not present a detectable resonance at -600 ppm, indicating that extra-framework Sn in this material was either absent or was present below the detectability limit of the measurement.²³ In contrast, small quantities of extra-framework Sn were observed for both post-synthetic samples. The absence of extra-framework Sn in 1Sn-Beta_{HDT} can be attributed to a more effective incorporation of tin by the hydrothermal methodology.⁵ Although the dominant resonance in all samples was found in the region attributable to isomorphously-substituted Sn species (-650 to -750 ppm), differences in the chemical shift and intensity of the signals were observed. As shown in figure 17 of this chapter, 1Sn-Beta_{SSI} and 1Sn-Beta_{PA} show different chemical shifts for the Sn speciation present in the samples, the former shows a main peak at -720 ppm whereas the latter exhibits a main resonance at -690 ppm and another smaller species at -737 ppm. In the 1Sn-Beta_{HDT}, a main resonance at -690 ppm was observed, alongside a less intense resonance at -737. The molecular understanding of how the differences in chemical shift relates to the properties of hydrated Sn species is the topic of debate in the scientific community. Although diverse and sometimes contradictory assignments are reported in the literature, it is reasonable to assume that the shifting of these signals can be related to changes in the active site properties such as T-sites location, Sn-O-Si bond angle and degree of hydration.^{3,23,31,32} In this light, it is notable how the pre-activation of 1Sn-Beta_{SSI} results in NMR signals comparable to those found in the hydrothermal sample, suggesting that common active site properties – and potentially performance – may be found for these catalysts.

In figure 13, it was shown how the pre-activation treatment of 1Sn-Beta_{SSI} leads to slight textural alterations of the material, which were evident by DRIFTS. Therefore a DRIFTS study of the three catalysts was undertaken (figure 20). As can be seen, the spectrum of 1Sn-Beta_{PA} shows an increased contribution of isolated silanol groups ($\equiv\text{Si-OH}$, 3740 cm^{-1}), a decrease in the magnitude of H-bonding interactions ($3200\text{-}3600\text{ cm}^{-1}$),²⁷⁻²⁹ and a decrease in intensity characteristic of internal defect sites (960 cm^{-1}) when compared to the spectrum of 1Sn-Beta_{SSI}.^{35,36} Taken together, these changes indicate that the material becomes less defective and more hydrophobic following pre-activation. Interestingly, Sn-Beta_{HDT} already exhibited very low signals in these regions, in agreement with previous reports which show how this material possess a low number of defect sites and larger crystallite sizes.⁴

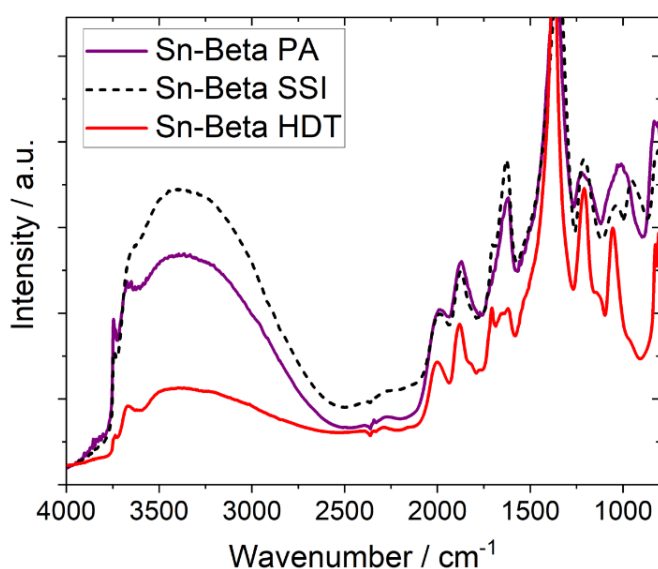


Figure 20. DRIFT spectra of 1Sn-Beta_{SSI} (dashed line), 1Sn-Beta_{PA} (solid purple line) and 1Sn-Beta_{HDT} (red line) recorded at 25 °C.

To better evaluate the changes in hydrophilic properties between the samples, vapour sorption studies were performed using water as adsorbate.⁴ Figure 21 presents the water sorption isotherms for the three samples of Sn-Beta prepared by each methodology. From these, it is clear that drastic differences are observed between 1Sn-Beta_{HDT} and 1Sn-Beta_{SSI}. 1Sn-Beta_{HDT} was found to adsorb approximately 20 times less water than 1Sn-Beta_{SSI}, confirming the highly hydrophobic nature of this material. As already shown in the chapter, although both post-synthetic samples adsorb much higher quantities of water, it is notable that 1Sn-Beta_{PA} demonstrated a substantial (ca. 30 %) decrease in hydrophilicity in comparison to 1Sn-Beta_{SSI}. This finding confirms that in addition to possessing a different active site structure, 1Sn-Beta_{PA} is also somewhat more hydrophobic than 1Sn-Beta_{SSI}. Taken together, the preliminary characterisation suggests that pre-activation modifies the active site and the textural properties of 1Sn-Beta_{SSI}. Although the resulting sample (1Sn-

Beta_{PA}) seems to possess active Sn sites more comparable to 1Sn-Beta_{HDT}, it maintains lattice properties more similar to 1Sn-Beta_{SSI}.

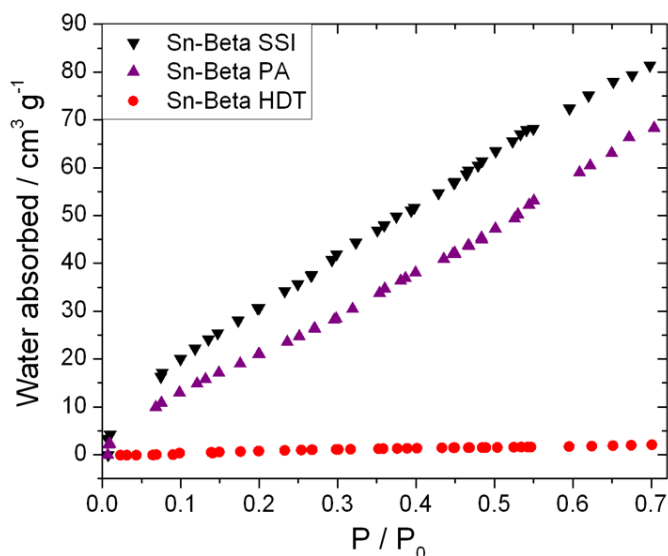


Figure 21. Water sorption isotherms of 1Sn-Beta_{SSI} (top series, black downward triangles) 1Sn-Beta_{PA} (middle series, purple triangles) and 1Sn-Beta_{HDT} (bottom series). Experimental details: Isotherm gathered at 20 °C from 0 to 0.7 P/P₀.

4.4.2 α -hydroxy-esters production and influence of promoters

To better determine the relevance of the changes of the lattice and active sites of Sn-Beta following pre-activation with respect to the performance of the materials, kinetic studies of each sample were performed. The materials were tested for the retro-aldol fragmentation of glucose to the α -hydroxy-esters methyl lactate (ML) and methyl vinyl glycolate (MVG).¹¹⁻¹³ This reaction was chosen both for its industrial interest, and due to the fact it possesses a more complex reaction network in comparison to other Sn-Beta catalysed reactions, which could better highlight the differences between the materials.^{33,37}

Figure 22 presents the initial kinetic data gathered during the continuous conversion of glucose over the three catalyst samples. In these initial experiments, glucose conversion was performed at 160 °C, at conditions previously reported (1 % wt. glucose in methanol, 160 °C, 24 h period of operation) in the absence of any reaction promoters (no water, no alkali).^{1,2,9,10} A high Weight Hourly Space Velocity (WHSV) of 4.752 h⁻¹ was chosen so that some rate limiting reactant was present even at t₀, in order to allow immediate deactivation of the catalyst to be observed, and hence obtain a rapid evaluation of the intrinsic stability of each catalyst.^{17,38}

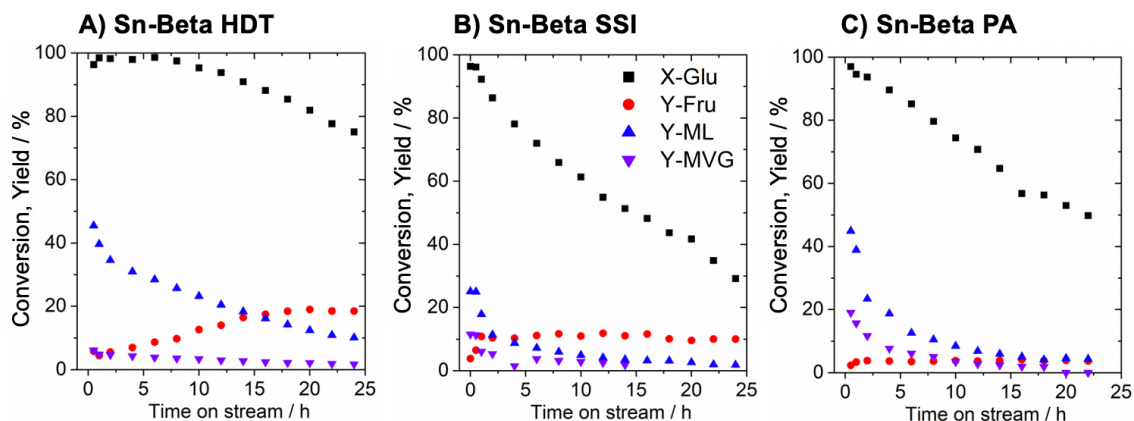


Figure 22. Glucose upgrading carried out at 160 °C by A) 1Sn-Beta_{PA}, B) 1Sn-Beta_{HDT} and C) 1Sn-Beta_{SSI} in pure methanol. Conversion (X) of glucose and yield at the time t (Y) of the products (Fructose, ML and MVG) are plotted against time on stream. Experimental details: 1 % wt. glucose in methanol, 160 °C, 20 bar, 100 mg catalyst, flow of reactant: 1 mL min⁻¹.

To evaluate the initial activity of each catalyst, the distribution of products during time on stream kinetic were evaluated by High Performance Liquid Chromatography (HPLC) (figure 22A-C). Since all catalysts were tested at identical reaction conditions (WHSV and temperature), the time on stream kinetics are directly comparable. In line with previous reports, 1Sn-Beta_{SSI} exhibited poorer performance than 1Sn-Beta_{HDT}, as evidenced by the lower yields of ML and MVG obtained in the presence of this catalyst (combined ML+MVG yield of 36 versus 46 %, respectively, registered at 0.5 hours of time on stream). However, the pre-activated material (1Sn-Beta_{PA}) exhibited a ML yield comparable to that of 1Sn-Beta_{HDT} (46 %). Moreover, 1Sn-Beta_{PA} resulted in the highest yields of MVG being obtained (19 %, compared to < 5 % for 1Sn-Beta_{HDT}). As such, it is clear that the pre-activation protocol identified during glucose isomerisation is also applicable as a method to improve the performance of Sn-Beta for retro-aldol fragmentation. This finding therefore reveals that the pre-activation of Sn-Beta not only improves the general activity of the material, but it also improves its selectivity towards valuable products in this reaction network. Although pre-activation resulted in interesting improvements in productivity and selectivity, 1Sn-Beta_{HDT} still exhibited the highest levels of stability across the catalysts series (Figure 22A-C). In fact, deactivation rate constants calculated on the basis of glucose conversion were calculated to be 0.043 h⁻¹, 0.089 h⁻¹ and 0.074 h⁻¹ for Sn-1Beta_{HDT}, 1Sn-Beta_{SSI} and 1Sn-Beta_{PA}, respectively (figure 23).²⁶

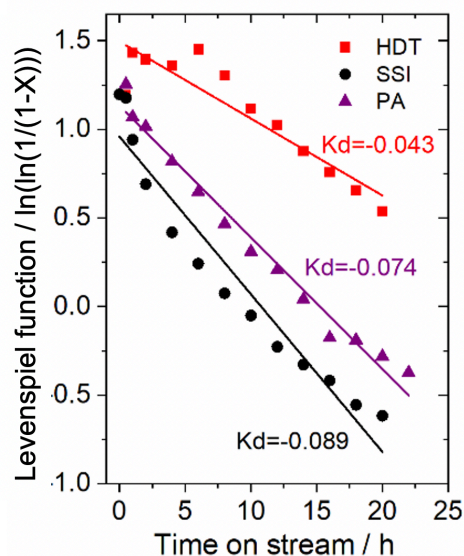


Figure 23. Deactivation constant for continuous glucose upgrading to ML and MVG in methanol at 160 °C carried out by different preparations of Sn-Beta. Experimental details: 1 % wt. glucose in methanol, 160 °C, 20 bar, 100 mg catalyst, flow of reactant: 1 mL min⁻¹.

Notably, the trend in rate of deactivation (HDT < PA < SSI) appears to correlate to the preference of the catalysts to interact with methanol, as evidenced by methanol adsorption data showed in Chapter 3 (Section 3.3.5). The catalyst most prone to adsorb methanol (1Sn-Beta_{SSI}) deactivated more rapidly than the catalyst least likely to adsorb the solvent (1Sn-Beta_{HDT}).

Although the data presented in figure 22 already demonstrated some beneficial aspects of pre-activation, the deactivation of Sn-Beta in these conditions is still rapid. As shown in Chapter 2, the stability of Sn-Beta can be enhanced by addition of small amounts of water to the reaction feed, the presence of which minimises alkoxylation and/or condensation of the sites during continuous operation conditions.^{1,2} Therefore, to understand if these catalysts were all sensitive to the same mechanism of deactivation, and whether their stability could be improved by addition of water, the retro-aldol fragmentation of glucose was carried out in a solution of methanol:water 99:1, but at otherwise-identical conditions to those described in figure 22.

To show the full kinetics of reaction, and to give at the same time clear and intuitive understanding on the perturbation of the system, in the remaining part of the chapter two different figures will be shown for each set of kinetic experiment. The first figure will show the full kinetic data with the reaction intermediates displayed, and the second figure will show a comparison with the reaction carried out in pure methanol. In this last set of images, only the conversion of glucose and yield of ML are shown to favour simpler understanding of the improvements due to the changing in the system.

Figure 24 shows the full kinetic of reaction in methanol:water 99:1 at 160 °C carried out by each preparation of Sn-Beta zeolite. Figure 24 presents the kinetic data for 1Sn-Beta_{HDT}, 1Sn-Beta_{SSI} and 1Sn-Beta_{PA} respectively, when each reaction was performed in

methanol:water 99:1. In those figures, comparison is made between the original reaction run in pure methanol (black symbols, kept as a standard reference throughout the remaining manuscript), and the reaction in methanol:water 99:1 (blue).

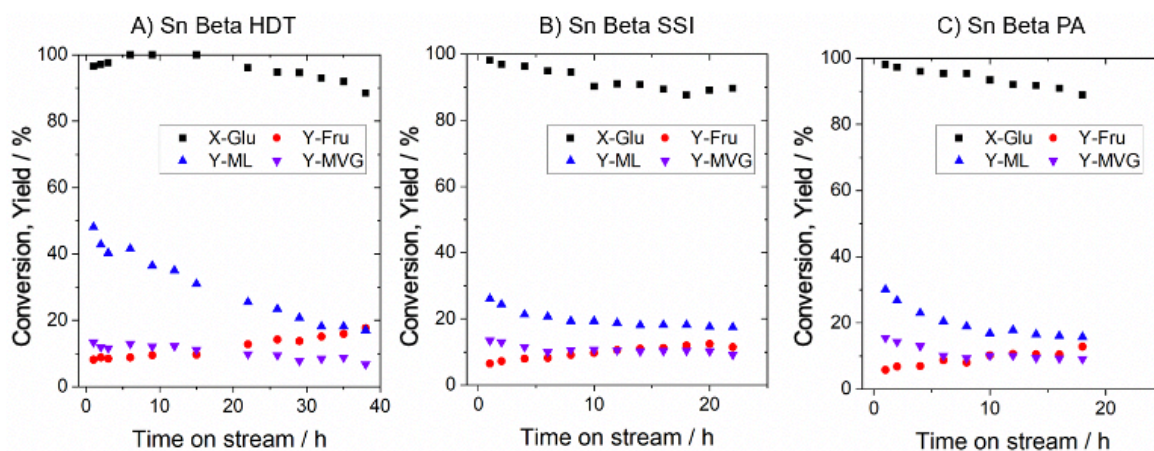


Figure 24 Kinetic data for continuous glucose upgrading to ML and MVG carried out by different preparations of Sn-Beta in methanol:water 99:1 at 160 °C. Conversion (X) of glucose and yield at the time t (Y) of the products (Fructose, ML and MVG) are plotted against time on stream. Experimental details: 1 % wt. glucose in methanol:water 99:1, 160 °C, 20 bar, 100 mg catalyst, flow of reactant: 1 mL min⁻¹.

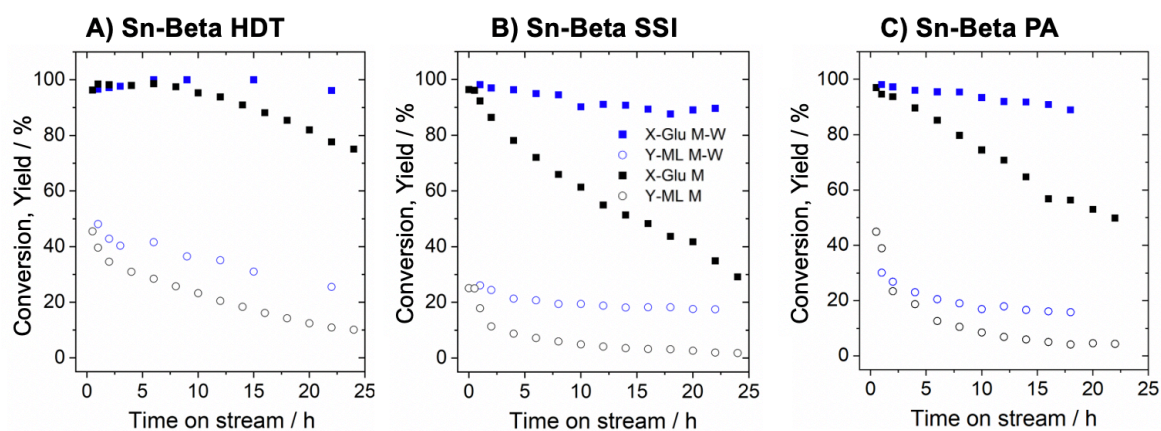


Figure 25. Glucose upgrading carried out at 160 °C by A) 1Sn-Beta_{PA}, B) 1Sn-Beta_{HDT} and C) 1Sn-Beta_{SSI} in methanol:water 99:1. Conversion (X) of glucose and yield at the time t (Y) of the products (ML) are plotted against time on stream. Experimental details: 1 % wt. glucose in methanol:water 99:1, 160 °C, 20 bar, 100 mg catalyst, flow of reactant: 1 mL min⁻¹.

Interestingly, Figure 25A-C shows how all the catalysts improved in stability once water was added to the feed of reaction, showing how at least one form of deactivation over the first 20 h for these materials can be suppressed by addition of water, in line with the findings shown in Chapter 2.¹ Notably, the addition of water enhanced the stability of each catalyst to a different degree, which resulted in each catalyst displaying comparable levels of stability following perturbation by water (figure 26). As such, the perturbation of water benefited 1Sn-Beta_{SSI} the most, as this material showed the most rapid rate of deactivation

in pure methanol. The effect was evidently smaller for the hydrothermal zeolite, which already showed good stability in pure methanol.

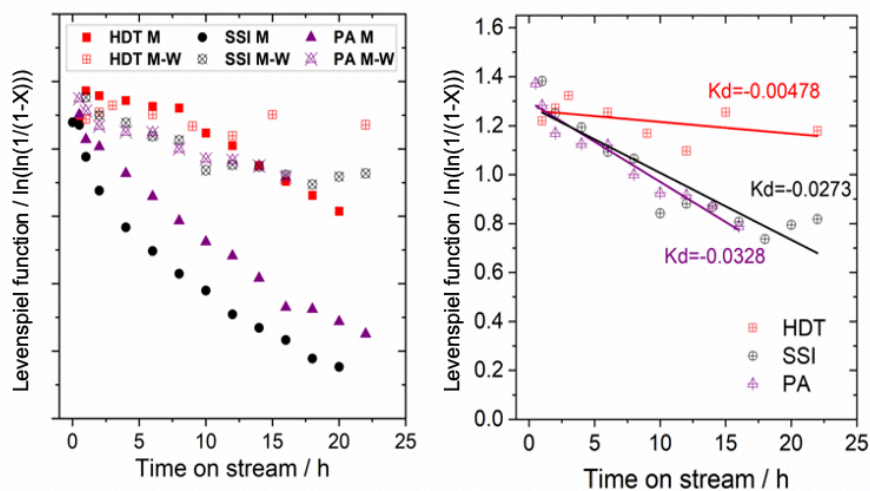


Figure 26. (Left) Rate of deactivation for 1Sn-Beta_{HDT} (squares), 1Sn-Beta_{SSI} (circles) and 1Sn-Beta_{PA} (triangles) in pure methanol (filled symbols) and in methanol:water 99:1 (empty symbols). (Right) Deactivation constant value for for 1Sn-Beta_{HDT} (squares), 1Sn-Beta_{SSI} (circles) and 1Sn-Beta_{PA} (triangles) in methanol:water 99:1.

Analysis of the product distribution shown in the kinetic data reported in figure 25A-C revealed some minor changes to the selectivity of the catalysts upon addition of water. However, the overall selectivity of each reaction at the same rate of glucose conversion was similar for the processes in pure methanol and methanol:water (figure 27). As such, the presence of water does not modify the intrinsic selectivity performance of the catalyst. Due to this, in the presence of water, 1Sn-Beta_{HDT} was the best performing catalyst of the series, but still achieved only 50% selectivity to ML.

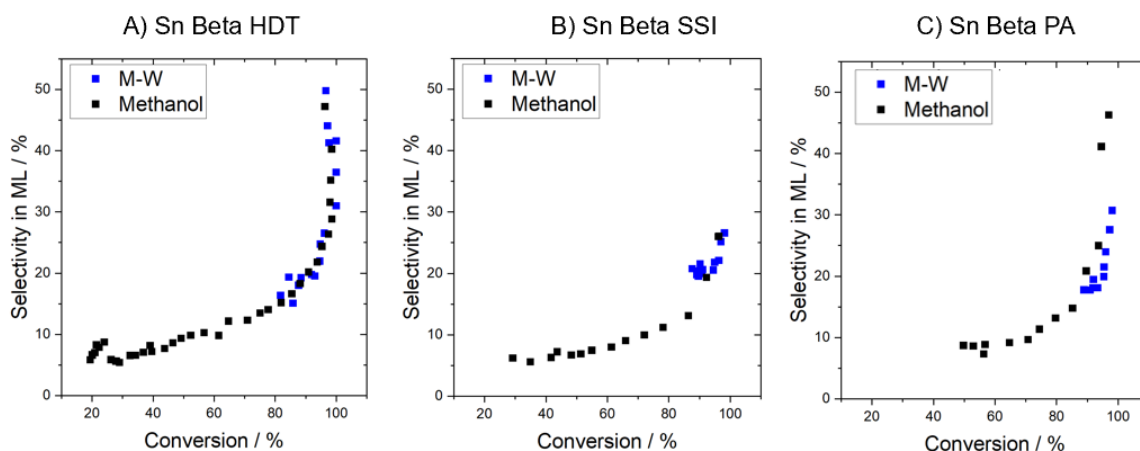


Figure 27. Selectivity to ML plotted against conversion of glucose in methanol:water (99:1) at 160 °C for different Sn-Beta preparations. Experimental details: 1 % wt. glucose in methanol:water 99:1, 160 °C, 20 bar, 100 mg catalyst, flow of reactant: 1 mL min⁻¹.

Although improved stability was achieved following addition of 1 % wt. water, the selectivity of the process in methanol:water 99:1 was still low (50 % selectivity in ML). This low level of selectivity emphasises the high reactivity and multifunctionality of Sn-Beta in being able to catalyse different reaction paths (Chapter 1, Section 1.12).³⁷ Previous studies have shown how adding small quantities of alkali salts to the glucose conversion system can improve the selectivity of Sn-Beta towards retro-aldol products.^{9,10,37} It has been proposed that the effect of alkali salts arises from their ability to exchange protons present in the active site environment, thereby minimising the partial Brønsted acidity of the material. To determine the susceptibility of the catalyst series to alkali, and hence to gain further understanding of the effect of pre-activation, the Sn-Beta materials were tested for glucose upgrading at 160 °C in presence of alkali salts (KCl), to test the tendency of the materials to interact with the potassium promoter. In this series of experiments, water was not added to the reaction feed so as to understand the contribution of alkali to the reaction alone. KCl was used as alkali promoter in this chapter as it possesses a wider range of suitable concentration than other promoters, such as K₂CO₃, and it can therefore be introduced into the feed in a slight excess without compromising performance.³⁹

Figure 28 therefore shows the full kinetic for glucose upgrading carried out at 160 °C in presence of alkali salts (KCl, 4 mg L⁻¹). An immediate increase of selectivity towards ML and MVG is notable, with 1Sn-Beta_{PA} and 1Sn-Beta_{HDT} showing already ca. 80 % yield towards these α -hydroxy-esters.

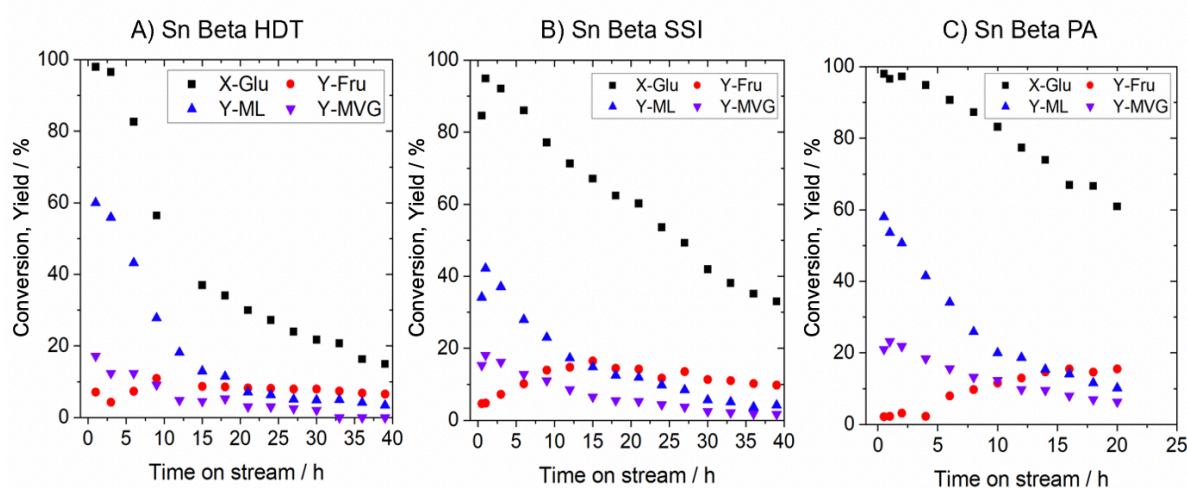


Figure 28 Kinetic data for continuous glucose upgrading to ML and MVG in methanol in presence of alkali salts (KCl) at 160 °C. Conversion (X) of glucose and yield at the time t (Y) of the products (Fructose, ML and MVG) are plotted against time on stream. Experimental details: 1 % wt. glucose in methanol (KCl 4 mg L⁻¹), 160 °C, 20 bar, 100 mg catalyst flow of reactant: 1 mL min⁻¹.

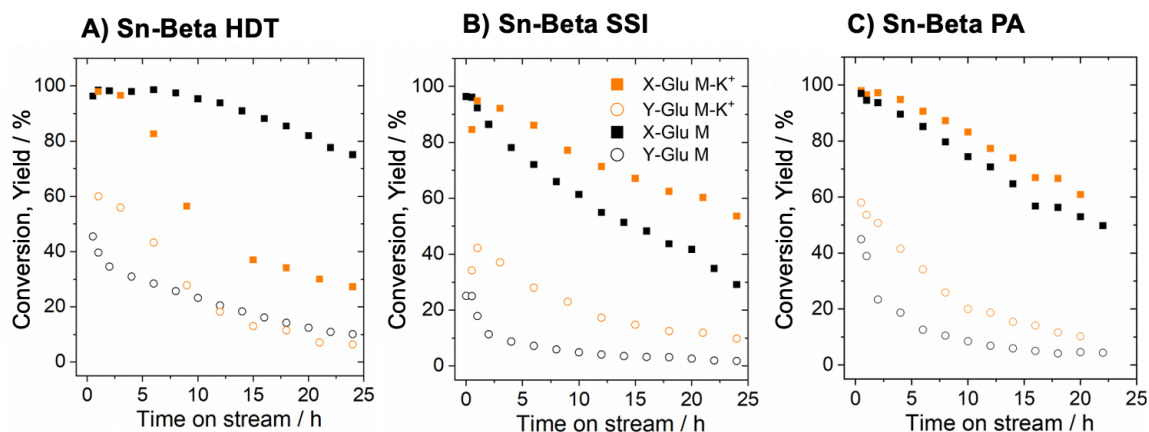


Figure 29. Glucose upgrading carried out at 160 °C by A) 1Sn-Beta_{PA}, B) 1Sn-Beta_{HDT} and C) 1Sn-Beta_{SSI} in methanol with alkali salts (KCl). Conversion (X) of glucose and yield at the time t (Y) of the products (ML) are plotted against time on stream. Experimental details: 1 % wt. glucose in methanol (KCl 4 mg L⁻¹), 160 °C, 20 bar, 100 mg catalyst, flow of reactant: 1 mL min⁻¹.

As can be seen, the addition of KCl to the reaction feed substantially improves the overall selectivity to retro-aldol products in all cases. This occurs due to an important increase (around 15-25 %) of MVG and ML lactate yields for all the materials, in addition to a decrease in the amount of glucose converted non-selectively, as evidenced by the improved carbon balance. These results show how alkali salts are able to channel the selectivity of these materials to the retro-aldol products, which are some of the products of major industrial interests amongst those that can be produced by Sn-Beta during glucose upgrading. In the presence of alkali, combined retro-aldol product yields were highest for Sn-Beta_{HDT} and Sn-Beta_{PA}, which reached a maximum of 80 % in both cases.

Although the increment in selectivity for this range of products is extremely interesting, the time on stream data (Figures 29A-C) shows how the stability of each catalyst is impacted differently in the presence of alkali salts (figure 30). In fact, whereas the stability of both post synthetic Sn-Beta materials (PA and SSI) was increased marginally upon addition of alkali, resulting in both materials showing a similar level of stability, the stability of 1Sn-Beta_{HDT} was lowered drastically in the presence of potassium salts. In particular an abrupt deactivation in the first 20 h of reaction was detected with 1Sn-Beta_{HDT} in presence of potassium salts. Accordingly, although all samples are susceptible to the selectivity benefits of alkali, the addition of alkali is overall not beneficial for 1Sn-Beta_{HDT}.

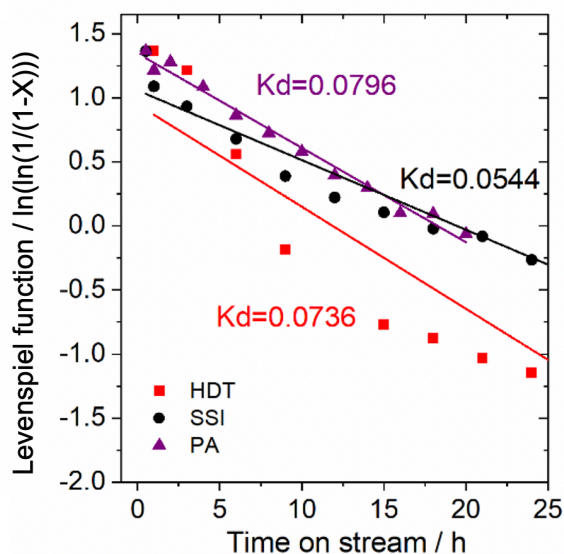


Figure 30. Deactivation constant for continuous glucose upgrading to ML and MVG in methanol in presence of alkali salts (KCl) at 160 °C. Experimental details: 1 % wt. glucose in methanol (KCl 4 mg L⁻¹), 160 °C, 20 bar, 100 mg catalyst, flow of reactant: 1 mL min⁻¹.

To understand whether the stabilising effect of water could be used in synergy with the effect of alkali, a final series of reactions was performed in methanol:water 99:1 in the presence of alkali salts. Figure 31 shows the full kinetic of reaction for glucose upgrading carried out at 160 °C in methanol:water 99:1 and alkali for the different preparations of Sn-Beta, whereas figure 32 presents the conversion and yield in ML for this system in comparison with the one in pure methanol. Due to the beneficial effect of water in maximising the stability of each catalyst, these final experiments were run for a total of 70 h on stream, to better magnify the differences in catalyst performance.

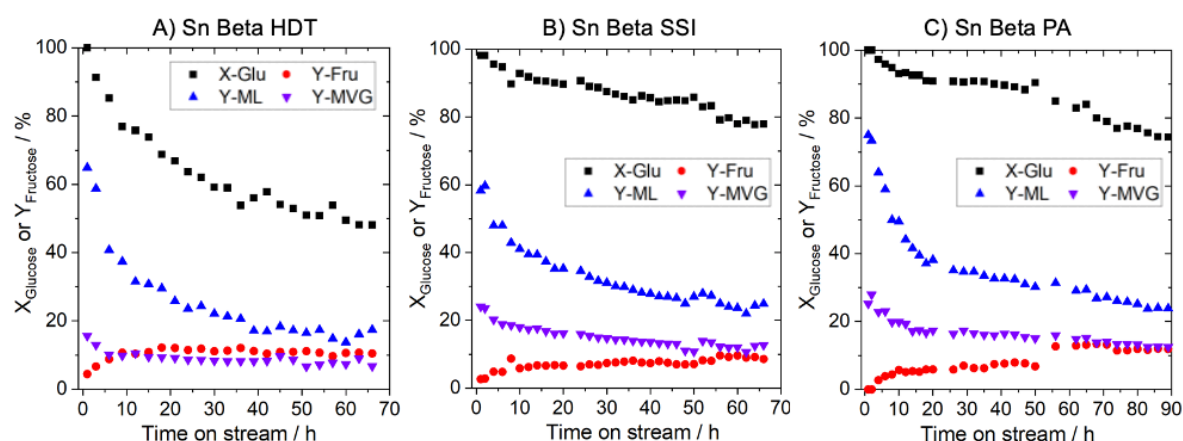


Figure 31. Kinetic data for continuous glucose upgrading to ML and MVG in methanol:water (99:1) in presence of alkali salts (KCl) at 160 °C. Conversion (X) of glucose and yield at the time t (Y) of the products (Fructose, ML and MVG) are plotted against time on stream. Experimental details: 1 % wt. glucose in methanol:water 99:1 (KCl 4 mg L⁻¹), 160 °C, 20 bar, 100 mg catalyst, flow of reactant: 1 mL min⁻¹.

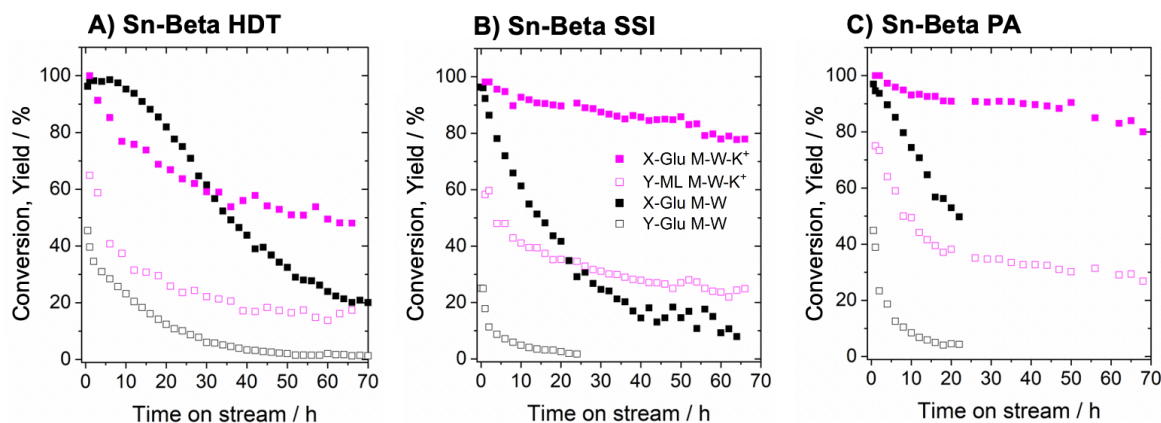


Figure 32. Glucose upgrading carried out at 160 °C by A) 1Sn-Beta_{PA}, B) 1Sn-Beta_{HDT} and C) 1Sn-Beta_{SSI} in methanol:water (99:1) with alkali salts (KCl). Conversion (X) of glucose and yield at the time t (Y) of the products (ML) are plotted against time on stream. Experimental details: 1 % wt. glucose in methanol:water 99:1 (KCl 4 mg L⁻¹), 160 °C, 20 bar, 100 mg catalyst, flow of reactant: 1 mL min⁻¹.

In the presence of water and alkali, an increased yield of the desired retro-aldol products was attained for 1Sn-Beta_{PA}, which showed the highest yield in ML and MVG along the series (Figure 32A-C).^{11,40,41} Although the retro-aldol product yield experienced a decrease with time on stream on account of deactivation at the very high levels of WHSV, steady state yields of 35 % and 20 % were maintained for ML and MVG, respectively, over 70 h of time on stream for 1Sn-Beta_{PA}. In contrast, the steady state yields of ML and MVG over 1Sn-Beta_{SSI} and 1Sn-Beta_{HDT} were at least 10 % lower. Interestingly, the best result in terms of stability was also achieved by 1Sn-Beta_{PA} and 1Sn-Beta_{SSI} (Figure 32B-D), which experienced only a 20 % loss of conversion over 70 h of time on stream. 1Sn-Beta_{HDT} instead experienced 50 % activity loss in the same time window (full kinetic plot available in figure 33). Clearly, the beneficial impact of water in promoting the stability of 1Sn-Beta_{HDT} is outweighed by the negative impact of alkali for the same material, as indicated in figure 29A.

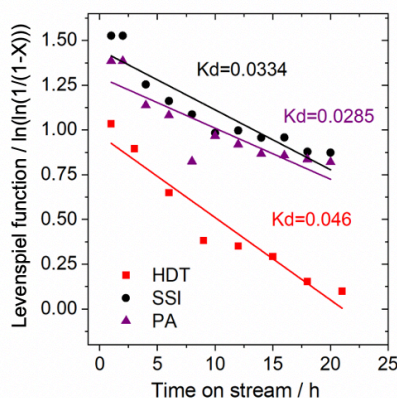


Figure 33. Deactivation constant for continuous glucose upgrading to ML and MVG carried out by different preparations of Sn-Beta zeolite in methanol:water (99:1) in presence of alkali salts (KCl) at 160 °C. Experimental details: 1 % wt. glucose in methanol:water 99:1 (KCl 4 mg L⁻¹), 160 °C, 20 bar, 100 mg catalyst, flow of reactant: 1 mL min⁻¹.

This set of data gathered in presence of alkali and water demonstrate for the first time the superiority of a post-synthetic sample of Sn-Beta over a hydrothermally prepared material, from both a selectivity and a stability prospective. To analyse the different performance of all these materials in these different conditions in a more rigorous way, the productivity of each catalyst for retro-aldol product formation (ML and MVG) in the presence of water and alkali was calculated (figure 34) alongside the Levenspiel deactivation rate constant for the same reactions (figure 34, value of k_d calculated in the first 20 h on stream as shown in figure 33). From this, it is clear that in the presence of water and alkali, the productivity to useful products is maximised with 1Sn-Beta_{PA}. Furthermore, 1Sn-Beta_{PA} also showed the lowest rate of deactivation in the series in the presence of water and alkali. Whilst a lower deactivation rate was achieved by the hydrothermal Sn-Beta process carried out in the presence of water but the absence of alkali (figure 26), the yields obtained in the absence of alkali with 1Sn-Beta_{HDT} were some 25 % lower than those obtained with 1Sn-Beta_{PA} at optimal operational conditions. As the post synthetic preparations of Sn-Beta do not show any loss of stability upon adding of alkali salts, it is clear that combining the lattice properties of post-synthetic Sn-Beta with the right active site speciation generates a superior material for glucose upgrading.

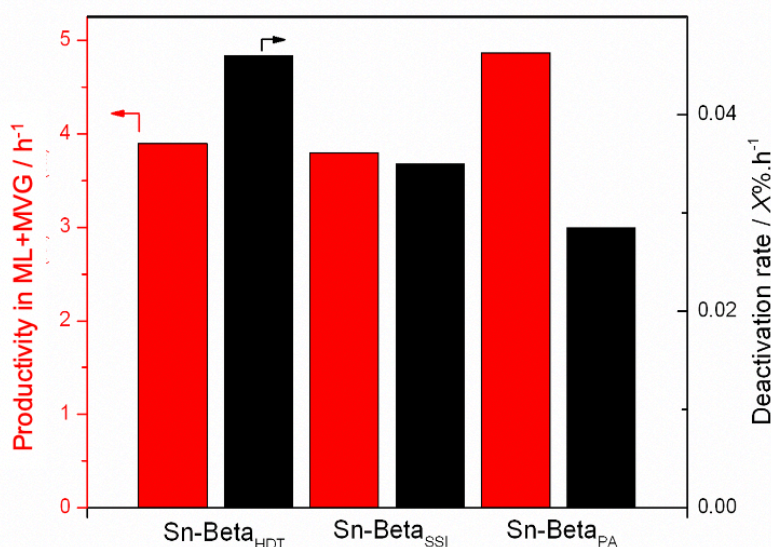


Figure 34. Combined RA productivity (ML+MVG) and deactivation rate constants during glucose upgrading in methanol:water (99:1) with alkali salts (KCl) for 1Sn-Beta_{HDT}, 1Sn-Beta_{SSI} and 1Sn-Beta_{PA}. Experimental details: 1 % wt. glucose in methanol:water 99:1 (KCl 4 mg L⁻¹), 160 °C, 20 bar, 100 mg catalyst, flow of reactant: 1 mL min⁻¹.

4.5 Conclusions

In this chapter, it was demonstrated that substantial improvements to the activity and stability of Sn-Beta occur following suitable regeneration of the catalyst by thermal treatment. Indeed, following thermal treatment of a partially deactivated sample of Sn-Beta, its relative activity for glucose isomerisation was found to increase by a factor of two. Through a combination of spectroscopic (^{119}Sn CPMG MAS NMR, DRIFTS, vapour sorption) and kinetic methodologies, it was revealed that this effect occurs due to solvothermal reorganisation of the catalyst, which results in the generation of a new active environment characterised by improved accessibility, higher reactivity and increased hydrophobicity. In doing so, was therefore demonstrated that surprising improvements to catalyst activity and stability can be achieved even for well-optimised catalytic materials, due to operation in the reactor. By understanding the processes that govern these changes, it was showed that various pre-activation protocols can be employed to induce the same changes in active site environment in short periods of time simply by treating the fresh catalyst in solvent at elevated temperature and pressure prior to operation, which results in improved performance being readily attained without extensive operation of the catalyst being required.

In the second part of the chapter an extensive study of the performance of Sn-Beta after pre-activation for glucose upgrading to α -hydroxy-esters was carried out. Alongside this catalyst 1Sn-Beta_{HDT} and 1Sn-Beta_{SSI} were tested as well to understand how the pre-activated material was performing in comparison to these catalysts. It was shown how the catalyst is not only intrinsically more active and more stable than its parent zeolite (Sn-Beta_{SSI}), but it also shows a positive response to the reaction promoters (alkali and water). Finally 1Sn-Beta_{PA} proved to be superior in glucose upgrading to α -hydroxy-esters than 1Sn-Beta_{HDT}, which until now was known as the catalyst material and preparation methodology yielding the best performing Sn-Beta zeolite (Chapter 3). These findings allowed to understand which Sn speciation and framework properties are required for producing a highly selective, stable and active Sn-Beta zeolite for glucose upgrading, these features will be the guidelines for possible future catalyst preparations.

Although the “pre-activation” of Sn-Beta yielded to interesting results for the glucose upgrading to α -hydroxy-esters, the performance of this catalyst for GI still needs to be improved. Only a selectivity of 40-50 % at 50 % conversion during continuous GI was detected (figure 1 Right). Even if Sn-Beta maintained a good level of stability for this reaction thanks the adding of water, these results are far from the ones achieved by bio-enzymatic routes.^{42,43} Further developments are therefore needed for this process to catalyse economically and selectively the isomerisation of glucose to fructose.

4.6 Reference

- (1) Padovan, D.; Tolborg, S.; Botti, L.; Taarning, E.; Sádaba, I.; Hammond, C. Overcoming Catalyst Deactivation during the Continuous Conversion of Sugars to Chemicals: Maximising the Performance of Sn-Beta with a Little Drop of Water. *React. Chem. Eng.* **2018**, 3(2), 155-163
- (2) Padovan, D.; Botti, L.; Hammond, C. Active Site Hydration Governs the Stability of Sn-Beta during Continuous Glucose Conversion. *ACS Catal.* **2018**, 8, 7131–7140.
- (3) Kolyagin, Y. G.; Yakimov, A. V.; Tolborg, S.; Vennestrøm, P. N. R.; Ivanova, I. I. Application Of ¹¹⁹Sn CPMG MAS NMR for Fast Characterization of Sn Sites in Zeolites with Natural ¹¹⁹Sn Isotope Abundance. *J. Phys. Chem. Lett.* **2016**, 7 (7), 1249–1253.
- (4) Hammond, C.; Conrad, S.; Hermans, I. Simple and Scalable Preparation of Highly Active Lewis Acidic Sn-Beta *Angew. Chemie - Int. Ed.* **2012**, 51 (47), 11736–11739.
- (5) Botti, L.; Navar, R.; Tolborg, S.; Martinez-Espin, J. S.; Padovan, D.; Taarning, E.; Hammond, C. Influence of Composition and Preparation Method on the Continuous Performance of Sn-Beta for Glucose-Fructose Isomerisation. *Top. Catal.* **2019**, 62 (17–20), 1178–1191.
- (6) Corma, A.; Domine, M. E.; Nemeth, L.; Valencia, S. Al-Free Sn-Beta Zeolite as a Catalyst for the Selective Reduction of Carbonyl Compounds (Meerwein-Ponndorf-Verley Reaction). *J. Am. Chem. Soc.* **2002**, 124 (13), 3194–3195.
- (7) Blasco, T.; Cambor, M. A.; Corma, A.; Esteve, P.; Guil, J. M.; Martínez, A.; Perdigón-Melón, J. A.; Valencia, S. Direct Synthesis and Characterization of Hydrophobic Aluminum-Free Ti-Beta Zeolite. *J. Phys. Chem. B* **1998**, 102 (1), 75–88.
- (8) Canos, A. C.; Valencia, V.; Us, I. L.; Domine, M. E.; Es, V. (12) United States Patent. **2001**, 1 (12).
- (9) Tolborg, S.; Sádaba, I.; Osmundsen, C. M.; Fristrup, P.; Holm, M. S.; Taarning, E. Tin-Containing Silicates: Alkali Salts Improve Methyl Lactate Yield from Sugars. *ChemSusChem* **2015**, 8 (4), 613–617.
- (10) Elliot, S. G.; Tosi, I.; Meier, S.; Martinez espin, J.; Tolborg, S.; Taarning, E. Stoichiometric Active Site Modification Observed by Alkali Ion Titrations of Sn-Beta. *Catal. Sci. Technol.* **2019**.
- (11) Dusselier, M.; De Clercq, R.; Cornelis, R.; Sels, B. F. Tin Triflate-Catalyzed Conversion of Cellulose to Valuable (α -Hydroxy-) Esters. *Catal. Today* **2017**, 279, 339–344.
- (12) Sølvhøj, A.; Taarning, E.; Madsen, R. Methyl Vinyl Glycolate as a Diverse Platform Molecule. *Green Chem.* **2016**, 18 (20), 5448–5455.
- (13) Dewaele, A.; Meerten, L.; Verbelen, L.; Eyley, S.; Thielemans, W.; Van Puyvelde, P.; Dusselier, M.; Sels, B. Synthesis of Novel Renewable Polyesters and Polyamides with Olefin Metathesis. *ACS Sustain. Chem. Eng.* **2016**, 4 (11), 5943–5952.
- (14) Dewaele, A.; Meerten, L.; Verbelen, L.; Eyley, S.; Thielemans, W.; Van Puyvelde, P.; Dusselier, M.; Sels, B. Synthesis of Novel Renewable Polyesters and Polyamides with Olefin Metathesis. *ACS Sustain. Chem. Eng.* **2016**, 4 (11), 5943–5952.
- (15) Kolyagin, Y. G.; Yakimov, A. V.; Tolborg, S.; Vennestrøm, P. N. R.; Ivanova, I. I. Application of ¹¹⁹Sn CPMG MAS NMR for Fast Characterization of Sn Sites in Zeolites with Natural ¹¹⁹Sn Isotope Abundance. *J. Phys. Chem. Lett.* **2016**, 7 (7), 1249–1253.
- (16) Yakimov, A. V.; Kolyagin, Y. G.; Tolborg, S.; Vennestrøm, P. N. R.; Ivanova, I. I. ¹¹⁹Sn MAS NMR Study of the Interaction of Probe Molecules with Sn-BEA: The Origin of Penta- and Hexacoordinated Tin Formation. *J. Phys. Chem. C* **2016**, 120 (49), 28083–28092.

- (17) Hammond, C. Intensification Studies of Heterogeneous Catalysts: Probing and Overcoming Catalyst Deactivation during Liquid Phase Operation. *Green Chem.* **2017**, *19* (12), 2711–2728.
- (18) Takasaki, Y. Kinetic and Equilibrium Studies on D-Glucose-d-Fructose Isomerization Catalyzed by Glucose Isomerase from *Streptomyces* Sp. *Agric. Biol. Chem.* **1967**, *31* (3), 309–313.
- (19) Son, P. A.; Nishimura, S.; Ebitani, K. Preparation of Zirconium Carbonate as Water-Tolerant Solid Base Catalyst for Glucose Isomerization and One-Pot Synthesis of Levulinic Acid with Solid Acid Catalyst. *React. Kinet. Mech. Catal.* **2014**, *111* (1), 183–197.
- (20) Vanelderden, P.; Snyder, B. E. R.; Tsai, M. L.; Hadt, R. G.; Vancauwenbergh, J.; Coussens, O.; Schoonheydt, R. A.; Sels, B. F.; Solomon, E. I. Spectroscopic Definition of the Copper Active Sites in Mordenite: Selective Methane Oxidation. *J. Am. Chem. Soc.* **2015**, *137* (19), 6383–6392.
- (21) Al-Nayili, A.; Yakabi, K.; Hammond, C. Hierarchically Porous BEA Stannosilicates as Unique Catalysts for Bulky Ketone Conversion and Continuous Operation. *J. Mater. Chem. A* **2015**, *00*, 1–10.
- (22) Kolyagin, Y. G.; Yakimov, A. V.; Tolborg, S.; Vennestrøm, P. N. R.; Ivanova, I. I. Direct Observation of Tin in Different T-Sites of Sn-BEA by One- and Two-Dimensional ¹¹⁹Sn MAS NMR Spectroscopy. *J. Phys. Chem. Lett.* **2018**, *9* (13), 3738–3743.
- (23) Wolf, P.; Liao, W. C.; Ong, T. C.; Valla, M.; Harris, J. W.; Gounder, R.; van der Graaff, W. N. P.; Pidko, E. A.; Hensen, E. J. M.; Ferrini, P.; et al. Identifying Sn Site Heterogeneities Prevalent Among Sn-Beta Zeolites. *Helv. Chim. Acta* **2016**, *99* (12), 916–927.
- (24) Hammond, C.; Padovan, D.; Al-Nayili, A.; Wells, P. P.; Gibson, E. K.; Dimitratos, N. Identification of Active and Spectator Sn Sites in Sn-β Following Solid-State Stannation, and Consequences for Lewis Acid Catalysis. *ChemCatChem* **2015**, *7* (20), 3322–3331.
- (25) Botti, L.; Navar, R.; Tolborg, S.; Martinez-Espin, J. S.; Padovan, D.; Taarning, E.; Hammond, C. Influence of Composition and Preparation Method on the Continuous Performance of Sn-Beta for Glucose-Fructose Isomerisation. *Top. Catal.* **2019**, *62* (17–20), 1178–1191.
- (26) O. Levenspiel, *Chemical Reaction Engineering*, (Eds.: John Wiley & Sons: New York), **1999**; ch. 21, p 473
- (27) Zecchina, A.; Bordiga, S.; Spoto, G.; Marchese, L.; Petrini, G.; Leofanti, G.; Padovan, M. Silicalite Characterization. 2. IR Spectroscopy of the Interaction of Carbon Monoxide with Internal and External Hydroxyl Groups. *J. Phys. Chem.* **1992**, *96* (12), 4991–4997.
- (28) Zecchina, A.; Bordiga, S.; Spoto, G.; Marchese, L.; Petrini, G.; Leofanti, G.; Padovan, M. Silicalite Characterization. 1. Structure, Adsorptive Capacity, and IR Spectroscopy of the Framework and Hydroxyl Modes. *J. Phys. Chem.* **1992**, *96* (12), 4985–4990.
- (29) Scarano, D.; Zecchina, A.; Bordiga, S.; Geobaldo, F.; Spoto, G.; Petrini, G.; Leofanti, G.; Padovan, M.; Tozzola, G. Fourier-Transform Infrared and Raman Spectra of Pure and Al-, B-, Ti- and Fe-Substituted Silicalites: Stretching-Mode Region. *J. Chem. Soc. Faraday Trans.* **1993**, *89* (22), 4123–4130.
- (30) Gounder, R.; Davies, M. E. Beyond shape selective catalysis with zeolites: hydrophobic void spaces in zeolites enable catalysis in liquid water. *AIChE J.* **2013**, *59* (9), 3349–3358.
- (31) Wolf, P.; Valla, M.; Rossini, A. J.; Comas-Vives, A.; Núñez-Zarur, F.; Malaman, B.; Lesage, A.; Emsley, L.; Copéret, C.; Hermans, I. NMR Signatures of the Active Sites in Sn-β Zeolite. *Angew. Chemie - Int. Ed.* **2014**, *53* (38), 10179–10183.

- (32) Wolf, P.; Valla, M.; Núñez-Zarur, F.; Comas-Vives, A.; Rossini, A. J.; Firth, C.; Kallas, H.; Lesage, A.; Emsley, L.; Copéret, C.; et al. Correlating Synthetic Methods, Morphology, Atomic-Level Structure, and Catalytic Activity of Sn- β Catalysts. *ACS Catal.* **2016**, *6* (7), 4047–4063.
- (33) Holm, M. S.; Saravanamurugan, S.; Taarning, E. Conversion of Sugars to Lactic Acid Derivatives Using Heterogeneous Zeotype Catalysts. *Science (80-.)*. **2010**, *328* (5978), 602–605.
- (34) Yakimov, A. V.; Kolyagin, Y. G.; Tolborg, S.; Vennestrøm, P. N. R.; Ivanova, I. I. Accelerated Synthesis of Sn-BEA in Fluoride Media: Effect of H₂O Content in the Gel. *New J. Chem.* **2016**, *40* (5), 4367–4374.
- (35) Sushkevich, V. L.; Kots, P. A.; Kolyagin, Y. G.; Yakimov, V.; Marikutsa, A. V.; Ivanova, I. I. Origin of Water-Induced Brønsted Acid Sites in Sn-BEA Zeolites Origin of Water-Induced Brønsted Acid Sites in Sn-BEA Zeolites. **2019**.
- (36) Courtney, T. D.; Chang, C. C.; Gorte, R. J.; Lobo, R. F.; Fan, W.; Nikolakis, V. Effect of Water Treatment on Sn-BEA Zeolite: Origin of 960 Cm⁻¹FTIR Peak. *Microporous Mesoporous Mater.* **2015**, *210*, 69–76.
- (37) Tolborg, S.; Meier, S.; Sádaba, I.; Elliot, S. G.; Kristensen, S. K.; Saravanamurugan, S.; Riisager, A.; Fristrup, P.; Skrydstrup, T.; Taarning, E. Tin-Containing Silicates: Identification of a Glycolytic Pathway via 3-Deoxyglucosone. *Green Chem.* **2016**, *18* (11), 3360–3369.
- (38) Scott, S. L. A Matter of Life(Time) and Death. *ACS Catal.* **2018**, *8* (9), 8597–8599.
- (39) Elliot, S. G.; Tolborg, S.; Madsen, R.; Taarning, E.; Meier, S. Effects of Alkali-Metal Ions and Counter Ions in Sn-Beta-Catalyzed Carbohydrate Conversion. *ChemSusChem* **2018**, *11* (7), 1198–1203.
- (40) Tang, B.; Li, S.; Song, W. C.; Yang, E. C.; Zhao, X. J.; Guan, N.; Li, L. Fabrication of Hierarchical Sn-Beta Zeolite as Efficient Catalyst for Conversion of Cellulosic Sugar to Methyl Lactate. *ACS Sustain. Chem. Eng.* **2020**, *8* (9), 3796–3808.
- (41) Guo, Q.; Fan, F.; Pidko, E. A.; Van Der Graaff, W. N. P.; Feng, Z.; Li, C.; Hensen, E. J. M. Highly Active and Recyclable Sn-MWW Zeolite Catalyst for Sugar Conversion to Methyl Lactate and Lactic Acid. *ChemSusChem*. 2013, pp 1352–1356.
- (42) Li, H.; Yang, S.; Saravanamurugan, S.; Riisager, A. Glucose Isomerization by Enzymes and Chemo-Catalysts: Status and Current Advances. *ACS Catal.* **2017**, *7* (4), 3010–3029.
- (43) Parker, K.; Salas, M.; Nwosu, V. C. High Fructose Corn Syrup : Production , Uses and Public Health Concerns. **2010**, *5*, 71–78.

Chapter 5

Hf-Beta zeolite: a new selective catalyst for continuous glucose isomerisation

The content of this chapter was published in the following manuscript:

Angew. Chemie Int. Ed. **2020**, DOI: 10.1002/anie.202006718

5.1 Introduction

In the introduction of the thesis (Chapter 1), it was shown how the glucose isomerisation reaction (GI) to fructose represents an important bottleneck for glucose upgrading to a plethora of chemical commodities with high added value.¹⁻⁴ This reaction is currently carried out in industry at mild temperatures (60-80 °C) in aqueous solution exploiting enzymatic catalysis.⁵⁻⁷ This process is characterised by high purity of the final mixtures which is a mandatory requirement for High Fructose Corn Syrup (HFCS) production as a food-related product which is the aim of this process.^{8,9}

On the other side, the fructose production for biomass upgrading does not have to meet this purity requirement, but it needs lower costs of production to be marketable as a competitive source of carbon to the classic fossil feedstock.^{10,11}

In the last decade, the efforts of the researcher for finding a suitable heterogeneous catalyst were conveyed in the development of Sn zeotypes which could catalyse this process with some of the requirements met.¹²⁻¹⁴ Nonetheless Sn containing zeolites have been shown to be not ideal for the GI reaction. In fact, the strong acidity of the Sn site, combined with the partial Brønsted acidic character of this material has been shown to lead to formation of several by-products.¹⁵

Therefore, the selectivity of the process is compromised by these parallel reactions. In Chapter 2 and 4 it was shown how different perturbations could improve the stability and the selectivity of Sn-Beta towards glucose cleavage to α -hydroxy-esters. However none of these perturbations managed to access a full selectivity towards fructose production.¹⁶⁻¹⁸ Consequently, a new type of catalyst with better intrinsic activity is clearly required for large scale GI to be performed with heterogeneous catalysis.

Therefore, in this chapter the surprising activity of Hf-Beta zeolite during continuous glucose isomerisation is explored. This material has never been reported to be active in this particular reaction, therefore discontinuous and continuous kinetic data are shown to benchmark its activity.^{18,19} Moreover the performance of this material is compared to the current best heterogeneous inorganic catalyst for this glucose isomerisation: Sn-Beta.¹²⁻¹⁴ In this comparison the emphasis is focalised on the performances in continuous reactors. In this system the material is in contact with the solvent at high temperature and pressures,

thus fluid dynamics and diffusion parameters are different in these conditions than in the classic batch systems, and they cannot be overlooked prior projecting a process scale-up.

5.2. Experimental details:

5.2.1 Catalyst synthesis

Hydrothermal synthesis of metal incorporated Beta zeolite was performed according to reference 20: 30.6 g of tetraethyl orthosilicate (TEOS, Sigma Aldrich, 98 %) was added to 33.1 g of tetraethylammonium hydroxide (TEAOH, Sigma Aldrich, 35 %) under careful stirring, forming a two-phase mixture. After 60-90 min, one phase was obtained and the desired amount of the metal source ($\text{SnCl}_4 \cdot 5\text{H}_2\text{O}$ or HfCl_4 or ZrCl_4 , Sigma Aldrich > 99.5 %) dissolved in 2.0 mL of H_2O was added dropwise. The solution was then left for 48 h under stirring until a viscous gel was formed. The gel was finalised by the addition of 3.1 g hydrofluoric acid (HF, Fischer Chemicals 50 %) in 1.6 g of demineralized H_2O yielding a solid gel with the molar composition; 1.0Si, 1:0.005 Metal, 1:0.02 Cl^- , 1:0.55 TEA^+ , 1:0.55 F^- , 1:7.5 H_2O , where the metal was either Sn, Hf or Zr. The obtained gel was transferred to a Teflon lined stainless steel autoclave and kept for 7 days at 140 °C to crystallise. The obtained crystals were filtered and washed with deionised water. Calcination at 550 °C (2 °C min^{-1}) for 6 h under static air was carried out in order to remove the organic template.

5.2.2 Catalyst Characterisation

X-ray diffraction (XRD) spectra were acquired using a PANalytical X'PertPRO X-ray diffractometer. A $\text{CuK}\alpha$ radiation source (40 kV and 30 mA) was utilised. Diffraction patterns were recorded between 6–55° 2θ (step size 0.0167°, time/step = 150 s, total time = 1 h).

Specific surface area was determined from nitrogen adsorption using the BET equation, and microporous volume was determined from nitrogen adsorption isotherms using the t-plot method. Porosimetry measurements were performed on a Quantachrome Autosorb-iQ-MP/XR, and samples were degassed prior to use (115 °C, 6 h, nitrogen flow).

DRIFT spectroscopy was performed in a Harrick praying mantis cell. The spectra were recorded on a Bruker Tensor Spectrometer over a range of 4000–650 cm^{-1} at a resolution of 2 cm^{-1} . Pyridine adsorption studies with DRIFT spectroscopy were performed on the pre-treated zeolite powder (heated to 100 °C for 30 min in nitrogen at 40 mL min^{-1} prior to adsorption). Pyridine was dosed onto the sample by passing the gas stream through a saturator module. Samples were maintained at 25 °C during adsorption of pyridine for 10 minutes. Afterwards the pyridine saturator was disconnected from the cell, and the temperature was increased at a rate of 5 °C min^{-1} up to 200 °C maintaining the samples under a gaseous stream of nitrogen. Spectra were recorded with an acquisition time smaller than 1 min.

Operando UV–Vis measurements were performed with a homemade tubular reactor equipped with a fiber optic UV–Vis probe. UV–Vis measurements were performed with a light source (Ocean Optics DH-2000), spectrometer (Maya 2000 Pro, Ocean Optics), and a

600- μm UV–Vis fiber. The light was directed onto an optically transparent reactor column, located within a heated aluminum block.

X-ray absorption spectra were collected on the B18 beamline, Diamond Light Source at the Harwell campus, UK. Samples were analysed as pellets in transmission mode at room temperature using the fast-scanning Si(111) double crystal monochromator. Data processing, including alignment, normalisation and background removal, was performed using the Demeter software package (Athena). Analysis of the EXAFS data was performed using IFEFFIT within the Artimus software package (Ravel, *Journal of Synchrotron Radiation*, 2005, 12, 537 and Newville, *Journal of Synchrotron Radiation*, 2001, 8, 322). 1st shell path lengths were fitted at all k weighted χ data using a k space window of $2.2 < k < 12$, $1.1 < R < 2.5$. The R range was extended to 4 when fitting 2nd shells. A standard of monoclinic HfO_2 was fitted using simplified paths of single paths for Hf-O first shell, Hf-Hf and second shell Hf-O distances as reported by Erenburg and co-workers.²¹ Successfully fitted second shell paths were applied to the fitting of catalyst EXAFS data, with path lengths and coordination numbers being refined. However no acceptable results were obtained when applying such second shell paths to the catalyst spectra.

5.2.3 Kinetic and analytical studies

Continuous GI reactions were performed in a plug flow, stainless steel tubular reactor. The catalyst was pelletised (size fraction 63 and 77 μm) and densely packed into a $\frac{1}{4}$ " stainless steel tube (4.1 mm internal diameter). Two plugs of quartz wool and a frit of 0.5 μm held the catalyst in place. Temperature control was achieved by a thermostatted oil bath at the desired reaction temperature, and pressurization was achieved by means of a backpressure regulator. Aliquots of the reaction solutions were taken periodically from a sampling valve placed after the reactor and analysed by an Agilent 1260 Infinity HPLC equipped with a Hi-Plex Ca^{2+} column and ELS detector and quantified against an external standard (sorbitol) added to the sample prior the injection. Conditions of each catalytic experiment are provided in table 1, and each entry will be recalled in the text when needed. The glucose employed as substrate was provided by Sigma Aldrich (>99.5 %, monohydrate), methanol anhydrous as solvent was provided by Sigma Aldrich (99.8 %). Standard of fructose, mannose, were provided by Sigma Aldrich (> 99.9 %).

Table 1. Experimental conditions for the continuous GI reaction showed along the manuscript.

Cat.	Temp. (°C)	Flow (mL min ⁻¹)	Catalyst. (g)	WHSV ^a (Kg Kg ⁻¹ h ⁻¹)	C.T. (τ) ^b (s)
Hf-Beta	110	0.65	0.1	3.1	8.4
Sn-Beta	110	1.5	0.1	7.2	3.6
Zr-Beta	110	0.1	0.1	0.48	54
Hf-Beta	140	1.5	0.1	7.2	3.6
Sn-Beta	140	1.5	0.1	7.2	3.6

^aWeight Hourly Space Velocity: mass of substrate flowed per hour over 1 kg of catalyst (Equation 10 in the equation appendix) ^bContact time: time of interaction between the substrate and the catalyst (equation 2 in the equation appendix)

High field liquid NMR analysis on the samples were recorded on a Bruker Avance III 800 MHz spectrometer equipped with a TCI cryoprobe at 25 °C. The samples analysed were dried under a flow of nitrogen at 25 °C and successively re-diluted in deuterated methanol. ¹H-¹³C HSQC spectra were acquired by sampling the FID in the ¹H and ¹³C dimensions by 1024 and 512 complex data points, respectively, during acquisition times of 142 milliseconds (¹H) and 18 milliseconds (¹³C). All spectra were processed with ample zero filling in both dimensions using Bruker Topspin 3.5 pl6.

GI batch studies were performed in a pressurised ACE tubular glass reactor thermally controlled by a hot oil bath on an IKA hot plate. 4 g of reactant solution (1 % wt. glucose in methanol) and the catalysts were placed inside the reactor in order to maintain a glucose/metal molar ratio equal to 50. Samples were periodically collected and analysed by HPLC as described above.

5.3 Results and Discussion

5.3.1 Kinetic studies.

A series of Sn-, Hf-, Zr- and Ti-Beta zeolite was synthesized by fluoride-media hydrothermal. The crystalline structure of each material framework was confirmed by X-Ray diffraction analysis (figure 1). Throughout this whole chapter all the catalysts encountered are synthesised by fluoride media hydrothermal synthesis with a 1 % wt. of metal loading. Therefore it will not be used any nomenclature to distinguish between preparations and loadings. As such all the materials mentioned in this chapter can be considered as 1 % wt. metal loaded hydrothermally synthesized by fluoride media (HDT). Complimentary porosimetry analysis corroborated the successful synthesis of each material, based on their specific surface areas and microporous volumes (table 2).

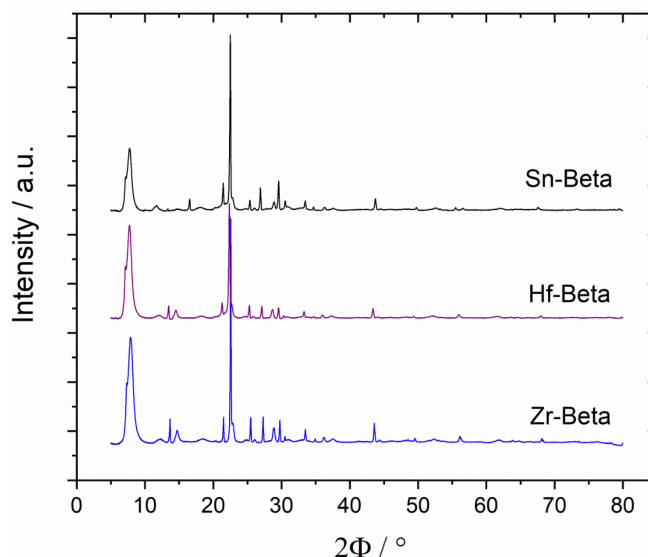


Figure 1. XRD analysis on Hf-Beta (purple), Sn-Beta (black), Zr-Beta (blue).

Table 2. Physical, chemical and reactivity data for various Lewis acidic silicates

Catalyst	SSA (m ² g ⁻¹)	V _{micro} (cm ³ g ⁻¹)	Si/M (molar)	TOF GI (h ⁻¹)	S _{Fru} at X _{Glu} = 20 %
Sn-Beta	398	0.21	198	95	68 %
Zr-Beta	414	0.21	189	16	45 %
Ti-Beta	390	0.20	204	15	56 %
Hf-Beta	404	0.22	202	0	-

Porosity data determined by N₂ isotherms; Si/M molar ratio determined by ICP-MS. Turnover frequency (TOF) values calculated from batch GI experiments at t = 2 min. Reaction conditions: 1 % wt. glucose in MeOH, 4 g reaction solution, glucose/metal ratio of 50, 110 °C, autogenic pressure.

Interesting behaviour was observed for these catalysts when tested in continuous glucose isomerisation to fructose (GI). In continuous processes, reactants are continuously pumped over a suspended solid catalyst bed, and the reaction occurs during the time the mixture resides on the catalyst within the reactor. Such reactors are widely employed in the base chemical industry, due to their increased levels of productivity, safety and scalability.^{22,23} Figure 2 and figure 3 show the time on stream data for two particular Lewis acidic silicates, Sn-Beta (figure 2) and Hf-Beta (figure 3), for continuous GI at 110 °C, alongside their Levenspiel (equation 5 in the appendix equation) plots for determination of deactivation rate.

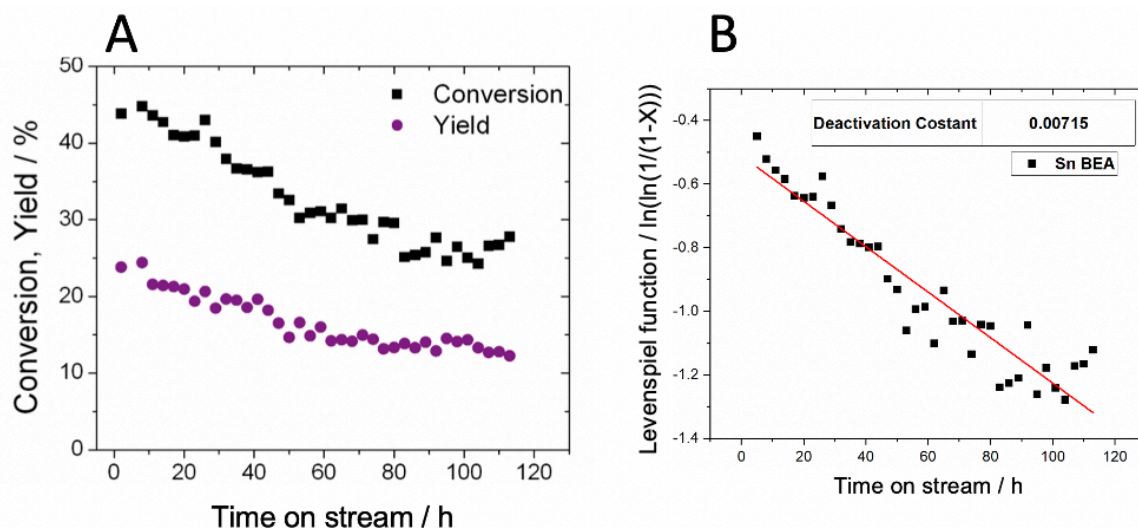


Figure 2. (Left) Time on stream data for Sn-Beta. (Right) Levenspiel function for deactivation constant (K_d) calculation for Sn-Beta during the continuous isomerisation of glucose to fructose. Conversion (X) of glucose and yield at the time t (Y) of products (Fru) is plotted against time on stream. Experimental details: 1 % wt. glucose in methanol, 110 °C, 10 bar, 1.5 mL min⁻¹ of flow over 100 mg of catalyst.

As can be seen (figure 2 Left), Sn-Beta exhibited an initially high level of substrate conversion (45 %) (equation 3 in the equation appendix), in line with its high activity during batch processing. However, relatively rapid deactivation was observed, resulting in more than 40 % loss of activity over the course of 113 h on stream. A single deactivation regime was observed, characterized by a deactivation rate constant²⁴ of 0.0715 X%.h⁻¹ (figure 2 Left). In contrast, Hf-Beta exhibited a very different kinetic profile. After an initial induction period lasting 20 h, during which time the catalysts exhibited a (relatively) lower level of activity, Hf-Beta gained sufficient activity to reach similar levels of conversion to Sn-Beta. Over the final 72 h on stream, Hf-Beta reached an almost steady state level of activity, with conversion and yield fluctuating by the typical experimental error of the testing and analytical protocols (5-8 %), and maintained its high level of conversion and fructose yield throughout. After the initial period of induction, a deactivation constant of 0.00281 X%.h⁻¹ was determined, demonstrating Hf-Beta to be a more stable catalyst than Sn-Beta for GI following the induction period (figure 2 Right).

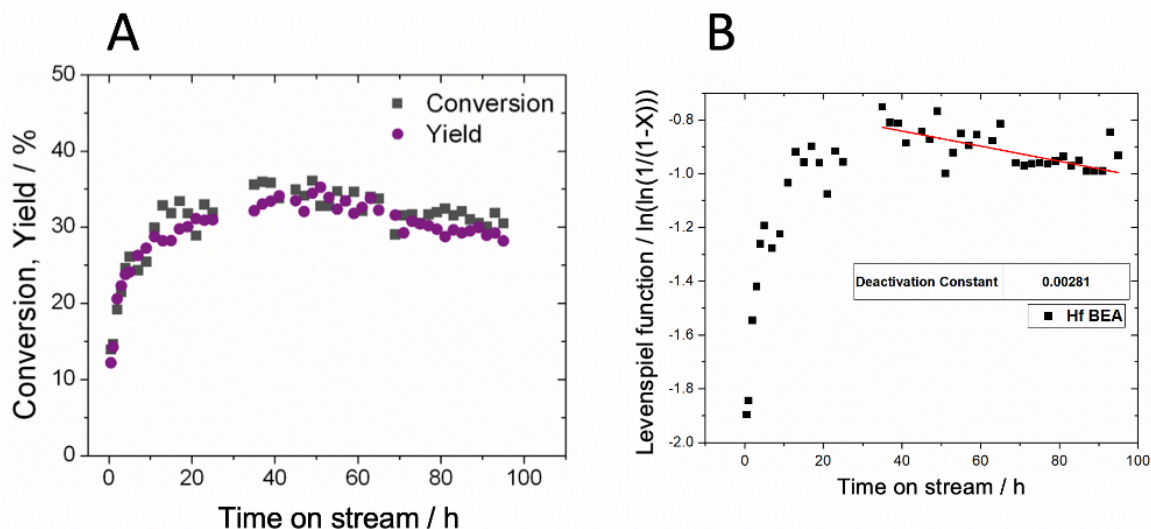


Figure 3. (Left) Time on stream data for Hf-Beta. (Right) Levenspiel function for deactivation constant (K_d) calculation for Hf-Beta during the continuous isomerisation of glucose to fructose. Conversion (X) of glucose and yield at the time t (Y) of the products (Fructose) are plotted against time on stream. Experimental details: 1 % wt. glucose in methanol, 110 °C, 10 bar, 0.65 mL min⁻¹ of flow over 100 mg of catalyst.

In addition to demonstrating higher levels of stability, analysis of the product distribution reveals Hf-Beta to be substantially more selective to fructose than the Sn-containing analogue. When comparing the fructose selectivity at all levels of conversion (equation 8 in the equation appendix) (*iso-conversion* analysis, figure 4 Left), Hf-Beta was approximately 80-100 % more selective than the state of the art Sn-Beta catalyst, converting glucose solely to fructose and mannose, the two thermodynamic products expected from GI,³ at a carbon balance level of 100 %. In contrast, at the levels of conversion explored during this study, only around half of the glucose was converted to fructose by Sn-Beta. Additionally, a substantial (> 20 %) loss of carbon balance was observed over Sn-Beta (figure 4 Right), indicating that species other than glucose, fructose and mannose were formed over this catalyst. It is thus clear that in addition to being more stable, Hf-Beta is substantially more selective than Sn-Beta. This is especially important, since catalytic systems exhibiting poor selectivity result in the requirement of extensive, expensive separation procedures, and waste valuable resources.

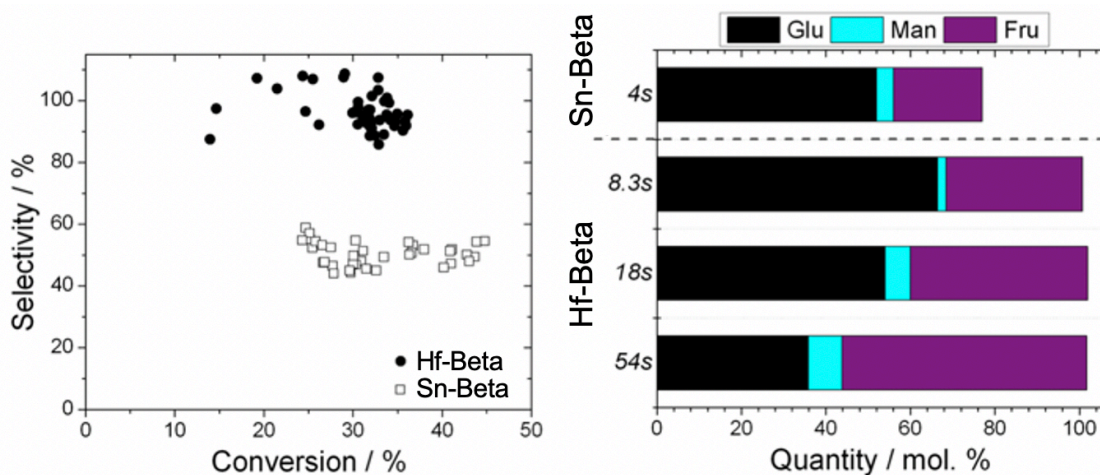


Figure 4. (Left) Conversion versus selectivity profile for Sn- and Hf-Beta. (Right) Product distribution achieved with Sn- and Hf-Beta at various contact times between 4 and 54 seconds. Experimental details: 1 % wt. glucose in methanol, 110 °C , 10 bar.(Sn-Beta) 1.5 mL min⁻¹ and (Hf-Beta) 0.65 mL min⁻¹ of flow over 100 mg of catalyst

To truly evaluate the selectivity performance of Hf-Beta, particularly with respect to Sn-Beta, the extent of reaction was increased by extending the reactant contact time *i.e.* the amount of time the reactant contacts the catalyst bed within the reactor (equation 2 in the equation appendix). As can be seen, increasing the contact time of glucose over Hf-Beta from 8 seconds to 54 seconds increased the quantity of glucose converted, from 33.6 % to 66.2 %. Yet, despite operating at extremely high conversion, the excellent selectivity of Hf-Beta remained, resulting in an unprecedented single-pass fructose yield of 57.9 % being achieved (equation 9 in the equation appendix). Notably, no loss of carbon balance was observed in this run, strongly indicating that competitive and/or consecutive side reactions remained absent even at high levels of conversion. In fact, the product distribution achieved at these conditions is representative of the thermodynamic equilibrium mixture, representing the first time chemocatalysis has been able to achieve this feat in GI.^{25,26}

Curiously, Hf-Beta catalyst performance at 110 °C was achieved only after a certain period of time in the reactor, during which period the intrinsic activity of the catalyst increased by approximately a factor of three to five (figure 3). To understand the nature of this induction period in which the catalyst increased in activity over 20 h of time on stream, a simple experiment was performed flowing the catalyst in the solvent of reaction (methanol) for 20 h at 110 °C. Interestingly in figure 5 is clear how Hf-Beta does not show any induction period when treated in methanol for 20 h, and high levels of activity and selectivity are observed from the first moments glucose was introduced into the reactor. This demonstrates that the origin of this behaviour is due to a surprising interaction with the solvent.

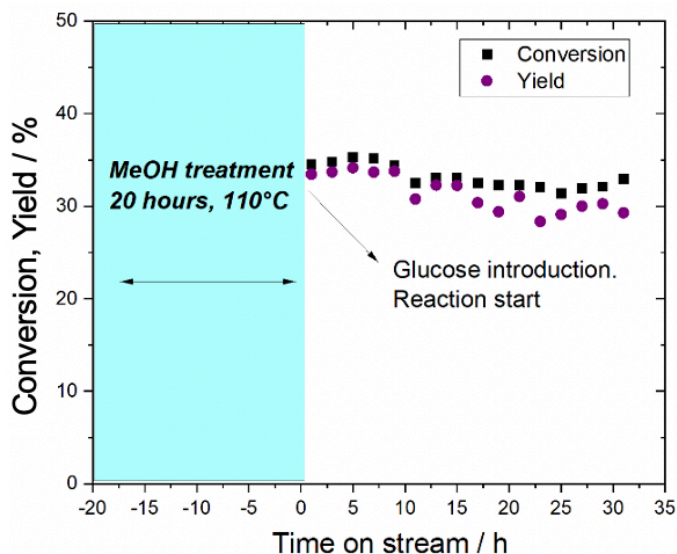


Figure 5. Catalytic performance of Hf-Beta for continuous glucose isomerisation to fructose following treatment in methanol flow for 20 h at 110 °C prior to introduction of glucose in the feed. Experimental details: 1 % wt. glucose in methanol, 110 °C , 10 bar, 0.65 mL min⁻¹ of flow over 100 mg of catalyst. The methanol wetting was performed at 110°C maintaining 0.65 mL min⁻¹ of flow over 100 mg of catalyst.

The same behaviour was exhibited by Zr-Beta zeolite (figure 6), this material after induction in methanol exhibited a high level of selectivity in line with Hf-Beta. Nonetheless the activity shown by Zr-Beta was approximately 9-10 times lower than Hf-Beta at identical conditions.

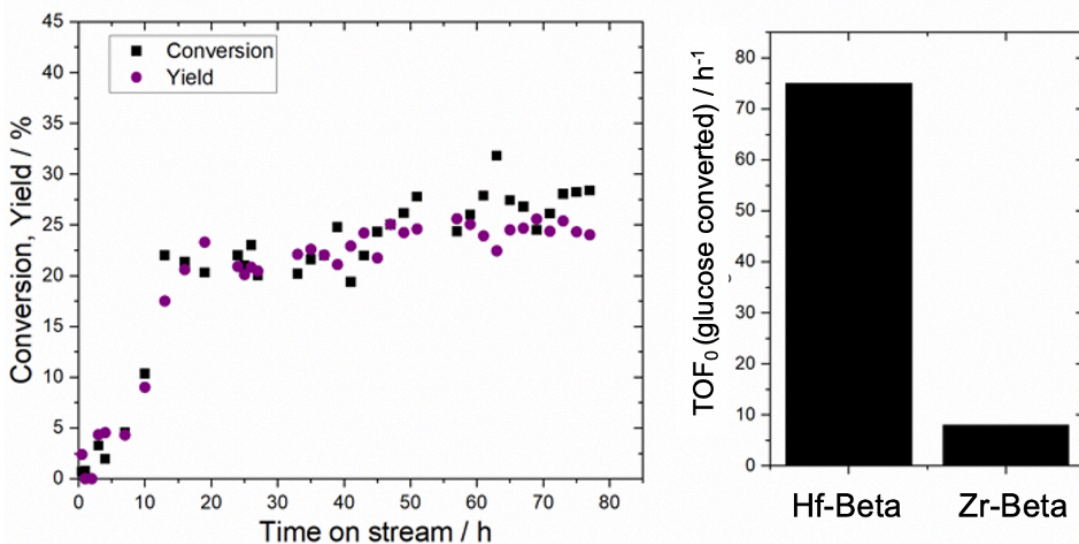


Figure 6. (Left) Catalytic performance of Zr-Beta for continuous glucose isomerisation to fructose at 110 °C. (Right) comparison in activity during continuous GI at 110 °C in methanol for Hf-Beta and Sn-Beta. Experimental details: 1 % wt. glucose in methanol, 110 °C, 10 bar. (Zr-Beta) 0.1 mL min⁻¹ and (Hf-Beta) 0.65 mL min⁻¹ of flow over 100 mg of catalyst.

To understand the nature of the overall reaction network, and hence to better understand the origin of the improved performance of Hf-Beta relative to Sn-Beta, detailed studies of

the product distribution observed during both extended reactions were performed. Firstly, *operando* UV-Vis was performed during continuous GI over Sn-Beta and Hf-Beta, according to the benchmarked procedure in Chapter 2 (2.3.3).¹⁶ The kinetic data obtained with the *operando* reactor matches the data obtained in the conventional flow reactor (figure 7). Both experiments were tailored so that similar levels of substrate conversion were attained during the reaction periods, ensuring similar stages of the reaction coordinate were monitored.¹⁶

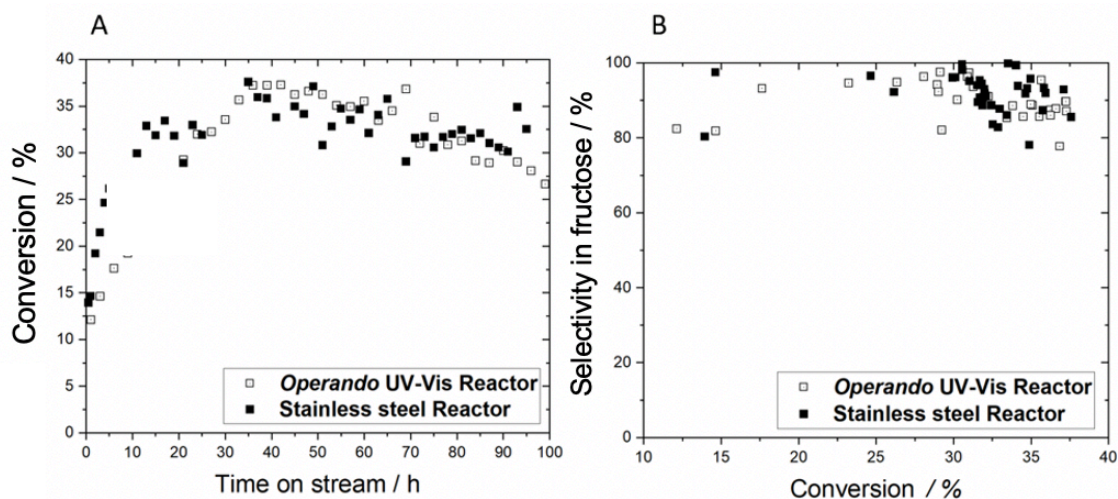


Figure 7. (Left) Catalytic performance of Hf-Beta for continuous glucose isomerisation to fructose at 110 °C in the *operando* reactor (empty symbol) and in the stainless steel reactor (black symbols). (Right) Conversion in glucose plotted against selectivity in fructose for GI catalysed by Hf-Beta in the *operando* reactor (empty symbol) and in the stainless steel reactor (black symbols). Experimental details: 1 % wt. glucose in methanol, 110 °C, 10 bar, 0.65 mL min⁻¹ of flow over 100 mg of catalyst.

The resulting spectra of the first and 50 h on stream under the UV-Vis probe are shown in Figure 8. In line with the work presented in Chapter 2, spectra are presented in difference mode, so that optical features formed during the reaction exhibit positive signals, whereas optical features decreasing during the reaction exhibit negative signals. Both catalysts exhibited a strong, positive absorption at 300-360 nm, related to an interaction between the active site of the catalyst and the substrate (*i.e.* M-glucose absorptions, Chapter 2, 2.3.3).¹⁶ Both catalysts also exhibited a negative signal at high energy (< 250 nm). This signal was demonstrated in Chapter 2 to arise from interactions between the active site and the reaction solvent (methanol), and that the extent of this negative signal correlates with loss of activity for Sn-Beta.¹⁶ However, for both catalysts, the magnitude of this negative signal is relatively low, consistent with their relatively high levels of stability compared to other catalysts, such as Sn-Beta materials prepared by post-synthetic methods, which are more prone to methanol-induced deactivation

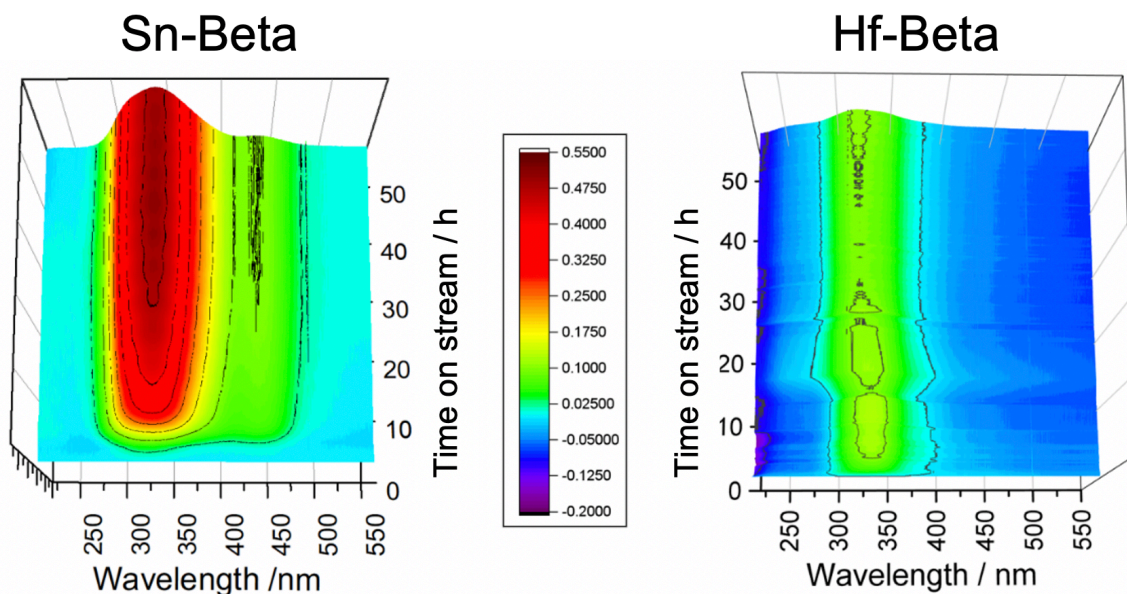


Figure 8. *Operando* UV-Vis measurements for Sn-Beta (Left) and Hf-Beta (Right) catalysed GI at 110 °C, permitting the absorption spectra of the system to be measured continuously alongside the kinetics of the system. Experimental details: 1 % wt. glucose in methanol, 110 °C, 10 bar. (Sn-Beta) 1.5 mL min⁻¹ and (Hf-Beta) 0.65 mL min⁻¹ of flow over 100 mg of catalyst.

Of particular interest, however, is the absorption found at lower energy (*ca.* 400-480 nm). The signal of this band is plotted in figure 9 against the selectivity in fructose of the system in which the catalyst is performing, it is possible to see how its intensity inversely correlated to the selectivity of Sn-Beta, *i.e.* lower selectivity to fructose was observed when there was a large absorption at 400-480 nm. It is notable that this signal was totally absent from the *operando* UV-Vis measurement of Hf-Beta, further suggesting that this feature relates to a by-product in the system and further indicating the improved selectivity of Hf-Beta. The complete understanding of the transformation related to this 400-480 nm UV-Vis band is beyond the scope of this chapter, but is fully explored in the following chapter (Chapter 6).

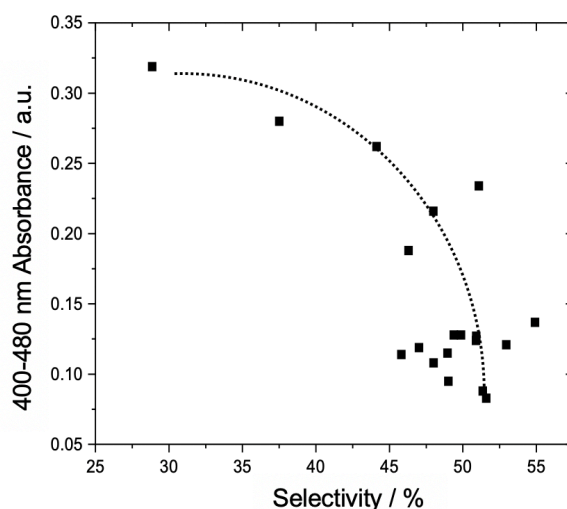


Figure 9. Correlation between the absorption observed between 400-480 nm in the spectrum of Sn-Beta catalysed glucose isomerisation and the selectivity to fructose exhibited by the catalyst.

To gain further insight into the relative performances of Hf- and Sn Beta, ^1H - ^{13}C HSQC NMR spectroscopy was used to obtain an unbiased representation of the by-product formation when using either catalyst. Various by-products in the Lewis acid catalysed conversion of glucose have previously been described using ^1H - ^{13}C HSQC NMR assays, thus facilitating the characterization of post-reaction solutions.^{15,27} Figure 10A-D shows the ^1H - ^{13}C HSQC NMR spectra for Sn- and Hf Beta catalysed GI at 110 °C across various spectral regions. The ^1H - ^{13}C HSQC method is employed as it provides roughly 30-times higher sensitivity than analogous one-dimensional ^{13}C NMR measurements, whilst providing dramatic improvements in resolution due to its two-dimensional nature. The spectra of both reactions were sampled at different points of time on stream, so that samples of exactly the same level of conversion (20 %) were measured (10 % and 19 % yield of fructose for Sn Beta and Hf Beta, respectively). As such, the spectra are presented normalised to the quantity of remaining glucose, as verified by qNMR standardisation and chromatographic techniques (HPLC-ELSD). Accordingly, the volumes of the signals associated to unconverted glucose are identical in both spectra (figure 10A). Consistent with chromatographic measurements, signals attributed to fructose were much more intense for Hf-Beta over Sn-Beta, verifying the improved yield to fructose observed over Hf-Beta, and the improved selectivity of the catalyst. Moreover, a similar quantity of mannose was observed during both catalytic experiments at 110 °C. However, a number of additional species were observed from the reaction catalysed over Sn-Beta, none of which were observed for Hf-Beta catalysis. The by-products included methyl fructosides and the branched aldohexose hamamelose, in addition to various glycolytic end products including trans-2,5,6-trihydroxy-3-hexenoic acid methyl ester (THM) and various 3-deoxy- γ -lactones. In previous works focused upon high temperature glucose conversion over Sn-Beta, it has been hypothesized that glycolytic end products, such as THM, occur *via* the retro-Michael dehydration of hexoses to the key intermediate, 3-deoxyglucosone (3DG), over Lewis acidic centres.^{15,28} However, dehydration reactions are also readily catalyzed by Brønsted acidic functionalities.^{15,29} Thus, the origin of these products exclusively over Sn-Beta could relate to different types of acidity in Sn- and Hf-Beta, and/or differences in the active site environment of both materials.

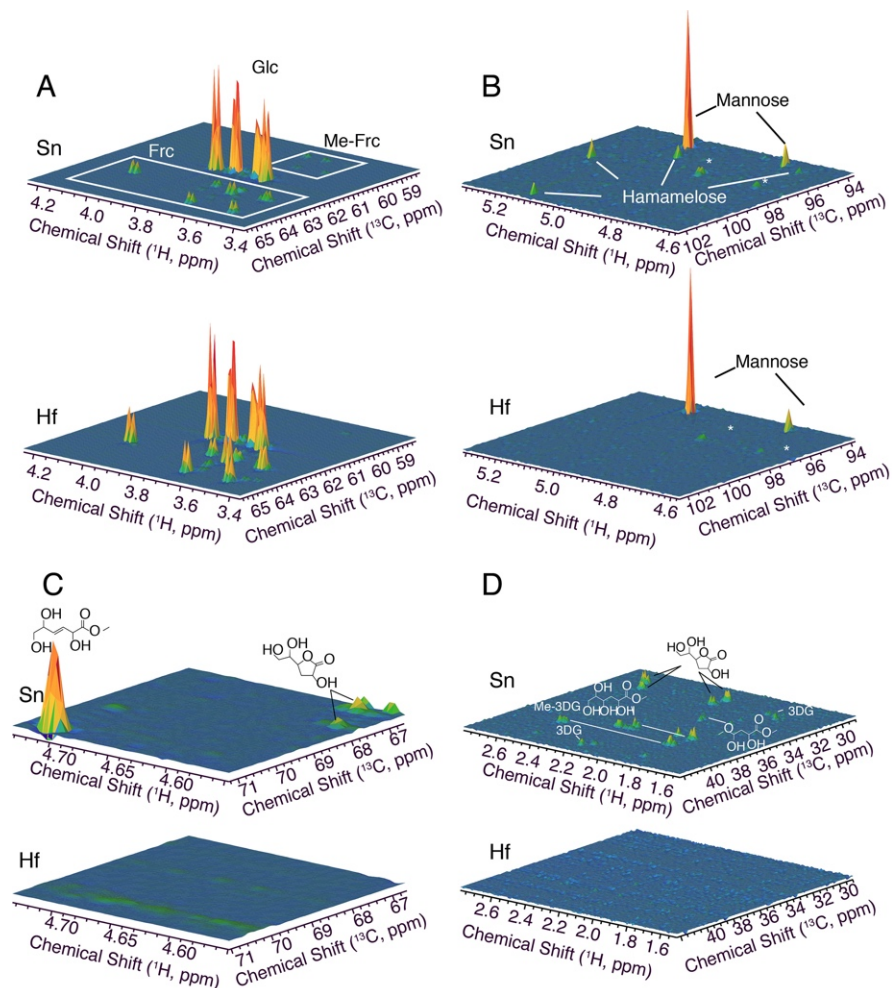


Figure 10. ^1H - ^{13}C HSQC NMR spectra for NMR analyses of the reaction effluent from Sn- and Hf-Beta catalysed GI at 110 °C. Spectra were acquired at 25 °C on an 800 MHz spectrometer equipped with a cryogenically cooled probe. The spectra provide an unbiased picture of the vastly reduced by-product formation when using Hf-Beta instead of Sn-Beta. Experimental details: 1 % wt. glucose in methanol, 110 °C, 10 bar. (Sn-Beta) 1.5 mL min⁻¹ and (Hf-Beta) 0.65 mL min⁻¹ of flow over 100 mg of catalyst.

These analyses were provided by our collaborator Dr. S. Meier, at Denmark Technical University (DTU), DK

5.3.2 Spectroscopic analysis of Hf-Beta

To gain a better understanding of the performance of Hf-Beta, and to compare its structure and active site speciation to that previously established for Sn-Beta, spectroscopic studies of Hf-Beta were performed. Unfortunately, the low gyromagnetic ratio of Hf, its large quadrupole moment, its high-energy absorption feature ($\lambda_{\text{max}} < 200$ nm), coupled with its dilute number of active sites (Si/M = 202), prohibits its characterisation by classical site-selective methods, such as solid state NMR and UV-Vis spectroscopy. As such, very little information is available concerning the active site speciation of Hf-Beta, although much more is known about Sn-Beta.³⁰⁻³³ Accordingly, direct and indirect studies were achieved by means of X-Ray Absorption Spectroscopy (XAS) and chemisorption studies coupled with Infra-red spectroscopy (cIR).

Hf L₃ edge X-ray Absorption Fine Structure (XAFS) analysis was used to gain insight into the Hf active site within the catalyst before and after reaction. While the majority of XAS studies of zeolites are performed after dehydration, in this case was chosen to perform analysis on hydrated samples that are more representative of the materials used during this study (samples were stored at ambient temperature and pressure prior to and following use).

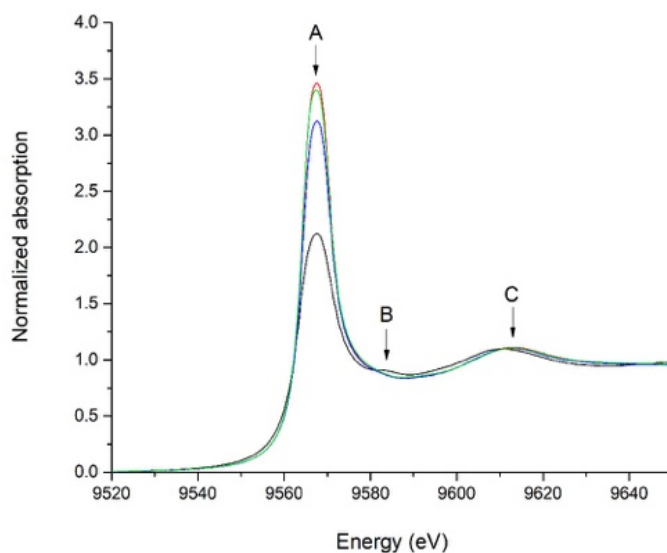


Figure 11. Hafnium L₃-edge XANES of Hf-Beta catalyst and monoclinic HfO₂. (Red) fresh catalyst; (green) methanol treated catalyst; (blue) used catalyst; (black) HfO₂. (A) White line feature; (B) multiple scattering Hf-O-Hf; (C) EXAFS oscillation.

These data were gathered by Dr. Kondrat S. in the Diamond Light Source synchrotron at Harwell (UK)

Figure 11 shows the X-ray Absorption Near Edge Structure (XANES) data of the catalyst, prior to and post reaction or methanol treatment, and that of a monoclinic HfO₂ standard. The adsorption edge of all catalyst samples, as determined by the maxima of the first derivative of the data, was found to be at 9564.4 eV compared to 9563.4 eV in the monoclinic HfO₂. The 1 eV shift in adsorption edge of the catalyst compared to HfO₂ was coupled with a significant increase in the white line feature labelled A (feature associated with $2p \rightarrow 5d$ transition) in the catalyst samples. It is proposed that the formal oxidation state of Hf (IV) is present in all samples and the observed differences indicate a change in the local environment of Hf within the catalyst compared to the monoclinic HfO₂ standard. Also, of note is the subtle difference in white line intensity between the catalyst samples, with the intensity being greatest in the fresh sample, followed by the methanol treated and the post reaction samples. Feature B is seen in the XANES of HfO₂ but not in Hf-Beta at any stage of reaction and is attributed to a Hf-O-Hf multiple scattering process involving atoms in the second shell. The absence of this feature in the Hf-Beta catalyst further suggests a different coordination of oxygen to Hf in Hf-Beta compared to bulk HfO₂.

To obtain more detailed information about the local structure of Hf in these samples, Hf L₃-edge extended X-ray Absorption Fine Structure (EXAFS) studies were performed (figure 12). The k^x weighted χ data and corresponding magnitude of the Fourier transform (FT) data of the samples is shown in figure 10 Right. The first feature in both the catalyst and HfO₂ FT data can be assigned to Hf-O scattering paths, while features between 2.5 and 4 Å are associated with Hf-Hf and second shell Hf-O paths. It is evident from simple observation of the non-phase corrected FT data that the first Hf-O feature is at a shorter distance in the catalyst samples compared to HfO₂, and that second shell Hf-O and/or Hf-Hf paths are much less significant.

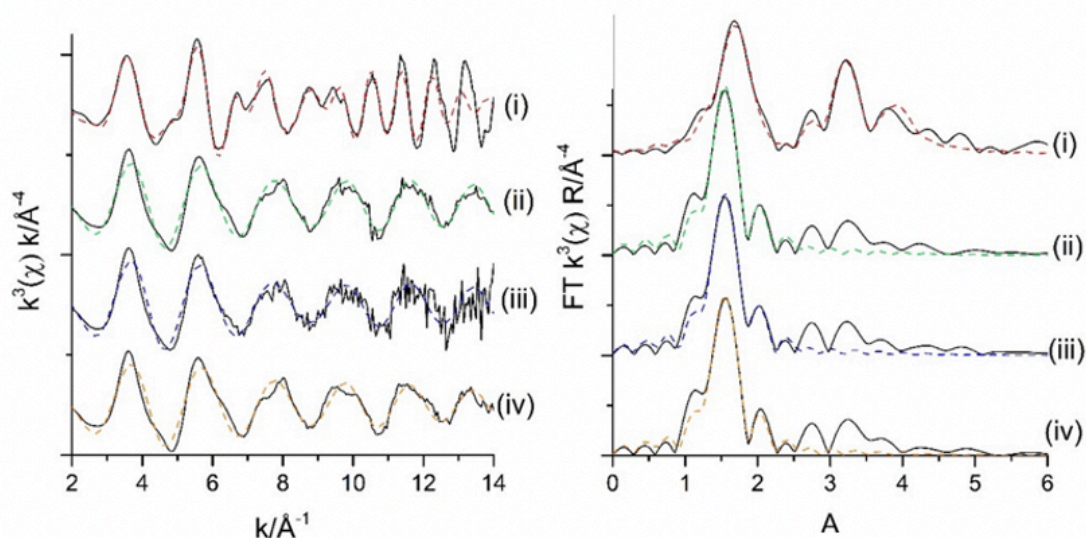


Figure 12. Hafnium L₃-edge EXAFS of Hf-Beta catalyst and monoclinic HfO₂. A) k^3 weighted χ data; B) Magnitude of Fourier Transform. Samples: (i) monoclinic HfO₂; (ii) fresh catalyst; (iii) used catalyst; (iv) methanol treated catalyst. Fitted data overlaid onto spectra in dashed colour.

These data were gathered by Dr. Kondrat S. in the Diamond Light Source synchrotron at Harwell (UK)

Fitting of the EXAFS data, shown in table 3, revealed two clear first shell Hf-O paths in the catalyst samples compared to the single fitted path in the monoclinic HfO₂. The first Hf-O path in all the catalysts was found to be at 2.00 Å, and was determined to have a coordination number of 4. Based on these values and on previous XAS studies of Sn-Beta materials,³⁴ this path can be directly attributed to Hf atoms present in a tetrahedral environment in the BEA zeolite framework. A second Hf-O distance, at 2.20 Å length and with a coordination number of 2, could also be determined. Since this second distance is notably longer than the average first shell distance of monoclinic or orthorhombic HfO₂, it is highly unlikely that the second Hf-O distance arises from bulk HfO₂ species. This is further supported by the observation that attempts at fitting a second shell Hf-Hf and/or Hf-O paths using models applicable for monoclinic or orthorhombic HfO₂ were unsatisfactory for all catalyst samples.³⁵ As such, the second Hf-O distance could either be due to water bound

to the Hf atoms present within the framework, or to a small fraction of the Hf within the sample being present as HfO_x clusters.

Whilst the absence of HfO_x standards makes impossible to conclusively distinguish between these options, the obvious lack of HfO₂, coupled previous XAS studies of Sn-Beta³⁴ materials prior to and following dehydration, makes it possible to propose that the second Hf-O distance relates to the coordination of two water molecules to the otherwise-tetrahedrally coordinated active sites. Thus, it was concluded that at least the major fraction of Hf is within the BEA zeolite framework and is present as a hydrated isomorphously substituted lattice atom at ambient conditions. The lack of changes in the amplitude of features between 2.5 and 4 Å in the catalyst samples post operation, coupled with the constant coordination numbers for first shell Hf-O species, suggests that none of the Hf species present in the sample do change in quantity or structure during reaction, consistent with the excellent stability of the catalyst.

Table 3. EXAFS fitting data of Hf-Beta catalysts and a monoclinic HfO₂ standard. Fitting parameters: $2.2 < k < 12$, $1.1 < R < 2.5$ (4 for mono-HfO₂).

Sample	Path	CN	R (Å)	2σ ² (Å ²)	E _r (eV)	R-factor
Mono-HfO ₂	Hf-O (1) ^b	7 ^c	2.12(1)	0.011(1)	7(1)	0.007
	Hf-Hf (1) ^b	7 ^c	3.42(1)	0.008(1)		
	Hf-O (2) ^b	7 ^c	3.70(3)	0.013(5)		
	Hf-Hf (2) ^b	4 ^c	4.00(1)	0.005(2)		
Hf-Beta (fresh)	Hf-O (1)	4.5(8)	2.00(2)	0.003(2)	7(1)	0.007
	Hf-O (2)	2.1(5)	2.20(4)	0.004 ^d		
Hf-Beta (used)	Hf-O (1)	4.5(8)	2.00(2)	0.004(2)	8(1)	0.005
	Hf-O (2)	2.4(5)	2.20(2)	0.004 ^d		

^a Multiple path lengths fitted as a single path (i.e Hf-O(1) comprises of 7 different path lengths); ^b Coordination numbers (CN) fixed to known crystallographic values;³⁶ ^c 2σ² defined as 1.2 of 2σ² of Hf-O(1).

These data were gathered by Dr. Kondrat S. in the Diamond Light Source synchrotron at Harwell (UK)

Although is possible to conclude that both Sn- and Hf-containing Beta possess isomorphously substituted Lewis acidic centres, recent studies have indicated that the substitution of different Lewis acids into the lattice can lead to the genesis of very different acidic properties.^{31,37} Thus, to gain insight into the acidic properties of Sn-Beta and Hf Beta, chemisorption IR spectroscopy (cIR) was performed with pyridine as a probe molecule that is sensitive to both Lewis and Brønsted acidic centres (figure 11).^{38,39} Figure 13 shows the IR spectra of pyridine adsorbed on Hf- and Sn-Beta in the 1650-1425⁻¹ region, following dosing with pyridine vapour at room temperature, and subsequent outgassing up to 200 °C to

remove gaseous and weakly bound pyridine, according to the method of Harris *et al.*⁴⁰ Spectra were background corrected by subtraction of the spectrum of the zeolite catalyst prior to dosing.

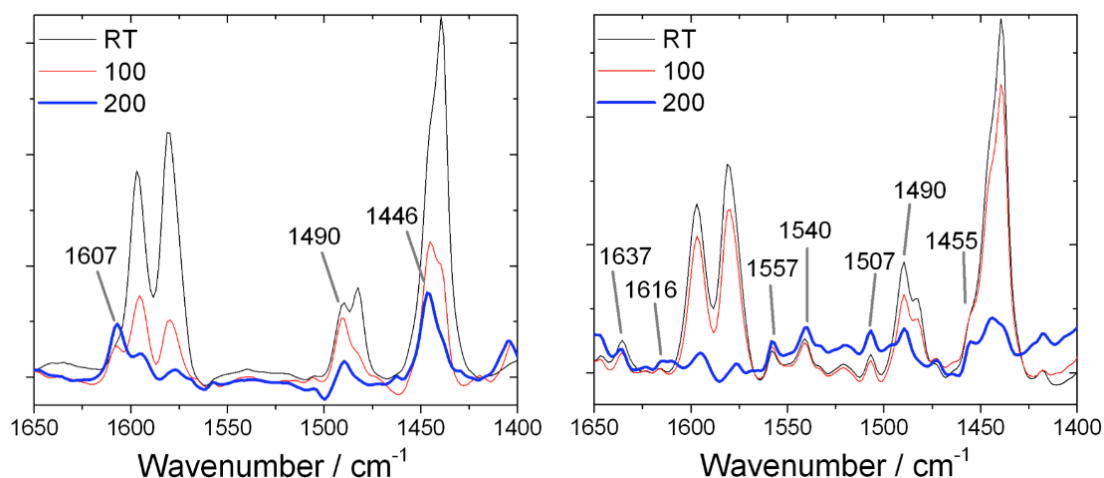


Figure 13. Chemisorption FTIR studies following the interaction of pyridine over (Left) Hf-Beta, and (Right) Sn-Beta.

Based on previous studies of pyridine adsorption⁴¹ and the behaviour of the vibrations upon thermal treatment, three main classes of vibrations could be assigned; i) vibrations related to physisorbed and/or hydrogen bonded pyridine (1597, 1580, 1482, 1440 cm^{-1}); ii) vibrations arising from coordination of pyridine to Lewis acid centres (1620-1600, 1455-1445 cm^{-1}), and; iii) vibrations related to pyridine protonated by Brønsted acid centres (1637, 1540 cm^{-1}).^{40,41} Since physisorbed and/or hydrogen bonded pyridine vibrations do not relate to the active sites of the catalysts, and vibrations at 1490 cm^{-1} can be generated both by Lewis and Brønsted acid sites, these bands are not discussed further.

By interrogation of the cIR profiles (figure 13), two major observations could be made. Firstly, although both samples exhibited vibrations related to interaction of pyridine with Lewis acidic centres, the stretching frequencies of these vibrations were present at higher values for Sn-Beta than Hf-Beta (1616 vs. 1607 cm^{-1} , and 1455 vs. 1446 cm^{-1} , respectively). This indicates stronger activation of pyridine by Sn-Beta compared to Hf-Beta.⁴¹ Secondly, whilst vibrations associated to the protonation of pyridine were clearly generated by Sn-Beta (particularly at 1637 and 1540 cm^{-1}), such vibrations were totally absent from the spectra of Hf-Beta. Thus, it can be concluded that Sn-Beta possesses relatively strong Lewis acid sites alongside Brønsted acidic active sites, whereas Hf-Beta only contains Lewis acid active sites, which are of a lower strength to those found in Sn-Beta. The observation of Brønsted acidity in Sn-Beta is supported by recent NMR studies,^{38,39} whilst the weaker Lewis acid strength of Hf-Beta relative to Sn-Beta is supported by ¹⁵N MAS NMR studies of various Lewis and Brønsted acidic silicates, as reported by Gunther *et al.*⁴²

5.3.3 Intensification of the process

Given its much improved selectivity and stability relative to Sn-Beta, the potential of Hf-Beta for intensified GI was investigated. Of particular interest is whether its selectivity and stability can be maintained even at elevated temperatures, which would favour thermodynamic equilibrium yields and reactor productivity (equation 1 in the equation appendix) (Chapter 1, Section 1.8). Accordingly, the performance of Hf-Beta for GI was also investigated at 140 °C, and compared to the performance of a sample of Sn-Beta at the same temperature. Although increasing the reaction temperature from 110 to 140 °C markedly increases the quantity of glucose converted over Sn-Beta, the space-time-yield (equation 11 in the equation appendix) at 140 °C is only slightly higher than that obtained at 110 °C (2.2 vs. 1.8 g (Fru) cm⁻³ h⁻¹ respectively) for Sn-Beta. This minor increase is a likely consequence of the onset of competitive, consecutive and degradation reactions which are known to occur above 130 °C, as indicated by the significant loss of carbon balance in this reaction. In contrast, the excellent performance of Hf-Beta is maintained even at 140 °C, with fructose still produced at a selectivity > 90 % at an improved space-time-yield of 4.12 g (Fru) cm⁻³ h⁻¹. At these conditions, a continuous single pass yield of up to 50 % was achieved, with excellent stability observed over a 24 h period of operation (figure 14).

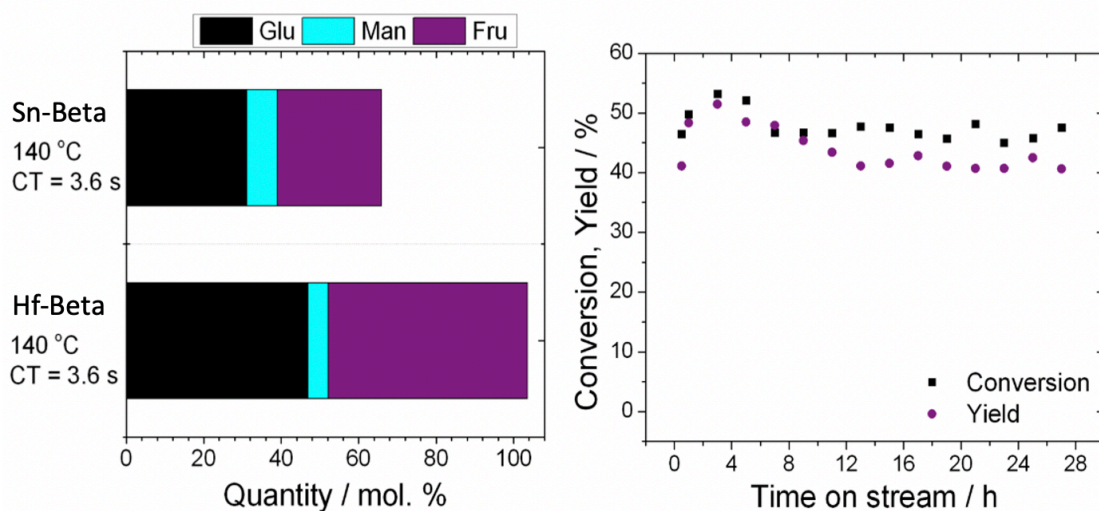


Figure 14. Kinetic data for the isomerisation of glucose to fructose over Sn- and Hf-containing Beta zeolites (A) Time on stream Hf-Beta at 140 °C (B). Experimental details: 1 % wt. glucose in methanol, 140 °C, 10 bar. (Sn-Beta) 1.5 mL min⁻¹ and (Hf-Beta) 1.5 mL min⁻¹ of flow over 100 mg of catalyst.

Furthermore, the induction period observed at 110 °C is almost completely eliminated at higher temperatures, resulting in a process that is highly productive, selective and stable from the very first moments of operation. Notably, separation of the product mixture by reduced pressure solvent recovery revealed that the isolated product formed at 140 °C is a white, crystalline solid, confirming the lack of browning due to sugars condensations even during high temperature operation (figure 15).

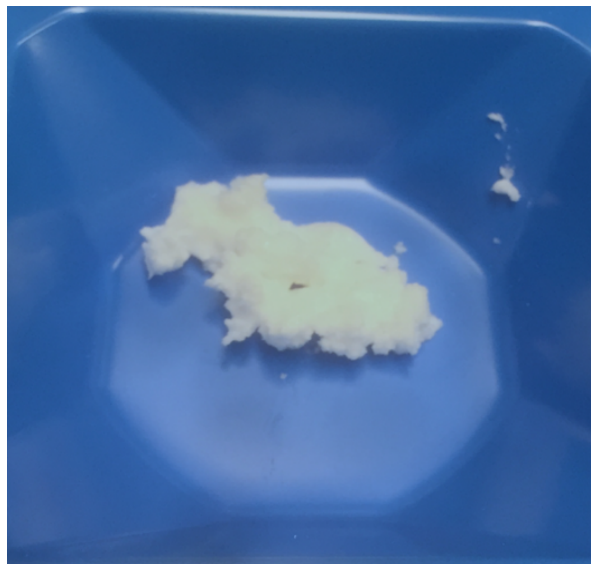


Figure 15. Colours of the sugar product purified from the isomerisation reaction catalysed by Hf-Beta zeolite conducted at 140 °C with 50 % conversion and 98 % selectivity. Experimental details: 1 % wt. glucose in methanol, 140 °C, 10 bar, 1.5 mL min⁻¹ of flow over 100 mg of catalyst.

5.4 Conclusion

The work exposed in this chapter of the thesis presents the discovery of how Hf-Beta zeolite can be a stable, active and selective heterogeneous catalyst for glucose isomerisation. This is the first time that in the literature is reported a inorganic catalyst able to produce such elevated yields in fructose (>50 %) without compromising the selectivity of the process. Furthermore, the elevated selectivity allowed production a highly pure product, which present a clean, white colour; this can be essential for downstream applications.

Moreover, the possibility to run this process a relatively high temperatures (100-140°C) allows, not only to increase the productivity, but also to shift the thermodynamic equilibrium towards the fructose production being this transformation endothermic.^{3,41} These advantages are not accessible when using enzymes considering the low stability at temperature of 80°C and above.^{6,7} During this chapter, it was also shown how Zr-Beta can achieve similar level of selectivity to Hf-Beta, although its activity is significantly lower.

5.5 Reference

- (1) Collard, F. X.; Blin, J. A Review on Pyrolysis of Biomass Constituents: Mechanisms and Composition of the Products Obtained from the Conversion of Cellulose, Hemicelluloses and Lignin. *Renew. Sustain. Energy Rev.* **2014**, *38*, 594–608.
- (2) Zhang, X.; Wilson, K.; Lee, A. F. Heterogeneously Catalyzed Hydrothermal Processing of C5-C6 Sugars. *Chem. Rev.* **2016**, *116* (19), 12328–12368.
- (3) Assary, R. S.; Kim, T.; Low, J. J.; Curtiss, L. A. Glucose and Fructose to Platform Chemicals : Understanding the Thermodynamic Landscapes of Acid-Catalysed Reactions Using High-Level Ab Initio Methods W. **2012**, 16603–16611.
- (4) Aellig, C.; Hermans, I. Continuous D-Fructose Dehydration to 5-Hydroxymethylfurfural Under Mild Conditions. **2012**, 1737–1742.
- (5) Choudhary, V.; Pinar, A. B.; Lobo, R. F.; Vlachos, D. G.; Sandler, S. I. Comparison of Homogeneous and Heterogeneous Catalysts for Glucose-to-Fructose Isomerization in Aqueous Media. *ChemSusChem* **2013**, *6* (12), 2369–2376.
- (6) Li, H.; Yang, S.; Saravanamurugan, S.; Riisager, A. Glucose Isomerization by Enzymes and Chemo-Catalysts: Status and Current Advances. *ACS Catal.* **2017**, *7* (4), 3010–3029.
- (7) Bandlish, R. K.; Michael Hess, J.; Epting, K. L.; Vieille, C.; Kelly, R. M. Glucose-to-Fructose Conversion at High Temperatures with Xylose (Glucose) Isomerases From *Streptomyces murinus* and Two Hyperthermophilic *Thermotoga* Species. *Biotechnol. Bioeng.* **2002**, *80* (2), 185–194.
- (8) Parker, K.; Salas, M.; Nwosu, V. C. High Fructose Corn Syrup : Production , Uses and Public Health Concerns. **2010**, *5*, 71–78.
- (9) Lima, D. M.; Fernandes, P.; Nascimento, D. S.; Cássia, R. De; Ribeiro, L. F.; Assis, S. A. De. Fructose Syrup : A Biotechnology Asset. **2011**, *9862* (4), 424–434.
- (10) Eerhart, A. J. J. E.; Faaij, A. P. C.; Patel, M. K. Replacing Fossil Based PET with Biobased PEF; Process Analysis, Energy and GHG Balance. *Energy Environ. Sci.* **2012**, *5* (4), 6407–6422.
- (11) White, J. S. Sucrose , HFCS , and Fructose : History , Manufacture , Composition , Applications , and Production. **2014**.
- (12) Moliner-Marín, M.; Roman-Leshkov, Y.; Davis, M. E.; Nikolla, E. Isomerisation of glucose to fructose by means of Lewis acid-zeolite catalysts. **2011**, *2* (19), 1–23. EP3067362A1
- (13) Moliner, M.; Román-Leshkov, Y.; Davis, M. E. Tin-Containing Zeolites Are Highly Active Catalysts for the Isomerization of Glucose in Water. *Proc. Natl. Acad. Sci. U. S. A.* **2010**, *107* (14), 6164–6168.
- (14) Dijkmans, J.; Gabriels, D.; Dusselier, M.; de Clippel, F.; Vanelderen, P.; Houthoofd, K.; Malfliet, A.; Pontikes, Y.; Sels, B. F. Productive Sugar Isomerization with Highly Active Sn in Dealuminated Beta Zeolites. *Green Chem.* **2013**, *15*, 2777–2785.
- (15) Tolborg, S.; Meier, S.; Sádaba, I.; Elliot, S. G.; Kristensen, S. K.; Saravanamurugan, S.; Riisager, A.; Frstrup, P.; Skrydstrup, T.; Taarning, E. Tin-Containing Silicates: Identification of a Glycolytic Pathway via 3-Deoxyglucosone. *Green Chem.* **2016**, *18* (11), 3360–3369.
- (16) Padovan, D.; Botti, L.; Hammond, C. Active Site Hydration Governs the Stability of Sn-Beta during Continuous Glucose Conversion. *ACS Catal.* **2018**, *8* (8), 7131–7140.
- (17) Elliot, S. G.; Tosi, I.; Meier, S.; Martinez-Espin, J. S.; Tolborg, S.; Taarning, E. Stoichiometric Active Site Modification Observed by Alkali Ion Titrations of Sn-Beta. *Catal. Sci. Technol.* **2019**, *9* (16), 4339–4346.

- (18) Holm, M. S.; Saravanamurugan, S.; Taarning, E. Conversion of Sugars to Lactic Acid Derivatives Using Heterogeneous Zeotype Catalysts. *Science (80-.)*. **2010**, *328* (5978), 602–605.
- (19) Luo, H. Y.; Lewis, J. D.; Román-Leshkov, Y. Lewis Acid Zeolites for Biomass Conversion: Perspectives and Challenges on Reactivity, Synthesis, and Stability. *Annu. Rev. Chem. Biomol. Eng.* **2016**, *7* (1), 663–692.
- (20) Tolborg, S.; Katerinopoulou, A.; Falcone, D. D.; Sadaba, I.; Osmundsen, C. M.; Davis, R. J.; Taarning, E.; Fristrup, P.; Holm, M. S. Incorporation of Tin Affects Crystallization, Morphology, and Crystal Composition of Sn-Beta. *J. Mater. Chem. A* **2014**, *2* (47), 20252–20262
- (21) Erenburg, S. B.; Trubina, S. V.; Kvashnina, K. O.; Kruchinin, V. N.; Gritsenko, V. V.; Chernikova, A. G.; Markeev, A. M. Short-Range Order in Amorphous and Crystalline Ferroelectric Hf_{0.5}Zr_{0.5}O₂. *J. Exp. Theor. Phys.* **2018**, *126* (6), 816–824.
- (22) Costandy, J. G.; Edgar, T. F.; Baldea, M. Switching from Batch to Continuous Reactors Is a Trajectory Optimization Problem. *Ind. Eng. Chem. Res.* **2019**, *58* (30), 13718–13736.
- (23) Hammond, C. Intensification Studies of Heterogeneous Catalysts: Probing and Overcoming Catalyst Deactivation during Liquid Phase Operation. *Green Chem.* **2017**, *19* (12), 2711–2728.
- (24) Levenspiel, O. *Chemical Reaction Engineering*; 1999; Vol. 38.
- (25) Takasaki, Y. Kinetic and Equilibrium Studies on D-Glucose-d-Fructose Isomerization Catalyzed by Glucose Isomerase from *Streptomyces* Sp. *Agric. Biol. Chem.* **1967**, *31* (3), 309–313.
- (26) Son, P. A.; Nishimura, S.; Ebitani, K. Preparation of Zirconium Carbonate as Water-Tolerant Solid Base Catalyst for Glucose Isomerization and One-Pot Synthesis of Levulinic Acid with Solid Acid Catalyst. *React. Kinet. Mech. Catal.* **2014**, *111* (1), 183–197.
- (27) Saravanamurugan, S.; Riisager, A.; Taarning, E.; Meier, S. Mechanism and Stereoselectivity of Zeolite-Catalysed Sugar Isomerisation in Alcohols. *Chem. Commun.* **2016**, *52* (86), 12773–12776.
- (28) Dusselier, M.; VanWouwe, P.; deClippel, F.; Dijkmans, J.; Gammon, D. W.; Sels, B. F. Mechanistic Insight into the Conversion of Tetrose Sugars to Novel α -Hydroxy Acid Platform Molecules. *ChemCatChem* **2013**, *5* (2), 569–575.
- (29) Saravanamurugan, S.; Tosi, I.; Rasmussen, K. H.; Jensen, R. E.; Taarning, E.; Meier, S.; Riisager, A. Facile and Benign Conversion of Sucrose to Fructose Using Zeolites with Balanced Brønsted and Lewis Acidity. *Catal. Sci. Technol.* **2017**, *7* (13), 2782–2788.
- (30) Harris, R. K.; Becker, E. D.; Cabral de Menezes, S. M.; Goodfellow, R.; Granger, P. NMR Nomenclature: Nuclear Spin Properties and Conventions for Chemical Shifts. IUPAC Recommendations 2001. International Union of Pure and Applied Chemistry. Physical Chemistry Division. Commission on Molecular Structure and Spectroscopy. *Magn. Reson. Chem.* **2002**, *40* (7), 489–505.
- (31) Boronat, M.; Concepción, P.; Corma, A.; Renz, M.; Valencia, S. Determination of the Catalytically Active Oxidation Lewis Acid Sites in Sn-Beta Zeolites, and Their Optimisation by the Combination of Theoretical and Experimental Studies. **2005**, *234*, 111–118.
- (32) Kolyagin, Y. G.; Yakimov, A. V.; Tolborg, S.; Vennestrøm, P. N. R.; Ivanova, I. I. Direct Observation of Tin in Different T-Sites of Sn-BEA by One- and Two-Dimensional ¹¹⁹Sn MAS NMR Spectroscopy. *J. Phys. Chem. Lett.* **2018**, *9* (13), 3738–3743.
- (33) Wolf, P.; Valla, M.; Rossini, A. J.; Comas-Vives, A.; Núñez-Zarur, F.; Malaman, B.; Lesage, A.; Emsley, L.; Copéret, C.; Hermans, I. NMR Signatures of the Active Sites in Sn-Beta Zeolite. *Angew. Chemie - Int. Ed.* **2014**, *53* (38), 10179–10183.

- (34) Hammond, C.; Padovan, D.; Al-Nayili, A.; Wells, P. P.; Gibson, E. K.; Dimitratos, N. Identification of Active and Spectator Sn Sites in Sn- β Following Solid-State Stannation, and Consequences for Lewis Acid Catalysis. *ChemCatChem* **2015**, *7* (20), 3322–3331.
- (35) Iida, T.; Ohara, K.; Román-Leshkov, Y.; Wakihara, T. Zeolites with Isolated-Framework and Oligomeric-Extraframework Hafnium Species Characterized with Pair Distribution Function Analysis. *Phys. Chem. Chem. Phys.* **2018**, *20* (12), 7914–7919.
- (36) Whittle, K. R.; Lumpkin, G. R.; Ashbrook, S. E. Neutron Diffraction and MAS NMR of Cesium Tungstate Defect Pyrochlores. *J. Solid State Chem.* **2006**, *179* (2), 512–521.
- (37) Gunther, W. R.; Michaelis, V. K.; Griffin, R. G.; Roman-Leshkov, Y. Interrogating the Lewis Acidity of Metal Sites in Beta Zeolites with ¹⁵N Pyridine Adsorption Coupled with MAS NMR Spectroscopy. *J. Phys. Chem. C* **2016**, *120* (50), 28533–28544.
- (38) Sushkevich, V. L.; Kots, P. A.; Kolyagin, Y. G.; Yakimov, A. V.; Marikutsa, A. V.; Ivanova, I. I. Origin of Water-Induced Brønsted Acid Sites in Sn-BEA Zeolites. **2019**.
- (39) Zheng, A.; Liu, S. Bin; Deng, F. ³¹P NMR Chemical Shifts of Phosphorus Probes as Reliable and Practical Acidity Scales for Solid and Liquid Catalysts. *Chem. Rev.* **2017**, *117* (19), 12475–12531.
- (40) Harris, J. W.; Cordon, M. J.; Di Iorio, J. R.; Vega-Vila, J. C.; Ribeiro, F. H.; Gounder, R. Titration and Quantification of Open and Closed Lewis Acid Sites in Sn-Beta Zeolites That Catalyze Glucose Isomerization. *J. Catal.* **2016**, *335*, 141–154.
- (41) Bonino, F.; Damin, A.; Bordiga, S.; Lamberti, C.; Zecchina, A. Interaction of CD 3 CN and Pyridine with the Ti(IV) Centers of TS-1 Catalysts: A Spectroscopic and Computational Study. *Langmuir* **2003**, *19* (6), 2155–2161.
- Gunther, W. R.; Michaelis

Chapter 6

Mechanistic studies of continuous glucose upgrading over Lewis acid silicates by *operando* UV-Vis and HSQC NMR

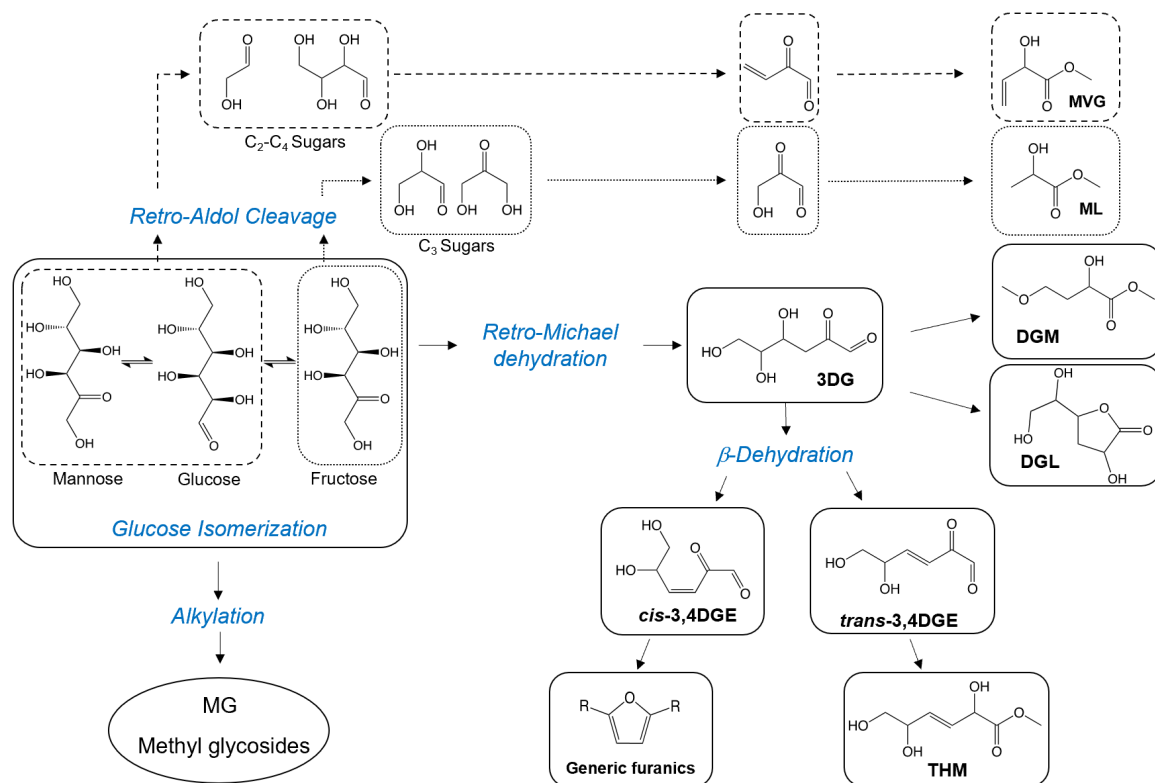
Manuscript submitted and in review process, ID: cs-2020-036382

ACS Catal.

6.1 Introduction

Throughout the whole manuscript several developments in sugars upgrading were discovered: the stabilising effect of water, the identification of the hydrothermal synthesis as the best material for glucose isomerisation, the pre-activation treatment for Sn-Beta zeolite and finally Hf-Beta zeolite as selective catalyst for glucose isomerisation to fructose. These discoveries allowed to understand the complexity of the transformation taking place throughout sugar upgrading and how even marginal modifications in the material can drastically impact on the selectivity and productivity of the process.

To highlight the complexity and diverse transformations taking place throughout sugars upgrading previous study on glucose upgrading by Sn-Beta zeolite released by Tolborg *et al.*¹ shows how this process can yield to a plethora of products: *trans*-2,5,6-trihydroxy-3-hexenoic methyl ester (THM) and furanics such as 5-(hydroxymethyl)furfural (HMF), derived from β -dehydration of 3 deoxy-D-erythrosulose (3-DG) (β -dehydration products); methyl lactate (ML) and methyl vinyl glycolate (MVG), derived from retro-aldol cleavage of hexoses (RA products); fructose and mannose, as products of glucose isomerization (GI products); methyl-glycosides, by alkylation of the monosaccharides in solution (alkylation products); and finally 3-deoxy- γ -lactones (3DGL), formed by ring closure of 3DG. Whilst the ability of Sn-Beta to catalyse so many reactions makes it a very interesting catalyst, it also makes control of the selectivity of the catalyst towards a precise chemical pathway very challenging. This is especially problematic in the context of process design, process economics and sustainable carbon management.²



Scheme 1. Scheme of the several reactions that are involved in the glucose upgrading catalysed by Sn-Beta zeolite.

Although experimental works have shown that the catalyst composition,³⁻⁵ preparation methodology^{4,6,7} and reaction conditions (temperature⁸, presence of alkali^{1,9} and/or water^{7,10}) can impact the final product distribution attained when converting glucose over Sn-Beta, relatively few studies have addressed how these stimuli impact the final reaction outcome. Moreover, the impact of catalyst deactivation on these pathways has not yet been studied, and few studies have addressed the correlation between catalyst structure and selectivity in the overall reaction network.

A major obstacle towards addressing these questions is the lack of spectroscopic insight into the operating catalyst active site structures. In particular, the conditions at which glucose upgrading is carried out (liquid phase, 80-170 °C, <25 bar when operating continuously⁷), makes *in situ* study of this system challenging. Consequently, existing structure-activity-lifetime relationships have relied on the correlation of kinetic data to various *ex situ* methodologies (e.g. MAS NMR),¹¹⁻¹⁴ and/or to probe molecule studies that monitor the interaction of Sn-Beta with model compounds such as CD₃CN and pyridine.¹⁵⁻¹⁷ Although useful to benchmark the functionality of the catalyst, *ex situ* characterization methods have limitations, and probe molecules on their own cannot fully represent the real environment of a catalytic reaction. An additional source of difficulty is that several of the compounds generated by Sn-Beta during these processes (*vide supra*) are not amenable to detection by routine chromatographic analyses, meaning that low carbon balances are

usually reported. Together, these hurdles have contributed to the slow development of accurate structure-activity-lifetime relationships.

In this chapter, it is developed a study following the activation of glucose over Sn- and Hf-silicate catalyst by *operando* UV-Vis spectroscopy. The technique was showed already in Chapter 2 of the manuscript and it effectively showed the interaction between Sn and the solvent (methanol), but without giving insight on the glucose-Sn interaction; after three years of project, several discoveries (such as stabilising effect of water and Hf-Beta as selective catalyst for GI) allowed to further expand the scope of the *operando* UV-Vis reactor for glucose isomerisation. This technique is performed at operational conditions (*in operando*, <170 °C, <25 bar) and is carried out in continuous flow, which allows the concurrent study of the deactivation of these interactions as a function of time on stream. To complement these studies, high-field liquid NMR measurements (¹H-¹³C HSQC) were used to cross-correlate the optical intermediates to various products in solution, and aid spectroscopic assignment of the optical intermediates.^{18,19} Along with providing additional mechanistic insight into these systems, these findings reveal that the selectivity of the catalyst also improves as a function of partial deactivation, due to preferential deactivation of non-selective reaction pathways.

6.2 Experimental details

6.2.1 Catalyst synthesis:

For the synthesis of post-synthetic Sn-Beta zeolite a commercial zeolite Al-Beta (Zeolyst, NH₄⁺-form, Si/Al = 19) was dealuminated by treatment in HNO₃ solution (13 M HNO₃, 100 °C, 20 mL g⁻¹ zeolite, 20 h). Solid-state stannation was achieved by grinding the appropriate amount of tin(II) acetate with the necessary amount of dealuminated zeolite for 10 minutes in a pestle and mortar. Following this procedure, the sample was heated in a combustion furnace (Carbolite MTF12/38/400) to 550 °C (10 °C min⁻¹ ramp rate) first in a flow of N₂ (3 h) and subsequently air (3 h) for a total of 6 h. Gas flow rates of 60 mL min⁻¹ were employed at all times.

The hydrothermal synthesis of Sn-Beta was performed following a procedure described in literature in reference 20: 30.6 g of tetraethyl orthosilicate (TEOS) was added to 33.1 g of tetraethylammonium hydroxide (TEAOH) under careful stirring, forming a two-phase system. After 60–90 min, one phase was obtained and the desired amount of the tin source, typically SnCl₄·5H₂O dissolved in 2.0 mL of H₂O, was added dropwise. The solution was then left for 48 h under stirring until a viscous gel was formed. The gel was finalised by the addition of 3.1 g HF in 1.6 g of demineralized H₂O yielding a solid gel with the molar composition; 1.0Si: 0.005Sn: 0.02Cl⁻: 0.55TEA⁺: 0.55F⁻: 7.5H₂O. The obtained gel was transferred in a Teflon lined stainless steel autoclave and kept for 7 days at 140 °C to crystallise. The obtained crystals were filtered and washed with deionised water.

Calcination at 550 °C (2 °C min⁻¹) for 6 h under static air was carried out in order to remove the organic template.

6.2.2 Catalyst Characterisation

Operando UV–Vis measurements were performed with a homemade tubular reactor equipped with a fiber optic UV–vis probe. UV–vis measurements were performed with a light source (Ocean Optics DH-2000), spectrometer (Maya 2000 Pro, Ocean Optics), and a 600-µm UV–vis fiber. The light was directed onto an optically transparent reactor column, located within a heated aluminum block.

6.2.3 Kinetic evaluation and analytical methods

Continuous glucose upgrading reaction were performed in a plug flow, stainless steel, tubular reactor. The catalyst was pelletised (size fraction 63 and 77 µm) and densely packed into a ¼" stainless steel tube (4.1 mm internal diameter). Two plugs of quartz wool and a frit of 0.5 µm held the catalyst in location. Temperature control was achieved by a thermostatted oil bath at the desired reaction temperature, and pressurization was achieved by means of a backpressure regulator. Aliquots of the reaction solutions were taken periodically from a sampling valve placed after the reactor and analysed by an Agilent 1260 Infinity HPLC equipped with a Hi-Plex Ca column and ELS detector and quantified against an external standard (sorbitol) added to the sample prior the injection.

High field liquid NMR analysis on the sample were recorded on a Bruker Avance III 800 MHz spectrometer equipped with a TCI cryoprobe at 25 °C. The samples analysed were dried from the protonated methanol under flow of nitrogen at 25 °C and successively re-diluted in deuterated methanol.

The glucose employed as substrate was provided by Sigma Aldrich (>99.5 %, monohydrate), methanol anhydrous as solvent was provided by Sigma Aldrich (99.8 %), deionised water was added to the reaction feed. Standard of fructose, mannose, methyl lactate were provided by Sigma Aldrich (> 99.9 %). Methyl Vinyl Glycolate as standard was provided by Tokyo Chemicals Industry (>99.9 %). Dihydroxy-acetone as substrate was provided by Sigma-Aldrich (99.9 %).

6.3 Results and Discussion

6.3.1 Identification of optical intermediates by operando UV-Vis spectra

As described above, Sn-Beta is known to catalyse several selective and non-selective reaction pathways starting from glucose.¹ Although various reaction stimuli – including choice of catalyst, method of preparation and presence of additives to the reaction solution (particularly alkali and water)^{7,8,9} – affect the course of the glucose conversion reaction over Sn-Beta (equation 3 in the equation appendix), a dominating factor with respect to progress of the reaction is the choice of operational temperature.⁷ In particular, it has been established that GI is the dominant selective reaction pathway at temperatures of up to 110 °C, whereas RA processes become dominant as the temperature is increased beyond 110 °C.^{7,21}

Accordingly, preliminary *operando* UV-Vis studies were focused upon monitoring the conversion of glucose over Sn-Beta at various temperatures between 80 to 140 °C. Each *operando* experiment was performed with a 1 % wt. glucose in methanol feed solution, and identical flow rates (0.75 mL min^{-1}) and masses of catalyst were employed (100 mg catalyst) in each experiment. Each individual experiment was performed with fresh sample of catalyst, which in the case of these preliminary experiments was a sample of Sn-Beta containing 10 % wt. Sn, and which was prepared by Solid State Incorporation (henceforth 10Sn-Beta_{SSI}). Spectra were recorded after 0.5 h of time on stream, to minimise the impact of catalyst deactivation⁷ and all spectra were background corrected to the spectrum of the catalyst in a flow of pure methanol *i.e.* to the state of the catalyst prior to introduction of glucose. The *operando* UV-Vis spectra generated by these reactions are illustrated in figure 1. It is noted that although the absence of extinction coefficient values for these intermediates prohibits quantitative assessment of the spectra, relative comparisons of intensity as a function of reaction perturbation can be made, which allows empirical correlations across entire series to be undertaken.

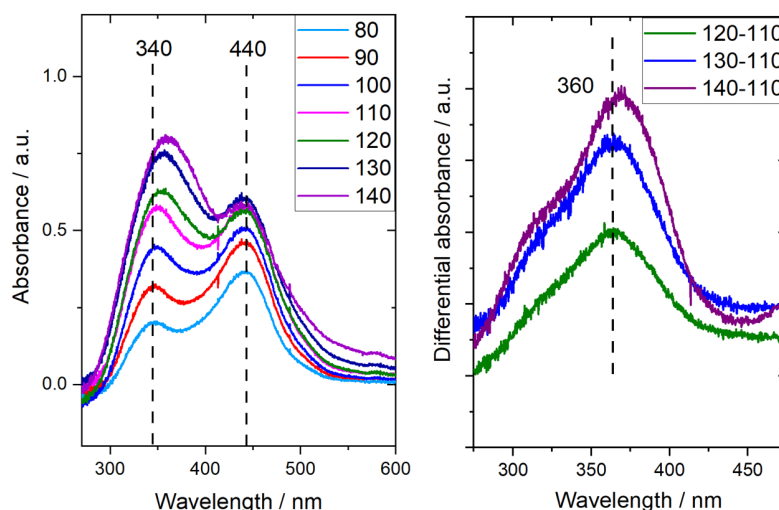


Figure 1. (Left) *Operando* UV-Vis for glucose conversion over 10Sn-Beta_{SSI} between 80-140 °C. (Right) Differential *operando* UV-Vis spectrum in the 250-450 nm region, achieved by subtracting the spectrum of the experiment at 110 °C from those generated between 120-140 °C. Experimental conditions: 1 % wt. glucose in methanol, 0.75 mL min^{-1} of flow over 100 mg of 10Sn-Beta_{SSI}, 15 bar.

As can be seen in figure 1, several absorption intermediates were generated during the interaction of glucose and 10Sn-Beta_{SSI}. At the lowest temperature studied (80 °C), spectra consisted of two clearly defined absorptions, centred at $\lambda = 340 \text{ nm}$ and 440 nm (henceforth, λ_{340} and λ_{440}). However, the behaviour of these features as a function of temperature differed substantially. The λ_{440} absorption was the most intense feature observed at 80 °C, but increased only marginally upon increasing the temperature from 80 to 110 °C, after which the intensity of the feature further plateaued. In contrast, the λ_{340} absorption was

present at a much lower intensity at 80 °C, but increased steeply at higher temperatures, reaching its maximum intensity at 140 °C (figure 1, left). Alongside these changes was an evident shift in the position of the λ_{340} feature upon increasing the temperature beyond 110 °C. Analysis of the differential spectra generated by subtraction of the 110 °C spectrum from those generated at higher temperature (figure 1, right) clearly revealed that this shift was caused by the generation of a contribution at λ_{360} , which beyond this temperature is increasing at a higher rate than the underlying absorption at $\lambda_{320-340}$.

Control experiments showed in Chapter 2 (Section 2.3.3) confirmed that the absorptions described in the previous section were only generated when glucose and Sn were both present in the system. Specifically, these absorptions were not formed when methanol was flowed over Sn-Beta, or when glucose was flowed over Sn-free zeolite Beta. To verify that these absorptions did not simply arise through formation of a chromophoric (by-)product of the reaction, the reaction effluent and standards of glucose and High Fructose Corn Syrup (HFCS, 42 % glucose) were also monitored by *ex situ* UV-Vis (figure 2). Interestingly, whilst the reaction effluent showed a broad absorption at high energy (250-300 nm), confirming the presence of some chromophoric by-product in the reaction solution, none of the standard solutions exhibited absorptions at 340 nm and 440 nm. As these bands were only formed in the presence of glucose and Sn, but did not relate to individual compounds formed during reaction, they can be assigned to transient species present on the catalyst due to the interaction between Sn and glucose.

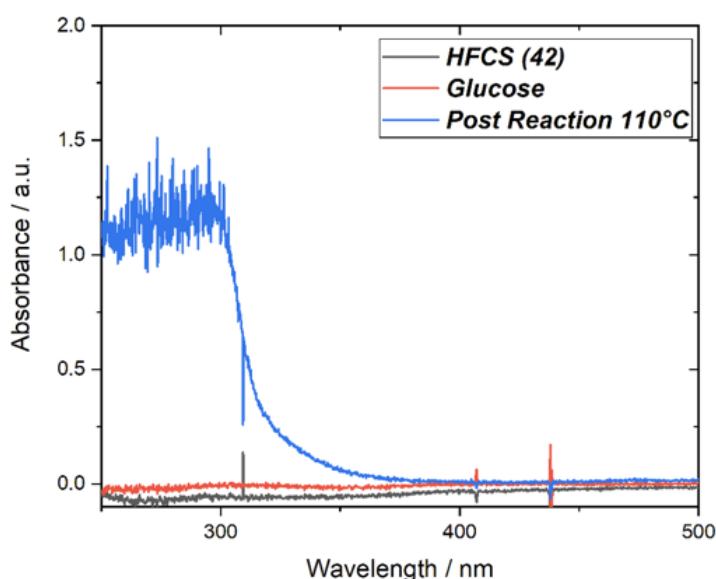


Figure 2. UV-Vis analysis *ex-situ* on glucose dissolved in methanol, 1 % wt. HFCS (42) dissolved in methanol and the effluent of glucose upgrading over Sn-Beta at 110 °C. Experimental conditions: 1 % wt. glucose in methanol, 0.750 mL min⁻¹ of flow over 100 mg of 10 Sn-Beta_{SS1}, 15 bar.

To determine the relevance of findings from figure 1, the reaction effluent of each experiment was analysed by classic chromatographic techniques (HPLC-ELSD/UV and GC-FID). In figure 3, the yields of the products are plotted against the temperature of each

reaction. Although all of the products detected by chromatographic techniques are generated by the Lewis acid active sites of the catalyst (no products were observed when Sn-free zeolite Beta was used as catalyst, Chapter 2, Section 2.3.3), and hence are examples of selective reaction products, they can be further categorised as GI products (fructose, mannose) and RA products (ML and MVG).

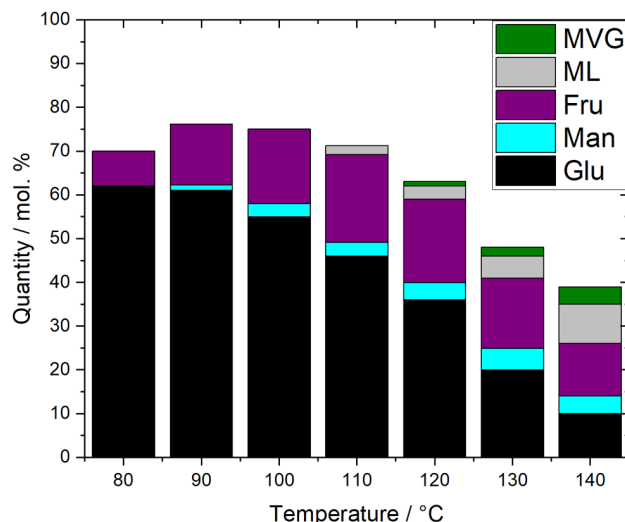


Figure 3. Yields of fructose, mannose (GI products), methyl lactate and methyl vinyl glycolate (RA products) at varying temperatures following the conversion of glucose by 10Sn-Beta_{SS1}. Experimental conditions: 1 % wt. glucose in methanol, 0.750 mL min⁻¹ of flow over 100 mg of 10 Sn-Beta_{SS1}, 15 bar.

At lower temperatures (80-110 °C), GI products were the dominant species in the reaction effluent, the yield of which increased from 7 % at 80 °C, to 26 % at 110 °C (figure 3). However, even at these low temperatures, a substantial decrease in carbon balance was observed. This loss suggests that by-products not amenable to chromatographic analysis were already present in the effluent even at low temperature. Notably, the carbon balance in each of these low temperature reactions was comparable (*ca.* 75 %), indicating that the by-products formed at low temperature were not strongly impacted by the increase in temperature in this range.

Interestingly, although increasing the temperature above 110 °C resulted in a substantial increase in the quantity of substrate converted – which increased from 55 % at 110 °C to >90 % at 140 °C – the overall yield of selective products (GI+RA) did not increase as substantially. Accordingly, a second major loss of carbon balance was observed in the higher temperature regime (>110 °C), the onset of which coincided with the generation of the λ_{360} features (figure 1, right). Alongside this loss, the distribution of selective products also changed in the higher temperature regime, and RA products accounted for an increasing fraction of the selective products in the effluent, in line with previous studies. Figure 3 thus confirms that the cumulative yield of the products, the distribution of products between GI and RA, the overall carbon balance (and hence, quantity of by-products), and

the intensity of the *operando* UV-Vis absorbances, all strongly depend upon the reaction temperature.

To gain further preliminary insight, the evolution of the *operando* UV-Vis spectra as a function of time on stream was investigated over a 13 h reaction period. In particular, the *operando* spectra of the glucose conversion reaction at 110 °C were evaluated at several stages of the continuous reaction period. This temperature was chosen as it provided a balance between the maximal yield of desired products (GI+RA), the carbon balance of the process, and the presence of all absorption features.

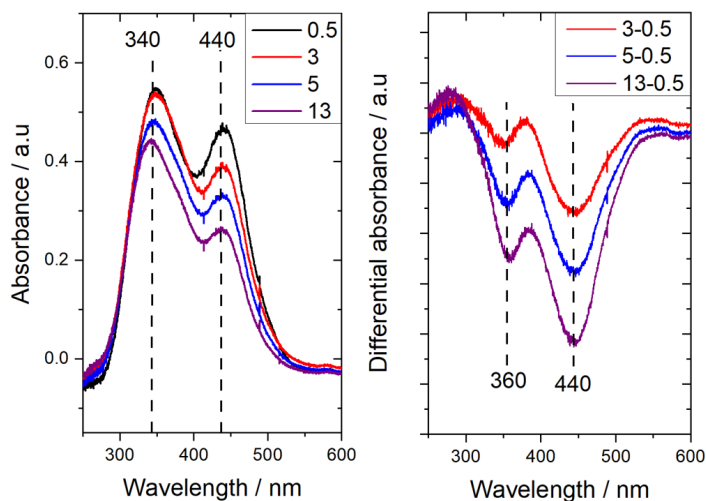


Figure 4. (Left) *Operando* UV-Vis spectrum from the conversion of glucose over 10Sn-Beta_{SSi} at 110 °C at various points of time on stream (0.5, 3, 5 and 10 h). (Right) Differential *operando* UV-Vis spectrum in the 250-600 nm region, obtained by subtracting the spectrum recorded at 0.5 h on stream from those at later points of time. Experimental conditions: 110 °C, 1 % wt. glucose in methanol, 0.750 mL min⁻¹ of flow over 100 mg of 10 Sn-Beta_{SSi}, 15 bar.

As can be seen (figure 4, left), over the course of 13 h on stream all the absorptions present in the *operando* UV-Vis spectra decreased. However, the rate of decrease differed markedly for the different bands in the spectra. For example, whereas the λ_{440} signal rapidly lost intensity over the first hours of reaction, the λ_{340} signal decreased much more gradually. Moreover, the λ_{340} band also shifted towards higher energy, suggesting a non-uniform loss of intensity in the 330-380 nm region. To clarify the changes observed as a consequence of time on stream, differential spectra were generated by subtracting the spectrum recorded at 0.5 h on stream from those collected at later times on stream. This indicated that the λ_{340} band was a congested feature of an absorbance at approximately 330-340 nm (henceforth λ_{330}), and a second absorbance at 360 nm (λ_{360}), which deactivated much faster over the first 10 h of the reaction. This finding indicates that although the λ_{360} feature observed in Figure 1 grows strongly at higher temperatures, it was already present at 110 °C, accounting for the progressive shift in the maxima at increasing temperature. As a consequence of the

loss of intensity at 360 and 440 nm, the λ_{340} UV-Vis band became the most dominant after 10 h on stream, with the majority of its intensity remaining after this operational period.

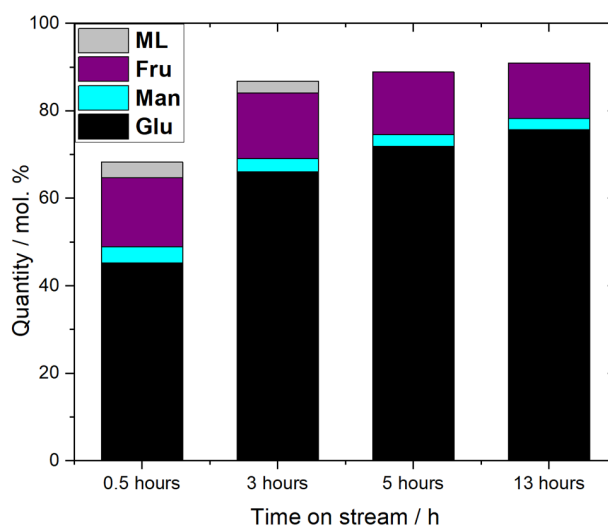


Figure 5. Kinetic data related to the conversion of glucose over 10Sn-Beta_{SSi} at 110 °C at various points of time on stream (0.5, 3, 5 and 13 h). Experimental conditions: 110 °C, 1 % wt. glucose in methanol, 0.750 mL min⁻¹ of flow over 100 mg of 10 Sn-Beta_{SSi}, 15 bar.

Despite the decrease in absorbance observed over the 10 h reaction period, quantitative analysis of the reaction effluent revealed that the yield of selective (GI+RA) products only decreased slightly from 22 % to 16 % (figure 5). However, the quantity of glucose converted by the catalyst decreased much more dramatically (from 55 % to 22 % between 0.5 h and 10 h). As a consequence, the carbon balance of the reaction increased substantially over the first 10 h on stream (from 65 to 90 %, figure 5). The increased carbon balance indicates that undetected by-products were produced to a much lower level after 10 h on stream, thereby increasing the selectivity of the reaction system without directly affecting the selective reaction pathways themselves (equation 8 in the equation appendix).

Given that several of the products achieved by conversion of glucose are not amenable to detection by classical chromatographic means, further analysis of the post-reaction effluents was undertaken by high-field liquid NMR (¹H-¹³C HSQC NMR spectroscopy).^{16,17} This method provides roughly 30 times higher sensitivity compared to conventional 1D ¹³C NMR, whilst providing improved resolution due to its two-dimensional nature. As demonstrated in recent studies, the methodology can be used to describe several products from the Lewis acid catalysed conversion of glucose, and provides an unbiased representation of by-product formation since it is also sensitive to compounds that are not easily detected with classical chromatographic methods. The spectra of the two effluents measured by HSQC NMR (0.5 h and 13 h on stream) are shown in figure 6.

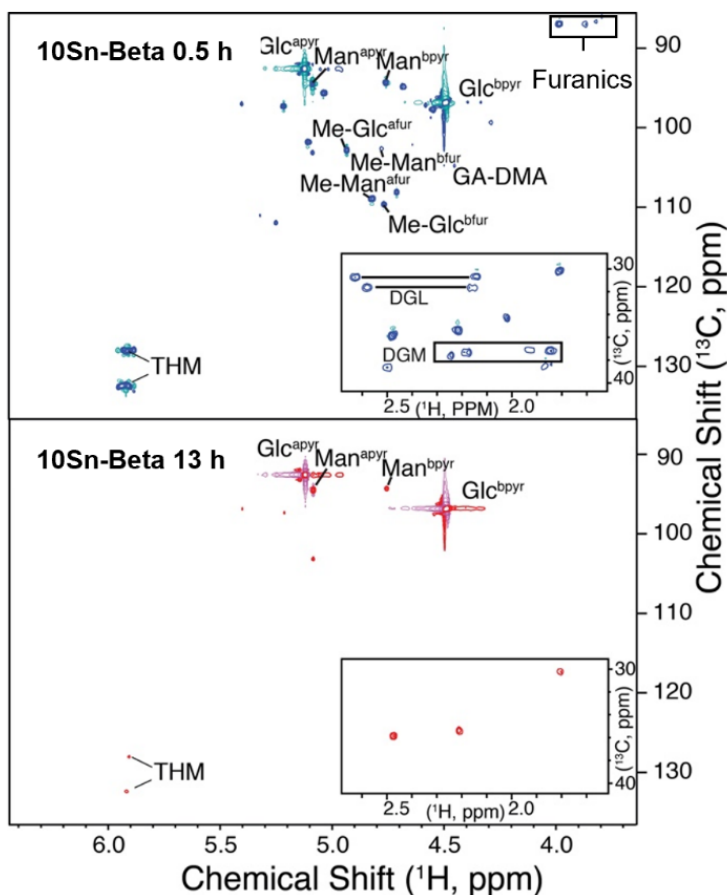


Figure 6. 2D ^1H - ^{13}C HSQC NMR on the effluent of the reaction reported in figure 5. Experimental conditions: 110 °C, 1 % wt. glucose in methanol, 0.750 mL min^{-1} of flow over 100 mg of 10Sn-Betassi, 15 bar.

These analyses were provided by our collaborator Dr. S. Meier, at Denmark Technical University (DTU), DK

2D ^1H - ^{13}C HSQC NMR spectra of the reaction effluent samples at 0.5 h and 10 h are displayed in figure 6. This analysis demonstrated that the 0.5 h reaction effluent contained high quantities of THM, 3DGL, 3-deoxy-gluconic methyl ester (DGM) and furanics. According to recent studies by Tolborg *et al.*¹, these molecules can all be produced from β -dehydration of the same intermediate (3DG), which is formed by retro-Michael dehydration of glucose. Notably, large quantities of alkylation products (methyl-glucoside and methyl-mannoside) were also present at 0.5 h of time on stream. The formation of alkylation products and β -dehydration products strongly decreased after 10 h of time on stream, at the same period of time as the intensity of λ_{440} and λ_{360} decreased, and the carbon balance of the reaction increased from 69 to 90 % (figure 4). Based on these observations, it can tentatively be ascribed that the λ_{330} absorption relates to selective reaction pathways (GI and/or RA), whereas absorptions at λ_{360} and λ_{440} relate to the generation of non-selective by-products.

6.3.2 Assignment of selective reaction pathways to *operando* spectra

To further verify these generalised assignments (λ_{330} = selective, and λ_{360} and λ_{440} = non-selective), a variety of additional *operando* UV-Vis experiments were performed. Firstly, *operando* UV-Vis was performed on a sample of Hf-containing zeolite Beta, which in Chapter 5 showed to be able to convert glucose into fructose and mannose solely at the thermodynamic equilibrium.

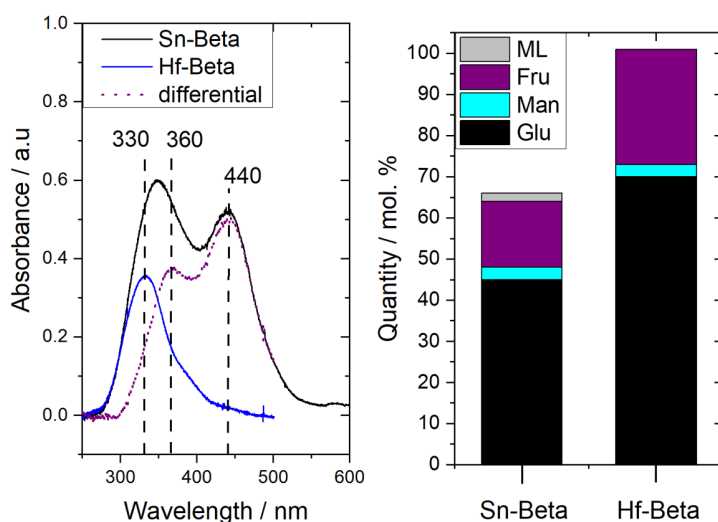


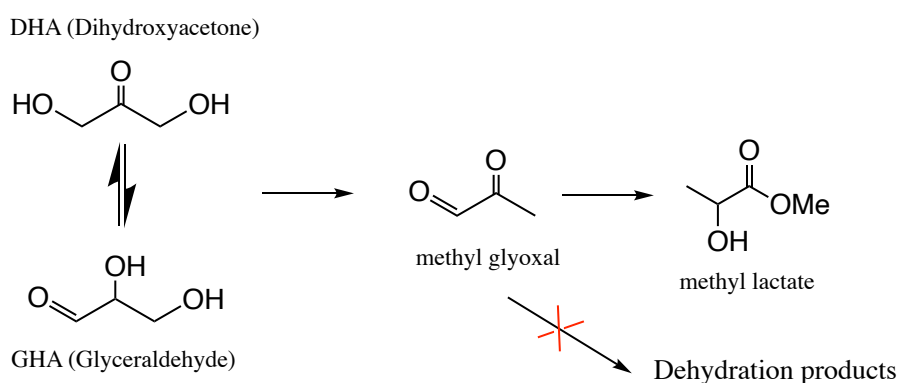
Figure 7. (Left) 2D *operando* UV-Vis spectra recorded during glucose conversion over Hf-Beta (blue line) and 10Sn-Beta_{SSI} (black line) at 110 °C. The dotted line is the differential spectrum achieved by subtraction of the Hf-Beta spectrum from that of 10Sn-Beta_{SSI}. (Right) Distribution of reactant and product species in the effluent of both reactions as monitored by chromatographic methods. Experimental conditions: (10Sn-Beta_{SSI}) 110 °C, 1 % wt. glucose in methanol, 0.750 mL min⁻¹ of flow over 100 mg of catalyst, 15 bar. (Hf-Beta) 110 °C, 1 % wt. glucose in methanol, 0.650 mL min⁻¹ of flow over 100 mg of catalyst, 15 bar

Figure 7 shows the *operando* UV-Vis spectrum generated by the catalytic conversion of glucose over Hf-Beta at 110 °C (Si/Hf molar ratio of 200), alongside that from the 10Sn-Beta_{SSI} catalysed reaction at otherwise identical conditions. Consistent with the data presented in figure 1, spectra recorded at 0.5 h on stream were used for evaluation. The catalyst was first activated in a flow of MeOH for 20 h prior to reaction. Whilst the *operando* UV-Vis spectra generated during glucose upgrading at 110 °C with Sn-Beta consisted of absorbances at λ_{440} , λ_{330} and λ_{360} , the spectra from Hf-Beta did not show any absorbance at λ_{440} (figure 7, left). Moreover, although the overall intensity of the spectrum was lower in the 330-380 nm region, this was clearly due to the absence of any a major absorbance at λ_{360} , as highlighted in the differential spectrum. Instead, a single well-defined absorbance at λ_{330} was observed.

Kinetic data generated during these experiments are shown in figure 7, right. In line with Chapter 5, the reaction effluent generated during the continuous conversion of glucose over Hf-Beta only contained detectable quantities of glucose, fructose and mannose, with no loss

of carbon balance observed. At the reaction conditions measured, the total yield of selective (GI) products when using Hf-Beta was 30 % (equation 9 in the equation appendix). In contrast, at the same conditions using 10Sn-Beta_{SSI} as catalyst, the level of conversion was much higher (55 %), but the total yield of selective products was only 24 %, confirming the poorer selectivity performance of Sn-Beta. Moreover, the carbon balance of the Sn-Beta reaction was also much lower, with approximately 35 % of the initial carbon being converted into undetected by-products. The presence of a single absorbance at λ_{330} for the catalyst exhibiting quantitative selectivity to GI and no loss in carbon balance supports assignment of the λ_{330} absorption to a selective conversion pathway, and the λ_{360} and λ_{440} bands to non-selective reaction pathways.

A key product in the reaction system is 3DG. This molecule is formed by retro-Michael dehydration of glucose, and it is reportedly a key intermediate in several selective pathways of the reaction (Scheme 1), including the retro-aldol and β -dehydration pathways. In order to aid the assignment of a signal for 3DG formation, the conversion of dihydroxyacetone (DHA) to ML was studied. During this reaction, retro-Michael dehydration of DHA to pyruvaldehyde (PVA) must occur in order for ML to be produced (Scheme 2). The reaction leading to PVA occurs *via* a pathway that is analogous to the formation of 3DG from glucose, and reportedly employs similar catalyst-substrate coordination. However, this reaction cannot lead to any further β -dehydration due to the absence of a hydroxyl-group at the C-3 atom.



Scheme 2. Scheme of reactions carried out by Sn-Beta during dihydroxyacetone conversion to methyl lactate.

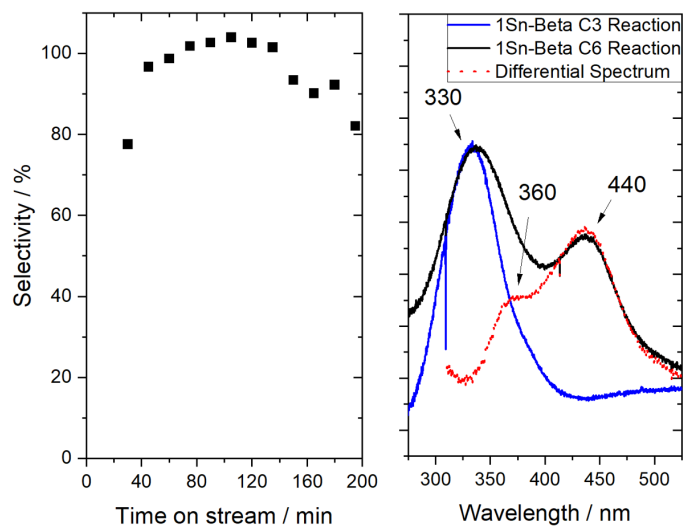


Figure 8. (Left) ML selectivity during the conversion of DHA to ML as a function of time on stream over 10Sn-Beta_{SSI} at 110 °C. (Right) 2D *operando* UV-Vis spectra generated during the conversion of DHA to ML over 10Sn-Beta_{SSI} at 110 °C, compared to the spectrum generated from the analogous reaction starting from glucose. Experimental conditions: 110 °C, 1 % wt. glucose in methanol, 0.750 mL min⁻¹ of flow over 100 mg of 1Sn-Beta_{SSI}, 15 bar.

The conversion of DHA to ML was performed at 110 °C with 1 % wt. Sn loaded Sn-Beta zeolite (henceforth 1Sn-Beta_{SSI}) as catalyst. This catalyst was chosen since previous results in literature show for this reaction a widespread use of low loading of Sn-Beta zeolite (<2 % wt. Sn).²² The absence of β -dehydration pathways results in ML formation at a selectivity close to 100 % throughout the reaction period (figure 8). Spectra generated by *operando* UV-Vis analysis of this reaction clearly demonstrate that the reaction is accompanied by a single absorption centred at λ_{330} , with very minimal absorption evident at λ_{360} and λ_{440} . To further probe these signals, the spectrum generated at 0.5 h time on stream during the conversion of DHA to ML over 1Sn-Beta_{SSI} was compared to the spectrum generated at the same time on stream during the glucose conversion reaction at otherwise identical conditions. The red line in the graph shows the differential graph between these two spectra, achieved by subtracting the DHA spectrum from that achieved from the glucose upgrading reaction. The differential spectrum clearly supports the observation that the C₃ reaction primarily exhibited an intense absorption at λ_{330} , whereas the C₆ reaction shows a dominant signal at λ_{330} , and significant absorptions at λ_{360} and λ_{430} . These findings support the hypothesis that the retro-Michael dehydration reaction intermediates are embedded beneath λ_{330} , allowing the λ_{330} band to be assigned to the coordination of Sn with carbonyl and hydroxyl group of the substrate molecule. It is noted that whilst the spectrum of the DHA reaction still shows a slight broadening at 360 nm, this most likely arises from the formation of traces of hexoses due to aldol condensation of two molecules of C₃ to hexose, which can then be transformed by the classic glycolytic pathways shown in scheme 1.

To further aid the assignment of the optical features related to 3DG, and later retro-aldol products, the effect of alkali on the reaction system was also investigated. It is widely reported in the literature that adding alkali salts to the reaction feed dramatically increases the selectivity of the glucose conversion reaction towards RA product formation.^{1,8} Accordingly, the impact of alkali addition was evaluated for 1Sn-Beta_{SSI} by recording the *operando* spectra of this catalyst in the absence and in the presence of alkali in the reaction feed. KCl (4 mg L⁻¹) was chosen as alkali additive because its wide range of effective concentration permits easier utilisation in continuous flow, and its limited basicity does not strongly impact glycoside formation, which could aid assignment of the non-selective bands indirectly.²³ This is in contrast to K₂CO₃ which strongly suppresses the alkylation pathway due to its basicity.²² The reaction was performed at high temperature (150 °C), since the effect of alkali is more pronounced during the formation of RA products formed during the high temperature selective pathway.^{1,9}

Figure 9 presents the *operando* UV-Vis spectra following the effect of alkali (KCl) during glucose conversion over 1Sn-Beta_{SSI}, and the kinetic data achieved from in both the presence and absence of alkali. Interestingly, in the presence of alkali, the system shows a much sharper λ_{330} absorption, a notable decrease in intensity for λ_{360} , and a very minor decrease in intensity for λ_{440} . The differential spectrum (red) of the two stages of reaction clarifies how the presence of alkali salts impacts the optical properties of the system, particularly the intensity of λ_{360} . The limited change in absorbance at 440 nm could be an early indication that this particular non-selective absorbance arises from glycoside formation, since the limited basicity of KCl has been shown to leave the alkylation pathway largely unaffected.¹⁹

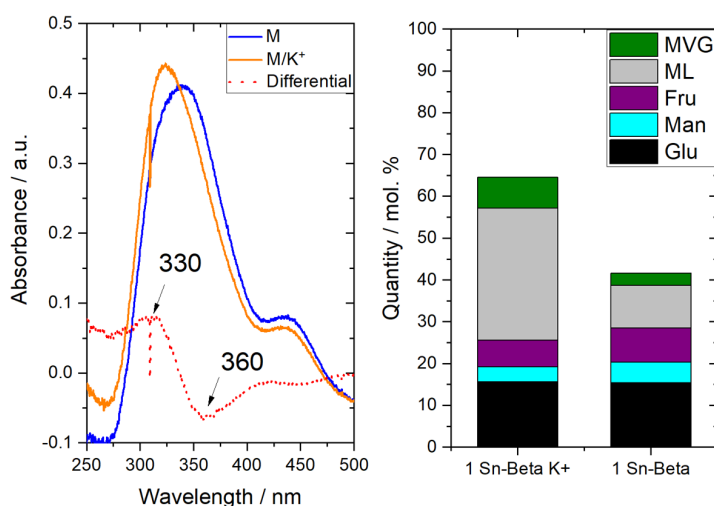
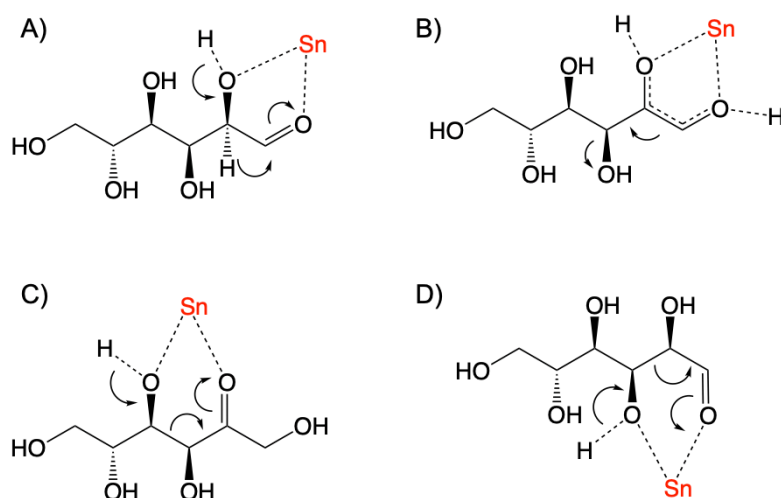


Figure 9. (Left) *Operando* UV-Vis spectra generated by the conversion of glucose by 1Sn-Beta_{SSI} in presence (orange line) and absence (blue line) of alkali salts at 150 °C (blue line). The red line shows the differential spectrum of these two spectra. (Right) Product distribution related to the *operando* spectra in of 1Sn-Beta in the presence and in the absence of alkali ions. Experimental conditions: 150 °C, 1 % wt. glucose in methanol (KCl, 4 mg L⁻¹), 0.750 mL min⁻¹ of flow over 100 mg of 1Sn-Beta_{SSI}, 15 bar.

When evaluating the impact of alkali on the kinetic performance of Sn-Beta (Figure 9, Right), the most evident impact is the substantial increase to ML yield from 12 to 40 % upon inclusion of alkali. As yields to GI products and the quantity of glucose converted are largely unchanged, the carbon balance increased dramatically upon addition of alkali, suggesting that much lower quantities of by-products were formed in the presence of alkali. The increase in the yield of retro-aldol products is accompanied by a clear increase in absorbance at λ_{330} . This shows that the optical features associated with retro-aldol formation are also embedded within the λ_{330} region. Moreover, the significant increase in carbon balance is also accompanied by a decrease in absorbance, primarily at λ_{360} . This further indicates that the 360 nm region is associated with non-selective by-products. From the data presented in this section, it is apparent that both the RA pathway and the GI pathway are characterised by an absorbance at λ_{330} . Although each pathway would likely require the coordination of different carbonyl and hydroxyl groups (scheme 3), this observation can be taken as evidence that both selective pathways proceed *via* similar catalyst-substrate intermediates, which has previously been proposed in the literature but has not previously been supported experimentally.²⁴⁻²⁶



Scheme 3. Reaction intermediates embedded beneath λ_{330} A) H-transfer intermediate for glucose isomerisation. B) Retro-Michael dehydration intermediate for 3DG from glucose. C) Retro-aldol cleavage of ketose to C3 sugars. D) Retro-aldol cleavage of hexoses to C₂ and C₄ sugars.

6.3.3. Assignment of non-selective pathways (λ_{440} and λ_{360}) to *operando* spectra

Correlation of spectroscopic and reactivity data strongly indicate that the λ_{330} feature relates to the selective conversion of glucose, either through isomerisation or retro-aldol fragmentation, whereas absorbances the λ_{360} and λ_{440} features arise from non-selective reaction pathways. These non-selective pathways include pathway derived from β -dehydration and alkylation, as evidenced by chromatographic analysis and NMR

spectroscopy. To better understand the relevance of the λ_{360} and λ_{440} features, additional correlations were sought, with the aim of assigning both features to a particular non-selective reaction pathway.

As demonstrated in figure 1, the two non-selective bands exhibit very different dependence on temperature. Specifically, whereas the λ_{440} feature was clearly generated at very low temperature but increased only marginally with reaction temperature, the λ_{360} feature was absent at low temperature but became dominant at higher temperature. Recently, Tolborg *et al.*¹ reported a study focused upon the prevalence of by-products during the catalytic conversion of glucose over Sn-Beta between temperatures of 90-180 °C. During this investigation, the authors revealed that by-products in the low temperature regime mainly consisted of glycosidic compounds such as methyl glucopyranoside (Me-Glu) and methyl fructofuranoside (Me-Fru). Upon raising the reaction temperature beyond 110 °C, contributions from glycosidic compounds decreased substantially, and by-products from β -dehydration and furanic production came to dominate. Graphic representation of the published data (figure 10) shows how the behaviour of these two classes of compounds differed markedly with temperature, with glycosidic products decreasing in abundance at increasing temperature, whereas β -dehydration products increased over the temperature range. Based on this behaviour, it can be hypothesised that the low temperature λ_{440} feature arises from glycosidic pathways, whereas the high temperature absorbance at λ_{360} arises from β -dehydration. Support of this preliminary assignment is gained from the observation that the addition of KCl (figure 9) decreased the magnitude of the λ_{360} feature to a much greater extent than λ_{440} , since it has been reported that KCl does not overly impact the glycosidic reaction pathway unlike more basic alkali additives.²²

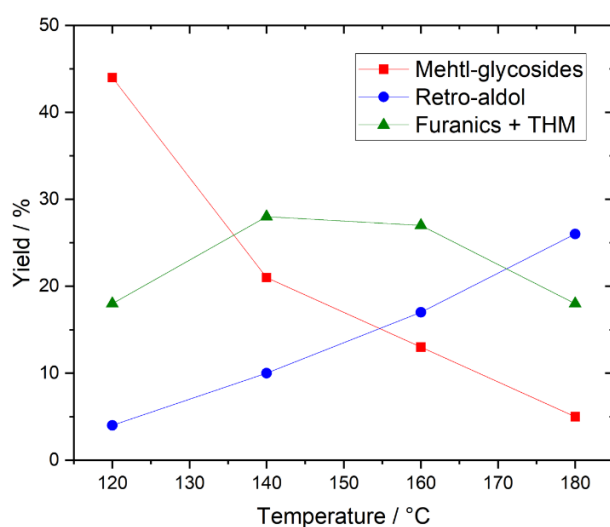


Figure 10. Graphic representation of the data shown by Tolborg *et al.*¹ the yields of methyl-glycosides (black), β -dehydration products (THM and furanics in blue) and retro-aldol products (MVG and ML in red) are plotted against the operative temperature for glucose upgrading by Sn-Beta zeolite.

To gain experimental support of this hypothesis, two additional catalytic samples were evaluated by *operando* UV-Vis. These two samples included Sn-Beta samples containing only 1 % wt. Sn, but which were prepared by different preparative methods (post-synthetic SSI and classical hydrothermal synthesis). These samples are henceforth denoted 1Sn-Beta_{SSI} and 1Sn-Beta_{HDT}, respectively. The basic characterisation of these samples (XRD, porosimetry, ¹¹⁹Sn MAS NMR) was recently reported in detail.⁶ In order to obtain maximum insight from these experiments, glucose conversion was performed at 130 °C, in order to stimulate generation of the λ_{360} feature, which only weakly contributed to the spectra at lower temperatures (figure 1).

Figure 11 Left presents the *operando* UV-Vis spectra of glucose upgrading carried out at 130 °C by the different samples of Sn-Beta, alongside the kinetic data obtained from each experiment. As can be seen, the spectrum obtained with 1Sn-Beta_{SSI} was consistent with that obtained for 10Sn-Beta_{SSI} at the same temperature. A strong absorbance in the 330-380 nm region was observed, alongside a somewhat less intense absorbance at λ_{440} . In contrast, the spectrum of 1Sn-Beta_{HDT} exhibited negligible absorbance related to λ_{440} , but exhibited much more intense absorbances in the 330-380 nm region. Along with increased absorbance in the 330-380 nm region, the maxima was also clearly shifted to λ_{330} .

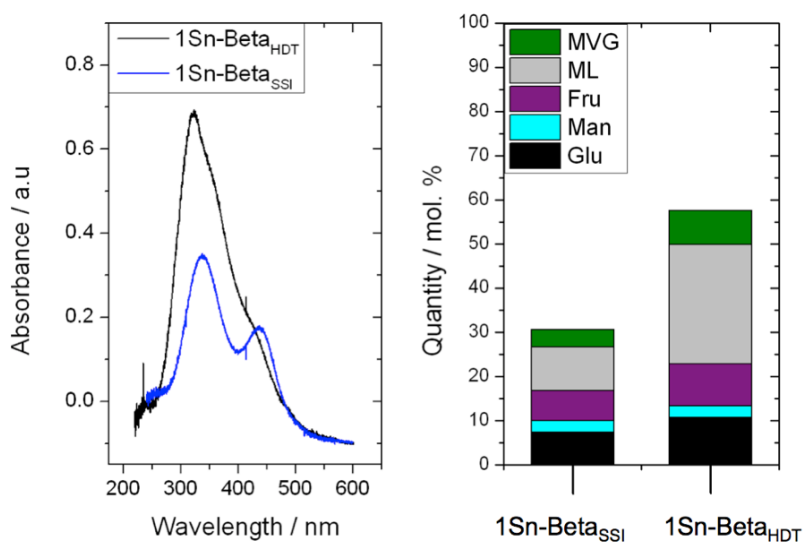


Figure 11. (Left) 2D spectra for *operando* glucose upgrading gathered for 30 min at 130 °C. the reaction was carried out by 1Sn-Beta_{SSI} (red line) and 1Sn-Beta_{HDT} (dark red dotted line). (Right) Composition of post-reaction materials produced by the catalysts characterized by 2D *operando* UV-Vis on the left. Experimental conditions: 130 °C, 1 % wt. glucose in methanol (KCl, 4 mg L⁻¹), 0.5 mL min⁻¹ of flow over 100 mg of 1Sn-Beta_{SSI}, 15 bar.

The product yields related to these two reactions and *operando* spectra are displayed in figure 11, Right. Whilst both experiments exhibited comparable levels of glucose conversion (ca. 90 %), much higher yields of selective products were obtained over 1Sn-Beta_{HDT} (45 %) than over 1Sn-Beta_{SSI} (22 %). This change in selectivity confirms the better performance

of the hydrothermal material for conversion of glucose, in line with previous kinetic studies. In the context of this study, the higher yield of selective products obtained with 1Sn-Beta_{HDT} correlates with its increased absorbance at 1Sn- to λ_{330} , and further supports assignment of the λ_{330} feature to the selective reaction pathways. However, substantial quantities of undetected by-products were clearly produced in both cases, as evidenced by the low carbon balances observed (30 % and 70 %, or 1Sn-Beta_{SSI} and 1Sn-Beta_{HDT}, respectively). Accordingly, the effluents of these reactions were also analysed by multiplicity edited ¹H-¹³C HSQC 2D NMR (figure 12).

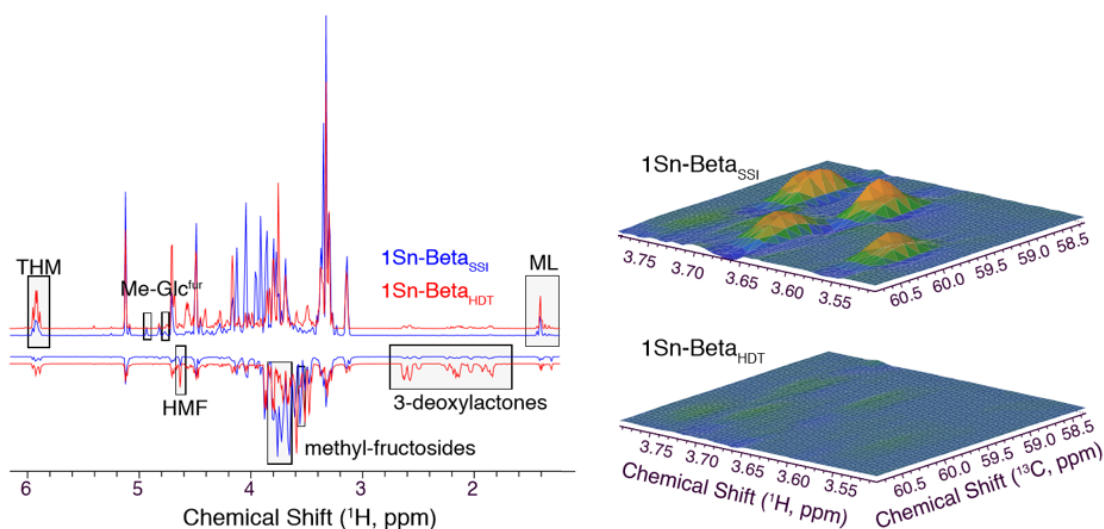


Figure 12. (left) Positive (CH and CH₃ groups) and negative (CH₂ groups) projections from edited 2D ¹H-¹³C HSQC NMR spectra recorded on the effluent of the *operando* UV-Vis glucose upgrading carried out by different preparations of Sn-Beta. (right) Spectral region containing the methyl-fructoside signal.

These analyses were provided by our collaborator Dr. S. Meier, at Denmark Technical University (DTU), DK

Projections for the ¹H-¹³C HSQC 2D spectra are shown in figure 12 left, where positive signals derive from carbons carrying one or three hydrogens, while negative intensities are derived for CH₂ groups. Signal related to Me-Glu and Me-Fru are highlighted at 4.7-4.9 ppm and at 3.6 ppm, the latter of which are shown in figure 12 right. It is clear that whilst 1Sn-Beta_{SSI} produces substantial quantities of Me-Glu and Me-Fru at these reaction conditions, 1Sn-Beta_{HDT} is not as effective in producing alkyl-glycosides. In contrast, the NMR spectra reveal that 1Sn-Beta_{HDT} yielded much larger quantities of lactones (2-2.5 ppm), and was much more effective at producing furanics and THM, as shown in figure 12 left (signals at 5.9 ppm and 4.6 ppm). Among the non-selective absorbances (λ_{360} , λ_{440}), 1Sn-Beta_{HDT} exhibited much higher intensity in the λ_{360} region, whereas 1Sn-Beta_{SSI} exhibit much larger absorption at λ_{440} . Based on these observations and the NMR experiments described above, absorption at λ_{360} can tentatively be attributed to by-products deriving from 3DG,

including β -dehydration products (THM, furanics) and lactones, whereas absorptions at λ_{440} can be assigned to alkyl-glycoside products.

Although each correlation is empirical in nature, the balance of evidence achieved from these studies (temperature dependence of the two non-selective absorbances, catalyst preparation, alkali) strongly indicates that λ_{440} arises from the (rapid/low temperature) formation of alkyl glycosides, whereas λ_{360} is related to β -dehydration pathways, resulting in the formation of THM and furanics.

6.3.4 Discussion on the nature of the UV-Vis absorptions

Having completed the assignments of the UV-Vis bands (λ_{330} = GI and RA , and λ_{360} = β -dehydration and λ_{440} = alkylation of monosaccharides), it is clear that each UV-Vis absorption is related to different transformation which are radically different between each other (scheme 1). As shown in figure 11, different materials have different tendency to promote a certain reaction pathway, therefore something relating the nature of the catalyst is responsible for channelling the reaction towards a determined path. To understand which particular property was responsible for this the effect of water was employed as a mean to probe the nature of each glucose-Sn interaction monitored by continuous *operando* UV-Vis glucose upgrading.

In Chapter 2 it has already been explained how the presence of water in the system improve the stability of the material over glucose isomerisation at 110 °C and glucose upgrading at 160 °C (Chapter 4). This effect is due to the continuous hydration that water is maintaining in the active site of Sn-Beta, as reported this continuous hydration avoid the condensation or alkoxylation of the open Sn site, such phenomenon is particularly pronounced in the first 20 h of the reaction.^{7,9} Therefore in figure 13 are reported the kinetic data gathered by *operando* UV-Vis glucose upgrading at 110 °C carried out by Sn-Beta in pure methanol and in methanol:water (90:10). This section of the project will exploit 10Sn-Beta_{SSI} as catalyst since this material was thoroughly used in Chapter 2 to understand the stabilising effect of water. As expected, the reaction carried out in pure methanol deactivates fast leading to a 50 % loss in activity in the first 5 h, whereas the catalyst in the methanol: water system is highly stable and experiences less than 10 % deactivation in the first 60 h.

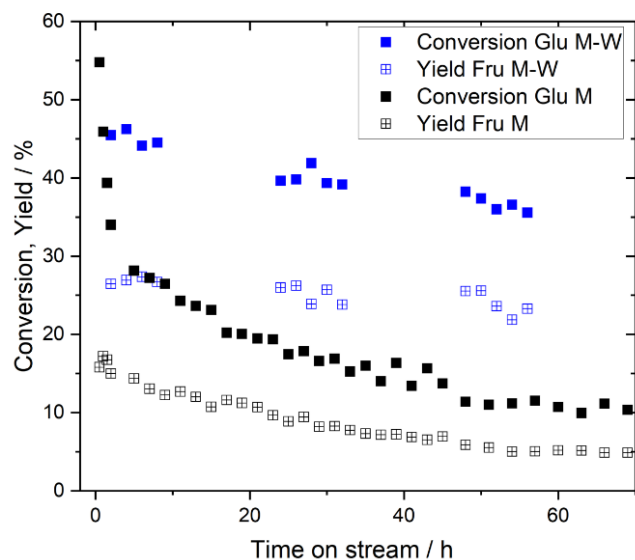


Figure 13. kinetic data for glucose isomerisation carried out in methanol (black symbols) and in methanol:water (90:10) (blue symbols) at 110 °C by 10Sn-Beta zeolite. Glucose conversion and fructose yield are plotted as a function of time on stream. Experimental conditions: 1 % wt glucose in methanol (or methanol:water 90:10, % wt.), 0.750 mL min⁻¹ of flow over 100 mg of 10 Sn-Beta_{SSI}, 15 bar.

The 2D *operando* UV-Vis spectra at 0.5 h of time on stream are gathered for these two systems in figure 14. Interestingly both systems have initial λ_{440} at similar intensity, whereas λ_{340} (that is formed by λ_{360} and λ_{330}) is roughly 20 % more intense when the reaction is carried out in presence of water. This might justify the pronounced difference in initial fructose yield for these systems. The lower intensity of λ_{340} in the pure methanol reaction can be in part explained by the Sn-methanol interaction which is already present at λ_{270} .

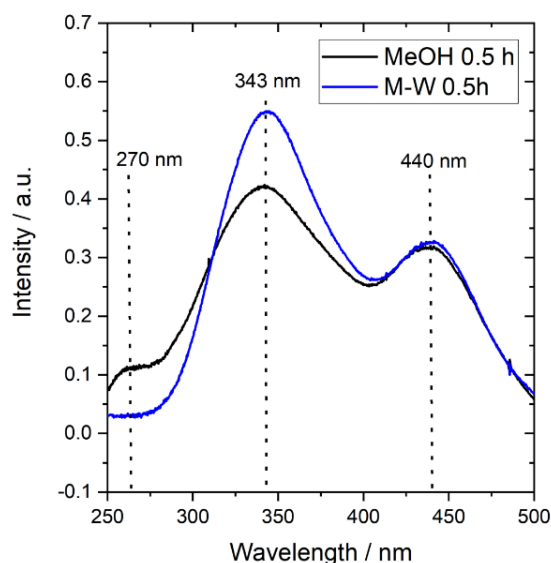


Figure 14. 2D *operando* UV-Vis glucose upgrading spectra gathered at 110 °C with 10Sn-Beta in (black) methanol and (blue) methanol:water (90:10). Experimental conditions: 1 % wt. glucose in methanol (or methanol:water 90:10, % wt.), 0.750 mL min⁻¹ of flow over 100 mg of 10 Sn-Beta_{SSI}, 15 bar.

To understand how the water was affecting the evolution of these absorptions, the spectroscopic data gathered from this system were compared by plotting the relative intensity of each specie against the time on stream of the reaction. As can be seen in figure 15 dramatically different deactivation was detected between the two systems. In figure 15 left the reaction carried out in methanol shows an important deactivation of λ_{440} which intensity at the end of the reaction is only 30 % of the initial. The λ_{360} band shows an important deactivation losing 40 % of its initial intensity, the λ_{330} band is the less affected by deactivation losing only 25-30 % of its initial intensity. Interestingly this band shows an induction in the first 2 h in line with the yield of fructose in figure 13 for the related system. When the reaction is carried out in methanol:water (90:10) the bands shows a slower deactivation, which is in agreement with the kinetic in figure 13, but interestingly the trend of deactivation is similar for all the absorptions. λ_{360} and λ_{440} show exactly same trend of deactivation losing only 30% of their intensity in 45 h. λ_{330} instead loses 20 % of its intensity in 45 h.

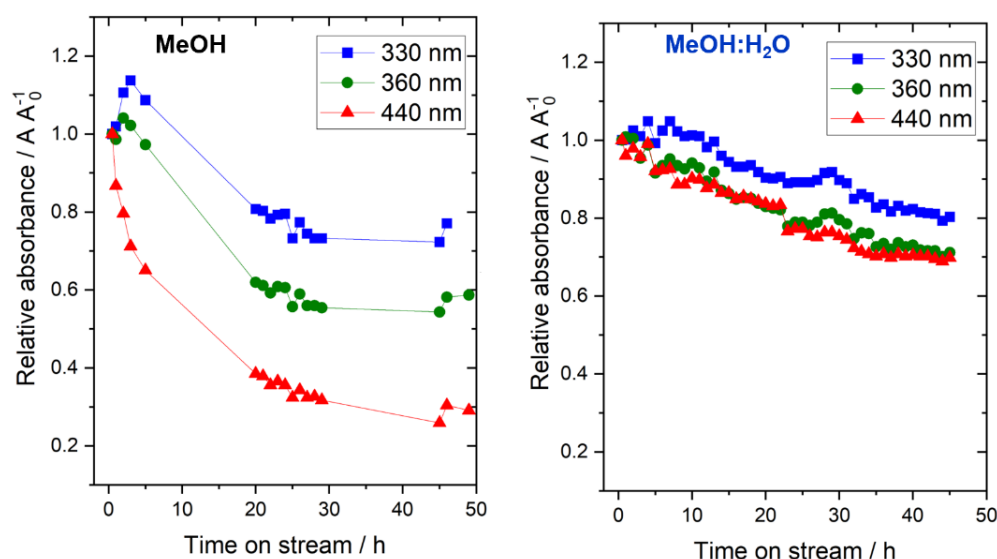


Figure 15. Relative absorbance of each *operando* UV-Vis band plotted against time on stream for 50 h of continuous glucose upgrading carried out by 10Sn-Beta at 110 °C in (left) methanol and (right) methanol:water (90:10). Experimental conditions: 1 % wt. glucose in methanol (or methanol:water 90:10, wt.), 0.750 mL min⁻¹ of flow over 100 mg of 10 Sn-Beta_{SS1}, 15 bar.

These results show clearly how λ_{360} and λ_{440} undergo a softer deactivation when traces of water are present in the reaction media, this strictly related these bands to the presence of protons in the material, which (in agreement with Chapter 2) are maintained by the presence of water in the reaction media.

A further proof for this correlation is presented by the alkali experiment (figure 9), the presence of alkali in fact is known to be responsible for the proton exchanges with alkali cations in the near vicinity of the Sn-active site.^{8,27} This experiment shows clearly how λ_{330}

is not affected by this exchange of protons, whereas λ_{360} immediately loses intensity incrementing in this way the selectivity of the system towards ML switching of non-selective pathways as THM and furanic productions. This results clearly show how the proton presence in Sn-Beta zeolite is impacting the stability and the selectivity of the catalyst. Furthermore, is interesting to note how the two absorptions strongly related to the presence of proton in the system (λ_{360} and λ_{440}) are responsible for two different pathways and have different response to different perturbation and synthesis preparations. This suggests the presence of different typologies of “active” proton in the material, this is already been shown from different NMR studies,^{28,29} but further characterisation of these protonic sites is beyond the scope of this work.

6.3.5 Use of operando UV-Vis to probe mechanistic phenomena

Having assigned the various optical signals for intermediates that are generated during the continuous conversion of glucose over Sn-Beta, the efficacy of the method to provide new information on various kinetic phenomena of the system was evaluated. In particular, the utility of *operando* UV-Vis spectroscopy to better explain the deactivation processes occurring during continuous operation was explored.

Operando UV-Vis was employed to monitor the continuous isomerisation of glucose to fructose over 10Sn-Beta_{SSI} in methanol at 110 °C during a 50 h period of operation (figure 16). The kinetic data generated during the *operando* reaction shows that the system was characterized by an initially steep rate of deactivation over the first 5-10 h on stream, during which period conversion decreased from 55 % to approximately 30 %. Over longer periods of operation, conversion continued to decrease albeit at a slower rate, eventually reaching a level of 15 % after 50 h on stream. Although full selectivity towards fructose was not reached even at low rates of conversion, it is notable that the selectivity of the reaction was much lower at the initial stages of operation. Analysis of the time on stream data by the Levenspiel function revealed that deactivation occurred in three distinct stages over 10Sn-Beta_{SSI} at these operational conditions.³⁰ These stages were characterised by deactivation rate constants of 0.17 (stage 1, 0-7 h), 0.03 (stage 2, 7-25 h) and 0.01 (stage 3, 25-50 h) $X\% \cdot h^{-1}$ (equation 5 in the equation appendix).

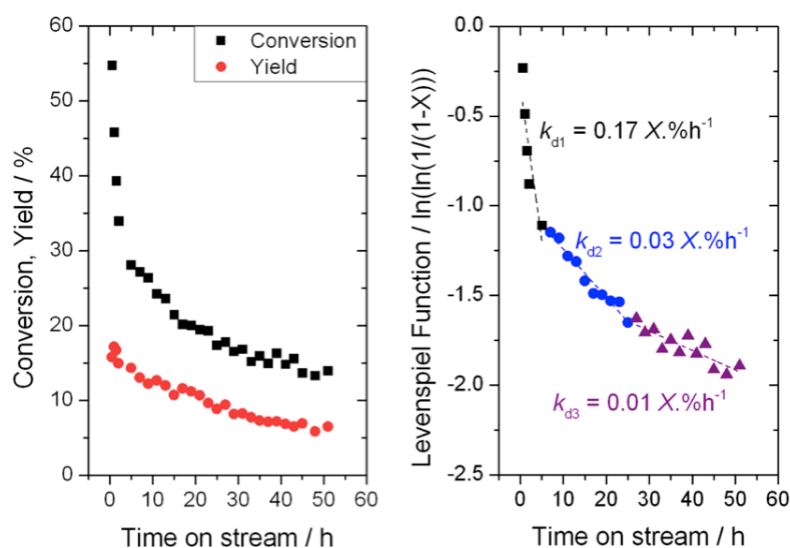


Figure 16. Kinetic data for glucose conversion over 10Sn-Beta_{SSI} at 110 °C in methanol. (Left) Glucose conversion and fructose yield are plotted as a function of time on stream. (Right) Levenspiel function, demonstrating the deactivation constant of the reaction in different stages of operation. Experimental conditions: 1 % wt. glucose in methanol, 0.750 mL min⁻¹ of flow over 100 mg of 10 Sn-Beta_{SSI}, 15 bar.

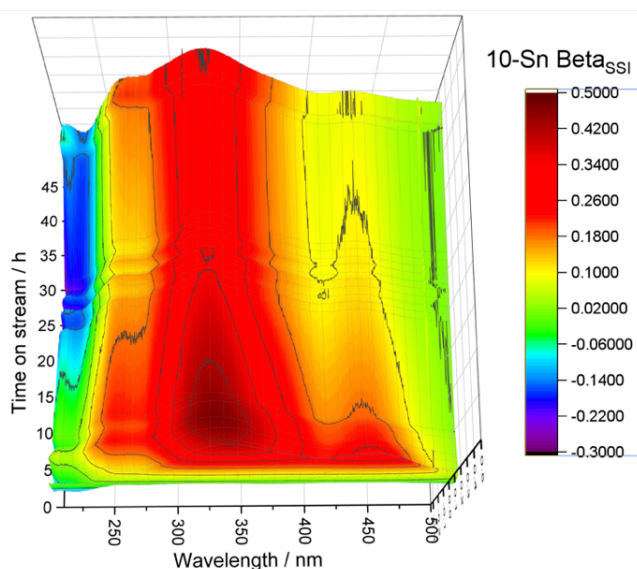


Figure 17. *Operando* UV-Vis spectrum for glucose upgrading over 10Sn-Beta_{SSI} at 110 °C in methanol. Experimental conditions: 1 % wt. glucose in methanol, 110 °C, 0.750 mL min⁻¹ of flow over 100 mg of 10 Sn-Beta_{SSI}, 15 bar.

The *operando* UV-Vis spectra generated throughout the operational period are shown in figure 17 in differential mode, in which the spectrum recorded prior to introducing glucose into the feed (time = 0 h), is subtracted from each spectrum. Warm colours (red) depict increased absorption relative to the fresh catalyst in methanol, whereas cold colours (blue) represent a decrease in absorption relative to the fresh catalyst in methanol.

Based on the functional changes of the material as detailed above, correlations of the *operando* UV-Vis spectra to the kinetic data were undertaken. Over the first hours on

stream, conversion decreased rapidly ($k_{d1} = 0.17 \text{ X}\%.\text{h}^{-1}$) from a maximum of 55 % at 0.5 h to 28 % at 5 h on stream and the fructose yield also decreased, albeit more slowly, from 18 % to 15 %. The most evident change in the *operando* UV-Vis spectra over time was the dramatic decrease in intensity of the λ_{440} feature (figure 18, k_{d1}). Taken together, the rapid decrease in glucose conversion, coupled only to a minor decrease in yield but a major decrease in absorbance at λ_{440} can be ascribed to rapid deactivation of the competitive alkylation pathway, in which glucose is converted to undesirable alkylated products, such as Me-Glu, which sequesters glucose into a non-reactive form.

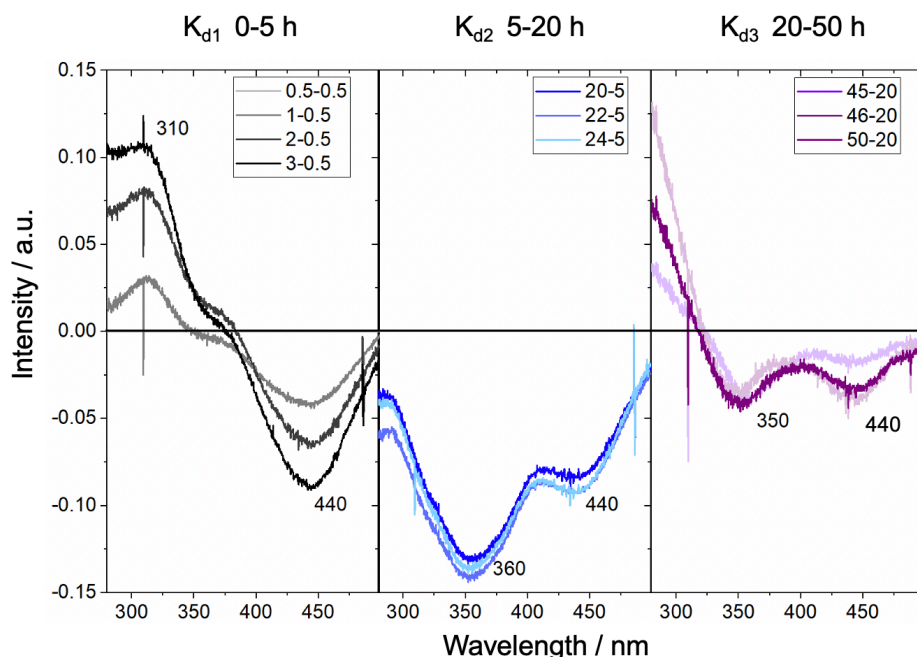


Figure 18. Differential spectra of the 2D *operando* UV-Vis glucose upgrading carried out at 110 °C in methanol by 10 Sn-Beta zeolite at different interval of time of stream (K_{d1} : 0.5 h to 5h) (K_{d2} : 5 h to 20 h) (K_{d3} : 20 h onwards). Experimental conditions: 1 % wt. glucose in methanol, 110 °C, 0.750 mL min^{-1} of flow over 100 mg of 10 Sn-Beta_{SS1}, 15 bar.

Over the following 20 h on stream (from 5 h to 25 h), conversion continued to decrease, albeit at a slower rate ($k_{d2} = 0.03 \text{ X}\%.\text{h}^{-1}$). During this period, the selectivity of the catalyst increased continually, since conversion decreased at a faster rate than yield. This observation indicates that an additional non-selective pathway was primarily deactivating in this regime. Over this time frame, a clear narrowing of the absorbance in the 330-380 nm region was observed, due to a loss of intensity at λ_{360} (Figure 18, k_{d2}). Increased selectivity of the catalyst alongside the decrease in intensity at λ_{360} is evidence that deactivation of the β -dehydration pathways occurred during this period, resulting in decreased formation of furanics and dehydration products, such as THM.

Over the remaining 25 h on stream (from 25-50 h), limited changes to the visible region were observed at 330 nm, suggesting that the selective pathway occurring at this temperature (GI) remains relatively unperturbed over the final period of operation. This

interpretation is supported by the relatively steady time on stream data obtained during this period, during which conversion and yield decreased minimally, and reaction selectivity was unaffected. However, at this stage, a (negative) high-energy signal at 220 nm clearly increased in magnitude. As reported in Chapter 2, this signal relates to deactivation of the catalyst through interaction with the solvent, which is the primary mechanism of deactivation for the selective pathways of the process at these operational conditions. Hence, relatively slow rate deactivation of the selective pathway of the reaction occurs in this time frame. Taken together, *operando* UV-Vis analysis demonstrates that the deactivation of Sn-Beta during glucose conversion is non-trivial and non-homogeneous, and is characterised by several events occurring at different periods of time, each of which impact the activity and selectivity of the system to different degrees.

In addition to providing mechanistic insight, the findings generated by *operando* UV-Vis indicate that the catalyst becomes more selective during operation as a consequence of more rapid deactivation of the non-selective reaction pathways associated with alkylation (λ_{440}) and β -dehydration (λ_{360}). To verify if this was the case, a final kinetic experiment was performed to evaluate the selectivity of the catalyst during different stages of continuous operation (figure 15). In this experiment, glucose conversion was performed over 10Sn-Beta_{SSI} at 150 °C firstly at a flow rate of 2 mL min⁻¹. Consistent with the experiment at 110 °C (figure 19), rapid deactivation occurred over the first 20 h of operation, with conversion decreasing from 80 % to 22 %. Over this time frame, relatively low quantities of selective products were observed in the effluent.

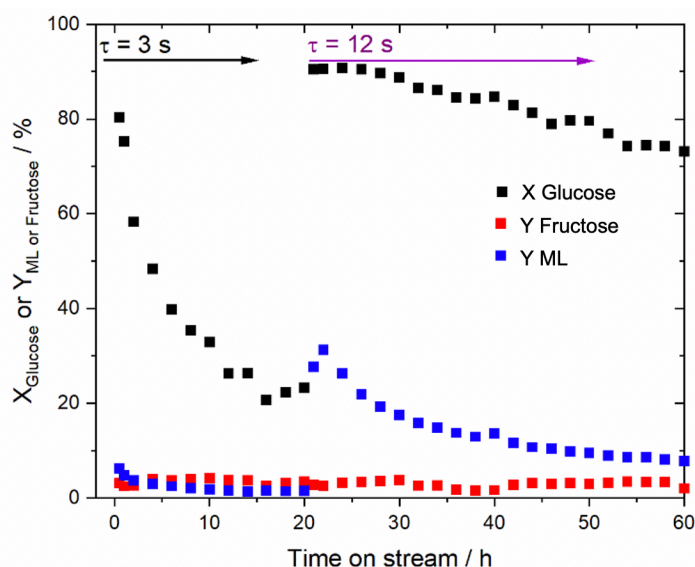


Figure 19. Kinetic data for glucose conversion over 10Sn-Beta_{SSI} at 150 °C in methanol at two different flow rate regimes. Conversion (X) of glucose and yield at the time t (Y) of the products (Fructose and ML) is plotted against time on stream. Experimental conditions: 1 % wt. glucose in methanol, 150 °C, 2 mL min⁻¹ of flow (0.5 mL min⁻¹ after 20 h) over 100 mg of 10 Sn-Beta_{SSI}, 20 bar.

After 20 h, the flow rate of the feed was decreased from 2.0 to 0.5 mL min⁻¹, thereby increasing the contact time of the reaction from 3s to 12s (equation 2 in the equation appendix), and allowing glucose conversion to be raised back to the initial level of conversion. In doing so, it is clear that the catalytic process was substantially more selective after 20 h on stream than during the earlier stages of reaction. The change in selectivity supports the observations made by *operando* UV-Vis, and confirms that the catalyst becomes intrinsically more selective during continuous operation due to more rapid deactivation of the non-selective reaction pathways attributed to alkylation and β -dehydration.

6.4 Conclusion

This study follows the catalytic conversion of glucose over the Lewis acidic silicates, Sn-Beta and Hf-Beta, at operational conditions (<170 °C, <25bar) in a continuous flow reactor equipped with *operando* UV-Vis spectroscopy. Three transient absorption features related to the activation and conversion of glucose at various conditions were detected, at 330 nm, 360 nm and 440 nm. Spectroscopic (high-field ¹H-¹³C HSQC NMR) and kinetic cross-experiments allow each of these Sn-glucose interactions to be assigned to a particular class of selective (330 nm) and non-selective (360, 440 nm) products. The non-selective absorptions were found to arise from β -dehydration products of glucose and alkylation products respectively. All non-selective pathways, including glucose isomerisation and retro-aldol products, were present at 330 nm, confirming that a common catalyst-substrate interaction is responsible for all of these pathways.

Based on the findings of *operando* UV-Vis, elements of the deactivation of stannosilicate catalysts during continuous operation were probed. These studies demonstrated that deactivation during glucose conversion is non-uniform, with different reaction pathways losing activity at different rates. In particular, the non-selective reaction pathways associated with alkylation (440 nm) deactivated fastest, followed by deactivation of the β -dehydration pathways (360 nm). Accordingly, the catalyst was found to increase in selectivity following partial deactivation, allowing its performance in later stages of the reaction cycle to be increased substantially. More broadly, the findings presented in this manuscript provide additional mechanistic insight into the glucose conversion process over Lewis acidic zeolites, and also provide a new way for researchers to characterise such catalysts for biomass conversion without requiring probe molecules.

6.5 Reference

- (1) Tolborg, S.; Meier, S.; Sádaba, I.; Elliot, S. G.; Kristensen, S. K.; Saravanamurugan, S.; Riisager, A.; Fristrup, P.; Skrydstrup, T.; Taarning, E. Tin-Containing Silicates: Identification of a Glycolytic Pathway via 3-Deoxyglucosone. *Green Chem.* **2016**, *18* (11), 3360–3369.
- (2) Ennaert, T.; Van Aelst, J.; Dijkmans, J.; De Clercq, R.; Schutyser, W.; Dusselier, M.; Verboekend, D.; Sels, B. F. Potential and Challenges of Zeolite Chemistry in the Catalytic Conversion of Biomass. *Chem. Soc. Rev.* **2016**, *45* (3), 584–611.
- (3) Hammond, C.; Padovan, D.; Al-Nayili, A.; Wells, P. P.; Gibson, E. K.; Dimitratos, N. Identification of Active and Spectator Sn Sites in Sn- β Following Solid-State Stannation, and Consequences for Lewis Acid Catalysis. *ChemCatChem* **2015**, *7* (20), 3322–3331.
- (4) Dijkmans, J.; Gabriels, D.; Dusselier, M.; de Clippel, F.; Vanelderen, P.; Houthoofd, K.; Malfliet, A.; Pontikes, Y.; Sels, B. F. Productive Sugar Isomerization with Highly Active Sn in Dealuminated Beta Zeolites. *Green Chem.* **2013**, *15*, 2777–2785.
- (5) Li, P.; Liu, G.; Wu, H.; Liu, Y.; Jiang, J. G.; Wu, P. Postsynthesis and Selective Oxidation Properties of Nanosized Sn-Beta Zeolite. *J. Phys. Chem. C* **2011**, *115* (9), 3663–3670.
- (6) Botti, L.; Navar, R.; Tolborg, S.; Martinez-Espin, J. S.; Padovan, D.; Taarning, E.; Hammond, C. Influence of Composition and Preparation Method on the Continuous Performance of Sn-Beta for Glucose-Fructose Isomerisation. *Top. Catal.* **2019**, *62* (17–20), 1178–1191.
- (7) Wolf, P.; Liao, W. C.; Ong, T. C.; Valla, M.; Harris, J. W.; Gounder, R.; van der Graaff, W. N. P.; Pidko, E. A.; Hensen, E. J. M.; Ferrini, P.; et al. Identifying Sn Site Heterogeneities Prevalent Among Sn-Beta Zeolites. *Helv. Chim. Acta* **2016**, *99* (12), 916–927.
- (8) Padovan, D.; Tolborg, S.; Botti, L.; Taarning, E.; Sádaba, I.; Hammond, C. Overcoming Catalyst Deactivation during the Continuous Conversion of Sugars to Chemicals: Maximising the Performance of Sn-Beta with a Little Drop of Water. *React. Chem. Eng.* **2018**, *3* (2), 155–163.
- (9) Tolborg, S.; Sádaba, I.; Osmundsen, C. M.; Fristrup, P.; Holm, M. S.; Taarning, E. Tin-Containing Silicates: Alkali Salts Improve Methyl Lactate Yield from Sugars. **2015**, No. MI, 613–617.
- (10) Padovan, D.; Botti, L.; Hammond, C. Active Site Hydration Governs the Stability of Sn-Beta during Continuous Glucose Conversion. *ACS Catal.* **2018**, *8*, 7131–7140.
- (11) Yakimov, A. V.; Kolyagin, Y. G.; Tolborg, S.; Vennestrøm, P. N. R.; Ivanova, I. I. ^{119}Sn MAS NMR Study of the Interaction of Probe Molecules with Sn-BEA: The Origin of Penta- and Hexacoordinated Tin Formation. *J. Phys. Chem. C* **2016**, *120* (49), 28083–28092.
- (12) Wolf, P.; Valla, M.; Núñez-Zarur, F.; Comas-Vives, A.; Rossini, A. J.; Firth, C.; Kallas, H.; Lesage, A.; Emsley, L.; Copéret, C.; et al. Correlating Synthetic Methods, Morphology, Atomic-Level Structure, and Catalytic Activity of Sn- β Catalysts. *ACS Catal.* **2016**, *6* (7), 4047–4063.
- (13) Kolyagin, Y. G.; Yakimov, A. V.; Tolborg, S.; Vennestrøm, P. N. R.; Ivanova, I. I. Direct Observation of Tin in Different T-Sites of Sn-BEA by One- and Two-Dimensional ^{119}Sn MAS NMR Spectroscopy. *J. Phys. Chem. Lett.* **2018**, *9* (13), 3738–3743.
- (14) Kolyagin, Y. G.; Yakimov, A. V.; Tolborg, S.; Vennestrøm, P. N. R.; Ivanova, I. I. Application Of ^{119}Sn CPMG MAS NMR for Fast Characterization of Sn Sites in Zeolites with Natural ^{119}Sn Isotope Abundance. *J. Phys. Chem. Lett.* **2016**, *7* (7), 1249–1253.
- (15) Boronat, M.; Concepción, P.; Corma, A.; Renz, M.; Valencia, S. Determination of the Catalytically Active Oxidation Lewis Acid Sites in Sn-Beta Zeolites, and Their Optimisation by the Combination of Theoretical and Experimental Studies. **2005**, *234*, 111–118.

- (16) Zheng, A.; Liu, S. Bin; Deng, F. 31P NMR Chemical Shifts of Phosphorus Probes as Reliable and Practical Acidity Scales for Solid and Liquid Catalysts. *Chem. Rev.* **2017**, *117* (19), 12475–12531.
- (17) Gunther, W. R.; Michaelis, V. K.; Griffin, R. G.; Roman-Leshkov, Y. Interrogating the Lewis Acidity of Metal Sites in Beta Zeolites with 15N Pyridine Adsorption Coupled with MAS NMR Spectroscopy. *J. Phys. Chem. C* **2016**, *120* (50), 28533–28544.
- (18) Saravanamurugan, S.; Riisager, A.; Taarning, E.; Meier, S. Mechanism and Stereoselectivity of Zeolite-Catalysed Sugar Isomerisation in Alcohols. *Chem. Commun.* **2016**, 52 (86), 12773–12776.
- (19) Elliot, S. G.; Tolborg, S.; Sádaba, I.; Taarning, E.; Meier, S. Quantitative NMR Approach to Optimize the Formation of Chemical Building Blocks from Abundant Carbohydrates. *ChemSusChem* **2017**, *10* (14), 2990–2996.
- (20) Tolborg, S.; Katerinopoulou, A.; Falcone, D. D.; Sadaba, I.; Osmundsen, C. M.; Davis, R. J.; Taarning, E.; Fristrup, P.; Holm, M. S. Incorporation of Tin Affects Crystallization, Morphology, and Crystal Composition of Sn-Beta. *J. Mater. Chem. A* **2014**, *2* (47), 20252–20262.
- (21) Holm, M. S.; Saravanamurugan, S.; Taarning, E. Conversion of Sugars to Lactic Acid Derivatives Using Heterogeneous Zeotype Catalysts. *Science* **2010**, *328* (5978), 602–605.
- (22) Taarning, E.; Saravanamurugan, S.; Holm, M. S.; Xiong, J.; West, R. M.; Christensen, C. H. Zeolite-Catalyzed Isomerization of Triose Sugars. *ChemSusChem* **2009**, *2* (7), 625–627
- (23) Elliot, S. G.; Tolborg, S.; Madsen, R.; Taarning, E.; Meier, S. Effects of Alkali-Metal Ions and Counter Ions in Sn-Beta-Catalyzed Carbohydrate Conversion. *ChemSusChem* **2018**, *11* (7), 1198–1203.
- (24) Yang, G.; Pidko, E. A.; Hensen, E. J. M. The Mechanism of Glucose Isomerization to Fructose over Sn-BEA Zeolite: A Periodic Density Functional Theory Study. *ChemSusChem* **2013**, *6* (9), 1688–1696.
- (25) Dusselier, M.; VanWouwe, P.; deClippel, F.; Dijkmans, J.; Gammon, D. W.; Sels, B. F. Mechanistic Insight into the Conversion of Tetrose Sugars to Novel α -Hydroxy Acid Platform Molecules. *ChemCatChem* **2013**, *5* (2), 569–575.
- (26) Román-Leshkov, Y.; Davis, M. E. Activation of Carbonyl-Containing Molecules with Solid Lewis Acids in Aqueous Media. *ACS Catal.* **2011**, *1* (11), 1566–1580.
- (27) Elliot, S. G.; Tosi, I.; Meier, S.; Martinez-Espin, J. S.; Tolborg, S.; Taarning, E. Stoichiometric Active Site Modification Observed by Alkali Ion Titrations of Sn-Beta. *Catal. Sci. Technol.* **2019**, *9* (16), 4339–4346.
- (28) Sushkevich, V. L.; Kots, P. A.; Kolyagin, Y. G.; Yakimov, A. V.; Marikutsa, A. V.; Ivanova, I. I. Origin of Water-Induced Brønsted Acid Sites in Sn-BEA Zeolites. **2019**.
- (29) Conrad, S.; Wolf, P.; Müller, P.; Orsted, H.; Hermans, I. Influence of Hydrophilicity on the Sn β -Catalyzed Baeyer–Villiger Oxidation of Cyclohexanone with Aqueous Hydrogen Peroxide. *ChemCatChem* **2017**, *9* (1), 175–182.
- (30) Levenspiel, O. *Chemical Reaction Engineering*; 1999; Vol. 38.

Chapter 7

Conclusions and pertaining challenges

7.1 Next challenges and discussion

During the introduction of the thesis, (Chapter 1) elements of the last two decades of research on catalytic biomass upgrading catalysed by Sn-Beta were presented. During this period, several studies were performed on this material allowing researchers to gain insights of its reactivity and its active site conformation. Although these results were essential for understanding the catalytic potential of Sn-Beta, at the beginning of this project (2016) little was known regarding its possible applicability on a real process aiming to produce chemical commodities with a real economic gain. Therefore in this manuscript, relevant attention was given to the performance of Sn-Beta in terms of stability on a continuous process for glucose upgrading. Stability is often an overlooked property of a catalyst in the academic environment, where activity is usually the property that researchers seek in catalytic research. However good catalyst stability is a paramount property that a material needs to possess for ensuring the economic feasibility of a process. Furthermore, mechanistic studies of catalyst stability are not trivial and require sophisticated *in-situ* and *operando* characterisations making this study appealing and challenging also from a technological point of view.

Probably the most important discovery regarding the stability of the catalyst during continuous transformation was achieved in Chapter 2, where the stabilising effect of water was thoroughly described and analysed. In this work, over 1500 h of continuous sugars upgrading was achieved by Sn-Beta.^{1,2} This piece of work eventually opened a lot of question on “*how*” the deactivation is taking place. Interesting elucidation on this topic was given in Chapter 6, where it was finally shown that the deactivation of Sn-Beta is not a uniform process, but the different reactions carried out by Sn-Beta have different deactivation profiles (Chapter 6, scheme 1 and figure 18). Moreover it was also shown how different preparations of Sn-Beta are able to catalyse preferably different pathways showing a different behaviour of the catalyst as a function of the active sites speciation and preparation procedure. In particular, higher performances for glucose upgrading were originally achieved by the hydrothermal preparation of Sn-Beta zeolite as demonstrated by Chapter 3 and Chapter 6, where analytic and spectroscopic studies highlighted the effectiveness of this preparation.

This finding encouraged the research for a new kind of post-synthetical treatment which could improve Sn-Beta activity, and in Chapter 4 this research resulted in the “pre-activation protocol” for Sn-Beta, which improved the activity, stability and selectivity of this material towards glucose upgrading. In Chapter 4, it was shown how these enhancements in performance were strongly related to a change in hydrophobicity and active site speciation

of the material. Although these hypotheses were in line with previous literature, which empirically correlated better performances to higher hydrophobicity of the material,³ a deeper understanding of this correlation could be achieved here. Particularly, the transformation of the active site after “pre-activation” was thought to be linked to the improvement in performance (Chapter 4, Section 4.3.3). However, further investigation at this point was not pursued.

This research could be further expanded through a more complete characterisation of Sn-Beta by the method proposed by Kolyagin *et al.*⁴ The methodology here proposed enables the assignment of a ¹¹⁹Sn-NMR speciation to a precise T-site in the zeolite framework; a similar study on the “pre-activated” catalyst might enable researchers to understand whether a changing in T-site position of Sn is the cause of the improvement in the catalyst performance, or whether other factors, such as increased hydrophobicity, are solely responsible for improved performance.

Further understanding in this matter is needed also in correlating the properties of Sn-Beta zeolite to a precise chemical pathway. In particular, in Chapter 6 it was shown how hydrothermal Sn-Beta is more prone to produce retro-aldol (RA) products than its post-synthetic analogue, and how the presence of protons in the active site environment of Sn-Beta can result in the formation of non-selective products, such as alkyl-glycosides and β -dehydration products. Unfortunately, I did not succeed throughout this project to analyse the properties of the protons in Sn-Beta zeolite, nor to understand the cause of the higher tendency of the hydrothermal Sn-site to selectively cleave C₆ sugars to yield methyl lactate (ML) and methyl vinyl glycolate (MVG). These challenges are still open for future researchers to further expand this area of research.

A big contribution in understanding the catalyst behaviour in continuous glucose upgrading was given by the development of a novel continuous *operando* UV-Vis reactor. This reactor allowed to monitor in real time the interaction between the solvent and the reaction substrate with the catalyst, recording in the meanwhile trustworthy kinetic data. This was the first time a continuous *operando* UV-Vis reactor was employed on a liquid-solid phase system at temperature <170 °C and at 20 bar of pressure. This analysis highlighted a strong interaction between the solvent and the active site of Sn-Beta zeolite (Chapter 2, 2.3.3); in particular this interaction seemed to have played an important role throughout the developments of the project:

- 1- Sn-Beta deactivation showed to be originated by the Sn-methanol interaction (Chapter 2); this kind of deactivation showed to be more accentuated for post-synthetic preparation of Sn-Beta zeolite (Chapter 3) and was found to be possible to overcome this interaction by adding traces of water to the catalyst environment (Chapter 2).
- 2- The “pre-activation” protocol of Sn-Beta was clearly originated by a solvent-catalyst interaction prior calcination at 550 °C (Chapter 4), leading to transformation in material

properties, which improved the material performances in terms of activity, selectivity and stability.

- 3- Hf-Beta zeolite showed to be active for glucose isomerisation (GI) only after a 20 h induction period in methanol, which enabled the catalyst to achieve performances never shown previously (Chapter 5).

The nature of these catalyst-solvent interactions are still not yet completely understood and further studies are required to better understand these phenomena to forecast catalyst behaviour in the scale up of a chemical process. This study will be paramount for the chemical industry in the next decade; in fact several processes for biomass upgrading need to be developed for shifting away from fossil feedstock and comply with future requirement for CO₂ emissions.^{5,6} These processes will employ oxygenated molecules, characterised by high boiling points, making the development of continuous liquid processes essential for this purpose.⁷ When compared to the classic gas phase reactions, the phenomena taking place in these processes are more complex since the catalyst will be immersed in a solvent which most of the time is not inert in the catalytic process, but it might interact with the catalyst (as shown in for this system).⁸ Therefore a deep mechanistic study on such catalyst-solvent interactions will be essential to ensure the best performance of a process ensuring its economic sustainability.

Finally particular emphasis in the manuscript was reserved for the enhancement in selectivity of some of the processes involving glucose upgrading, particular in Chapter 4 for the first time in the literature a full selectivity in RA products was achieved by Sn-Beta zeolite, even though if only for small amount of time on stream. Similarly, in Chapter 5 for the first time a fully selective, heterogenous chemocatalytic glucose isomerisation (GI) reaction was achieved. As explained in Chapter 1 (Section 1.8), GI represent an important bottleneck for the upgrading of glucose to important chemical commodities, due to the high operative costs characteristic of the enzymatic process, which is nowadays industrially applied. Although the findings of these discoveries are important, further experiments are necessary for scaling up these processes.

In particular, throughout the thesis, a generally high Weight Hourly Space Velocity (WHSV, equation 10 in the equation index) was applied to facilitate catalyst deactivation and favour its mechanistic study (Chapter 2). Consequently, although these conditions showed in some case high productivity, immediate catalyst deactivation was a consequence. Therefore to proceed in the process scale-up these results need to be replicated at lower WHSV, with a higher excess of catalyst, which will reduce the productivity of the process but it will allow a longer lifetime of the process to more relevant industrial conditions.

Furthermore, throughout the whole manuscript a concentration of only 1 % wt. glucose was used for glucose upgrading. This quantity was chosen due to the low solubility of glucose in methanol, and it was sufficient to move the first steps in the continuous sugar upgrading.

However to improve the economy of the process higher concentration of the substrate are required, and thanks to adding of water in the reaction feed, up to 10 % wt. of sugars can be dissolved in the reaction feed. Therefore, these processes need to be re-evaluated in these intensified conditions to understand how to scale-up these reactions in the best way. However, selectivity is not the only key to industrialisation of a process; another sector, which development is paramount for the efficiency of the process is the product separation. This part of the process is also often overlooked, but it represents an impacting voice on the variable costs for a chemical plant. Therefore, further developments in this area are necessary to better separate the final products. Discoveries in this area might in fact dictate different conditions also for the upstream processes.⁹

In general, the developments achieved throughout this PhD brought interesting results that I believe might have a positive impact on the field. Nonetheless, the project of the Bio-refinery is still far from being reality, and fossil feedstock remains the most important source of carbon for polymer and base chemical production. Refinery processes for fossil feedstock were developed slowly throughout the course of the last century passing through different innovations which enabled humanity to transform this carbon source in an optimal, cost effective manner. The profound differences in chemical properties between fossil-feedstock and biomass partially justify the lack of knowledge, and the hurdles encountered in the last two decades in creating a new set of processes for commodity chemical production from this renewable source of carbon. Therefore, in the next decades the scientific community is expected to deliver a new asset of chemical processes able to eliminate the use of petroleum for the production of plastic and energy, decreasing drastically anthropologic carbon emission. This projection can be supported by past experience in developing refinery processes, which was carried out with less effective technological assets. Although it is true that this contemporary technological edge can catalyse the completion of the bio-refinery, it is simplistic assuming that a pure technological comparison can be representative of the pace at which scientific progress is moving today in this sector.

A parallel socio-economic thinking can outline different prospects for the progression of this specific area of chemistry; to understand that it is crucial to realise in which economic environment the refinery of fossil-feedstock was developed, and the difference with the contemporary situation.

Important development in oil distillation were reached during the second world war, where the war-competition dictated technological progress in several technological fields. After the world wars, years of peace and prosperity in the western countries lead to economic growth sustained by consumerism and international commercial exchanges. In these years demand for new material and technology created the conditions for companies to invest in developing new products able to satisfy an existing demand. Today, a different urge is driving a drastic change in technology. In fact, there is no real demand for new plastic materials by consumers, but environmental factors are creating the conditions for which companies need to invest capital for different sources of carbon or energy. This implies that

these new investments will not bring an increment in revenue, but rather they will nurture the creation of an alternative source of income to the already existing one.

Moreover, the wealth and the dimensions of the main chemical industries brought these companies to have a financial structure that leads to a more risk-adverse management, and hence which does not now find the same stimuli to invest in new technology as in the 50's or 60's. Governments, with the intent to boost investment in a less-conservative direction, have tried to artificially create the urge for disruptive technologies introducing taxation on emission (externalities) or banning chemicals and/or processes which did not adhere at environmental friendly norms. Although this effectively helped in creating new technologies, it did not give yet the strong change of direction, which was expected.

This situation might represent an interesting opportunity for academia and small entrepreneur, who should aim to develop the intellectual properties for big scale biomass upgrading processes. Historically, academic catalysis research was pointed principally towards solving fundamental questions, trying to open new pathways of technological growth. In the next years, this approach might need to be revised, and this revolution may already be slowly taking place. Top-ranking universities are ever more trying to expand their focus towards financing small businesses (start-up, spin-offs...) for developing new intellectual properties or even real businesses competitive to the market.

This approach might be beneficial for the field of biomass upgrading, in fact if spin-offs founded by governments or universities have the possibility to grow, the bigger chemical firms will be pushed to keep-up with them and even absorb them, revolutionising their processes and their business. Unfortunately, entrepreneurship in chemical industry is not easily accessible, practical experiments in R&D have high costs and process developing might requires several years of costs before creating actual earnings. This might be one of the reasons that has allowed big chemical firms to run without new and fresh competition for the last decades, contributing somehow to a conservative approach in business development.

Therefore, governments and academia must embrace diversified policies in investing capital in new small businesses, and at the same time impose new fees and constrains on CO₂ emissions. This diversified approach will force big chemistry firms to develop new technologies not only to adhere to the more strict and rigid regulations but also to maintain the pace with the technological disruption of bold and new enterprises.

Although this last discussion is far from being strictly chemically-related, I believe it is essential after a PhD course of study to embrace a vision of the socio-economical factors which surround our daily struggle in the laboratories. These considerations can aid in focusing capitals and energy in the right target to achieve to bring new and disruptive technologies to the market.

7.2 Next Challenges: bullet-points

As described above this project moved the first step towards the application of Sn-Beta and Hf-Beta on large scale processing, effectively showing the catalyst stability in continuous set-up. Although these findings are innovative and represent an important advancement from previous literature, several improvements are required to ensure the applicability of Sn-Beta on a real scale processing. This small paragraph will shortly present a clear lists of bullet points that needs to be covered to move forward the project. Although these points were partially reported in the previous section, more concise and clear instructions are herein reported from a technological prospective:

- 1) The substrate for this reaction was glucose monohydrate from Sigma-Aldrich, however a more scalable process will use glucose syrup industrially produced by starch enzymatic hydrolysis (90 % glucose in water). Therefore this substrate needs to be tested to prove the compatibility with the catalyst.
- 2) The systems explored need to be able to process higher concentration of sugars to ensure economically favourable conditions. Therefore, the optimisation of these processes for higher feed concentration is essential.
- 3) The systems herein studied are working at elevated WHSV (weight hourly space velocity). To maintain high level of conversion for longer time the process needs to be able to maintain a good selectivity in excess of catalyst. Therefore, optimisation of this parameter is needed.
- 4) Alternatively to point 3 reactor designs must be evaluated for overcome steep catalyst deactivation. This point relates to a more technological approach, which might need interdisciplinary collaborations.

Alongside these points lays the necessity to face more fundamental questions, which were brought to light during the development of the project. These issues might not directly affect the applicability of Sn-Beta on large scale processing, but are raising interesting questions on the catalyst response to liquid-solid interaction in continuous flow. The possible answer to these question are potentially helpful for a broad range of application and can be covered in these points:

- 1) Solvent-catalyst interactions needs to be studied during continuous operations. It has been brought to light in this project how methanol-catalyst interaction are responsible for Sn-Beta deactivation (Chapter 2), Sn-Beta pre-activation (Chapter 4) and Hf-Beta activation (Chapter 5). These interaction were not previously detected in batch conditions and their nature may play an important role in the developments of liquid-solid continuous processes.
- 2) The operando UV-Vis reactor on glucose upgrading has shown great insights, and its applicability needs to be further supported showing experimental proofs of how the technique is recording the spectra on the surface of the material.

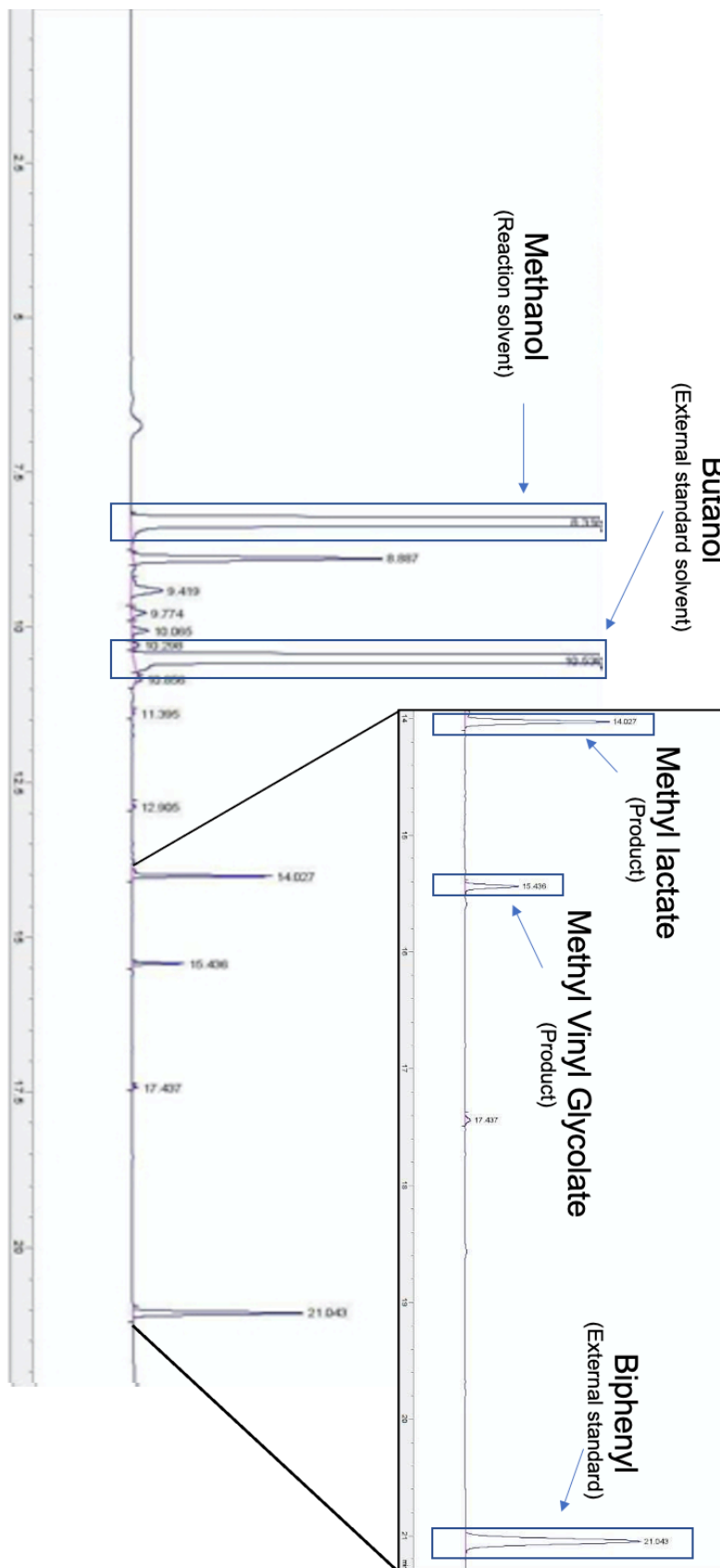
7.3 Reference

- (1) Padovan, D.; Botti, L.; Hammond, C. Active Site Hydration Governs the Stability of Sn-Beta during Continuous Glucose Conversion. *ACS Catal.* **2018**, *8* (8), 7131–7140.
- (2) Padovan, D.; Tolborg, S.; Botti, L.; Taarning, E.; Sádaba, I.; Hammond, C. Overcoming Catalyst Deactivation during the Continuous Conversion of Sugars to Chemicals: Maximising the Performance of Sn-Beta with a Little Drop of Water. *React. Chem. Eng.* **2018**, *3* (2), 155–163.
- (3) Cordon, M. J.; Hall, J. N.; Harris, J. W.; Bates, J. S.; Hwang, S. J.; Gounder, R. Deactivation of Sn-Beta Zeolites Caused by Structural Transformation of Hydrophobic to Hydrophilic Micropores during Aqueous-Phase Glucose Isomerization. *Catal. Sci. Technol.* **2019**, *9* (7), 1654–1668.
- (4) Kolyagin, Y. G.; Yakimov, A. V.; Tolborg, S.; Vennestrøm, P. N. R.; Ivanova, I. I. Direct Observation of Tin in Different T-Sites of Sn-BEA by One- and Two-Dimensional ^{119}Sn MAS NMR Spectroscopy. *J. Phys. Chem. Lett.* **2018**, *9* (13), 3738–3743.
- (5) Climent, M. J.; Corma, A.; Iborra, S. Conversion of Biomass Platform Molecules into Fuel Additives and Liquid Hydrocarbon Fuels. *Green Chem.* **2014**, *16* (2), 516.
- (6) Huber, G. W.; Iborra, S.; Corma, A. Synthesis of Transportation Fuels from Biomass: Chemistry, Catalysts, and Engineering. *Chem. Rev.* **2006**, *106* (9), 4044–4098.
- (7) Vennestrøm, P. N. R.; Osmundsen, C. M.; Christensen, C. H.; Taarning, E. Beyond Petrochemicals: The Renewable Chemicals Industry. *Angew. Chemie - Int. Ed.* **2011**, *50* (45), 10502–10509.
- (8) Hammond, C. Intensification Studies of Heterogeneous Catalysts: Probing and Overcoming Catalyst Deactivation during Liquid Phase Operation. *Green Chem.* **2017**, *19* (12), 2711–2728.
- (9) Thoma, C.; Konnerth, J.; Sailer-Kronlachner, W.; Solt, P.; Rosenau, T.; Herwijnen, H. W. G. Current Situation of the Challenging Scale-Up Development of Hydroxymethylfurfural Production. *ChemSusChem* **2020**, *13*, 1–22.

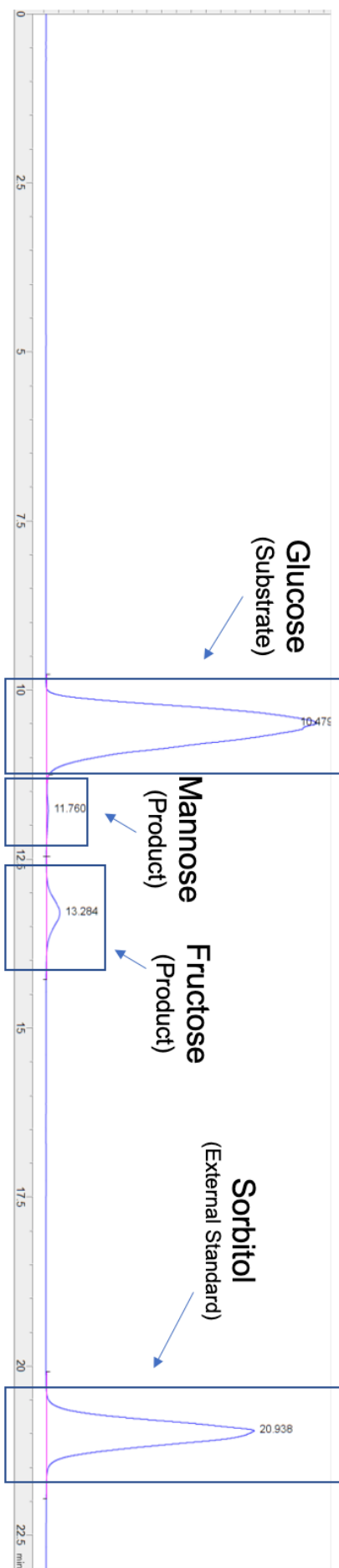
Appendix "A": Equations Appendix

1. $Productivity = \frac{Kg_{products}}{K_{catalyst} \cdot h}$
2. $Contact\ time = \tau\ (min) = \frac{volume_{(catalyst\ bed)}}{flow\ rate}$
3. $Conversion = X_{reactant} = \frac{mol_{reactant\ (0)} - mol_{reactant\ (t)}}{mol_{reactant\ (0)}}$
4. $Relative\ performance = \frac{Conversion, X(t)}{Conversion, X(0)}$
5. $Levenspiel\ deactivation\ rate = \ln\left(\ln\left(\frac{[Glu]_0}{[Glu]_t}\right)\right) = \ln(k \cdot \tau) - \ln \cdot k_d t$
6. $TOF_0 = moles_{(converted)} \cdot moles_{S_n}^{-1} \cdot h^{-1}$
7. $Substrate\ turnover = \frac{\sum_0^t mol\ (Substrate)}{n\ (S_n)}$
8. $Selectivity = S = \frac{(Y_{product})}{(X_{Glucose})}$
9. $Yield = Y_{product} = \frac{mol_{product\ (t)}}{mol_{reactant\ (0)}}$
10. $Weight\ Hourly\ Space\ Velocity\ (WHSV) = \frac{Kg_{reactant}}{h \cdot Kg_{catalyst}}$
11. $Space - Time - Yield = \frac{Kg_{products}}{m_{catalyst}^3 \cdot h}$

Appendix "B": GC-Chromatogram



Appendix "C": ELSD-HPLC-Chromatogram





Cite this: *React. Chem. Eng.*, 2018, 3, 155

Overcoming catalyst deactivation during the continuous conversion of sugars to chemicals: maximising the performance of Sn-Beta with a little drop of water†

Daniele Padovan,‡^a Søren Tolborg, ^b Luca Botti,^a Esben Taarning,^b Irantzu Sádaba*^b and Ceri Hammond ^{*a}

Producing chemicals from renewable resources represents one of the key challenges in chemical science. Whilst catalytic methods for converting renewables to chemicals offer several advantages over biological approaches, the solid catalysts developed to date are typically plagued by rapid rates of deactivation, prohibiting their greater exploitation. Here, we demonstrate, for the first time, that a Sn-containing zeolite, Sn-Beta, is capable of continuously converting saccharide solutions to value added chemicals with high levels of activity, selectivity and stability. For both the isomerisation of glucose to fructose, and the conversion of fructose to alkyl lactates, we observe that the addition of up to 10% of water to the methanol/sugar reaction feed increases reactivity by a factor of 2.5, and catalyst stability by one order of magnitude. Continuous operation for up to 1366 h (57 days) is demonstrated, with only limited loss of activity being observed over this period of time. Post-reaction characterisation indicates that the addition of water influences several elements of the catalytic system, which cooperatively result in improved performance.

Received 26th October 2017,
Accepted 24th November 2017

DOI: 10.1039/c7re00180k

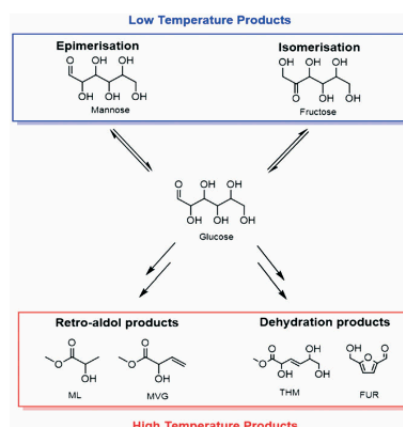
rsc.li/reaction-engineering

Introduction

Fossil resources are the feedstock for over 90% of all organic chemicals on an industrial scale. Given the finite nature of these resources, developing more sustainable routes to platform and commodity chemicals is an essential task. In this regard, the conversion of renewable sugar streams into valuable chemicals is one of the major targets.^{1–5} Catalytic methodologies exhibit several advantages *versus* fermentative transformations with respect to overall productivity of the system. They are also, in general, more robust and benefit from economy of scale. However, sufficient stability of solid catalysts in the polar solvents required for sugar conversion, such as water and methanol, has yet to be achieved, prohibiting greater exploitation of such technologies.^{6–8}

The isomerisation of glucose to fructose (GI),^{9–13} and the production of alkyl lactates from saccharides through retro-aldol chemistry^{14,15} are two examples of renewable chemical processes whereby catalytic methods offer several potential advantages over fermentative methods (Scheme 1). GI is a

key step for the production of high fructose corn syrup (HFCS, 8 Mt a⁻¹), and for the transformation of hexoses to renewable furanic platform molecules (Scheme 1).^{16,17} Additionally, methyl lactate (ML) is a very attractive bio-monomer for the production of renewable plastics, and other co-products formed during ML production, such as methyl vinyl glycolate (MVG), also have potential for application in the



Scheme 1 General scheme demonstrating the products that can be obtained by the catalytic conversion of sugars with Sn-Beta at both low (<140 °C) and high (>140 °C) temperature.

^a Cardiff Catalysis Institute, Cardiff University, Park Place, Cardiff, CF10 3AT, UK. E-mail: hammond4@cardiff.ac.uk

^b Haldor Topsøe A/S, New Business R&D, Haldor Topsøes Allé 1, 2800-Kgs. Lyngby, Denmark. E-mail: irsz@topsoe.com

† Electronic supplementary information (ESI) available. See DOI: 10.1039/c7re00180k

‡ These authors contributed equally.

Active Site Hydration Governs the Stability of Sn-Beta during Continuous Glucose Conversion

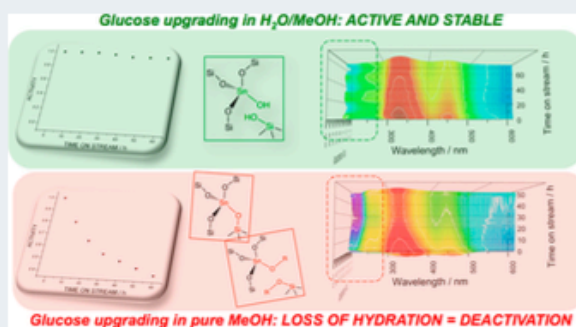
Daniele Padovan,[‡] Luca Botti,[‡] and Ceri Hammond*[§]

Cardiff Catalysis Institute, School of Chemistry, Cardiff University, Cardiff, CF10 3AT, United Kingdom

Supporting Information

ABSTRACT: The stability of Sn-Beta for the continuous upgrading of hexoses is improved dramatically upon the addition of small amounts of water to the methanol/sugar reaction feed, despite water itself being an unfavorable solvent. Herein, the molecular level origin of this effect is investigated. Spectroscopic studies of the catalytic materials pre-, post- and during operation, with *operando* UV-vis, ¹¹⁹Sn CPMG MAS NMR, DRIFTS-MS, TGA, TPD/O-MS, and porosimetry, are coupled to additional kinetic studies, to generate detailed structure–activity–lifetime relationships. In doing so, we find that the addition of water influences two particular processes—fouling and active site modification. However, mitigating the second is the most crucial role of water. Indeed, in the absence of water, the loss of Sn–OH and Si–OH sites occurs. Notably, these changes in active site hydration correlate to deactivation and reactivation of the system. The consequences of these findings, both for mechanistic understanding of the system and to the design of alternative regeneration methods, are also discussed.

KEYWORDS: Biomass upgrading, Sugar conversion, Zeolites, Tin, *in situ* Spectroscopy



INTRODUCTION

The production of important commodity chemicals from renewable resources represents a focal point of contemporary chemical research.^{1–5} Given their abundance and functionality, cellulose-based derivatives are the most viable source of carbon for the production of chemicals. Whereas several possible strategies exist for converting such feedstock into chemicals, selective catalytic methodologies offer several advantages, particularly in the context of process intensification. Of particular interest is the conversion of highly functionalized molecules such as glucose and fructose, which can be obtained following depolymerization of cellulose. In this respect, the heterogeneous catalyst Sn-Beta (Sn-β) is of prime interest, having been shown to be highly active and selective for a range of processes such as (i) fructose production via glucose–fructose isomerization;^{6–10} (ii) generation of renewable monomers such as alkyl lactates,^{11,12} furanics,^{13,14} and methyl vinyl glycolate;^{15,16} (iii) H₂-free reduction of carbonyl compounds via catalytic transfer hydrogenation;¹⁷ and (iv) Baeyer–Villiger oxidation of (renewable) ketones with H₂O₂ as oxidant.^{18–20}

Possessing an ability to operate continuously, without exhibiting excessive levels of deactivation, is one of the most important properties a promising heterogeneous catalyst must exhibit in order to be suitable for industrialization.^{21,22} As such, study and optimization of the stability of the catalyst under continuous conditions is paramount. In contrast to fossil feedstock, the highly oxygenated nature of sugar-based

substrates necessitates processing in the liquid phase. The addition of the solvent, alongside the chelating substrates present in solution, can dramatically impact the stability of a solid material, particularly when elevated pressures and temperatures are required for sufficient levels of macroscopic performance to be achieved.^{23,24} As such, despite the significant interest in catalytic sugar upgrading, development of robust catalytic materials capable of continuous operation has lagged behind, prohibiting greater intensification.

Recently, we demonstrated that dramatic improvements to the stability of Sn-β, during both glucose–fructose isomerization and the conversion of fructose to methyl lactate, could be achieved by adding small quantities of water to the conventional sugar/methanol feed, despite water itself being highly unfavorable as a solvent.²⁵ In fact, upon the addition of water (1–10 wt %) to the feed, reactivity was found to increase by a factor of 2.5, and catalyst stability improved by 1 order of magnitude. Combined, these permitted continuous operation to be achieved for up to 57 days without major losses in activity.²⁵

Herein, we investigate the molecular-level origin of this surprising effect. Spectroscopic studies of the catalytic materials pre-, post- and during operation, with *operando* UV-vis, ¹¹⁹Sn CPMG MAS NMR, DRIFTS-MS, TGA, TPO-

Received: May 4, 2018

Revised: June 11, 2018

Published: June 15, 2018



Influence of Composition and Preparation Method on the Continuous Performance of Sn-Beta for Glucose-Fructose Isomerisation

Luca Botti¹ · Ricardo Navar¹ · Søren Tolborg² · Juan S. Martinez-Espin² · Daniele Padovan¹ · Esben Taarning² · Ceri Hammond¹

Published online: 19 November 2018
© The Author(s) 2018

Abstract

The stability, activity and selectivity of various Sn-Beta catalysts are investigated to identify how the composition of the catalyst, in addition to its method of preparation, impact its ability to continuously isomerise glucose to fructose. Increasing the Sn loading in post-synthetically prepared catalysts leads to a decrease of both activity and stability. Accordingly, materials containing dilute amounts of Sn appear to be most suitable for continuous operation. Furthermore, the method of preparation has a profound impact on the overall performance of the catalyst. In fact, preparation of Sn-Beta by hydrothermal synthesis results in improvements of both activity and stability, with respect to the post-synthetic preparation of an otherwise-analogous material. The improved resistance of hydrothermal Sn-Beta is attributed, through a combination of operando UV-Vis, TPD-MS and vapour adsorption isotherms, to its greater resistance to deactivation by methanol (the reaction solvent). Complementary ¹¹⁹Sn CPMG MAS NMR experiments also indicate the presence of different Sn sites in the hydrothermal material, which, alongside the presence of a less adsorptive siliceous matrix, may be intrinsically less prone to solvent interaction than those present in post-synthetic Sn-Beta.

Keywords Sugar conversion · Continuous flow · Glucose · Renewables · Sn-Beta · Zeolites

1 Introduction

With fossil fuel depletion becoming ever greater, researchers are increasingly focusing their efforts on sustainability. Within this area, one of the major targets is the search for alternative sources of carbon for chemical production. In this context, renewable carbon resources, such as cellulosic biomass, may provide a solution [1–3]. Cellulose is a biopolymer constituted by a chain of glucose monomers. Once depolymerised into its constituent units, it can subsequently be converted into higher value commodity compounds, some

notable examples including 5-(hydroxymethyl)furfural [4], methyl lactate [5] and methyl vinyl glycolate [6]. Whilst its significant stability makes the direct conversion of glucose into 5-(hydroxymethyl)furfural and methyl lactate challenging, its isomer, fructose, can readily be converted into them. As such, the catalytic isomerisation of glucose to fructose represents a key step in the production of cellulose-derived chemicals.

At present, glucose isomerisation is achieved through enzymatic catalysis. However, although the bio-catalytic route is highly selective, it requires strict operational conditions, leading to a process with a low degree of flexibility. As such, the development of a solid catalyst capable of performing this reaction via heterogeneous catalytic methods in a scalable manner is highly desirable [7–9]. Amongst various solid catalysts capable of performing the glucose isomerisation reaction, the zeolite Sn-Beta has been shown to be one of the most promising materials. Furthermore, Sn-Beta has also been shown to be exceptionally active for the related conversion of hexoses to methyl lactate and methyl vinyl glycolate through retro-aldol chemistry. The outstanding catalytic ability of Sn-Beta for carbohydrate valorisation has

Electronic supplementary material The online version of this article (<https://doi.org/10.1007/s11244-018-1078-z>) contains supplementary material, which is available to authorized users.

✉ Ceri Hammond
hammondc4@cardiff.ac.uk
<http://blogs.cardiff.ac.uk/hammond/>

¹ Cardiff Catalysis Institute, School of Chemistry, Cardiff University, Park Place, Cardiff CF10 3AT, UK

² Haldor Topsøe A/S, Sustainable Chemicals, Haldor Topsøes Allé 1, 2800 Lyngby, Denmark

Thermal Regeneration of Sn-Containing Silicates and Consequences for Biomass Upgrading: From Regeneration to Preactivation

Luca Botti, Daniele Padovan, Ricardo Navar, Søren Tolborg, Juan S. Martinez-Espin, and Ceri Hammond*



Cite This: *ACS Catal.* 2020, 10, 11545–11555



Read Online

ACCESS |



Metrics & More



Article Recommendations



Supporting Information

ABSTRACT: Minimizing catalyst deactivation and developing regeneration protocols are critical challenges in the area of biomass upgrading. Herein, we investigate the regeneration of Sn-containing zeolites for the continuous conversion of glucose. In doing so, we reveal that permanent changes to the properties of the catalyst occur following continuous operation and regeneration, resulting in surprising improvements to performance during subsequent operational cycles. Through a combination of characterization (^{119}Sn CPMG MAS NMR, DRIFTS, and vapor sorption) and kinetic methodologies, we reveal that improved performance arises from restructuring of the catalyst, which causes the active-site environment to become more accessible, more hydrophobic, more reactive, and more stable.

Based on these findings, we demonstrate how these positive changes can be emulated without resorting to extended operation, by optimizing pretreatment of the catalyst prior to reaction. This process, termed preactivation, involves treatment of the fresh catalyst in a flow of methanol at 110 °C for 0.5 h, prior to its heat treatment at 550 °C in air for 3 h. This relatively rapid procedure allows substantial improvements to catalyst activity and stability to be achieved in a permanent fashion prior to the first operational cycle.

KEYWORDS: biomass conversion, deactivation, glucose, zeolites, solvent effects



INTRODUCTION

The conversion of renewables to commodity chemicals is a major topic of contemporary research.^{1–3} Of particular interest is the catalytic conversion of renewable compounds such as glucose, fructose, and xylose, each of which can be obtained by depolymerization of lignocellulose, the major constituent of renewable terrestrial biomass.^{4,5} As these compounds are highly functionalized, they can be used as platform molecules for the synthesis of chemicals, provided that an active, selective, and stable catalyst can be found to mediate their conversion into forms of relevance to society.⁶ Among such catalysts, Lewis acidic zeolites such as Sn-Beta are some of the most promising, as they are active and selective for a range of desirable chemical processes, including glucose-fructose isomerization;^{7–12} the conversion of renewable saccharides to important monomers such as alkyl lactates and methyl vinyl glycolate;^{13–16} the catalytic transfer hydrogenation of oxygenated compounds;¹⁷ and the Baeyer–Villiger oxidation of (renewable¹⁸) ketones with H_2O_2 as an oxidant.¹⁹

In addition to demonstrating high levels of activity and selectivity, promising heterogeneous catalysts must also be able to operate continuously, without exhibiting excessive rates of deactivation.^{20–22} Thus, in addition to optimizing activity and selectivity, the study of the stability of the catalyst under continuous conditions is paramount. Recently, we demonstrated that the stability of Sn-Beta for the valorization of

hexoses could be enhanced dramatically by adding small quantities of water to the sugar/methanol reaction feed.²³ In doing so, we could continuously catalyze the conversion of various hexoses for up to 57 days, without experiencing significant levels of deactivation. Through spectroscopic and kinetic methods, we attributed this improvement to *in situ* regeneration of the active sites by interaction with the correct solvent species.²⁴ Because of the excellent stability of Sn-Beta in the presence of small quantities of water, the impact of thermal regeneration in terms of catalyst longevity and performance was not fully explored in our previous study.²⁴ However, for a continuous process to be viable, it is essential that regeneration methods can be applied to the catalyst over multiple operational cycles, in order that sufficient levels of catalyst productivity can be achieved (in terms of kg of product produced per kg of catalyst) when catalyst deactivation is inevitably encountered.

As such, here, we present a study of the deactivation and regeneration of Sn-Beta catalysts during the continuous

Received: May 27, 2020

Revised: September 9, 2020

Published: September 10, 2020



**Heterogeneous Catalysis** Hot Paper

How to cite:

International Edition: doi.org/10.1002/anie.202006718

German Edition: doi.org/10.1002/ange.202006718

Solvent-Activated Hafnium-Containing Zeolites Enable Selective and Continuous Glucose–Fructose Isomerisation

Luca Botti, Simon A. Kondrat, Ricardo Navar, Daniele Padovan, Juan S. Martinez-Espin, Sebastian Meier, and Ceri Hammond*

Abstract: The isomerisation of glucose to fructose is a critical step towards manufacturing petroleum-free chemicals from lignocellulosic biomass. Herein we show that Hf-containing zeolites are unique catalysts for this reaction, enabling true thermodynamic equilibrium to be achieved in a single step during intensified continuous operation, which no chemical or biological catalyst has yet been able to achieve. Unprecedented single-pass yields of 58% are observed at a fructose selectivity of 94%, and continuous operation for over 100 hours is demonstrated. The unexpected performance of the catalyst is realised following a period of activation within the reactor, during which time interaction with the solvent generates a state of activity that is absent in the synthesised catalyst. Mechanistic studies by X-ray absorption spectroscopy, chemisorption FTIR, operando UV/Vis and ^1H - ^{13}C HSQC NMR spectroscopy indicate that activity arises from isolated Hf^{IV} atoms with monofunctional acidic properties.

Introduction

Pressing environmental and societal concerns are driving researchers to develop new processes with minimised reliance on fossil resources.^[1] In this context, sustainable chemical manufacture is a major challenge, since over 95% of the organic chemicals currently employed in the chemical industry are sourced from coal, oil and natural gas.^[2] Amongst renewable resources, lignocellulosic biomass is especially promising, given its abundance, high chemical functionality

and geographic diversity. Yet, its use as a chemical feedstock requires the development of selective catalytic technologies that are able to transform this valuable feedstock into useful end products in an economically and environmentally efficient manner.

The isomerisation of glucose to fructose (GI) is a key step towards converting glucose (the most abundant fraction of lignocellulose) into a variety of commercially relevant chemicals, including furanics, levulinates and unsaturated hydroxyesters.^[3] Although enzymes catalyse GI to single pass fructose yields of up to 42%,^[4] development of a solid (heterogeneous) catalyst capable of performing this reaction would be an important step forward, both by improving operational flexibility (temperature, pH, feed purity)^[5] and facilitating process intensification.^[6] To date, it has become generally appreciated that tin (Sn) containing zeolites (particularly Sn-BEA) possess the greatest potential for chemo-catalytic GI.^[7] Zeolites are crystalline, microporous silicates, which in the case of Sn-BEA is a three-dimensional silicate containing dilute amounts of Lewis acidic Sn^{IV} atoms within its lattice.^[8] However, although the high activity of Sn-BEA for GI has received widespread attention, several negative aspects of its performance are less appreciated, such as its poor stability in the polar solvents required for biomass conversion,^[9] and its tendency to catalyse a variety of competitive and/or degradation reactions at operational conditions.^[10] The latter is especially problematic, as it wastes a precious resource^[1b] and negatively impacts process economics. However, no better alternatives to Sn-BEA have yet been found. Consequently, heterogeneous catalysis is unable to reach the levels of performance exhibited by enzymes, and renewable chemical production by scalable chemo-catalytic methods remains limited by the enduring bottleneck of selective glucose isomerisation.

Here we show that hafnium (Hf)-containing zeolites are uniquely able to perform GI at unprecedented levels of selectivity, even at commercially relevant operational conditions. The optimal catalyst (Hf-BEA, Hf/Si molar ratio = 202, prepared by hydrothermal synthesis^[11]) achieves single pass fructose yields of 58%, at a fructose selectivity of 94%, even during continuous operation for over 100 h on stream. Its unique performance is maintained even at elevated temperature (< 140 °C), which is an advantage over biological catalysts that are only active at low temperature, where thermodynamics favours the reactant side of equilibrium, and reactor productivity is limited.^[7b] Structure-activity relationships indicate that activity arises from isolated Hf^{IV} atoms with monofunctional acidic properties, which permit high

*] L. Botti, C. Hammond
Department of Chemical Engineering
Imperial College London
London, SW7 2AZ (UK)
E-mail: ceri.hammond@imperial.ac.uk

L. Botti, R. Navar, D. Padovan
Cardiff Catalysis Institute, Cardiff University
Cardiff, CF10 3AT (UK)

S. A. Kondrat
Department of Chemistry, Loughborough University
Loughborough (UK)

J. S. Martinez-Espin
Haldor Topsøe A/S
Haldor Topsøes Allé 1, 2800-Kgs. Lyngby (Denmark)

S. Meier
Department of Chemistry, Technical University of Denmark
Kemitorvet Building 207, 2800-Kgs. Lyngby (Denmark)

Supporting information and the ORCID identification number(s) for the author(s) of this article can be found under:
<https://doi.org/10.1002/anie.202006718>.